University of Alberta

Comparative Surface Thermodynamic Analysis of New Fluid Phase Formation in Various Confining Geometries

by:

Leila Zargarzadeh

A thesis submitted to the Faculty of Graduate Studies and Research in partial fulfillment of the requirements for the degree of

Master of Science

in

Chemical Engineering

Department of Chemical and Materials Engineering

©Leila Zargarzadeh
Spring 2012
Edmonton, Alberta

Permission is hereby granted to the University of Alberta Libraries to reproduce single copies of this thesis and to lend or sell such copies for private, scholarly or scientific research purposes only. Where the thesis is converted to, or otherwise made available in digital form, the University of Alberta will advise potential users of the thesis of these terms.

The author reserves all other publication and other rights in association with the copyright in the thesis and, except as herein before provided, neither the thesis nor any substantial portion thereof may be printed or otherwise reproduced in any material form whatsoever without the author's prior written permission.

به جهان خرّم از آنم که جهان خرّم از اوست

عاشقم بر همه عالم که همه عالم از اوست

"In the world I am blissful, as the world is blessed with God's essence

I am in love with the entire universe, as it is filled with God's presence"

Saadi

To my parents

and

in loving memory of my grandmother, Batoul Shamshiri

Abstract

For a pure bulk (unconfined) fluid, phase transition happens at the saturation pressure. In contrast, for a fluid inside a confinement of small size (commonly below micrometers), vapour and liquid coexistence may happen at pressures other than the saturation pressure; or an expected phase transition might be prevented due to tight confinement of a specific geometry. Practical examples include fluids confined in miniaturized systems, catalysts, membranes, and reservoir rocks.

This thesis makes a comparative study, using thermodynamic stability analysis, of new phase formation out of a confined fluid, for three different confinement geometries of conical pit, plate–plate, and sphere–plate. Both the formation of liquid out of vapour and vapour out of liquid are studied for each geometry. Effects of different parameters: the equilibrium contact angle, the confinement solid separation, and the sphere size for the sphere–plate case, are investigated. The conclusions of this comparative study are extendable to other geometries.

Acknowledgements

I express my sincere gratitude wholeheartedly to my supervisor, Dr. Janet A.W. Elliott, for her precious guidance, constructive discussions, constant encouragement, immense patience, enduring support, and her enthusiasm.

I would like to thank my examining committee: Dr. Thomas Thundat, Dr. Subir Bhattacharjee, Dr. Hongbo Zeng, and Dr. Zhenghe Xu, for their time and valuable challenging discussion.

I was fortunate to have great teachers and mentors throughout my life. I am much indebted to all my school teachers in my home country, Iran, and to the great professors of my undergraduate years at Shiraz University, and master studies at University of Alberta. I am especially appreciative of Dr. Sona Raeisi, Dr. Nasir Mehranbod, Dr. Shahab Ayatollahi, Dr. MohammadReza Rahimpour, and Dr. GholamReza Karimi at Shiraz University.

I gratefully acknowledge Fatemeh Eslami for stimulating scientific discussions, sharing the literature, and above all for our great friendship.

It is a pleasure to pay tribute to all my friends in Edmonton with whom I have celebrated different occasions. I am also grateful to all my friends throughout my life for their camaraderie which has continued regardless of distance, in particular to Nazanin Zarei, for her emotional support during the fourteen years of our friendship.

I wish to express my great love and gratitude to my beloved family: To my mother, Shahin Neshatdoost, and my father, Ahmad Zargarzadeh, for their endless love, unconditional support, encouragement, and prayers. To my brother, Amin, for his support and encouragement, and all he taught me in his unique creative way. To my sister, Maryam, for her deep feelings, support, and caring, especially during the years of my master's studies in Edmonton.

I would also like to convey thanks to each and every individual who helped in the realization of this thesis.

The financial support of this research by Natural Sciences and Engineering Research Council of Canada (NSERC) is highly appreciated. A portion of this research was funded by Dr. Zhenghe Xu's NSERC industrial chair in Oil Sands Engineering.

Leila Zargarzadeh

January 2012

Table of Contents

1. Introduction 1

1.1. Confined fluids in applications 3

1.2. Models to describe confined fluids 4

1.3. Scope of this thesis 10

1.4. Outline of chapters 12

2. Review of Required Surface Thermodynamics 15

2.1. Conditions for equilibrium 16

2.1.1. Thermal equilibrium: Temperature of bulk phases and interfaces at equilibrium conditions 19

2.1.2. Chemical equilibrium: Chemical potential of component *i* in bulk phases and interfaces at equilibrium conditions 20

2.1.3. Mechanical equilibrium: Laplace–Young equation 21

2.1.4. Young equation 24

2.2. Merging conditions for equilibrium: The Kelvin equation 25

2.3. Thermodynamic potential (Free energy) 29

2.4. Equilibrium states and stability analysis 32

2.5. Summary 34

3. Governing Equations and Common Definitions for a Liquid–Vapour System inside a Confined Solid Geometry 35

3.1. Introduction 35

3.2. Negligibility of gravitational effects *37*

3.3. Finding the Conditions for Equilibrium of the System *38*

3.3.1. Constraints of the system 41

3.3.2. Conditions for equilibrium 43

3.3.2.1. Conditions for equilibrium in the case of liquid formation out of a vapour phase 44

3.3.2.2. Conditions for equilibrium in the case of vapour formation out of a liquid phase 46

3.4. Free energy of the system *49*

3.4.1. Free energy for liquid formation out of a vapor bulk phase 50

3.4.2. Free energy of vapor formation out of a bulk liquid phase 52

3.5. Reference state for free energy *55*

3.6. Fluid material properties *59*

3.7. Effect of the bulk phase pressure on the sign of the Kelvin radius (R_C) *60*

3.7.1. Effect of the bulk phase pressure on the sign of R_C for the case of liquid formation out of a bulk vapour phase 60

3.7.2. Effect of the bulk phase pressure on the sign of R_C for the case of vapour formation out of a bulk liquid phase 63

3.8. Transition contact angle *65*

3.9. Summary *66*

4. Liquid–vapour system inside a conical pit 68

4.1. Liquid phase formation from a bulk vapour phase inside a conical pit *69*

4.1.1. Stability of the liquid phase being formed from a bulk vapour phase inside a conical pit: concave meniscus 76

4.1.1.1. Effect of equilibrium contact angle on the stability of the system for liquid phase formation out of a bulk vapour phase inside a conical pit: concave meniscus 78

4.1.1.2. Effect of the cone apex angle on the stability of the system for liquid formation out of a bulk vapour phase inside a conical pit: concave meniscus 82

4.1.2. Stability of the liquid phase being formed from a bulk vapour phase inside a conical pit: convex meniscus 84

4.1.2.1. Effect of equilibrium contact angle on the stability of the system for liquid phase formation out of a bulk vapour phase inside a conical pit: convex meniscus.....85

4.1.2.2. Effect of cone apex angle on the stability of the system for liquid phase formation out of a bulk vapour phase inside a conical pit: convex meniscus 88

4.2. Vapour phase formation from a bulk liquid phase inside a conical pit 90

4.2.1. Stability of the vapour phase being formed from a bulk liquid phase inside a conical pit: concave meniscus 93

4.2.1.1. Effect of equilibrium contact angle on the stability of the system for vapour phase formation out of a bulk liquid phase inside a conical pit: concave meniscus 94

4.2.1.2. Effect of cone apex angle on the stability of the system for vapour phase formation out of a bulk liquid phase inside a conical pit: concave meniscus 95

4.2.2. Stability of the vapour phase being formed from a bulk liquid phase inside a conical pit: convex meniscus 96

4.2.2.1. Effect of equilibrium contact angle on the stability of the system for vapour phase formation out of a bulk liquid phase inside a conical pit: convex meniscus 98

4.2.2.2. Effect of cone apex angle on the stability of the system for vapour phase formation out of a bulk liquid phase inside a conical pit: convex meniscus 98

4.3. Conclusion 99

5. Liquid–vapour system between two flat plates 106

5.1. Liquid phase formation from a bulk vapour phase between two flat plates 107

5.1.1. Stability of the liquid phase being formed from a bulk vapour phase between two flat plates: concave meniscus (θ < 90°).....111

5.1.1.1. Effect of equilibrium contact angle on the stability of the system for liquid phase formation out of a bulk vapour phase between two flat plates: concave meniscus 113

5.1.1.2. Effect of the flat plate separation distance on the stability of the system for liquid phase formation out of a bulk vapour phase between two flat plates: concave meniscus 118

5.1.2. Stability of the liquid phase being formed from a bulk vapour phase between two flat plates: convex meniscus (θ > 90°).....119

5.1.2.1. Effect of equilibrium contact angle on the stability of the system for liquid phase formation out of a bulk vapour phase between two flat plates: convex meniscus 122

5.1.2.2. Effect of the flat plate separation distance on the stability of the system for liquid phase formation out of a bulk vapour phase between two flat plates: convex meniscus 124

5.2. Vapour phase formation from a bulk liquid phase between two flat plates 126

5.2.1. Stability of the vapour phase being formed from a bulk liquid phase between two flat plates: concave meniscus (θ > 90°).....129

5.2.1.1. Effect of equilibrium contact angle on the stability of the system for vapour phase formation out of a bulk liquid phase between two flat plates: concave meniscus 132

5.2.1.2. Effect of the flat plate separation distance on the stability of the system for vapour phase formation out of a bulk liquid phase between two flat plates: concave

meniscus

…….135

5.2.2. Stability of the vapour phase being formed from a bulk liquid phase between two flat plates: convex meniscus (θ < 90°).....137

5.2.2.1. Effect of equilibrium contact angle on the stability of a vapour phase being formed from the liquid phase between two flat plates: convex meniscus 140

5.2.2.2. Effect of the flat plate separation distance on the stability of a vapour phase being formed from the liquid phase between two flat plates: convex meniscus.....142

5.3. Conclusion 144

6. Liquid–vapour system between a sphere and a flat plate 153

6.1. Liquid phase formation from a bulk vapour phase between a sphere and a flat plate …….155

6.1.1. Stability of the liquid phase being formed from a bulk vapour phase between a sphere and a flat plate: concave meniscus.....159

6.1.1.1. Effect of equilibrium contact angle on the stability of the system for liquid phase formation out of a bulk vapour phase between a flat plate and a sphere: concave meniscus …….162

6.1.1.2. Effect of the solid surface separation distance on the stability of the system for liquid phase formation out of a bulk vapour between a sphere and a flat plate: concave meniscus.....166

6.1.1.3. Effect of solid sphere size on the stability of the system for a liquid phase being formed out of a bulk vapour phase between a flat plate and a sphere: concave meniscus……..174

6.1.2. Stability of the liquid phase being formed from a bulk vapour phase between a sphere and a flat plate: convex meniscus.....177

6.1.2.1. Effect of equilibrium contact angle on the stability of the system for liquid phase formation out of a bulk vapour phase between a flat plate and a sphere: convex meniscus ……179

6.1.2.2. Effect of the solid surface separation distance on the stability of the system for liquid phase formation out of a bulk vapour between a sphere and a flat plate: convex meniscus……180

6.1.2.3. Effect of solid sphere size on the stability of the system for liquid phase formation out of a bulk vapour phase between a flat plate and a sphere: convex meniscus ……183

6.2. Vapour phase formation from a bulk liquid phase between a sphere and a flat plate ……185

6.2.1. Stability of the vapour phase being formed from a bulk liquid phase between a sphere and a flat plate: concave meniscus……189

6.2.1.1. Effect of the equilibrium contact angle on the stability of the system for vapour phase formation out of a bulk liquid phase between a flat plate and a sphere: concave meniscus……192

6.2.1.2. Effect of the solid surface separation distance on the stability of the system for liquid phase formation out of a bulk vapour between a sphere and a flat plate: concave meniscus……195

6.2.1.3. Effect of solid sphere size on the stability of the system for a vapour phase being formed out of a bulk liquid phase between a flat plate and a sphere: concave meniscus ……201

6.2.2. Stability of the vapour phase being formed from a bulk liquid phase between a sphere and a flat plate: convex meniscus……204

6.2.2.1. Effect of equilibrium contact angle on the stability of the system for vapour phase formation out of a bulk liquid phase between a flat plate and a sphere: convex meniscus ……206

6.2.2.2. Effect of the solid surface separation distance on the stability of the system for vapour phase formation out of a bulk liquid between a sphere and a flat plate: convex meniscus ……207

6.2.2.3. Effect of solid sphere size on the stability of the system for vapour phase formation out of a bulk liquid phase between a flat plate and a sphere: convex meniscus ……210

6.3. Conclusion ……212

7. Conclusion ……223

7.1. New phase formation – two types based on the curvature shape: concave or convex ……224

7.1.1. New phase formation with concave meniscus ……224

7.1.2. New phase formation with convex meniscus ……227

7.2. Effect of equilibrium contact angle on the stability of the system when a new phase is formed from a confined fluid ……229

7.2.1. Effect of equilibrium contact angle, for new phase formation with concave meniscus ……229

7.2.2. Effect of equilibrium contact angle for new phase formation with convex meniscus ……231

7.3. Effect of solid separation distance ……232

7.3.1. Effect of solid separation distance for new phase formation with concave meniscus ……234

7.3.2. Effect of solid separation distance, for new phase formation with convex meniscus 237

7.4. Effect of sphere size for the geometry of a sphere and a flat plate 238

7.5. Results implication 239

References 242

Index 246

List of Tables

Table 3-1 Capillary length of H_2O at 20^oC and n–dodecane at 24^oC.....38

Table 3-2 Constraints of the system for liquid phase formation from a bulk vapour phase. 43

Table 3-3 Constraints of the system for vapour phase formation from a bulk liquid phase. 43

Table 3-4 Conditions for equilibrium for the cases of (a) liquid formation out of a bulk vapour phase and (b) vapour formation out of a bulk liquid phase based on type of solid–liquid and solid–vapour interfaces. Liquid and vapour phases are made up of component (1) and the solid phase is purely component (2). 48

Table 3-5 Free energy of the system for the cases of (a) liquid formation out of a bulk vapour phase and (b) vapour formation out of a bulk liquid phase. Liquid and vapour phases are made up of component (1) and the solid phase is purely component (2). 55

Table 3-6 Forms of free energy with respect to the reference condition, for two cases of liquid formation out of a bulk vapour phase and vapour formation out of a bulk liquid phase. Liquid and vapour phases are made up of component (1) and the solid phase is purely component (2). 59

Table 3-7 H_2O and n–dodecane properties at specified temperature. 60

Table 3-8 Amount of the coefficient $\frac{\bar{R}T^V}{P_\infty v_\infty^L}$ and range of $\frac{P^V}{P_\infty}$ for positive or negative R_C for two components: H_2O and n–dodecane. 62

Table 3-9 Amount of the coefficient $\frac{\bar{R}T^V}{P_\infty v_\infty^L}$ and range of $\frac{P^L}{P_\infty}$ for positive or negative R_C for two components: H_2O and n–dodecane. 64

Table 4-1 Liquid volume and the surface areas for liquid phase formation from the bulk vapour phase in a conical pit.....75

Table 4-2 Vapour volume and the surface areas for vapour phase formation from the bulk liquid phase in a conical pit. 91

Table 4-3 Summary of liquid phase formation out of a bulk vapour phase and vapour phase formation out of a bulk liquid phase inside a conical pit with a half apex angle of β, and effect of the involved parameters. In this table θ denotes the equilibrium contact angle being measured from inside the denser phase (liquid), θ_t is the *transition contact angle*, R_1 (= R_2) is the principal radius of curvature of the liquid-vapour interface, P^L denotes the liquid pressure, and P^V is the vapour pressure. 101

Table 5-1 The liquid volume, the solid–liquid and the liquid–vapour surface areas for a liquid bridge between two flat plates. 109

Table 5-2 The vapour volume, the solid–liquid and the solid–vapour surface areas for a vapour bridge between two flat plates. 128

Table 5-3 Summary of liquid phase formation out of a bulk vapour phase and vapour phase formation out of a bulk liquid phase between two flat plates, and the effect of the equilibrium contact angle, θ, and the plate separation distance, H, on the stability of the system. $\boldsymbol{\theta_t}$ is the transition contact angle, R_1 & R_2 are the principal radii of the liquid-vapour interface, P^L is the liquid phase pressure, and P^V is the vapour phase pressure. 146

Table 6-1 Liquid volume, solid–liquid and liquid–vapour surface area for liquid bridge formation between a flat plate and a sphere. 158

Table 6-2 Relative differences in the free energy level of the maximum and minimum points as a result of a certain number of degrees (2°) change in the contact angle for the case of liquid formation with concave meniscus out of a bulk vapour phase. 166

Table 6-3 Vapour volume, solid–vapour and liquid–vapour surface areas for vapour bridge formation between a flat plate and a sphere. 188

Table 6-4 Concave vapour formation between a flat plate and a sphere, relative differences in the free energy levels of the maximum and minimum points as a result of a certain number of degrees (2°) change in the contact angle, for water at 20°C, P^L=1.1P_∞, H=0.5R_C (300μm), R_p=10^3×R_C.....195

Table 6-5 Summary of liquid phase formation out of a bulk vapour phase and vapour phase formation out of a bulk liquid phase between a flat plate and a sphere, and the effects of the equilibrium contact angle, θ, the separation distance, H, and the sphere size, R_P, on the stability of the system. $\boldsymbol{\theta_t}$ is the transition contact angle, R_1 & R_2 are the principal radii of the liquid-vapour interface, P^L is the liquid phase pressure, and P^V is the vapour phase pressure. 213

Table 7-1 Curves of free energy vs. new phase size for new phase formation with concave meniscus.....225

Table 7-2 Curves of free energy vs. new phase size for new phase formation with convex meniscus.....228

Table 7-3 Effect of contact angle on curves of free energy vs. new phase size for new phase formation with concave meniscus. The solid line shows the free energy as contact angle gets farther from the transition contact angle. 230

Table 7-4 Effect of contact angle on curves of free energy vs. new phase size for new phase formation with convex meniscus. The solid line shows the free energy as contact angle gets farther from the transition contact angle.....232

Table 7-5 Comparison of free energy vs. size of the new phase at the start point (new phase size =0) for zero separation distance (H=0), and nonzero separation distance (H≠0). 234

Table 7-6 Effect of solid separation on curves of free energy vs. new phase size for new phase formation with concave meniscus. The dashed curve is the initial condition. The solid line shows the free energy as the walls' separation increases (cone apex (β) or surface

distance (H) increases from that of the dashed line). The dot-dashed curve represents unfavourability of new phase formation with concave meniscus inside a gap between two flat plates or a sphere–plate, as H increases over a certain distance (approximately by $|\mathbf{R_C cos\theta}|$). 235

Table 7-7 Effect of solid separation on curves of free energy vs. new phase size for new phase formation with convex meniscus. The dashed curve is the initial condition. The solid line shows the free energy as the walls' separation increases (cone apex angle (β) or surface distance (H) increases from that of the dashed line). The dot-dashed curve represents unfavourability of new phase formation with convex meniscus between two flat plates as H decreases over a certain distance (approximately by $|\mathbf{R_C cos\theta}|$). 237

Table 7-8 Complete picture of thermodynamic stability analysis for confined fluid inside confinements of different geometries 240

List of Figures

Figure 1-1 Schematic of a liquid bridge with a concave meniscus inside three different confinement geometries: (a) inside a conical pit, (b) between two flat plates, and (c) between a sphere and a flat plate. 2

Figure 2-1 Illustration of principal radii of curvature for an arbitrary interface 22

Figure 2-2 A typical system having interaction with its surroundings 29

Figure 2-3 Schematic of a possible free energy of the system vs. volume of a new phase: Equilibrium states are extrema of the plot where maximum points are unstable equilibria, local minimum points are meta–stable and an absolute minimum is the stable condition. (Adopted with permission from the Candidacy presentation of Fatemeh Eslami, December 2010) 33

Figure 3-1 Liquid formation with concave meniscus in different solid geometries, each to be discussed in a separate chapter: (a) Inside a conical pit, (b) Between two parallel solid plates, and (c) Between a spherical solid particle and a flat plate. 36

Figure 3-2 (a) Contact angle measurement convention demonstrated in the two cases of liquid formation out of a vapour phase and vapour formation out of a liquid phase inside a conical pit. The transition meniscus is shown as a dotted line. (b) Getting 10° closer to the transition contact angle, equivalent to an increase in the contact angle for the case of liquid formation and a decrease in the contact angle for the case of vapour formation. 66

Figure 4-1 Schematic of liquid formation inside a conical pit and definition of cone apex angle 2β, contact angle $\boldsymbol{\theta}$, principal radii of curvature R_1=R_2, radius of the three–phase contact circle W, the height of interface h, the distance between the highest and the lowest

parts of the liquid–vapour interface h′, and half–filling angle of the new phase Ø, for cases of a) concave ($\boldsymbol{\theta} < 90° - \beta$) and b) convex ($\boldsymbol{\theta} > 90° - \beta$) meniscus.....70

Figure 4-2 Free energy vs. scaled size of the liquid phase formed out of a bulk vapour phase for H_2O at 20°C, P^V=0.9P_∞, contact angle of θ=0° (concave meniscus), and solid half angle of β=10°. 77

Figure 4-3 Effect of equilibrium contact angle, θ, on the free energy of the liquid phase formed out of a bulk vapour phase for H_2O at 20°C and P^V=0.9P_∞, and solid half angle of β=10°, for various contact angles that result in a concave meniscus: (a) Free energy vs. scaled radius of curvature, (b) Free energy vs. volume of the liquid phase. 79

Figure 4-4 Comparing the effect of a certain number of degrees (5°) change in the equilibrium contact angle on the free energy of the system when a liquid phase is formed out of a bulk vapour phase for H_2O at 20°C and P^V=0.9P_∞ and solid half angle of β=10º for various contact angles that result in a concave meniscus. (a) Far from the transition contact angle, (b) Close to the transition contact angle.....80

Figure 4-5 Effect of cone apex angle on the free energy of the system when a liquid phase is formed out of a bulk vapour phase for H_2O at 20°C and P^V=0.9P_∞ and θ=0° (concave meniscus). (a) Free energy vs. scaled radius of curvature, (b) free energy vs. volume. 83

Figure 4-6 Free energy vs. scaled size of liquid phase formed out of a bulk vapour phase for H_2O at 20°C and P^V=1.1P_∞, contact angle of θ=180° (convex meniscus), and solid half angle of β=10°. 85

Figure 4-7 Effect of equilibrium contact angle on the free energy vs. volume of the liquid phase formed out of a bulk vapour phase for H_2O at 20°C and P^V=1.1P_∞, and solid half angle of β=10°, for various contact angles that result in a convex meniscus. (a) Free energy vs. scaled radius of curvature, (b) Free energy vs. volume of the liquid phase. 86

Figure 4-8 Comparing the effect of a certain number of degrees (5°) change in the equilibrium contact angle on the free energy of the system when a liquid phase is formed out of a bulk vapour phase for H_2O at 20°C and P^V=1.1P_∞ and solid half angle of β=10° for various contact angles that result in a convex meniscus. (a)Far from the transition contact angle, (b) Close to the transition contact angle.....87

Figure 4-9 Effect of cone apex angle on the free energy of the system when a liquid phase is formed out of a bulk vapour phase for H_2O at 20°C and P^V=1.1P_∞ and θ=180° (convex meniscus). (a) Free energy vs. scaled radius of curvature, (b) Free energy vs. volume. 89

Figure 4-10 Schematic of liquid formation inside a conical pit and the definition of cone apex angle 2β, contact angle $\boldsymbol{\theta}$, principal radii of curvature R_1=R_2, radius of the three−phase contact circle W, height of interface h, distance between the highest and the lowest parts of the liquid−vapour interface h′, and half−filling angle of the new phase ∅, for cases of a) concave ($\boldsymbol{\theta} > 90° + \beta$) and b) convex ($\boldsymbol{\theta} < 90° + \beta$) meniscus.....91

Figure 4-11 Free energy vs. scaled size of vapour phase formed out of a bulk liquid phase for H_2O at 20°C and P^L=1.1P_∞, contact angle of θ=180° (concave meniscus), and solid half angle of β=10°. 94

Figure 4-12 Effect of equilibrium contact angle on the free energy vs. volume of the vapour phase formed out of a bulk liquid phase for H_2O at 20°C and P^L=1.1P_∞ and solid half angle of β=10°, for various contact angles that results in a concave meniscus.....95

Figure 4-13 Effect of cone apex angle on the free energy vs. volume of the vapour phase formed out of a bulk liquid phase for H_2O at 20°C and P^L=1.1P_∞ and θ=180° (concave meniscus). 96

Figure 4-14 Free energy vs. scaled size of the vapour phase formed out of a bulk liquid phase for H_2O at 20°C and P^L=0.9P, contact angle of θ=0° (convex meniscus), and solid half angle of β=10°. 97

Figure 4-15 Effect of equilibrium contact angle on the free energy vs. volume of the vapour phase formed out of a bulk liquid phase for H_2O at 20°C and P^L=0.9P_∞ and solid half angle of β=10°, for various contact angles that result in a convex meniscus. 98

Figure 4-16 Effect of cone apex angle on the free energy vs. volume of the vapour phase formed out of a bulk liquid phase for H_2O at 20°C and P^L=0.9P_∞ and θ=0° (convex meniscus). 99

Figure 5-1 Schematic of a liquid bridge – a) concave ($\boldsymbol{\theta} < \mathbf{90}°$) and b) convex ($\boldsymbol{\theta} > \mathbf{90}°$) – between two flat plates, where θ is the equilibrium contact angle, r is the radius of the circle approximating the vertical section of the liquid–vapour interface, d is the liquid bridge half width, H is the distance between the two plates, y_1 is the three phase contact with the lower plate and y_2 is the three phase contact with the upper plate. 108

Figure 5-2 (a) Free energy vs. scaled liquid bridge half width ($\frac{\mathbf{d}}{\mathbf{R_C}}$) between two flat plates, for n–dodecane at 24°C, P^V=0.9P_∞, $\boldsymbol{\theta}$= 0°, and H=0.97R_C, (b) Magnification of the region close to d = 0. 112

Figure 5-3 (a) Effect of the equilibrium contact angle on the curve of free energy vs. liquid bridge half width between two flat plates, for n–dodecane at 24°C, P^V=0.9P_∞, for various contact angles less than 90° (concave meniscus), and H=0.97R_C, (b) Magnification of the unstable equilibrium point. 114

Figure 5-4 Comparison of the effect of a specific number of degrees change (2°) in the equilibrium contact angle on the free energy of liquid formation with a concave meniscus ($\boldsymbol{\theta}$< 90°) between two flat plates, for n–dodecane at 24°C, P^V=0.9P_∞, and

H=0.97R_C (a) far from the transition contact angle, (b) Closer to the transition contact angle.....115

Figure 5-5 Specific changes (2º) in the contact angle affect the free energy of liquid formation with a concave meniscus ($\theta < 90^o$) between two flat plates, for n−dodecane at 24°C, P^V=0.9P_∞, and H=0.97R_C. The relative difference in the free energy gets less important far from the transition contact angle in the case of having an energy barrier (a,b), becomes maximum when the energy curve changes to monotonically increasing, and gets less important as one gets closer to the *transition contact angle* in the case of monotonically increasing curves (d,e,f). 117

Figure 5-6 (a) Effect of the flat plate separation distance on the curve of free energy vs. liquid bridge half width between two flat plates, for n−dodecane at 24°C, P^V=0.9P_∞, θ=0°,(b) Magnification of the unstable equilibrium point. 118

Figure 5-7 (a) Free energy vs. scaled liquid bridge half width ($\frac{\mathbf{d}}{\mathbf{R_C}}$) between two flat plates, for n−dodecane at 24°C, P^V=1.1P_∞, $\boldsymbol{\theta}$ = 160°, and H=0.97$|R_C|$, (b) Magnification of the region close to d = 0. 121

Figure 5-8 (a) Effect of the equilibrium contact angle on the curve of free energy vs. liquid bridge half width between two flat plates, for n−dodecane at 24°C, P^V=1.1P_∞, for various contact angles higher than 90° (convex meniscus), and H=0.97$|R_C|$, (b) Magnification of the unstable equilibrium point. 123

Figure 5-9 (a) Effect of the flat plate separation distance on the curve of free energy vs. liquid bridge half width between two flat plates, for n−dodecane at 24°C, P^V=1.1P_∞, θ=160°, (b) Magnification of the unstable equilibrium point.....125

Figure 5-10 Schematic of a vapour bridge – a) concave ($\boldsymbol{\theta} > 90°$) and b) convex ($\boldsymbol{\theta} < \mathbf{90}°$) – between two flat plates, where θ is the equilibrium contact angle, r is the radius of the circle approximating the vertical section of the liquid−vapour interface, d is the vapour bridge half width, H is the distance between the two plates, y_1 is the three

phase contact with lower plate and y_2 is the three phase contact with the upper plate. 127

Figure 5-11 (a) Free energy vs. scaled vapour bridge half width ($\frac{d}{R_C}$) between two flat plates, for water at 20°C, P^L=1.1P_∞, θ=180°, and H=0.97R_C, (b) Magnification of the region close to d=0 131

Figure 5-12 (a) Effect of the equilibrium contact angle on the curve of free energy vs. vapour bridge half width between two flat plates, for water at 20°C, P^L=1.1P_∞, for various contact angles higher than 90° (concave meniscus), and H=0.97R_C, (b) Magnification of the unstable equilibrium point. 133

Figure 5-13 Comparison of the effect of a specific number of degrees (2°) change in the equilibrium contact angle on the free energy of vapour formation with a concave meniscus (θ > 90°) between two flat plates, for water at 20°C, P^V=1.1P_∞, and H=0.97R_C (a) far from the transition contact angle, (b) Closer to the transition contact angle.....134

Figure 5-14 (a) Effect of the flat plate separation distance on the free energy vs. vapour bridge half width between two flat plates, for water at 20°C, θ =180°, and P^L=1.1P_∞, (b) Magnification of the unstable equilibrium point. 136

Figure 5-15 (a) Free energy vs. scaled vapour bridge half width ($\frac{d}{R_C}$) between two flat plates, for water at 20°C, P^L=0.9P_∞, θ=20°, and H=0.97$|R_C|$, (b) Magnification of the region close to d=0. 139

Figure 5-16 (a) Effect of the equilibrium contact angle on the free energy vs. vapour bridge half width between two flat plates, for water at 20°C, P^L=0.9P_∞, for various contact angles less than 90° (convex meniscus), and H=0.97$|R_C|$, (b) Magnification of the unstable equilibrium point. 141

Figure 5-17 (a) Effect of the flat plate separation distance on the free energy vs. vapour bridge half width between two flat plates, for water at 20°C, θ =20°, and P^L=0.9P_∞, (b) Magnification of the unstable equilibrium point. 143

Figure 6-1 Schematic of a liquid bridge –a) concave and b) convex– between a flat plate and a sphere, where θ_1 and θ_2 are the equilibrium contact angles for the lower and upper surfaces, r is the radius of the circle approximating the vertical section of the liquid–vapour interface, d is the liquid bridge half width, H is the distance between the sphere and the flat plate, α is the half filling angle of the liquid in the bridge, y_1 is the three phase contact with the lower particle, y_2 is the three phase contact with the upper particle, and R_P is the radius of the spherical particle.....156

Figure 6-2 (a) Free energy vs. scaled liquid bridge half width ($\frac{d}{R_C}$) between a flat plate and a sphere, for n–dodecane at 24°C, P^V=0.9P_∞, θ=0°, H=0.97R_C, R_p=2.5 cm, (b) Magnification of the region close to d=0.....161

Figure 6-3 (a) Effect of the equilibrium contact angle on the free energy vs. scaled liquid bridge half width between a flat plate and a sphere, for n–dodecane at 24°C, P^V=0.9P_∞, H=0.97R_C, R_p=2.5 cm, for various contact angles that result in concave meniscus (b) Magnification of the unstable equilibrium point. 163

Figure 6-4 Comparison of the effect of a specific number of degrees change (2°) in the equilibrium contact angle on the free energy of liquid formation with a concave meniscus between a flat plate and a sphere, for n–dodecane at 24°C, P^V=0.9P_∞, H=0.97R_C, R_p=2.5 cm, (a1) far from the transition contact angle, (b1) closer to the transition contact angle. (a2) and (b2) are magnifications of (a1) and (b1) respectively.....165

Figure 6-5 (a) Effect of the solid surface separation distance on the free energy vs. scaled liquid bridge half width between a flat plate and a sphere, for n–dodecane at 24°C, P^V=0.9P_∞, θ=0°, R_p=2.5 cm, (b) Magnification of the unstable equilibrium point. ...167

Figure 6-6 Energy level of the maximum and minimum points at sphere–plate separation distance close to the breakage distance for a liquid bridge between a flat plate and a sphere, for n–dodecane at 24°C, P^V=0.9P_∞, θ=0°, R_p=2.5 cm. 170

Figure 6-7 (a) Free energy vs. scaled liquid bridge half width between a flat plate and a sphere, for n–dodecane at 24°C, P^V=0.9P_∞, θ=0°, H=0, R_p=2.5 cm. (b) Magnification of the calculation at small bridge width. 173

Figure 6-8 (a) Effect of the solid sphere size on the free energy vs. scaled liquid bridge half width between a flat plate and a sphere, for n–dodecane at 24°C, P^V=0.9P_∞, θ=0°, H=0.97R_C and P^V=0.9P_∞, (b) Magnification of the unstable equilibrium point. 175

Figure 6-9 (a) Free energy vs. scaled liquid bridge half width ($\frac{d}{R_C}$) between a flat plate and a sphere, for n–dodecane at 24°C, P^V=1.1P_∞, θ=160°, H=0.97R_C, R_p=2.5 cm, (b) Magnification of the region close to d=0. 178

Figure 6-10 Effect of the equilibrium contact angle on the free energy vs. scaled liquid bridge half width between a flat plate and a sphere, for n–dodecane at 24°C, P^V=1.1P_∞, H=0.97$|R_C|$, R_P=2.5cm and, for various contact angles that result in a convex meniscus.....179

Figure 6-11 (a) Effect of the solid surface separation distance on the free energy vs. scaled liquid bridge half width between a flat plate and a sphere, for n–dodecane at 24°C, P^V=1.1P_∞, θ=160°, and R_p=2.5 cm, (b) Magnification of the unstable equilibrium point.....181

Figure 6-12 Curve of free energy vs. scaled liquid bridge half width between a flat plate and a sphere for n–dodecane at 24°C, P^V=1.1P_∞, θ =180°, H=0, and R_p=2.5 cm. 182

Figure 6-13 (a) Effect of the solid sphere size on the free energy vs. liquid bridge half width between a flat plate and a sphere, for n–dodecane at 24°C, P^V=1.1P_∞, θ=160°, and H=0.97$|R_C|$, (b) Magnification of the unstable equilibrium point 184

Figure 6-14 Schematic of a vapour bridge – a) concave and b) convex – between a flat plate and a sphere, where θ_1 and θ_2 are the equilibrium contact angles, r is the radius of the circle approximating the vertical section of the liquid–vapour interface, d is the vapour bridge half width, H is the distance between the two plates, α is the half filling angle of the vapour in the bridge, y_1 is the three phase contact with the lower soild surface, y_2 is the three phase contact with the upper solid surface, and R_P is the radius of the spherical particle 186

Figure 6-15 (a) Free energy vs. vapour bridge half width between a flat plate and a sphere, for water at 20°C, P^L=1.1P_∞, H=0.5R_C (300μm), θ=180°, R_p=10^3×R_C (62 cm), (b) Magnification of the region close to d=0. 191

Figure 6-16 (a) Effect of the equilibrium contact angle on the free energy vs. scaled vapour bridge half width between a flat plate and a sphere, for water at 20°C, P^L=1.1P_∞, H=0.5R_C (300μm), R_p=10^3×R_C (62 cm), for various contact angles that result in concave meniscus, (b) Magnification of the unstable equilibrium point. 193

Figure 6-17 Comparison of the effect of a specific number of degrees change (2°) in the equilibrium contact angle on the free energy of vapour formation with a concave meniscus between a flat plate and a sphere, for water at 20°C, P^L=1.1P_∞, H=0.5R_C (300μm), R_p=10^3×R_C (62 cm), (a1) far from the transition contact angle, (b1) closer to the transition contact angle. (a2) and (b2) are magnifications of (a1) and (b1) respectively.....194

Figure 6-18 Effect of the solid surface separation distance on the free energy vs. scaled liquid bridge half width between a flat plate and a sphere, for water at 20°C, P^L=1.1P_∞, θ=180°, R_p=10^3×R_C (62 cm), (b) Magnification of the unstable equilibrium point.....196

Figure 6-19 Energy levels of the maximum and minimum points at separation distances close to the breakage distance for a vapour bridge between a flat plate and a sphere, for water at 20°C, P^L=1.1P_∞, θ=180°, R_p=10^3×R_C (62 cm).....199

Figure 6-20 Free energy vs. vapour bridge half width between a sphere and a flat plate, for water at 20°C, P^L=1.1P_∞, θ=180°, H=0, R_p=10^3×R_C (62 cm), (b) Magnification of the curve at small value of bridge width. 200

Figure 6-21 Effect of the solid sphere size on the free energy vs. vapour bridge half width between a flat plate and a sphere, for water at 20°C, P^L=1.1P_∞, θ=180°, H=0.5×R_C (300μm), (b) Magnification of the unstable equilibrium point. 202

Figure 6-22 (a) Free energy vs. scaled vapour bridge half width between a flat plate and a sphere, for water at 20°C, P^L=0.9P_∞, θ=0°, H=0.5$|R_C|$(300μm), R_p=10^3×$|R_C|$(62 cm), (b) Magnification of the region close to d=0. 205

Figure 6-23 Effect of the equilibrium contact angle on the free energy vs. scaled vapour bridge half width between a flat plate and a sphere, for water at 20°C, P^L=0.9P_∞, H=0.5$|R_C|$(300μm), R_p=10^3×$|R_C|$ (62 cm). 206

Figure 6-24 Effect of the solid surface separation distance on the free energy vs. scaled vapour bridge half width between a flat plate and a sphere, for water at 20°C, P^L=0.9P_∞, θ=0°,R_p=10^3×$|R_C|$ (6.2 km), concave meniscus, (b) Magnification of the unstable equilibrium point. 208

Figure 6-25 Curve of free energy vs. scaled liquid bridge half width between a flat plate and a sphere for water at 20°C, P^L=0.9P_∞, θ=0°, H=0, and R_p=10^3×$|R_C|$(6.2 km). 209

Figure 6-26 Effect of the solid sphere size on the free energy vs. vapour bridge half width between a flat plate and a sphere, for water at 20°C, P^L=0.9P_∞, θ=0°, and H=0.5$|R_C|$(300μm), (b) Magnification of the unstable equilibrium point. 211

Nomenclature

A	Surface area
α	Half filling angle of the bridge for sphere–plate geometry
β	Half of the cone apex angle
Bo	Bond number
Δ	Difference
d	Bridge half width for a bridge between two flat plates, or between a sphere and a flat plate
F	Helmholtz free energy
∅	Half−filling angle of the new phase inside a cone
g	Standard gravity
G	Gibbs free energy
γ	Surface tension
h	Height of the interface (from apex of the cone) for liquid−vapour interface inside a cone
h'	Distance between the highest and the lowest parts of the liquid−vapour interface inside a cone
H	Distance of the closest approach between solids for two flat plates, or sphere–plate geometry
H_{Break}	Breakage distance
k	Number of components in a phase or interface
ℓ	Characteristic length of the new phase
ℓ_c	Capillary length
μ	Chemical potential

N	Number of molecules
P	Pressure
P_∞	Saturation pressure
r	Radius of the circle approximating the vertical section of a liquid–vapour interface between two flat plates, or between a sphere and a flat plate
$\overline{R}$	Universal gas constant, 8.314 $\frac{J}{mol.K}$
R_1 , R_2	Principal radii of curvature
R_{1e} , R_{2e}	Equilibrium principal radii of curvature
R_C	Kelvin radius
R_m	Mean radius of curvature
ρ	Density
S	Entropy (Extensive property)
S^C	Entropy of the composite system
T	Temperature
U	Internal energy (Extensive property)
θ	Contact angle
θ_e	Equilibrium contact angle
θ_t	***Transition contact angle***
V	Volume (Extensive property)
υ_∞^L	Specific volume of liquid at saturation pressure
W	Radius of the three phase contact circle for the liquid–vapour interface inside a cone
y_1	y position of three phase contact with the lower solid for a bridge between two flat plates, or between a sphere and a flat plate

y_2	y position of three phase contact with the upper solid for a bridge between two flat plates, or between a sphere and a flat plate

Superscripts

a	Typical bulk phase
b	Typical bulk phase
ab	Typical interface between phases a and b
L	Liquid phase
LV	Liquid−Vapour interface
R	Reservoir
S	Solid phase
SL	Solid−Liquid interface
SV	Solid−Vapour interface
V	Vapour phase

Subscripts

0	Reference condition
1	Component (1)
2	Component (2)
e	Equilibrium state
i	Typical component in a phase or interface
∞	Refers to saturation condition

1. Introduction

For a pure fluid inside a container with walls that are distant from one another (unconfined fluid), liquid−vapour equilibrium only happens at the saturation pressure. At saturation pressure, both the liquid and the vapour phases are stable in the bulk and are separated by a flat interface. At any pressure other than the saturation pressure only one phase is stable in the bulk phase; i.e. the vapour phase for pressures below the saturation pressure and the liquid phase for pressures above the saturation pressure.

In contrast, phase behaviour of a fluid may be affected as a result of confinement. At small−scale confinements of specific geometry, vapour and liquid phases may coexist at stable equilibrium even at pressures other than the saturation pressure. Also in very tight confinements, the predicted phase transition (from liquid to vapour or vice versa) might not happen.

In this thesis for each geometry of interest, fluid inside a confinement can be placed in one of four categories based on the initial phase type (liquid / vapour) and the pressure of the confined fluid (above/below the saturation pressure). Therefore a confined fluid is among one of these situations: ❶ confined vapour phase at pressures below the saturation pressure, ❷ confined vapour phase at pressures above the saturation pressure, ❸ confined liquid phase at pressures below the

saturation pressure, or ❹ confined liquid phase at pressures above the saturation pressure. Various phenomena are known to be produced by a confining geometry, in each of the preceding situations.

Situation ❶: At pressures below the saturation pressure, vapour is the stable phase in bulk (without confinement). If this vapour phase is confined by wettable walls, some liquid phase can condense out of and coexist with this vapour phase at pressures below the saturation pressure (although the liquid phase is not stable in bulk, i.e. without confinement, at this pressure). Formation of liquid out of a bulk vapour phase inside a confinement of wettable walls at pressures below the saturation pressure is well known as *capillary condensation* [1]. A sketch of capillary condensation is shown in Figure 1-1 for three different confining geometries of interest. It is worth pointing out that wettable walls are made up of a solid material that results in the concave meniscus inside any confinement.

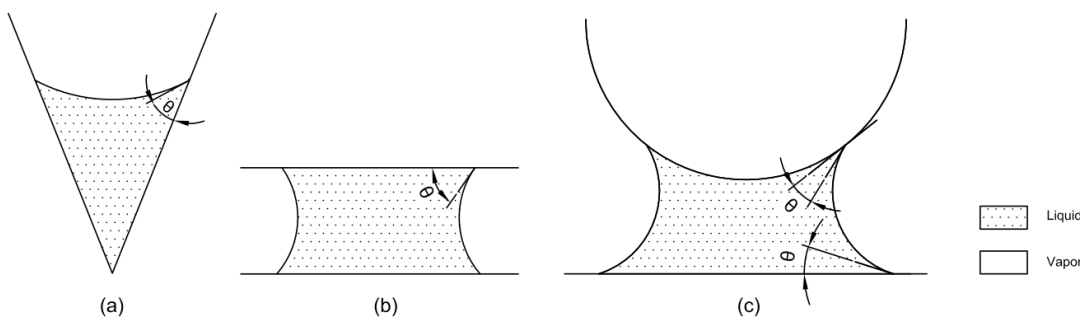

Figure 1-1 Schematic of a liquid bridge with a concave meniscus inside three different confinement geometries: (a) inside a conical pit, (b) between two flat plates, and (c) between a sphere and a flat plate.

Situation ❷: Tightly confined vapour inside a confinement with non–wettable walls (solid material for which the contact angle is in the range of 90º to 180º)

might not change into liquid even though the vapour pressure is above the saturation pressure, and the stable phase in bulk is liquid.

Situation ❸: A liquid phase at pressures below the saturation pressure and confined with wettable walls, may or may not transform into vapour depending on how tight the confinement is. This is interesting because at pressures below the saturation pressure the stable phase in bulk is vapour, and not liquid.

Situation ❹: Liquid is the stable phase in bulk when the pressure is above the saturation pressure. If this liquid is confined by non-wettable walls, some vapour evaporation (with concave meniscus) and hence coexistence of liquid and vapour may happen, even though the pressure is above the saturation pressure. This phenomenon is called *capillary evaporation* [1, 2].

These phenomena inside a confinement happen as a result of two factors: i) high surface−to−volume ratio of the new born phase, ii) different interfacial tension of solid material with liquid and vapour, which results in curved liquid−vapour interface and hence in pressure difference across the interface [3].

1.1. Confined fluids in applications

Confined fluid phenomena are of great practical importance in oil and gas, chemical and pharmaceutical industries, many geophysical phenomena, and increasingly fabrication and function of miniaturized system, among many others.

There are several cases where these phenomena are beneficially employed. Liquid phase sintering and foam stabilizing with particles are industrial examples of applying capillary condensation [4]. Capillary condensation has been employed for separation purposes such as methanol– hydrogen separation in inorganic membranes [5]. Also pore size distribution of porous materials such as mesoporous molecular sieve (MMS) is primarily assessed based on adsorption isotherms of capillary condensation [6].

On the other hand, there are many cases where confined fluids have unfavourable results which are to be prevented. Adhesion problems happen, as a result of capillary condensation, in miniaturized (<1mm) system components of micro- and nano- electro-mechanical systems (MEMS and NEMS), telecommunications, automotive industry, surgery, etc, both during fabrication and operation of the system components [7]. In brittle solids, capillary condensation has a consequence of crack propagation [8]. Both in storage and processing of powdered materials, capillary condensation of water from relatively humid air cause some problems [9].

Understanding the basics of confined fluid behaviour results in better design, either to employ or prevent these phenomena. The next section reviews some of the previous studies.

1.2. Models to describe confined fluids

Both applying and preventing these phenomena require a close study of the phenomena and various parameters that are involved. Lord Kelvin (Thomson) was

the first who explained capillary condensation for the case of vapour–liquid coexistence [2, 7]. Since then several studies have been performed.

Many experimental studies have been performed, mostly for capillary condensation, to achieve a better understanding of confined fluid phenomena. For example, atomic force microscopy (AFM) has been widely used, in which various tip shapes and materials (with different wettability), and different separation distances from the tip can be studied. AFM results showed that the capillary force is sensitive to ambient humidity (relative vapour pressure, i.e. the ratio of vapour pressure to the saturation pressure), and tip / particle wettability [10]. In several other works, the formation or disappearance of liquid bridges as a result of a decrease or an increase in separation distance of solid surfaces in the surface force apparatus (SFA) has been studied experimentally [11, 12].

Many theoretical models of confined fluid behaviour have been developed to reduce the cost of trial and error (experiments) in design. Various existing models can be categorized, as presented by Chau in his thesis [7], in three groups based on the application scale: 1) Macroscopic models that consider phases to be uniform. These models are valid down to a scale of several nanometres (approximately 5nm). 2) Molecular scale models which consider each particle of the fluid individually. Molecular dynamics, Monte Carlo simulations, and Lattice models are different methods under this category. Even with today's fastest computers, these models are only applicable to very small geometry problems (for particle number of less than 10^6, or equivalently over a scale of less than approximately 30

nm). 3) Mixed models as a compromise between microscopic and macroscopic approaches, including Density Functional Theory. Although these methods demand less computing time, they are still only applicable to small scales (less than 100 nm)[7].

Up until now, macroscopic models have been employed more commonly due to the wide range of size (from above approximately 5nm to several millimetres) they can predict [7] at a "much reduced computational cost" [10].

Most of such macroscopic modeling efforts investigate the phenomena from a mechanical point of view. The focus is to develop some relation to calculate the adhesion force between particles of different geometries as a result of the capillary bridge (capillary neck) for capillary condensation, or capillary evaporation phenomena. However most of these models are dedicated to capillary condensation for various fundamental geometries, such as the gap between plate–plate [9], sphere–plate [9, 10, 13, 14], cone–plate [9, 10, 13, 14] (also truncated cone–plate[10]) , cylinder–plate [13, 14], sphere–sphere [9, 14, 15]and cone–cone [9, 14] among many others.

Even in studies from the mechanical point of view with the focus on force calculation, some subtle equilibrium thermodynamic assumptions are made. In some of these studies, the exact shape of the meniscus of the new phase is calculated (through the Kelvin equation, equation (2.20)) assuming perfect thermodynamic equilibrium between the confined phase and the new phase that forms out of the confined phase [10]. The results from equilibrium assumptions are in good agreement with surface–force apparatus results, for example in atomic force

microscope (AFM) where the contact is typically between 0.1 to 1 second [13]. Many others use the toroidal approximation for the shape of the bridge, as it was in good agreement with the exact shape calculations [9].

Another approach of modeling the confined fluid behaviour is thermodynamic stability analysis. In this approach, first an appropriate free energy of the system is determined, then stability of the new phase formation out of a confined fluid is investigated through the trend of the free energy vs. size of the new phase. It can be determined whether the phase transition is possible, and if so whether the whole initial phase turns into the new phase, or the initial and new phase can coexist at equilibrium [16-18] . This approach has also been used to describe other surface phenomena, such as the ease of heterogeneous nucleation on fluid surfaces, compared to rigid surfaces [19].

Fewer articles can be found using this approach; however the results of such studies predict several observations and reveal the reason behind many phenomena:

Through such thermodynamic stability analysis, vapour formation and growth from a liquid −gas solution in a system of constant mass and volume within bone cells (modeled by a conical pit) is shown to be one potential reason of cell death after decompression [20].

In some other studies, surface roughness in contact with a liquid–gas solution (with gas concentration in the liquid being slightly greater than the equilibrium value) at constant pressure and temperature and with system boundaries closed to mass

transfer was analysed with surface thermodynamic. There surface roughness was represented by conical pits. It was found from thermodynamic stability analysis that bubble nuclei (with convex meniscus, or equivalently confined in a wettable wall) can form in a stable condition [16].

For the sphere–plate geometry, the liquid capillary bridge with concave meniscus and only for a zero contact angle has been studied using thermodynamic stability analysis by Elliott and Voitcu[18]. The results of such study were able to predict the diffuse liquid–vapour interface that has been previously observed at some certain separation distance (breakage distance), above which liquid bridge formation is thermodynamically impossible. For small separation distance (below the breakage distance), they found that the free energy as a function of the size of the bridge has two extrema, where the smaller one is a maximum point, corresponding to a nucleation barrier and the larger one is a minimum point, corresponding to the stable bridge. That study also noted the plate–plate case, as the extreme of the sphere–plate in which the sphere radius is infinity [18] .

Also the equilibrium shape of the bridging bubble between two colloidal spheres of identical size was found by minimization of the constrained Gibbs free energy (obtained from statistical methods in some of Attard's other article [21]) and a polynomial expansion describing the shape [22]. Attard showed a microscopic bridging bubble to be stable for hydrophobic spheres at small separation distances [22] . He proposed the force as a result of the bridging bubble to be responsible for the long–range attraction between hydrophobic surfaces in water. From this

thermodynamic analysis, the hysteresis in formation / disappearance of the bridging bubble on the approach and separation of the spheres is also explained [22].

Capillary bridging with concave meniscus (for the case where a phase inside the capillary completely wets the surfaces) was also studied from the thermodynamic point of view with a different free energy than the Elliott and Voitcu article [18], for either a liquid bridge or a vapour bridge inside the gap in the sphere–plate geometry. Andrienko et al. considered the free energy of the system as the sum of the bulk and the surface terms [2]. Without further explanation, they then describe each of these terms: The surface term is a result of the difference in surface tensions of the interfaces between solid–new phase and solid–initial phase, assuming the sharp interface limit (interface with no volume). The bulk term is due to the difference in chemical potentials of the phase–separated components inside the bridge (new phase) and in the initial bulk phase. In the first part of their article, they considered a cylinder approximation for the bridge volume and surface area. They got the same number of extrema (two extrema) in the excess free energy as Elliott and Voitcu [18], and stated that the larger bridge corresponds to the minimum (stable) point. They had also found that bridging (where the bridge had concave meniscus) is impossible for distances greater than a certain amount ($\frac{2\gamma^{LV}}{\Delta\mu}$ where γ^{LV} is the liquid–vapour interfacial tension and $\Delta\mu$ is the difference in the chemical potential of the phase–separated components inside the bridge and the bulk). They also calculated the interaction force from the derivative of free energy with respect to the separation distance of the sphere and the plate [2].

1.3. Scope of this thesis

This thesis is aimed to theoretically study new fluid phase formation out of a confined fluid with the thermodynamic stability analysis [16, 18] approach. The problem is investigated under conditions of constant temperature and constant pressure of the initial confined fluid, and zero gravity (or for negligible gravitational effects). The system is closed to mass transfer. The solid of the confinement is considered to be made up of a non-volatile, non-dissolving component and is also insoluble to the fluid. Solid surfaces are considered to be ideal [23], i.e. smooth, rigid, homogenous, with no appreciable vapour pressure. Assuming the fluid to be single component (pure), reduces the complexity of the problem, for the purpose of making a comparative study for various geometries with various affecting parameters.

While various confinement geometries have been investigated in literature (as discussed in section 1.2), only a few works have performed a comparative study of different geometries (examples of which can be found in references [9, 13]). Such comparative studies are especially rare for studies with the thermodynamic stability approach. In this thesis confined fluids in three different confinement geometries of conical pit (in chapter 4), the gap between two flat plates (in chapter 5), and the gap between a sphere and a flat plate (in chapter 6), are fully investigated.

Each of these geometries is of interest on its own, as it represents some real case. Conical pits are widely used to model surface roughness [16]. The plate–plate geometry is considered representative of a slit [8]. The sphere–plate geometry has

been used in several modeling works such as for nanoscale particles interacting with a surface in humid ambient conditions [10], in an atomic force microscope (AFM) and a surface force apparatus (SFA) [2, 24] .

To investigate new phase formation in each geometry, thermodynamic stability analysis is performed: Initially it is considered that a new phase with a meniscus shape of interest (concave or convex) is formed out of a confined phase. Then using surface thermodynamics, the free energy (thermodynamic potential) of such a system is developed and analysed for a series of virtual states (sizes) of the system, to figure out whether such new phase formation is favourable, and the system can evolve to some stable equilibrium condition [16].

Effects of several different important parameters have been examined for each geometry and in each chapter. These parameters include:

1) Effect of the equilibrium contact angle: The equilibrium contact angle may change due to different reasons, such as different solid material, surface manipulation, and adsorption at the solid−liquid interface [25]. The equilibrium contact angle affects the thermodynamic stability of the system.
2) Geometrical characteristics of the confinement: Solid surface separation distance (equivalent to the cone apex angle, and plate–plate or sphere–plate separation distance) is an important factor to be considered in stability analysis of the confined fluid.

   In the sphere–plate geometry, sphere size is also another factor that has to be considered.

Some pieces of this thesis reproduce the results of previous literature: Liquid bridge formation with concave meniscus and contact angle equal to zero has been investigated for sphere–plate and plate–plate geometries [18] as discussed in section 1.2. Also the effect of the separation distance for both of those geometries, and the effect of the sphere size for sphere–plate case were explained in that study.

The contribution of this thesis is the comparative thermodynamic stability analysis of confined fluid for different geometries. A broad picture of the confined fluid behaviour and effect of important parameters is presented in the conclusion section of each chapter and in the conclusion chapter (chapter 7). From this comparative study, the behaviour of different other geometries can be predicted, even before the full study of the case.

1.4. Outline of chapters

This thesis is organized in 7 chapters:

Chapter 2 provides a review of surface thermodynamics background for analysing thermodynamic stability of new phase formation out of a confined fluid. The step by step procedure of this chapter is applicable to a variety of multiphase systems with any number of bulk phases and interfaces.

Chapter 3 presents the common topics of liquid phase formation out of confined vapour, and vapour phase formation out of confined liquid, which are applicable to any confinement, regardless of its geometry. These topics include negligibility of gravitational effects, conditions for equilibrium (Table 3-4), the appropriate free

energy (Table 3-5) and free energy with respect to some reference (Table 3-6), properties of fluid materials of interest, sign of the Kelvin radius according to initial confined fluid pressure, and the newly introduced (to the author's best knowledge) concept of the ***transition contact angle***. Each of the presented equations and definitions are then applied through chapters 4 to 6 to find the equilibrium state of confined fluids in various confinement geometries.

In each of chapters 4 to 6, four different possibilities are investigated: liquid formation with a concave meniscus out of a confined vapour phase, liquid formation with a convex meniscus out of a confined vapour phase, vapour formation with a concave meniscus out of a confined liquid phase, and vapour formation with a convex meniscus out of a confined liquid phase.

Chapter 4 develops stability analysis of four possible liquid–vapour systems inside a conical pit. Effects of the equilibrium contact angle and the cone apex angle are investigated for each of the four cases.

Chapter 5 studies thermodynamic stability of four possible liquid–vapour systems inside a gap between two flat plates. Effects of the equilibrium contact angle and the flat plate separation distance on the stability of each of the cases are presented.

Chapter 6 is about thermodynamic stability of four possible liquid–vapour systems between a sphere and a flat plate. Effects of the equilibrium contact angle, the separation distance between the sphere and the plate, and the sphere size are then

investigated for each of the four cases. Some of the modeling outputs of this chapter are validated in comparison with some experimental results.

Chapter 7 summarizes the big picture of different geometries of chapters 4 to 6, and the effect of different parameters (equilibrium contact angle, solid surface separation distance, and the sphere size for the sphere–plate geometry).

In the whole thesis, Mathematica is used for computational purposes and graph production. Through initial efforts using MATLAB, round–off errors brought about some unexpected trends in the graphs. On the other hand run time of the MATLAB program increased dramatically when parameters were changed to SYMBOLIC and Variable precision arithmetic (VPA) was used. I have found Mathematica to be more efficient (over MATLAB) in the problems of interest of this thesis where scales are so small. Figures representing different geometries are drawn with AutoCAD. All section headings, equations, figure numbers, and table numbers are cross-referenced (and have hyperlink) throughout the text, so that Ctrl+click can be used on the electronic version to jump to the targets.

2. Review of Required Surface Thermodynamics

The basic surface thermodynamics required for description of any new phase formation is explained in this chapter. The explanations and equations are presented in such a way as to be applicable to a variety of multiphase systems with any number of bulk phases and interfaces as the constituent subsystems. However, the concerns of this thesis are solid – liquid – vapour systems, which will be discussed in chapter 3. This review follows the steps in Elliott's class notes [26] which in turn refer to Callen [27] and Charles Ward's class notes [28], and was basically introduced by Gibbs [29].

Any multiphase system is considered as a composite system, consisting of a number of constituent simple subsystems. A simple system means that it is large enough for validity of macroscopic thermodynamics, is macroscopically homogenous, isotropic and uncharged; and is not acted on by electric, magnetic, or gravitational fields [27].

A composite system is in equilibrium if each of its subsystems is internally in equilibrium (no macroscopic, spontaneous changes happen, and all of the intensive properties are spatially uniform in that simple subsystem) and there is no net exchange of energy, mass or volume between the subsystems.

Thermodynamic stability of the system in equilibrium is analyzed through different steps in the following sections: In sections 2.1 and 2.2 the conditions for the system to be at equilibrium are determined. The procedure for finding the appropriate free energy of the system through its evolution to equilibrium is discussed in section 2.3. Section 2.4 is about the number and stability of the equilibrium states and the size of the new born phase at each equilibrium state.

2.1. Conditions for equilibrium

For any composite system at equilibrium the variation of the extensive entropy of the system plus reservoir is equal to zero. The composite system of concern is made up of different simple subsystems, either bulk or interface. The entropy of the composite system, S^C, can therefore be described in terms of its subsystems.

Around each test system (all the phases and interfaces of concern), it is assumed that a reservoir exists (denoted by superscript *R*) which by definition has constant extensive properties, i.e. the reservoir is so large that its extensive parameters are not altered after contact with the test system. At any equilibrium condition we have:

$$dS^R + dS^C = dS^R + \sum_a dS^a + \sum_{ab} dS^{ab} = 0 \qquad (2.1)$$

where dS^a is the variation of entropy for any bulk phase and dS^{ab} for any interface.

For a bulk phase, the fundamental equation of thermodynamics in its differential form, as mentioned in [27], is given by:

$$dU^a = T^a dS^a - P^a dV^a + \sum_{i=1}^{k} \mu_i^a \, dN_i^a \tag{2.2}$$

In equation (2.2), U, S, V, and N_i are extensive properties of the system representing internal energy, entropy, volume and number of moles of component i. T, P, and μ are intensive thermodynamic properties indicating temperature, pressure and chemical potential. k denotes the total number of components in the phase and the superscript a represents any bulk phase.

Also the fundamental equation in its differential form for the reservoir is:

$$dU^R = T^R dS^R - P^R dV^R + \sum_{i=1}^{k} \mu_i^R \, dN_i^R \tag{2.3}$$

For any interface denoted with superscript ab, the differential form of the fundamental equation of thermodynamics is given by [18]:

$$dU^{ab} = T^{ab} dS^{ab} + \gamma^{ab} dA^{ab} + \sum_{i=j}^{k} \mu_i^{ab} \, dN_i^{ab} \tag{2.4}$$

where $\begin{cases} j = 2 & \text{when } ab \text{ is a flat interface} \\ j = 1 & \text{when } ab \text{ is a curved interface} \end{cases}$

γ represents interfacial tension and A denotes area of the interface.

In equation (2.4) the summation starts from $j=2$ for flat (planar) interfaces according to "Gibbs dividing surface approximation" [29]. However, for curved interfaces the summation in equation (2.4) starts from $j=1$ according to "Gibbs

surface of tension approximation", i.e. all components are to be considered in the summation [29].

As indicated by equation (2.2), three terms contribute to any differential change in internal energy of a bulk phase: quasi–static heat flux (TdS), quasi–static expansion work ($-PdV$) and quasi–static chemical work ($\sum_{i=1}^{k} \mu_i \, dN_i$). For interfaces as shown in equation (2.4), the expansion work is replaced by the work of changing the surface area ($+\gamma dA$).

Note that equations (2.2) and (2.4) are property equations that are valid whether or not the variation was caused by a quasi–static process. In other words, the internal energy is a state function, rather than a path function, and only depends on the initial and final points. Hence changes in the internal energy can always be obtained from equations (2.2) and (2.4).

Rearrangement of equation (2.2) results in equation (2.5) for dS of the bulk phase:

$$\mathrm{dS^a} = \frac{1}{\mathrm{T^a}}\mathrm{dU^a} + \frac{\mathrm{P^a}}{\mathrm{T^a}}\mathrm{dV^a} - \sum_{\mathrm{i=1}}^{\mathrm{k}} \frac{\mu_\mathrm{i}^\mathrm{a}}{\mathrm{T^a}}\mathrm{dN_i^a} \tag{2.5}$$

For interfaces, rearranging equation (2.4) gives equation (2.6) for dS:

$$\mathrm{dS^{ab}} = \frac{1}{\mathrm{T^{ab}}}\mathrm{dU^{ab}} - \frac{\gamma^\mathrm{ab}}{\mathrm{T^{ab}}}\mathrm{dA^{ab}} - \sum_{\mathrm{i=j}}^{\mathrm{k}} \frac{\mu_\mathrm{i}^\mathrm{ab}}{\mathrm{T^{ab}}}\mathrm{dN_i^{ab}} \tag{2.6}$$

$$\begin{cases} \mathrm{j} = 2 & \text{when } ab \text{ is a flat interface} \\ \mathrm{j} = 1 & \text{when } ab \text{ is a curved interface} \end{cases}$$

Replacing the different terms of equation (2.1) by equations of the form of (2.5) and (2.6) leads to:

$$\frac{1}{T^R}dU^R + \frac{P^R}{T^R}dV^R - \sum_{i=1}^{k}\frac{\mu_i^R}{T^R}dN_i^R$$

$$+\sum_a\left[\frac{1}{T^a}dU^a + \frac{P^a}{T^a}dV^a - \sum_{i=1}^{k}\frac{\mu_i^a}{T^a}dN_i^a\right] \tag{2.7}$$

$$+\sum_{ab}\left[\frac{1}{T^{ab}}dU^{ab} - \frac{\gamma^{ab}}{T^{ab}}dA^{ab} - \sum_{i=j}^{k}\frac{\mu_i^{ab}}{T^{ab}}dN_i^{ab}\right] = 0$$

Equation (2.7) gives the conditions for equilibrium when solved for any virtual displacement around equilibrium, subject to constraints of the system. The procedure to get the equilibrium condition is to substitute constraints on changes in extensive properties (*dU*, *dV*, *dN*, *dA*) into equation (2.7) and rearrange the resulting equation by collecting like terms so that one has an equation of the form of coefficients multiplying independent variations. Each coefficient may then be set to zero resulting in specific conditions for equilibrium. These equilibrium conditions are discussed individually in the proceeding sections.

2.1.1. Thermal equilibrium: Temperature of bulk phases and interfaces at equilibrium conditions

For a system that can exchange energy with the reservoir,

$$dU^R + \sum_a dU^a + \sum_{ab} dU^{ab} = 0 \tag{2.8}$$

Substituting equation (2.8) as one of the constraints in equation (2.7) results in one of the conditions for equilibrium being equality of temperature of all bulk phases and interfaces with the reservoir temperature.

In the case of an isolated system,

$$dU^{R} = 0 \tag{2.9}$$

Hence the energy balance is:

$$\sum_{a} dU^{a} + \sum_{ab} dU^{ab} = 0 \tag{2.10}$$

Substituting equation (2.9) as one of the constraints in equation (2.7), leads to one of the conditions for equilibrium being equality of temperature of all bulk phases with all interfaces only, and not with the reservoir.

2.1.2. Chemical equilibrium: Chemical potential of component *i* in bulk phases and interfaces at equilibrium conditions

When component *i* can transfer between phases, and in the absence of any chemical reaction, the mole balance for component *i* is:

$$dN_i^{b} + \sum_{a} dN_i^{a} + \sum_{ab} dN_i^{ab} = 0 \tag{2.11}$$

According to equation (2.11) a differential change in the amount of moles of *i* in one arbitrary phase (say phase *b*) is equal to negative changes of that component in other phases and interfaces. Substituting equation (2.11) as a constraint in equation (2.7) results in equality of chemical potential of component *i* in all of the involved

bulk phases and interfaces at thermodynamic equilibrium conditions. In an open system that can exchange mass with the reservoir, this equality also exists between phases and interfaces and the reservoir.

For a non−volatile component *i* existing in a bulk phase *b*, no transfer of that component to other bulk phases would happen, although the component can still adsorb at interfaces in contact with the bulk phase, therefore:

$$\mathrm{dN_i^b} + \sum_{\mathrm{ab}} \mathrm{dN_i^{ab}} = 0 \tag{2.12}$$

Substituting equation (2.12) in equation (2.7) results in equality of chemical potentials of component *i* in its initial bulk phase and associated interfaces only ($\mu_i^b = \mu_i^{ab}$).

Equation (2.12) reduces to $dN_i^b = 0$ when all the involved interfaces are flat, and component *i* is chosen as the arbitrary component that is absent at the interface in the "Gibbs dividing surface approximation". As a result, no equality of chemical potential for that component is obtained as a condition for equilibrium.

2.1.3. Mechanical equilibrium: Laplace−Young equation

Both changes in the interfacial area (dA^{ab}) and changes in the volumes of the comprising phases (dV^a and dV^b) are dependent on curvature of the involved interface. When all these curvature dependant terms are substituted in equation (2.7), they result in the famous Laplace−Young equation as one of the conditions for equilibrium [18]:

$$P^a - P^b = \gamma^{ab}\left(\frac{1}{R_1} + \frac{1}{R_2}\right) \tag{2.13}$$

where P^a is the pressure of one side of the curvature, and P^b is the pressure of the other side of the curvature. R_1 and R_2 are the principal radii of curvature used to describe a curved surface at any point. As described by Middleman[30] and Hunter [31], at any point of an arbitrary surface, there is a pair of orthogonal curves; each of which can be approximated with the arc of a circle if the curves are of differential size. The radii of these two circular arcs are R_1 and R_2.

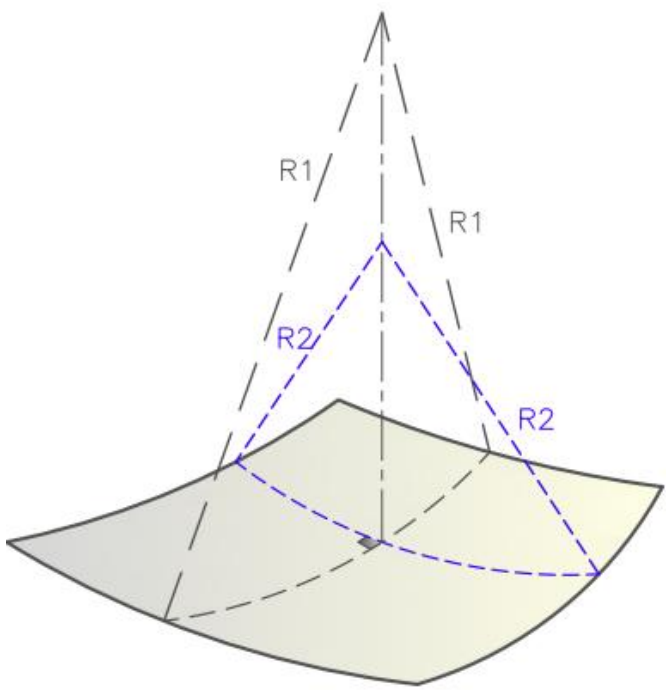

Figure 2-1 Illustration of principal radii of curvature for an arbitrary interface

This equation is also obtainable from a balance of the work done in forming the additional amount of surface, with the work corresponding to the pressure difference across the surface [32].

According to equation (2.13), in contrast to flat surfaces, at equilibrium conditions there is a pressure difference between the bulk phases on either side of a curved interface.

The mean radius of curvature, R_m, is then defined in terms of the principal radii of curvature as follows:

$$\frac{1}{R_m} = \frac{1}{2}\left(\frac{1}{R_1} + \frac{1}{R_2}\right) \tag{2.14}$$

and the Laplace−Young equation (2.13) can be described in term of this mean radius:

$$P^a - P^b = \frac{2\gamma^{ab}}{R_m} \tag{2.15}$$

The principal radii of curvature can be positive or negative, depending on which side of the interface the center of the circular arcs lies. Similarly to the presentation of Middleman[30], arbitrarily one side of the interface is chosen as the "inner" side assuming a positive sign, and the other side is chosen as the "outer" side with a negative sign. As a result, $\Delta P = +P_{inner} - P_{outer}$ and the radius of curvature has a positive sign when the center of the corresponding circular arc is located on the inner side and a negative sign when the center of the corresponding circular arc is located on the outer side. The principal radii of curvature then would have the same signs if both of the centers of their circular arcs are on the same side of the surface.

At equilibrium conditions in the absence of gravitational effects, as mentioned by Hunter[31], ΔP (which is equal to $P^a - P^b$) must be constant over all parts of the

interface; otherwise a fluid flow would occur. As a result, since γ^{ab} is also constant, the summation of the reciprocals of the principal radii of curvature $(\frac{1}{R_1} + \frac{1}{R_2})$ and hence R_m are to be constant according to equations (2.13) and (2.15). Therefore the interface would be a surface of constant mean curvature. It should be emphasized that this is only true in absence of any external fields such as gravity.

A spherical interface is an example of a surface with a constant mean curvature. For a spherical surface, both of the principal radii of curvature are the same $(R_1 = R_2 = R_m)$ with the same sign. Hence there will be a pressure difference of $\frac{2\gamma^{ab}}{R_1}$ $(= \frac{2\gamma^{ab}}{R_2})$ across the interface. Other examples of surfaces of constant curvature include a cylindrical interface, where one of the radii is infinity. Also it is worth mentioning that for a planar interface, $R_1 = R_2 = \infty$ and $P^a - P^b = 0$ in the Laplace−Young equation. This implies that the pressure is the same on both sides of any flat interface and for a given temperature, phase equilibrium occurs at a single pressure, known as the saturation pressure (P_∞) for the case of a liquid−vapor equilibrium.

2.1.4. Young equation

Depending on the system definition and constraints, some other equilibrium equation might be obtained after substitution of surface areas and bulk phase volume in terms of principal radii of curvature into equation (2.7) and solving the equation. For example, for a three phase solid–liquid–vapour system, the Young equation is obtained as one of the conditions for equilibrium [18]:

$$\gamma^{SV} - \gamma^{SL} = \gamma^{LV} \cos\theta \tag{2.16}$$

where θ is the equilibrium contact angle; the angle that the liquid−vapour interface makes with the solid surface, being measured from the liquid side, and in this work will be assumed to be determined when the solid material is specified. The superscripts *SV*, *SL* and *LV* indicate solid−vapour, solid−liquid, and liquid−vapour respectively.

2.2. Merging conditions for equilibrium: The Kelvin equation

Using some equations of state, the chemical potential of a specific component in each bulk phase can be described with respect to some reference condition. Equality of temperatures and chemical potentials of phases, as two of the conditions for equilibrium, might be combined to give a new relation between properties of the equation of state for each bulk phase, including pressure of each phase. If then this new relation is combined with the Laplace−Young equation, it leads to a formula for mean radius of curvature, based on pressure of one of the phases and the properties of the reference condition.

When the phases of concern are liquid and vapour, the equation is called the Kelvin equation (when the phases are solid and liquid it is called the Gibbs−Thomson equation [33]) and the mean radius of curvature is the Kelvin radius, R_C. The Kelvin radius is the mean radius of curvature at equilibrium conditions as determined from the Kelvin equation.

The Kelvin equation for a curved liquid−vapour interface, where both of the phases are single component (pure) is developed as follows:

Assuming the vapour phase to be an ideal gas yields as its chemical potential [18]:

$$\mu^{V}(T^{V},P^{V}) = \mu^{V}(T^{V},P_{\infty}) + \bar{R}T^{V}\ln(\frac{P^{V}}{P_{\infty}}) \tag{2.17}$$

where $\bar{R}$ is the universal gas constant which is equal to 8.314 $\frac{J}{mol.K}$ and P_{∞} is saturation pressure of the fluid in bulk.

Assuming the liquid phase to be incompressible, yields the following chemical potential for the liquid phase [18]:

$$\mu^{L}(T^{L},P^{L}) = \mu^{L}(T^{L},P_{\infty}) + \upsilon_{\infty}^{L}(P^{L} - P_{\infty}) \tag{2.18}$$

where υ_{∞}^{L} is specific volume of the pure liquid at the saturation pressure. From equality of temperature and chemical potential at equilibrium conditions, equating equations (2.17) and (2.18) results in equation (2.19):

$$\upsilon_{\infty}^{L}(P^{L} - P_{\infty}) = \bar{R}T^{V}\ln(\frac{P^{V}}{P_{\infty}}) \tag{2.19}$$

The Laplace−Young equation (2.15) is another equilibrium condition, describing the difference between P^{V} and P^{L} as a function of mean radius of curvature. Either of P^{V} or P^{L} can be described in terms of the other from equation (2.19) and combined with the Laplace−Young equation (2.15) to give a new equation for calculating the mean radius of curvature.

In the case of liquid formation, where the majority of the system is vapour (vapour is the initial, i.e. mother phase), P^L is described in terms of P^V using equation (2.19). Substituting P^L into equation (2.15) then yields the form of the Kelvin equation given below [34]:

$$R_C = \frac{2\gamma^{LV}}{(P^V - P_\infty) - \frac{\bar{R}T^V}{\upsilon_\infty^L}\ln\left(\frac{P^V}{P_\infty}\right)} \tag{2.20}$$

R_C in equation (2.20) is merely R_m at equilibrium conditions, i.e.:

$$R_C = \frac{1}{\frac{1}{2}\left(\frac{1}{R_{1,e}} + \frac{1}{R_{2,e}}\right)} \tag{2.21}$$

The signs of the principal radii of curvature are determined consistently according to the discussion in section 2.1.3. Considering the pressure difference as $P^V - P^L$, the radius has a positive sign if the center of the circular arc lies in the vapour phase and a negative sign if the center lies in the liquid phase.

Rearrangement of equation (2.20) in terms of $\frac{P^V}{P_\infty}$ (relative vapour phase pressure) yields:

$$R_C = \frac{2\gamma^{LV}}{P_\infty\left[\frac{P^V}{P_\infty} - 1\right] - \frac{\bar{R}T^V}{\upsilon_\infty^L}\ln\left(\frac{P^V}{P_\infty}\right)} \tag{2.22}$$

In the case of vapour formation out of a bulk liquid phase, P^V is described in terms of P^L using equation (2.19). After substitution of P^V in terms of P^L into equation

(2.15), the Kelvin equation is as follows (similar to the Kelvin equation for the case of bubble nucleation in a liquid–gas system [16, 17]) :

$$R_C = \frac{2\gamma^{LV}}{P^L - P_\infty \exp\left(\frac{\upsilon_\infty^L}{\overline{R}T^V}(P^L - P_\infty)\right)} \tag{2.23}$$

Equivalently equation (2.23) may be restated in terms of $\frac{P^L}{P_\infty}$ as:

$$R_C = \frac{2\gamma^{LV}}{P_\infty\left[\frac{P^L}{P_\infty} - \exp\left(\frac{\upsilon_\infty^L P_\infty}{\overline{R}T^V}\left(\frac{P^L}{P_\infty} - 1\right)\right)\right]} \tag{2.24}$$

The Kelvin equation is derived from macroscopic thermodynamic equations. However it has been shown by Powles [35] to be valid for microscopic drops above the size of validity of homogenous thermodynamics. For a clean system with no accumulation of contaminates, the Kelvin equation is obeyed by menisci with mean radius as low as eight times the molecular diameters of the material of interest [24] (for example down to 4 nm for cyclohexane as reported by Fisher and Israelachvili [24]). Also bulk thermodynamics and therefore the Kelvin radius are reported to be valid for mean radius of curvature greater than 5 nm for water (equivalent to relative vapour phase pressure of 0.9 when considering liquid drop formation) and at least 1 nm for cyclohexane (equivalent to relative vapour phase pressure of 0.1 when considering liquid drop formation) [36].

2.3. Thermodynamic potential (Free energy)

The next step in thermodynamic analysis of multiphase systems would be to determine the appropriate thermodynamic potential (free energy) of the system. A typical system may exchange energy, volume or mass with the reservoir (its surroundings), which means

$$\Delta U^R = -\Delta U$$
$$\Delta N_i^R = -\Delta N_i \qquad (2.25)$$
$$\Delta V^R = -\Delta V$$

where ΔU, ΔN_i , and ΔV denote changes in internal energy, number of molecules of component *i*, and volume of the system.

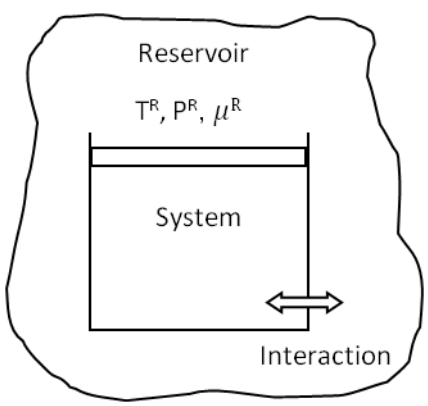

Figure 2-2 A typical system having interaction with its surroundings

The Euler relation for the reservoir is [16]:

$$U^R = T^R S^R - P^R V^R + \sum_{i=1}^{k} \mu_i^R N_i^R \qquad (2.26)$$

Both the system and the reservoir evolve to a new equilibrium state as a result of the interaction between the system and the reservoir. Acknowledging that by definition the reservoir intensive properties are constant, in evolution to a new equilibrium state the Euler relation leads to:

$$\Delta U^R = T^R \Delta S^R - P^R \Delta V^R + \sum_{i=1}^{k} \mu_i^R \Delta N_i^R \tag{2.27}$$

where Δ denotes the difference of two equilibrium states before and after the removal of the constraints. Substituting the relationships in (2.25) into equation (2.27) results in equation (2.28):

$$0 = \Delta U + T^R \Delta S^R + P^R \Delta V - \sum_{i=1}^{k} \mu_i^R \Delta N_i \tag{2.28}$$

Since the system plus reservoir are isolated, any spontaneous changes must cause their combined entropy to increase. Hence as the system plus reservoir evolves to equilibrium,

$$\Delta S + \Delta S^R \geq 0 \tag{2.29}$$

Substitution of equation (2.29) in equation (2.28) results in equation (2.30) [18]:

$$0 \geq \Delta U - T^R \Delta S + P^R \Delta V - \sum_{i=1}^{k} \mu_i^R \Delta N_i \tag{2.30}$$

where Δ indicates a difference between final and initial conditions, and ΔU, ΔS, ΔV, and ΔN_i show the changes in the system properties (other than the reservoir).

From the conditions for equilibrium that have been determined in section 2.1, the reservoir properties of T^R , P^R , μ_i^R are to be replaced by subsystem properties according to equilibrium conditions. According to the nature of the interactions between the system and the reservoir, some of the Δ's in equation (2.30) might be eliminated. For example to derive the free energy for a simple system which exchanges only energy and volume with the reservoir, and has a fixed number of moles, i.e. the system does not exchange mass with the reservoir ($\Delta N_i = 0$), equation (2.30) becomes:

$$[\mathrm{U} - \mathrm{TS} + \mathrm{PV}]_{\mathrm{final}} - [\mathrm{U} - \mathrm{TS} + \mathrm{PV}]_{\mathrm{initial}} \leq 0 \tag{2.31}$$

In equation (2.31), the part that appears inside the brackets is the thermodynamic potential function (free energy) for a closed simple system with walls that allow energy transfer and pressure balance through changes in volume. As a result, both the pressure and temperature are constant and imposed on the system by the surroundings. This is the free energy for many systems in chemical engineering where surface effects are negligible and is well known as the ***Gibbs free energy*** [27]:

$$\mathrm{G} = \mathrm{U} - \mathrm{TS} + \mathrm{PV} \tag{2.32}$$

Another well known free energy is the ***Helmholtz free energy***, which is the free energy of a closed system having constant volume ($\Delta V = 0$) with walls that allow energy transport (hence constant temperature), but not mass transport ($\Delta N_i = 0$) [27].

$$\mathrm{F} = \mathrm{U} - \mathrm{TS} \tag{2.33}$$

Any spontaneous change in the system is possible only if it results in a negative difference in the thermodynamic potential (free energy) according to equation (2.31). Equilibrium states (unstable, metastable, or stable) occur at the conditions under which equation (2.31) becomes zero. The stable equilibrium state occurs when increase is the only possible change in the free energy around the equilibrium state. The system is at its lowest free energy level (most stable) at the stable equilibrium state.

The potential energy of a system consisting of multiple phases and interfaces can be a combination of either of the famous free energies (Gibbs or Helmholtz) for each phase or interface, plus some extra terms. An example of this will be described in detail in chapter 3 for the solid−liquid−vapour systems of interest.

2.4. Equilibrium states and stability analysis

It is desirable to know the equilibrium size of a new phase that is formed. At equilibrium conditions the extensive properties of the system take on values that extremize the entropy of that system. As a result, the equilibrium states of the system can be obtained from the extremum of the curve of the free−energy vs. new−phase volume. Free energy, in the same way as any other energy, is only definable with respect to some reference condition. For thermodynamic stability analysis of new phase formation, it is convenient if the reference is considered to be an equilibrium condition at which none of the new phase and its resulting interfaces exist.

A schematic diagram of a possible free energy vs. new phase volume is presented in Figure 2-3 :

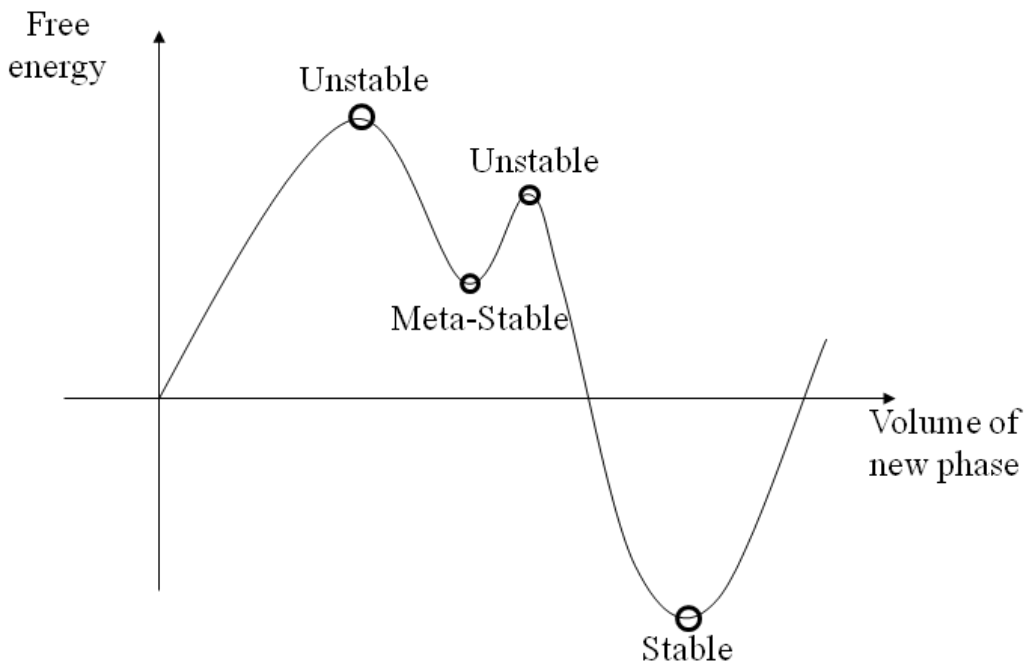

Figure 2-3 Schematic of a possible free energy of the system vs. volume of a new phase: Equilibrium states are extrema of the plot where maximum points are unstable equilibria, local minimum points are meta−stable and an absolute minimum is the stable condition. (Adopted with permission from the Candidacy presentation of Fatemeh Eslami, December 2010)

A maximum in the curve corresponds to an unstable equilibrium condition, while minimum points are respectively meta−stable or stable for a local or absolute minimum of the curve. For different systems, the curve might contain all or none of these types of equilibrium states. An ever−increasing curve indicates that new phase formation is unfavourable at the conditions of the system. In the case of a continously descending curve, the new phase will grow forever until all of the materials are changed to the new phase form.

Free−energy can also be plotted versus either of the radii of curvature (R_1 and R_2), and it will result in a similar format of curve with the same number of equilibrium states and identical free energy at the equilibrium states. It is worth mentioning that at any of the equilibrium states the constant mean radius of curvature is equal to the Kelvin radius, satisfying equation (2.21).

2.5. Summary

Well known surface thermodynamics background has been reviewed in this chapter. Thermodynamic stability analysis of new phase formation has been described. The first step is to find the equilibrium conditions of the system and the resultant equations, which was fully discussed in sections 2.1 and 2.2. In section 2.3, the second step, finding the appropriate free energy of the system, was explained. Finally section 2.4 clarified how to determine the number and stability of the equilibrium states (stable, unstable, or metastable) and the size of the new born phase at each equilibrium state.

The method being described in this chapter is applicable to a variety of multiphase systems with an arbitrary number of bulk phases and interfaces as the constituent subsystems.

3. Governing Equations and Common Definitions for a Liquid−Vapour System inside a Confined Solid Geometry

3.1. Introduction

Two cases of new phase formation are investigated in this thesis: liquid phase formation from a bulk vapour phase in a pore of a solid material, and vapour phase formation from a bulk liquid phase in a pore of a solid material. In either case three bulk phases of solid, liquid and vapour are involved.

Through the whole thesis, the liquid and the vapour phases are assumed to be pure, consisting of component (1). The solid is also pure and made up of a different component (2), which is non−volatile, non−dissolving, and is insoluble to component (1). The solid is ideal, which as defined by Ward and Neumann[23] , i.e. it is smooth, rigid, homogeneous, and has no appreciable vapour pressure. The reservoir is made up of any arbitrary component represented by *res*.

Different solid geometries, which are representative of various solid shapes in reality, are shown in Figure 3-1. In panel (a) of this figure, liquid is formed out of a vapour phase inside a solid conical pit. Panels (b) and (c) illustrate liquid capillary bridge formation between two solid particles, for various shapes of the particles. The moving piston at the top of each figure schematically represents the fact that the pressure of the bulk phase is constant and imposed by reservoir.

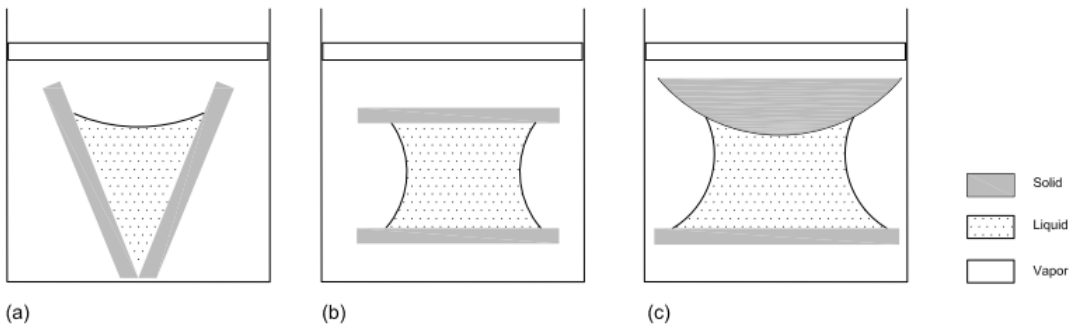

Figure 3-1 Liquid formation with concave meniscus in different solid geometries, each to be discussed in a separate chapter: (a) inside a conical pit, (b) between two parallel solid plates, and (c) between a spherical solid particle and a flat plate.

Although the volume of the new phase and the surface areas are functions of solid geometry, some basic equations are common between all geometries. The focus of this chapter is to develop general equations applicable for all cases mentioned above, regardless of the solid geometry. These equations are later used in the chapters specifically discussing the geometries.

Various details and governing equations common in all geometry types are discussed in the following sections. In section 3.2 the condition under which gravitational effects can be neglected are discussed. Section 3.3 explains conditions for equilibrium, based on the constraints of the system. In section 3.4 the energy that acts as the thermodynamic potential of the system through its evolution to

equilibrium is determined. Section 3.5 introduces the reference state, in comparison to which the thermodynamic potential (free energy) of the system can be calculated. The properties of the materials of interest in this research are presented in section 3.6. Section 3.7 clarifies how the sign of the mean radius of curvature of the liquid−vapour interface at the equilibrium condition (the Kelvin radius) changes as the bulk phase pressure changes from below the saturation pressure to above the saturation pressure. At the end, in section 3.8, a definition of the transition contact angle is introduced for the first time in the research related to curved menisci (to the best of the writer's literature review knowledge).

3.2. Negligibility of gravitational effects

In either case of liquid phase formation from a bulk vapour phase or vapour phase formation from a bulk liquid phase, when the new phase has a relatively small size, the gravitational force is negligible compared to the surface forces. The Bond number, *Bo*, (also called the Eötvös number, *Eo*) is an indicative dimensionless number of the relative importance of gravitational forces to surface forces.

$$\mathrm{Bo} = \frac{\Delta\rho g \ell^2}{\gamma} \tag{3.1}$$

where $\Delta\rho$ is the difference in the density of the two bulk phases on either side of the interface, g is standard gravity (9.8 ms^{-2}), ℓ is the characteristic length of the system and γ is the surface tension between the new phase and the mother phase. The density of the vapour phase is negligible in comparison to the density of the

liquid phase; therefore it is a good approximation to replace $\Delta\rho$ by the liquid density. [37]

The capillary length is then defined as a length at which the Bond number is one, hence gravity and surface forces are comparable.

$$\ell_c = \sqrt{\frac{\gamma}{\Delta\rho g}} \tag{3.2}$$

The gravitational effects can be neglected for a new phase of size well below the capillary length. [38]

Table 3-1 shows the capillary length in millimetres for two different materials at certain temperatures.

Table 3-1 Capillary length of H_2O at 20°C and n−dodecane at 24°C

Material	T (°C)	ρ ($\frac{kg}{m^3}$)	γ (mNm^{-1})	ℓ_c (mm)
H_2O	20	998.04	72.75	2.72
n−dodecane	24	746.45	25.03	1.85

All the properties can be obtained from a physical chemistry handbook. The properties in Table 3-1 were obtained from Perry and Green[39].

3.3. Finding the Conditions for Equilibrium of the System

For either of liquid phase formation from a bulk vapour phase or vapour phase formation from a bulk liquid phase, the equations that were developed in chapter 2 can be used if gravitational effects are negligible or under the assumption of no

gravitational fields. According to equation (2.1) the conditions for equilibrium for a liquid−vapour system confined to a solid geometry and surrounded by a reservoir are to be obtained from:

$$dS^{R} + dS^{S} + dS^{L} + dS^{V} + dS^{SL} + dS^{SV} + dS^{LV} = 0 \tag{3.3}$$

where superscripts *R*, *S*, *L*, *V*, *SL*, *SV*, and *LV* denote reservoir, solid, liquid, vapour, solid−liquid, solid−vapour, and liquid−vapour respectively.

In equation (3.3), *dS* for any bulk phase can be substituted by equation (2.5) and for any interface by equation (2.6). Terms that are to be considered in the summation in equation (2.6) depend on whether the interface is curved or flat. In both cases of liquid formation or vapour formation on the solid surface, the liquid−vapour interface is in general curved. Solid−liquid and solid−vapour interfaces may be either curved or flat depending on the geometry of the solid.

For the curved solid−liquid and solid−vapour interfaces, all the components are present at the solid−liquid and solid−vapour interfaces according to the "Gibbs surface of tension" approximation. After substituting equation (2.5) for each bulk phase and appropriate forms of equation (2.6) for curved solid−liquid, solid−vapour, and liquid−vapour interfaces, equation (3.3) becomes:

$$\left[\frac{1}{T^R}dU^R+\frac{P^R}{T^R}dV^R-\sum\frac{\mu_{res}^R}{T^R}dN_{res}^R\right]+\left[\frac{1}{T^S}dU^S+\frac{P^S}{T^S}dV^S-\frac{\mu_2^S}{T^S}dN_2^S\right]$$

$$+\left[\frac{1}{T^L}dU^L+\frac{P^L}{T^L}dV^L-\frac{\mu_1^L}{T^L}dN_1^L\right]+\left[\frac{1}{T^V}dU^V+\frac{P^V}{T^V}dV^V-\frac{\mu_1^V}{T^V}dN_1^V\right]$$

$$+\left[\frac{1}{T^{SL}}dU^{SL}-\frac{\gamma^{SL}}{T^{SL}}dA^{SL}-\frac{\mu_1^{SL}}{T^{SL}}dN_1^{SL}-\frac{\mu_2^{SL}}{T^{SL}}dN_2^{SL}\right] \tag{3.4}$$

$$+\left[\frac{1}{T^{SV}}dU^{SV}-\frac{\gamma^{SV}}{T^{SV}}dA^{SV}-\frac{\mu_1^{SV}}{T^{SV}}dN_1^{SV}-\frac{\mu_2^{SV}}{T^{SV}}dN_2^{SV}\right]$$

$$+\left[\frac{1}{T^{LV}}dU^{LV}-\frac{\gamma^{LV}}{T^{LV}}dA^{LV}-\frac{\mu_1^{LV}}{T^{LV}}dN_1^{LV}\right]=0$$

Alternatively, for the flat solid−liquid and solid−vapour interfaces, it is assumed that component (2) is chosen as the component that does not exist at flat solid−liquid and solid−vapour interfaces according to the "Gibbs dividing surface" approximation. After substituting equation (2.5) for each bulk phase, and appropriate forms of equation (2.6) for flat solid−liquid and solid−vapour interfaces, and for the curved liquid−vapour interface, equation (3.3) becomes:

$$\left[\frac{1}{T^R}dU^R+\frac{P^R}{T^R}dV^R-\sum\frac{\mu_{res}^R}{T^R}dN_{res}^R\right]+\left[\frac{1}{T^S}dU^S+\frac{P^S}{T^S}dV^S-\frac{\mu_2^S}{T^S}dN_2^S\right]$$

$$+\left[\frac{1}{T^L}dU^L+\frac{P^L}{T^L}dV^L-\frac{\mu_1^L}{T^L}dN_1^L\right]+\left[\frac{1}{T^V}dU^V+\frac{P^V}{T^V}dV^V-\frac{\mu_1^V}{T^V}dN_1^V\right]$$

$$+\left[\frac{1}{T^{SL}}dU^{SL}-\frac{\gamma^{SL}}{T^{SL}}dA^{SL}-\frac{\mu_1^{SL}}{T^{SL}}dN_1^{SL}\right] \tag{3.5}$$

$$+\left[\frac{1}{T^{SV}}dU^{SV}-\frac{\gamma^{SV}}{T^{SV}}dA^{SV}-\frac{\mu_1^{SV}}{T^{SV}}dN_1^{SV}\right]$$

$$+\left[\frac{1}{T^{LV}}dU^{LV}-\frac{\gamma^{LV}}{T^{LV}}dA^{LV}-\frac{\mu_1^{LV}}{T^{LV}}dN_1^{LV}\right]=0$$

3.3.1. Constraints of the system

The constraints of the system are:

- The system exchanges energy with the reservoir, and the combination of the system plus reservoir is isolated, hence:

$$dU^{R} + dU^{S} + dU^{L} + dU^{V} + dU^{SL} + dU^{SV} + dU^{LV} = 0 \tag{3.6}$$

From equation (3.6), one of the *dU*'s can be described in terms of the others.

- The system can exchange volume with the reservoir, due to the free movement of the piston shown in Figure 3-1.

$$dV^{R} + dV^{S} + dV^{L} + dV^{V} = 0 \tag{3.7}$$

The solid surface is considered to be rigid (no deformation). The solid surface is also assumed to be incompressible, i.e. no volume changes happen in the solid:

$$dV^{S} = 0 \tag{3.8}$$

From equation (3.7), one of the *dV*'s can be described in terms of the others.

- The system is closed and there is no mass exchange between the system and the reservoir.

$$dN^{R}_{res} = 0 \tag{3.9}$$

Component (1) can transfer between bulk phases and interfaces of the system, except to the solid phase which is composed purely of component (2).

$$dN_1^L + dN_1^V + dN_1^{SL} + dN_1^{SV} + dN_1^{LV} = 0 \tag{3.10}$$

Due to non−volatility, component (2) can only transfer from the solid phase to the solid−liquid and solid−vapour interface.

In the case of curved solid interfaces, according to the "Gibbs surface of tension" approximation, all components including component (2) are present at interface. Hence:

$$dN_2^S + dN_2^{SL} + dN_2^{SV} = 0 \tag{3.11}$$

or equivalently

$$dN_2^S = -dN_2^{SL} - dN_2^{SV} \tag{3.12}$$

When the solid−liquid and the solid−vapour interfaces are flat, component (2) is assumed not to be present at the interface according to the "Gibbs dividing surface" approximation, and non−volatility of this component results in:

$$dN_2^S = 0 \tag{3.13}$$

More convenient rearrangements of the above constraints for liquid phase formation from a bulk vapour phase are shown in Table 3-2.

Table 3-2 Constraints of the system for liquid phase formation from a bulk vapour phase.

Constraints of the system	Rearrangement of constraints for liquid phase formation from a bulk vapour phase
Equation (3.6)	$dU^V = -dU^R - dU^S - dU^L - dU^{SL} - dU^{SV} - dU^{LV}$
Equations (3.7) & (3.8)	$dV^V = -dV^R - dV^L$
Equation (3.10)	$dN_1^V = -dN_1^L - dN_1^{SL} - dN_1^{SV} - dN_1^{LV}$
Curved solid interface (3.12) Flat solid interface (3.13)	$dN_2^S = -dN_2^{SL} - dN_2^{SV}$ $dN_2^S = 0$

For vapour phase formation from a bulk liquid phase, the convenient rearrangements are as shown in Table 3-3.

Table 3-3 Constraints of the system for vapour phase formation from a bulk liquid phase.

Constraints of the system	Rearrangement of constraints for vapour phase formation from a bulk liquid phase
Equation (3.6)	$dU^L = -dU^R - dU^S - dU^V - dU^{SL} - dU^{SV} - dU^{LV}$
Equations (3.7) & (3.8)	$dV^L = -dV^R - dV^V$
Equation (3.10)	$dN_1^L = -dN_1^V - dN_1^{SL} - dN_1^{SV} - dN_1^{LV}$
Curved solid interface (3.12) Flat solid interface (3.13)	$dN_2^S = -dN_2^{SL} - dN_2^{SV}$ $dN_2^S = 0$

3.3.2. Conditions for equilibrium

In order to find the conditions for equilibrium, the constraints on the reservoir (equation (3.9)) and on the system (equation (3.8), and either Table 3-2 or Table 3-3) are to be substituted into equation (3.4) or (3.5), depending on whether the solid interfaces are curved or flat.

3.3.2.1. Conditions for equilibrium in the case of liquid formation out of a vapour phase

In the case of liquid formation from a bulk vapour phase, when the solid−liquid and solid−vapour interfaces are curved, the constraints from equations (3.8) and (3.9) and Table 3-2 are inserted into equation (3.4) and the result after rearrangement would be:

$$\begin{aligned}
&\left[\left(\frac{1}{T^R}-\frac{1}{T^V}\right)dU^R+\left(\frac{P^R}{T^R}-\frac{P^V}{T^V}\right)dV^R\right]\\
&+\left[\left(\frac{1}{T^S}-\frac{1}{T^V}\right)dU^S\right]\\
&+\left[\left(\frac{1}{T^L}-\frac{1}{T^V}\right)dU^L+\left(\frac{P^L}{T^L}-\frac{P^V}{T^V}\right)dV^L-\left(\frac{\mu_1^L}{T^L}-\frac{\mu_1^V}{T^V}\right)dN_1^L\right]\\
&+\left[\left(\frac{1}{T^{SL}}-\frac{1}{T^V}\right)dU^{SL}-\frac{\gamma^{SL}}{T^{SL}}dA^{SL}-\left(\frac{\mu_1^{SL}}{T^{SL}}-\frac{\mu_1^V}{T^V}\right)dN_1^{SL}-\left(\frac{\mu_2^{SL}}{T^{SL}}-\frac{\mu_2^S}{T^S}\right)dN_2^{SL}\right]\\
&+\left[\left(\frac{1}{T^{SV}}-\frac{1}{T^V}\right)dU^{SV}-\frac{\gamma^{SV}}{T^{SV}}dA^{SV}-\left(\frac{\mu_1^{SV}}{T^{SV}}-\frac{\mu_1^V}{T^V}\right)dN_1^{SV}-\left(\frac{\mu_2^{SV}}{T^{SV}}-\frac{\mu_2^S}{T^S}\right)dN_2^{SV}\right]\\
&+\left[\left(\frac{1}{T^{LV}}-\frac{1}{T^V}\right)dU^{LV}-\frac{\gamma^{LV}}{T^{LV}}dA^{LV}-\left(\frac{\mu_1^{LV}}{T^{LV}}-\frac{\mu_1^V}{T^V}\right)dN_1^{LV}\right]=0
\end{aligned} \tag{3.14}$$

For equation (3.14) to be true for any virtual displacement around the equilibrium, the coefficients multiplying each of the independent variations (dU^R, dV^R, dU^S, dU^L, dN_1^L, dU^{SL}, dN_1^{SL}, dN_2^{SL}, dU^{SV}, dN_1^{SV}, dN_2^{SV}, dU^{LV}, and dN_1^{LV}) are to be zero. Therefore equations (3.15) to (3.18) are obtained as equilibrium conditions for liquid formation out of a vapour phase:

$$T^R = T^S = T^L = T^V = T^{SL} = T^{SV} = T^{LV} \tag{3.15}$$

$$P^R = P^V \tag{3.16}$$

$$\mu_1^L = \mu_1^V = \mu_1^{SL} = \mu_1^{SV} = \mu_1^{LV} \tag{3.17}$$

$$\mu_2^S = \mu_2^{SL} = \mu_2^{SV} \tag{3.18}$$

The remaining terms in equation (3.14) yield the following condition for equilibrium:

$$\left(\frac{P^L}{T^L} - \frac{P^V}{T^V}\right) dV^L - \frac{\gamma^{SL}}{T^{SL}} dA^{SL} - \frac{\gamma^{SV}}{T^{SV}} dA^{SV} - \frac{\gamma^{LV}}{T^{LV}} dA^{LV} = 0 \tag{3.19}$$

Due to equality of temperatures according to equation (3.15), equation (3.19) can be simplified into:

$$\left(P^L - P^V\right) dV^L - \gamma^{SL} dA^{SL} - \gamma^{SV} dA^{SV} - \gamma^{LV} dA^{LV} = 0 \tag{3.20}$$

Equation (3.20) results in the Laplace−Young equation (2.14) and the Young equation (2.16) when dV^L, dA^{SL}, dA^{SV}, and dA^{LV} (which are interdependant) are described in terms of the principal radii of curvature of the liquid−vapour interface and the contact angle. The details of how Equation (3.20) leads to the Laplace−Young equation (2.14) and the Young equation (2.16) will be shown for the case of liquid formation with a concave meniscus inside a conical pit in chapter 4.

In the case of liquid formation from a bulk vapour phase with flat solid−liquid and solid−vapour interfaces, a similar procedure is used. Constraints from equations (3.8) and (3.9) and the equations from Table 3-2 are inserted into equation (3.5). As a result, for flat solid interfaces, equation (3.18) will be omitted as a condition for

equilibrium, while the other equilibrium conditions are the same as those of the curved case (Equations (3.15), (3.16), (3.17) and (3.20)).

3.3.2.2. Conditions for equilibrium in the case of vapour formation out of a liquid phase

The equilibrium conditions for the case of vapour formation out of a liquid phase with curved solid confinement surfaces, can be obtained from the same method as in section 3.3.2.1 by substituting equations (3.8) and (3.9) and the equations from Table 3-3 as constraints into equation (3.4), yielding:

$$
\begin{aligned}
&\left[\left(\frac{1}{T^R}-\frac{1}{T^L}\right)dU^R+\left(\frac{P^R}{T^R}-\frac{P^L}{T^L}\right)dV^R\right]\\
&+\left[\left(\frac{1}{T^S}-\frac{1}{T^L}\right)dU^S\right]\\
&+\left[\left(\frac{1}{T^V}-\frac{1}{T^L}\right)dU^V+\left(\frac{P^V}{T^V}-\frac{P^L}{T^L}\right)dV^V-\left(\frac{\mu_1^V}{T^V}-\frac{\mu_1^L}{T^L}\right)dN_1^V\right]\\
&+\left[\left(\frac{1}{T^{SL}}-\frac{1}{T^L}\right)dU^{SL}-\frac{\gamma^{SL}}{T^{SL}}dA^{SL}-\left(\frac{\mu_1^{SL}}{T^{SL}}-\frac{\mu_1^L}{T^L}\right)dN_1^{SL}-\left(\frac{\mu_2^{SL}}{T^{SL}}-\frac{\mu_2^S}{T^S}\right)dN_2^{SL}\right]\\
&+\left[\left(\frac{1}{T^{SV}}-\frac{1}{T^L}\right)dU^{SV}-\frac{\gamma^{SV}}{T^{SV}}dA^{SV}-\left(\frac{\mu_1^{SV}}{T^{SV}}-\frac{\mu_1^L}{T^L}\right)dN_1^{SV}-\left(\frac{\mu_2^{SV}}{T^{SV}}-\frac{\mu_2^S}{T^S}\right)dN_2^{SV}\right]\\
&+\left[\left(\frac{1}{T^{LV}}-\frac{1}{T^L}\right)dU^{LV}-\frac{\gamma^{LV}}{T^{LV}}dA^{LV}-\left(\frac{\mu_1^{LV}}{T^{LV}}-\frac{\mu_1^L}{T^L}\right)dN_1^{LV}\right]=0
\end{aligned}
\tag{3.21}
$$

For equation (3.21) to be true for any virtual displacement around the equilibrium, the coefficients multiplying each of the independent variations (dU^R, dV^R, dU^S, dU^V, dN_1^V, dU^{SL}, dN_1^{SL}, dN_2^{SL}, dU^{SV}, dN_1^{SV}, dN_2^{SV}, dU^{LV}, and dN_1^{LV}) are to be set to zero. Hence equations (3.22) to (3.25) are obtained as equilibrium conditions for liquid formation out of a vapour phase:

$$T^R = T^S = T^L = T^V = T^{SL} = T^{SV} = T^{LV} \tag{3.22}$$

$$P^R = P^L \tag{3.23}$$

$$\mu_1^L = \mu_1^V = \mu_1^{SL} = \mu_1^{SV} = \mu_1^{LV} \tag{3.24}$$

$$\mu_2^S = \mu_2^{SL} = \mu_2^{SV} \tag{3.25}$$

The remaining terms in equation (3.21) yield the following condition for equilibrium:

$$\left(P^V - P^L\right)dV^V - \gamma^{SL}dA^{SL} - \gamma^{SV}dA^{SV} - \gamma^{LV}dA^{LV} = 0 \tag{3.26}$$

If vapour formation out of the liquid phase happens at flat solid interfaces, equations (3.8) and (3.9) along with the appropriate equations for flat solid interfaces from Table 3-3 are to be inserted into equation (3.5). As a result, for flat solid interfaces, equation (3.25) will not be included in the conditions for equilibrium, while the other equilibrium conditions (equations (3.22), (3.23), (3.24), and (3.27)) are the same as those of the curved case.

A summary of the conditions for equilibrium in both cases of liquid formation out of a bulk vapour phase, and vapour formation out of a bulk liquid phase are presented in Table 3-4 parts (a) and (b) respectively.

Table 3-4 Conditions for equilibrium for the cases of (a) liquid formation out of a bulk vapour phase and (b) vapour formation out of a bulk liquid phase based on type of solid–liquid and solid–vapour interfaces. Liquid and vapour phases are made up of component (1) and the solid phase is purely component (2).

(a) Conditions for equilibrium for liquid formation out of a bulk vapour phase	
Curved SL and SV interfaces	$T^R = T^S = T^L = T^V = T^{SL} = T^{SV} = T^{LV}$ (3.15) $P^R = P^V$ (3.16) $\mu_1^L = \mu_1^V = \mu_1^{SL} = \mu_1^{SV} = \mu_1^{LV}$ (3.17) $\mu_2^S = \mu_2^{SL} = \mu_2^{SV}$ (3.18) $(P^L - P^V)dV^L - \gamma^{SL}dA^{SL} - \gamma^{SV}dA^{SV} - \gamma^{LV}dA^{LV} = 0$ (3.20)
Flat SL and SV interfaces	$T^R = T^S = T^L = T^V = T^{SL} = T^{SV} = T^{LV}$ (3.15) $P^R = P^V$ (3.16) $\mu_1^L = \mu_1^V = \mu_1^{SL} = \mu_1^{SV} = \mu_1^{LV}$ (3.17) $(P^L - P^V)dV^L - \gamma^{SL}dA^{SL} - \gamma^{SV}dA^{SV} - \gamma^{LV}dA^{LV} = 0$ (3.20)
(b) Conditions for equilibrium for vapour formation out of a bulk liquid phase	
Curved SL and SV interfaces	$T^R = T^S = T^L = T^V = T^{SL} = T^{SV} = T^{LV}$ (3.22) $P^R = P^L$ (3.23) $\mu_1^L = \mu_1^V = \mu_1^{SL} = \mu_1^{SV} = \mu_1^{LV}$ (3.24) $\mu_2^S = \mu_2^{SL} = \mu_2^{SV}$ (3.25) $(P^V - P^L)dV^V - \gamma^{SL}dA^{SL} - \gamma^{SV}dA^{SV} - \gamma^{LV}dA^{LV} = 0$ (3.26)
Flat SL and SV interfaces	$T^R = T^S = T^L = T^V = T^{SL} = T^{SV} = T^{LV}$ (3.22) $P^R = P^L$ (3.23) $\mu_1^L = \mu_1^V = \mu_1^{SL} = \mu_1^{SV} = \mu_1^{LV}$ (3.24) $(P^V - P^L)dV^V - \gamma^{SL}dA^{SL} - \gamma^{SV}dA^{SV} - \gamma^{LV}dA^{LV} = 0$ (3.26)

3.4. Free energy of the system

The next step is to find the thermodynamic potential (also called free energy) of the system that acts as the motivation in any evolution toward equilibrium. The system of interest is either liquid or vapour formation inside confined solid geometries with temperature and outer phase pressure controlled by a reservoir. It should be noted that while the pressure of the confined fluid is constant (controlled by the reservoir), the pressure of the new phase being formed out of a confined fluid is variable dependent onsize of that new phase. Hence Gibbs free energy cannot be a potential function of such system for which only one pressure is constant.

For the system of our concern, where only components (1) and (2) exist, equation (2.30) becomes:

$$0 \geq \Delta U - T^{R}\,\Delta S + P^{R}\,\Delta V - \mu_1^{R}\Delta N_1 - \mu_2^{R}\Delta N_2 \tag{3.27}$$

Each term of the above equation can be written using the constituent terms for the system:

$$\Delta U = \Delta U^{S} + \Delta U^{L} + \Delta U^{V} + \Delta U^{SL} + \Delta U^{SV} + \Delta U^{LV} \tag{3.28}$$

$$\Delta S = \Delta S^{S} + \Delta S^{L} + \Delta S^{V} + \Delta S^{SL} + \Delta S^{SV} + \Delta S^{LV} \tag{3.29}$$

Considering the incompressibility of the solid phase ($\Delta V^{S} = 0$), and Gibbs assumption of interfaces having no volume, then

$$\Delta V = \Delta V^{L} + \Delta V^{V} \tag{3.30}$$

Besides the system does not exchange mass with the reservoir, that is:

$$\Delta N_1 = 0 \quad \text{and} \quad \Delta N_2 = 0 \tag{3.31}$$

Inserting equations (3.28) to (3.31) into equation (3.27) leads to the following:

$$\begin{aligned} 0 \geq\ & \Delta U^S + \Delta U^L + \Delta U^V + \Delta U^{SL} + \Delta U^{SV} + \Delta U^{LV} \\ & -T^R\,(\Delta S^S + \Delta S^L + \Delta S^V + \Delta S^{SL} + \Delta S^{SV} + \Delta S^{LV}) + P^R\,(\Delta V^L + \Delta V^V) \end{aligned} \tag{3.32}$$

The reservoir properties of T^R and P^R are to be replaced according to the conditions for equilibrium, which are different depending on whether a vapour phase or a liquid phase is forming.

3.4.1. Free energy for liquid formation out of a vapor bulk phase

In the case of liquid formation out of a bulk vapor phase, where $P^R = P^V$, equation (3.32) is rearranged to

$$\begin{aligned} 0 \geq\ & \left[\Delta U^S - T^S\,\Delta S^S\right] + \left[\Delta U^L - T^L\,\Delta S^L\right] + \left[\Delta U^V - T^V\,\Delta S^V + P^V\,\Delta V^V\right] \\ & + \left[\Delta U^{SL} - T^{SL}\,\Delta S^{SL}\right] + \left[\Delta U^{SV} - T^{SV}\,\Delta S^{SV}\right] + \left[\Delta U^{LV} - T^{LV}\,\Delta S^{LV}\right] + P^V\,\Delta V^L \end{aligned} \tag{3.33}$$

According to the definitions of Helmholtz (F) and Gibbs (G) free energies (equations (2.33) and (2.32)), equation (3.33) is equivalent to:

$$\Delta(F^S + F^L + G^V + F^{SL} + F^{SV} + F^{LV} + P^V\,V^L) \leq 0 \tag{3.34}$$

Therefore the free energy of the system in which a liquid phase is being formed out of a vapor phase is

$$B = F^S + F^L + G^V + F^{SL} + F^{SV} + F^{LV} + P^V\,V^L \tag{3.35}$$

While the free energy of the whole system is B, each constituent subsystem has a specific free energy based on its constraints. For example for the solid phase with constant volume ($dV^S=0$) and temperature, the Helmholtz free energy is appropriate. The Gibbs free energy acts as the free energy of the vapor phase which has imposed temperature and pressure ($T^V=T^R$, and $P^V=P^R$). For the liquid phase where neither the volume nor the pressure is constant, some extra terms appear and the free energy is not in one of those well−known formats. This potential function in equation (3.35) has been presented previously [18].

The internal energies in equation (3.33) can be replaced with their equivalent forms from the Euler relation, which for bulk phases (a) is

$$\mathrm{U}^{\mathrm{a}} = \mathrm{T}^{\mathrm{a}}\,\mathrm{S}^{\mathrm{a}} - \mathrm{P}^{\mathrm{a}}\,\mathrm{V}^{\mathrm{a}} + \sum_{\mathrm{i}=1}^{\mathrm{k}} \mu_{\mathrm{i}}^{\mathrm{a}}\,\mathrm{N}_{\mathrm{i}}^{\mathrm{a}} \tag{3.36}$$

and for interfaces (ab) is

$$\mathrm{U}^{ab} = \mathrm{T}^{ab}\,\mathrm{S}^{ab} + \gamma^{ab}\,\mathrm{A}^{ab} + \sum_{i=\mathrm{j}}^{\mathrm{k}} \mu_i^{ab}\,\mathrm{N}_i^{ab} \tag{3.37}$$

$$\text{where} \begin{cases} \mathrm{j} = 2 & \text{when} \quad ab \text{ denotes a } flat \text{ interface} \\ \mathrm{j} = 1 & \text{when} \quad ab \text{ denotes a } curved \text{ interface} \end{cases}$$

As described in the previous section the liquid−vapor interface is curved and the solid−liquid and the solid−vapor interfaces may be curved or flat depending on the solid geometry.

Then the equivalent form of free energy for geometries with curved solid interfaces is:

$$B = \left[-P^{S}V^{S} + \mu_2^{S}N_2^{S}\right] + \left[-P^{L}V^{L} + \mu_1^{L}N_1^{L}\right] + \left[\mu_1^{V}N_1^{V}\right]$$
$$+ \left[\gamma^{SL}A^{SL} + \mu_1^{SL}N_1^{SL} + \mu_2^{SL}N_2^{SL}\right] + \left[\gamma^{SV}A^{SV} + \mu_1^{SV}N_1^{SV} + \mu_2^{SV}N_2^{SV}\right] \quad (3.38)$$
$$+ \left[\gamma^{LV}A^{LV} + \mu_1^{LV}N_1^{LV}\right] + P^{V}V^{L}$$

Also the equivalent form of free energy for geometries with flat solid interfaces, assuming that component (2) is chosen as the component not to exist at the solid interfaces, is:

$$B = \left[-P^{S}V^{S} + \mu_2^{S}N_2^{S}\right] + \left[-P^{L}V^{L} + \mu_1^{L}N_1^{L}\right] + \left[\mu_1^{V}N_1^{V}\right]$$
$$+ \left[\gamma^{SL}A^{SL} + \mu_1^{SL}N_1^{SL}\right] + \left[\gamma^{SV}A^{SV} + \mu_1^{SV}N_1^{SV}\right] \quad (3.39)$$
$$+ \left[\gamma^{LV}A^{LV} + \mu_1^{LV}N_1^{LV}\right] + P^{V}V^{L}$$

3.4.2. Free energy of vapor formation out of a bulk liquid phase

When a vapor is formed out of a liquid phase, $P^R = P^L$ and equation (3.32) is rearranged to:

$$0 \geq \left[\Delta U^{S} - T^{S}\Delta S^{S}\right] + \left[\Delta U^{L} - T^{L}\Delta S^{L} + P^{L}\Delta V^{L}\right] + \left[\Delta U^{V} - T^{V}\Delta S^{V}\right]$$
$$+\left[\Delta U^{SL} - T^{SL}\Delta S^{SL}\right] + \left[\Delta U^{SV} - T^{SV}\Delta S^{SV}\right] + \left[\Delta U^{LV} - T^{LV}\Delta S^{LV}\right] + P^{L}\Delta V^{V} \quad (3.40)$$

which is equivalent to:

$$\Delta\left(F^{S} + G^{L} + F^{V} + F^{SL} + F^{SV} + F^{LV} + P^{L}V^{V}\right) \leq 0 \quad (3.41)$$

Therefore the free energy of a system in which a liquid phase is being formed out of a vapor phase is

$$B = F^S + G^L + F^V + F^{SL} + F^{SV} + F^{LV} + P^L V^V \tag{3.42}$$

A similar potential function has been obtained by Ward and Levarte[16]for the case of vapour nuclei in solid surfaces contacting a liquid-gas solution.

The internal energies in equation (3.33) can be replaced with their equivalent forms from the Euler relation, according to equations (3.36) and (3.37).

Then the equivalent form of free energy for vapor phase formation for geometries with curved solid interfaces is:

$$\begin{aligned} B = {} & \left[-P^S V^S + \mu_2^S N_2^S\right] + +\left[\mu_1^L N_1^L\right] + \left[-P^V V^V + \mu_1^V N_1^V\right] \\ & + \left[\gamma^{SL} A^{SL} + \mu_1^{SL} N_1^{SL} + \mu_2^{SL} N_2^{SL}\right] + \left[\gamma^{SV} A^{SV} + \mu_1^{SV} N_1^{SV} + \mu_2^{SV} N_2^{SV}\right] \\ & + \left[\gamma^{LV} A^{LV} + \mu_1^{LV} N_1^{LV}\right] + P^L V^V \end{aligned} \tag{3.43}$$

Also the equivalent form of free energy for vapor formation for geometries with flat solid interfaces, assuming that component (2) is chosen as the component not to exist at solid interfaces, is:

$$\begin{aligned} B = {} & \left[-P^S V^S + \mu_2^S N_2^S\right] + +\left[\mu_1^L N_1^L\right] + \left[-P^V V^V + \mu_1^V N_1^V\right] \\ & + \left[\gamma^{SL} A^{SL} + \mu_1^{SL} N_1^{SL}\right] + \left[\gamma^{SV} A^{SV} + \mu_1^{SV} N_1^{SV}\right] \\ & + \left[\gamma^{LV} A^{LV} + \mu_1^{LV} N_1^{LV}\right] + P^L V^V \end{aligned} \tag{3.44}$$

The free energies for the cases of liquid formation out of a vapor phase and vapor formation out of a liquid phase are summarized in Table 3-5 parts (a) and (b) respectively:

Table 3-5 Free energy of the system for the cases of (a) liquid formation out of a bulk vapour phase and (b) vapour formation out of a bulk liquid phase. Liquid and vapour phases are made up of component (1) and the solid phase is purely component (2).

(a) Liquid formation out of a bulk vapour phase	
Free energy	$B = F^S + F^L + G^V + F^{SL} + F^{SV} + F^{LV} + P^V V^L$ (3.35)
Equivalent form of free energy for curved SL and SV interfaces	$B = \left[-P^S V^S + \mu_2^S N_2^S\right] + \left[-P^L V^L + \mu_1^L N_1^L\right] + \left[\mu_1^V N_1^V\right] + \left[\gamma^{SL} A^{SL} + \mu_1^{SL} N_1^{SL} + \mu_2^{SL} N_2^{SL}\right] + \left[\gamma^{SV} A^{SV} + \mu_1^{SV} N_1^{SV} + \mu_2^{SV} N_2^{SV}\right] + \left[\gamma^{LV} A^{LV} + \mu_1^{LV} N_1^{LV}\right] + P^V V^L$ (3.38)
Equivalent form of free energy for flat SL and SV interfaces	$B = \left[-P^S V^S + \mu_2^S N_2^S\right] + \left[-P^L V^L + \mu_1^L N_1^L\right] + \left[\mu_1^V N_1^V\right] + \left[\gamma^{SL} A^{SL} + \mu_1^{SL} N_1^{SL}\right] + \left[\gamma^{SV} A^{SV} + \mu_1^{SV} N_1^{SV}\right] + \left[\gamma^{LV} A^{LV} + \mu_1^{LV} N_1^{LV}\right] + P^V V^L$ (3.39)
(b) Vapour formation out of a bulk liquid phase	
Free energy	$B = F^S + G^L + F^V + F^{SL} + F^{SV} + F^{LV} + P^L V^V$ (3.42)
Equivalent form of free energy for curved SL and SV interfaces	$B = \left[-P^S V^S + \mu_2^S N_2^S\right] + \left[\mu_1^L N_1^L\right] + \left[-P^V V^V + \mu_1^V N_1^V\right] + \left[\gamma^{SL} A^{SL} + \mu_1^{SL} N_1^{SL} + \mu_2^{SL} N_2^{SL}\right] + \left[\gamma^{SV} A^{SV} + \mu_1^{SV} N_1^{SV} + \mu_2^{SV} N_2^{SV}\right] + \left[\gamma^{LV} A^{LV} + \mu_1^{LV} N_1^{LV}\right] + P^L V^V$ (3.43)
Equivalent form of free energy for flat SL and SV interfaces	$B = \left[-P^S V^S + \mu_2^S N_2^S\right] + \left[\mu_1^L N_1^L\right] + \left[-P^V V^V + \mu_1^V N_1^V\right] + \left[\gamma^{SL} A^{SL} + \mu_1^{SL} N_1^{SL}\right] + \left[\gamma^{SV} A^{SV} + \mu_1^{SV} N_1^{SV}\right] + \left[\gamma^{LV} A^{LV} + \mu_1^{LV} N_1^{LV}\right] + P^L V^V$ (3.44)

3.5. Reference state for free energy

Free energy can only be evaluated with respect to some reference state. It is convenient to consider the reference state as a situation in which none of the new phase has been formed. The reference state is denoted by subscript *0*, and is assumed to be an equilibrium state. [40]

In the case of liquid formation out of a vapor phase, the reference state has only solid phase, vapor phase and the solid−vapor interface existing. The free energy of the reference state for the case of a curved solid−vapor interface according to equation (3.38) is then:

$$B_0 = \left[-P_0^S V_0^S + \mu_{2,0}^S N_{2,0}^S\right] + \left[\mu_{1,0}^V N_{1,0}^V\right] + \left[\gamma_0^{SV} A_0^{SV} + \mu_{1,0}^{SV} N_{1,0}^{SV} + \mu_{2,0}^{SV} N_{2,0}^{SV}\right] \quad (3.45)$$

B_0 is literally the free energy of the equilibrium system when none of the new phase (liquid) is formed.

The total number of moles of each of the components (1) and (2) are constant according to constraints of the system, therefore:

$$N_{1,0}^V + N_{1,0}^{SV} = N_1^L + N_1^V + N_1^{SL} + N_1^{SV} + N_1^{LV} \quad (3.46)$$

$$N_{2,0}^S + N_{2,0}^{SV} = N_2^S + N_2^{SL} + N_2^{SV} \quad (3.47)$$

Also as another constraint, the surface area of the solid is constant:

$$A_0^{SV} = A^{SL} + A^{SV} \quad (3.48)$$

The solid is rigid (no deformation) and is incompressible, i.e. its volume is constant as another constraint of the system:

$$V_0^S = V^S \quad (3.49)$$

Since B_0 is the free energy of an equilibrium condition, for each component there exists the equality of chemical potential between the involved phase and interface, i.e.

$$\mu_{1,0}^{V} = \mu_{1,0}^{SV} \tag{3.50}$$

$$\mu_{2,0}^{S} = \mu_{2,0}^{SV} \tag{3.51}$$

The system is assumed to be large enough that the intensive properties in the solid phase, vapor bulk phase and at the solid−vapor interface are not changed after the formation of a small amount of liquid phase [40]. Therefore we assume:

$$P_0^S = P^S \tag{3.52}$$

$$\mu_{1,0}^{V} = \mu_1^{V}\,;\ \mu_{1,0}^{SV} = \mu_1^{SV} \tag{3.53}$$

$$\mu_{2,0}^{S} = \mu_2^{S}\,;\ \mu_{2,0}^{SV} = \mu_2^{SV} \tag{3.54}$$

$$\gamma_0^{SV} = \gamma^{SV} \tag{3.55}$$

When equations (3.46) to (3.55) are combined with equation (3.45) and the result is deducted from equation (3.38), the free energy expanded about the reference state is as follows:

$$\begin{aligned}
&\Delta B = B - B_0 = \\
&\left(P^V - P^L\right)V^L + \left(\gamma^{SL} - \gamma^{SV}\right)A^{SL} + \gamma^{LV}A^{LV} \\
&+\left(\mu_1^{L} - \mu_1^{V}\right)N_1^{L} + \left(\mu_1^{SL} - \mu_1^{V}\right)N_1^{SL} + \left(\mu_1^{SV} - \mu_1^{V}\right)N_1^{SV} + \left(\mu_1^{LV} - \mu_1^{V}\right)N_1^{LV} \\
&+\left(\mu_2^{SL} - \mu_2^{S}\right)N_1^{SL} + \left(\mu_2^{SV} - \mu_2^{S}\right)N_1^{SV}
\end{aligned} \tag{3.56}$$

Each of the terms of the above equation is essentially the difference between two intensive properties multiplied by an extensive property. Our interest is to find ΔB only in the small neighborhood of the equilibrium state. Each of the differences

between two intensive properties can be substituted by its Taylor expansion about the equilibrium state. For small virtual displacements around equilibrium states, terms that are directly proportional to the size of the virtual displacements can be neglected. Hence each of the differences between two intensive properties can be substituted by its quantity at equilibrium conditions [40]. Due to equality of chemical potentials at the equilibrium conditions (refer to Table 3-4 (a)), in equation (3.56) all the terms other than the first three terms are zero and equation (3.56) reduces to[18] :

$$\Delta B = B - B_0 = \left(P^V - P^L\right)V^L + \left(\gamma^{SL} - \gamma^{SV}\right)A^{SL} + \gamma^{LV}A^{LV} \tag{3.57}$$

For the above equation at equilibrium conditions, $(P^V - P^L)$ and $(\gamma^{SL} - \gamma^{SV})$ can be replaced by the Laplace−Young equation (equation (2.15)) and the Young equation (equation (2.16)) respectively. These substitutions transform equation (3.57) into the following equation:

$$\Delta B = B - B_0 = \gamma^{LV}\left(\frac{1}{R_1} + \frac{1}{R_2}\right)V^L + (-\gamma^{LV}\cos\theta)A^{SL} + \gamma^{LV}A^{LV} \tag{3.58}$$

where all of the R_1, R_2, and θ are evaluated at the equilibrium conditions.

Equation (3.58) can be written in terms of the Kelvin radius (R_C) [18] :

$$\Delta B = B - B_0 = \frac{2\gamma^{LV}}{R_C}V^L + (-\gamma^{LV}\cos\theta)A^{SL} + \gamma^{LV}A^{LV} \tag{3.59}$$

Following the same procedure for the flat solid−liquid and solid−vapor interfaces, the same equation as equation (3.58) represents the thermodynamic potential of the system of liquid formation out of a vapor.

For the case of vapor formation out of a liquid phase, the reference condition would be when no vapor is present. The thermodynamic potential is obtained from a similar procedure.

The free energies expanded about a reference state, for cases of liquid formation out of a vapor phase and vapor formation out of a liquid phase are summarized in Table 3-6:

Table 3-6 Forms of free energy with respect to the reference condition, for two cases of liquid formation out of a bulk vapour phase and vapour formation out of a bulk liquid phase. Liquid and vapour phases are made up of component (1) and the solid phase is purely component (2).

Liquid formation out of a vapour phase [18]	Vapour formation out of a liquid phase
$B - B_0 = (P^V - P^L)V^L + (\gamma^{SL} - \gamma^{SV})A^{SL} + \gamma^{LV}A^{LV}$ (3.57)	$B - B_0 = (P^L - P^V)V^V + (\gamma^{SV} - \gamma^{SL})A^{SV} + \gamma^{LV}A^{LV}$ (3.60)
$B - B_0 = \left(\frac{1}{R_1} + \frac{1}{R_2}\right)V^L + \left(-\gamma^{LV}\cos\theta\right)A^{SL} + \gamma^{LV}A^{LV}$ (3.58)	$B - B_0 = \left(\frac{1}{R_1} + \frac{1}{R_2}\right)V^V + \left(\gamma^{LV}\cos\theta\right)A^{SV} + \gamma^{LV}A^{LV}$ (3.61)
$B - B_0 = \frac{2\gamma^{LV}}{R_C}V^L + \left(-\gamma^{LV}\cos\theta\right)A^{SL} + \gamma^{LV}A^{LV}$ (3.59)	$B - B_0 = \frac{2\gamma^{LV}}{R_C}V^V + \left(\gamma^{LV}\cos\theta\right)A^{SV} + \gamma^{LV}A^{LV}$ (3.62)

3.6. Fluid material properties

The equations being developed so far can be applied to any confined fluid system, regardless of the constituent fluid component. However many experimental

investigations have been performed on H_2O in confining geometries. There are also some experiments on n−dodecane as the pure confined fluid. In order to compare our results with literature, throughout this thesis H_2O or n−dodecane is chosen as the pure component of the liquid and vapour phases. The properties of these two components at the specified temperature are presented in Table 3-7, and will be used in the following chapters.

Table 3-7 H_2O and n−dodecane properties at specified temperature.

Component	Temperature (ºC)	γ^{LV} (Nm^{-1})	P_∞ (Pa)	υ_∞^L (m^3kmol^{-1})
H_2O	20	0.07275 [31]	2339 [39]	0.01805 [39]
n−dodecane	24	0.02503 [41]	16.43 [39]	0.2282 [39]

3.7. Effect of the bulk phase pressure on the sign of the Kelvin radius (R_C)

The Kelvin radius, which is equal to the mean radius of curvature at equilibrium states, can be positive or negative; depending on the sign of the principal radii of curvature (equation (2.21)).The Kelvin radius with each sign is only possible at specific values of the bulk pressure. This will be discussed in two separate sections for the cases of liquid formation and vapour formation.

3.7.1. Effect of the bulk phase pressure on the sign of R_C for the case of liquid formation out of a bulk vapour phase

In the case of liquid formation, the bulk phase is the vapour phase. With the pressure difference being arbitrarily defined as $P^V - P^L$, the Kelvin radius can be obtained from equation (2.22). With the numerator ($2\gamma^{LV}$) being a positive number

in equation (2.22), the sign of R_C is determined based on the sign of the denominator, i.e.:

$$\begin{cases} R_C > 0 & \text{if} \quad \dfrac{P^V}{P_\infty} - 1 - \dfrac{\bar{R}T^V}{P_\infty \upsilon_\infty^L} \ln\left(\dfrac{P^V}{P_\infty}\right) > 0 \\ R_C < 0 & \text{if} \quad \dfrac{P^V}{P_\infty} - 1 - \dfrac{\bar{R}T^V}{P_\infty \upsilon_\infty^L} \ln\left(\dfrac{P^V}{P_\infty}\right) < 0 \end{cases} \tag{3.63}$$

For an ideal gas $\frac{\bar{R}T}{P\upsilon}$ is equal to unity. For any material, the denominator of $\frac{\bar{R}T^V}{P_\infty \upsilon_\infty^L}$ is much smaller than that of an ideal gas. Therefore regardless of the material, $\frac{\bar{R}T^V}{P_\infty \upsilon_\infty^L}$ is expected to be much greater than one.

Solving equation (3.63), with $\frac{\bar{R}T^V}{P_\infty \upsilon_\infty^L}$ much greater than one, shows that R_C is positive for $\frac{P^V}{P_\infty}$ less than one or greater than a very large value. The numerical amount of $\frac{\bar{R}T^V}{P_\infty \upsilon_\infty^L}$, as well as the range of $\frac{P^V}{P_\infty}$ for positive and negative R_C are shown in Table 3-8 , for two components of H_2O and n−dodecane, using the properties stated in Table 3-7.

Table 3-8 Amount of the coefficient $\frac{\bar{R}T^V}{P_\infty \upsilon_\infty^L}$ and range of $\frac{P^V}{P_\infty}$ for positive or negative R_C for two components: H_2O and n−dodecane.

Component	$\frac{\bar{R}T^V}{P_\infty \upsilon_\infty^L}$	$\frac{P^V}{P_\infty}$ range for $R_C > 0$	$\frac{P^V}{P_\infty}$ range for $R_C < 0$
H_2O	5.77×10^4	$\frac{P^V}{P_\infty} < 1$ or $\frac{P^V}{P_\infty} > 7.83\times10^5$	$1 < \frac{P^V}{P_\infty} < 7.83\times10^5$
n−dodecane	6.59×10^5	$\frac{P^V}{P_\infty} < 1$ or $\frac{P^V}{P_\infty} > 1.07\times10^7$	$1 < \frac{P^V}{P_\infty} < 1.07\times10^7$

Substituting the values for the saturation pressure (P_∞) from Table 3-7 into the criteria of Table 3-8 shows that a positive Kelvin radius is possible at bulk vapour pressures below the saturation pressure or above 1.83×10^9 Pa for H_2O and 1.76×10^8 Pa for n−dodecane (similarly above some extremely high pressures for other materials, due to $\frac{\bar{R}T^V}{P_\infty \upsilon_\infty^L}$ being much greater than one in equation (3.63)). The extreme high pressures resulting in positive Kelvin radius are not of interest. Eliminating those extremely high pressures, the range of bulk vapour pressure for each of positive or negative Kelvin radius is:

$$\begin{cases} R_C > 0 & \text{if} \quad \frac{P^V}{P_\infty} < 1 \\ R_C < 0 & \text{if} \quad \frac{P^V}{P_\infty} > 1 \end{cases} \tag{3.64}$$

According to equation (3.64) the Kelvin radius is positive at bulk vapour pressures below the saturation pressure, and is negative at bulk vapour pressures above the saturation pressure. It should be noted that at vapour pressure equal to saturation pressure, there would be no pressure difference along the interface (P^V=P^L) and the interface would be flat.

3.7.2. Effect of the bulk phase pressure on the sign of R_C for the case of vapour formation out of a bulk liquid phase

For the case of vapour formation, the bulk phase is the liquid phase. When the pressure difference is arbitrarily defined as $P^L - P^V$, equation (2.24) shows the Kelvin radius. In equation (2.24) with the positive numerator ($2\gamma^{LV}$), the sign of the denominator would determine the sign of R_C, hence:

$$\begin{cases} R_C > 0 & \text{if} \quad \dfrac{P^L}{P_\infty} - exp\left[\dfrac{P_\infty \upsilon_\infty^L}{\bar{R}T^V}\left(\dfrac{P^L}{P_\infty} - 1\right)\right] > 0 \\ R_C < 0 & \text{if} \quad \dfrac{P^L}{P_\infty} - exp\left[\dfrac{P_\infty \upsilon_\infty^L}{\bar{R}T^V}\left(\dfrac{P^L}{P_\infty} - 1\right)\right] < 0 \end{cases} \tag{3.65}$$

In section 3.7.1 it was explained that $\frac{\bar{R}T^V}{P_\infty \upsilon_\infty^L}$ is much greater than unity for any material at conditions of intrest. Then it can be concluded that $\frac{P_\infty \upsilon_\infty^L}{\bar{R}T^V}$ is much smaller than one regardless of the material. With $\frac{P_\infty \upsilon_\infty^L}{\bar{R}T^V}$ much less than unity, and after solving equation (3.65), it is found that R_C is negative for $\frac{P^L}{P_\infty}$ less than one or greater than a very large value. Numerical amounts of $\frac{P_\infty \upsilon_\infty^L}{\bar{R}T^V}$, and the criteria of $\frac{P^L}{P_\infty}$ for positive and negative R_C are shown in Table 3-9, for two components of H_2O and n−dodecane, using the properties stated in Table 3-7.

Table 3-9 Amount of the coefficient $\frac{P_\infty \upsilon_\infty^L}{\bar{R}T^V}$ and range of $\frac{P^L}{P_\infty}$ for positive or negative R_C for two components: H_2O and n−dodecane.

Component	$\frac{P_\infty \upsilon_\infty^L}{\bar{R}T^V}$	$\frac{P^L}{P_\infty}$ range for $R_C > 0$	$\frac{P^L}{P_\infty}$ range for $R_C < 0$
H_2O	1.73×10^{-5}	$1 < \frac{P^L}{P_\infty} < 7.83\times10^5$	$\frac{P^L}{P_\infty} < 1$ or $\frac{P^L}{P_\infty} > 7.83\times10^5$
n−dodecane	1.52×10^{-6}	$1 < \frac{P^L}{P_\infty} < 1.07\times10^7$	$\frac{P^L}{P_\infty} < 1$ or $\frac{P^L}{P_\infty} > 1.07\times10^7$

Substitution of saturation pressures (P_∞) from Table 3-7 into the criteria of Table 3-9 shows that negative Kelvin radii are possible at bulk liquid pressures below the saturation pressure or above 1.83×10^9 Pa for H_2O and 1.76×10^8 Pa for n−dodecane (similarly above some extremely high pressures for other materials, due to $\frac{P_\infty \upsilon_\infty^L}{\bar{R}T^V}$ being much less than one in equation (3.65)). The extreme high pressures resulting in negative Kelvin radius are not of interest. Eliminating those extremely high pressures ranges, the range of bulk liquid pressure for each of positive or negative Kelvin radius is:

$$\begin{cases} R_C > 0 & \text{if} \quad \frac{P^L}{P_\infty} > 1 \\ R_C < 0 & \text{if} \quad \frac{P^L}{P_\infty} < 1 \end{cases} \tag{3.66}$$

According to equation (3.66), the Kelvin radius is positive at bulk liquid pressures above the saturation pressure, and is negative at bulk liquid pressures below the saturation pressure. It should be noted that at liquid pressure equal to saturation pressure, there would be no pressure difference along the interface ($P^L = P^V$) and the interface would be flat.

3.8. Transition contact angle

For either case of liquid phase formation out of a bulk vapour phase or vapour formation out of a bulk liquid phase, the liquid−vapour meniscus might be concave or convex. Obviously there would be some contact angle at which the meniscus alters from being concave to being convex. This contact angle is called the ***transition contact angle***, and is denoted by θ_t.

Defining the ***transition contact angle*** allows us to describe the changes in the contact angle as getting closer to / farther from the ***transition contact angle***, rather than by increasing / decreasing the contact angle. This is especially helpful since there is a widely used convention of measuring the contact angle within the denser phase (liquid phase). The benefit of the ***transition contact angle*** is explained in more detail through the following example.

An example of two cases of liquid formation out of a bulk vapour phase and vapour formation out of a bulk liquid phase inside a conical pit is illustrated in Figure 3-2, where contact angles are measured from the liquid side. In part (a) while the shape of the concave meniscus is the same, the contact angle is 15° for the case of liquid formation and is 165° for the case of vapour formation. Consider that some surface manipulation changes the contact angle by 10° in part (b). For the case of liquid formation the contact angle is **increasing** to 25°, while for the case of the vapour formation it is **decreasing** to 155°. This change can uniquely be described as getting 10° closer to the ***transition contact angle***.

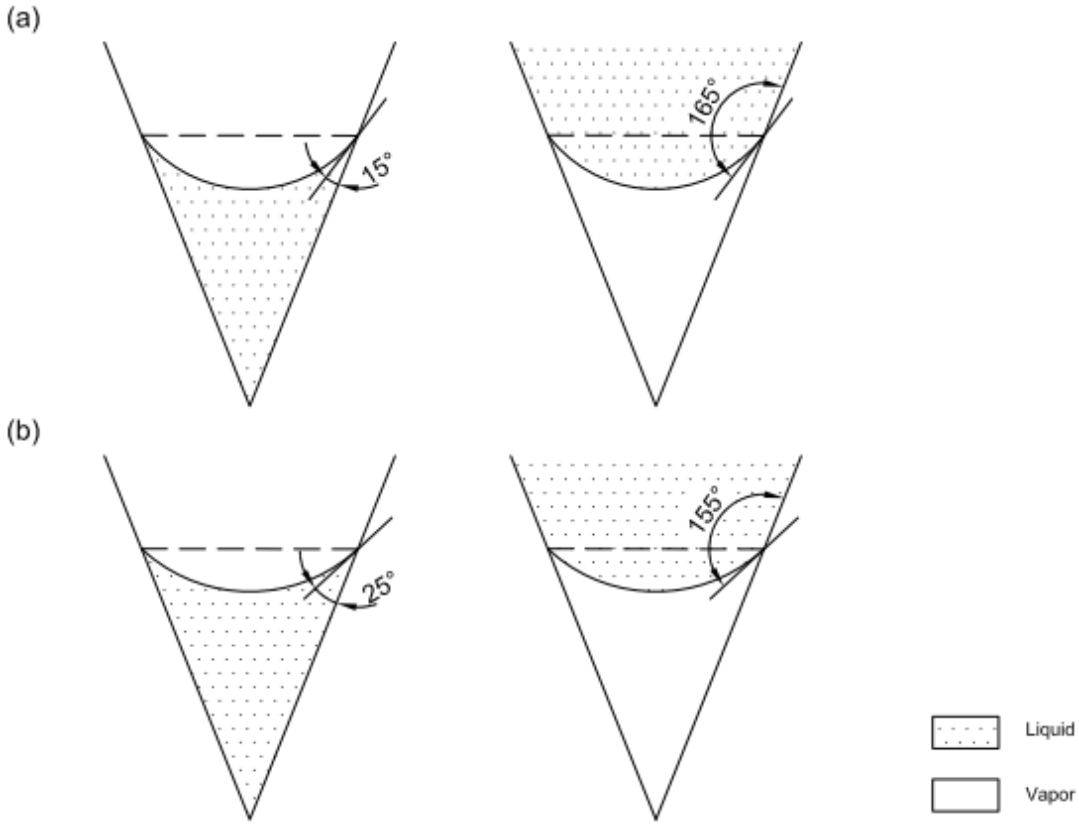

Figure 3-2 (a) Contact angle measurement convention demonstrated in the two cases of liquid formation out of a vapour phase and vapour formation out of a liquid phase inside a conical pit. The transition meniscus is shown as a dotted line. (b) Getting 10° closer to the transition contact angle, equivalent to an increase in the contact angle for the case of liquid formation and a decrease in the contact angle for the case of vapour formation.

3.9. Summary

This chapter covers all the governing equations, definitions, and material properties for two cases of liquid formation out of a bulk vapour phase and vapour formation out of a bulk liquid phase inside a confined geometry. These equations and definitions span across different geometries to be discussed in the following chapters.

The length below which the gravitational field can be neglected (capillary length) is presented for two components of interest at section 3.2. In section 3.3 conditions

for equilibrium of the system are derived, a summary of which can be found in Table 3-4. Through section 3.4 the appropriate free energies of the systems are determined, and summarized in Table 3-5. The reference condition as a basis of calculating the free energy level is introduced in section 3.5. Also the equations for the amount of the free energy with respect to the reference condition are presented in Table 3-6. Some material properties for H_2O and n−dodecane are reported in section 3.6 (Table 3-7). In section 3.7 the dependence of the sign of the Kelvin radius on the bulk phase pressure is discussed through two material specific cases of H_2O and n−dodecane (Table 3-8). The results were proven to be expandable to other components. Section 3.8 introduces ***transition contact angle*** as a helpful term in unifying the description of the changes in contact angle in either case of liquid or vapour formation.

4. Liquid−vapour system inside a conical pit

The first solid confinement geometry to be discussed is the conical pit. This geometry is of practical importance in many cases. For the focus of our study, the single component (pure) fluid being confined inside a cone, thermodynamic stability analysis is performed using the equations and definitions of chapter 3. The system is of constant mass and constant bulk phase pressure, imposed by the reservoir. For the solid shape of a conical pit, both the solid−liquid and the solid−vapour interfaces are *curved*.

Two possible liquid−vapour systems are discussed in detail in this chapter: liquid formation from a bulk vapour phase in section 4.1, and vapour formation from a bulk liquid phase in section 4.2. In either of these cases the meniscus might be concave or convex, each of which are discussed in separate sections: sections 4.1.1 and 4.1.2 are about liquid formation with concave and convex menisci respectively, where as vapour formation with concave and convex menisci are presented in sections 4.2.1 and 4.2.2 correspondingly. The effect of the equilibrium contact angle on the thermodynamic stability is discussed in sections 4.1.1.1, 4.1.2.1, 4.2.1.1, and 4.2.2.1 for liquid formation with concave or convex meniscus and vapour formation with concave or convex meniscus. Sections 4.1.1.2, 4.1.2.2,

4.2.1.2, 4.2.2.2 explain the effect of the cone apex angle in the different cases of liquid formation with concave or convex meniscus and vapour formation with concave or convex meniscus respectively. Section 4.3 presents the big picture of the stability analysis of both liquid and vapour formation inside a conical pit and the effect of different parameters discussed in the previous sections.

4.1. Liquid phase formation from a bulk vapour phase inside a conical pit

The constraints of the system are those that are stated in Table 3-2 for the *curved* solid interface. Conditions for equilibrium are as presented in Table 3-4 (a) (equation (3.15) to (3.20)), where the solid interfaces are *curved*. For this case, we will show how the Laplace−Young equation (2.13) and the Young equation (2.16) can be obtained from the conditions for equilibrium as stated in Table 3-4 (a).

Recall equation (3.20),

$$\left(P^{L} - P^{V}\right)dV^{L} - \gamma^{SL}dA^{SL} - \gamma^{SV}dA^{SV} - \gamma^{LV}dA^{LV} = 0 \tag{3.20}$$

where dV^{L}, dA^{SL}, dA^{SV}, and dA^{LV} are to be substituted in terms of the principal radii of curvature of the liquid−vapour interface and the contact angle.

Neglecting gravity, the pressure inside the liquid phase and the pressure inside the vapour phase would be constant; where from the Kelvin equation (equation (2.20)) it can be seen that in the liquid−vapour interface must be a surface of constant curvature. This constant curvature interface should meet the solid, which is in the form of a conical pit, at the same contact angle at every contact. Hence the

liquid−vapour interface can be considered to be part of a sphere, as it was assumed by Ward et. al.[20]. For the liquid−vapour interface to form part of a sphere, the principal radii of curvature are equal to each other, i.e. $R_1 = R_2 = R_C$.

The liquid–vapour interface might be either concave or convex. For this solid geometry (conical pit), and in the case of liquid formation from a bulk vapour phase the ***transition contact angle*** is $90° - \beta$, where β is half of the cone apex angle. Therefore the liquid−vapour interface is concave for contact angles $\theta < 90° - \beta$, and is convex for contact angles $\theta > 90° - \beta$. Liquid formation with concave or convex meniscus is illustrated in Figure 4-1.

It is a matter of geometrical calculations to develop the appropriate equations for V^L, A^{SL}, A^{SV}, and A^{LV}.

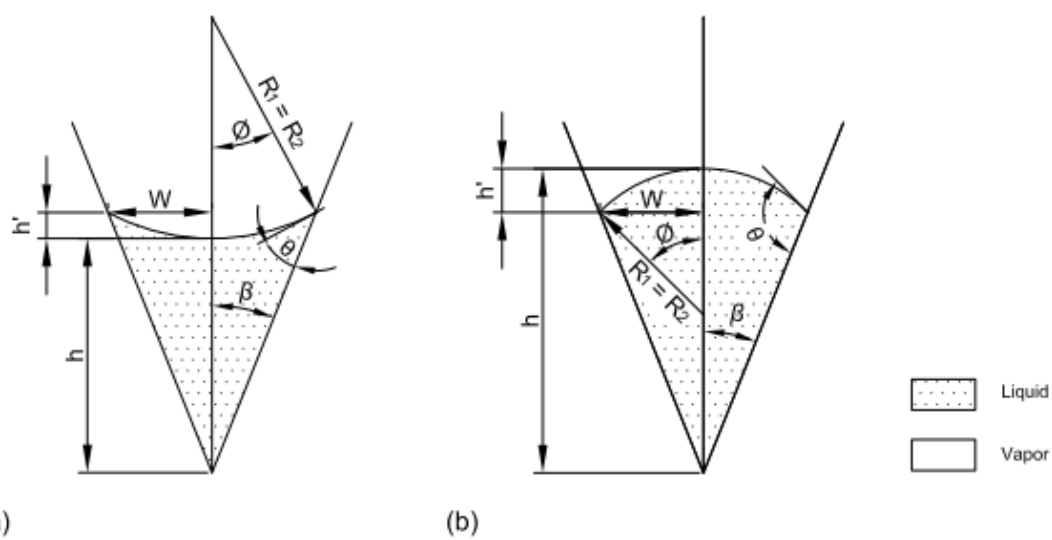

Figure 4-1 Schematic of liquid formation inside a conical pit and definition of cone apex angle 2β, contact angle θ, principal radii of curvature R_1=R_2, radius of the three−phase contact circle W, the height of interface h, the distance between the highest and the lowest parts of the liquid−vapour interface h′, and half−filling angle of the new phase ∅, for cases of a) concave ($\theta < 90° - \beta$) and b) convex ($\theta > 90° - \beta$) meniscus.

Using the formulas for the volume and the surface area of a cone and a spherical cap from a mathematics handbook such as Harris and Stocker [42], the volume of the liquid and the surface areas for the case of a concave meniscus ($\theta < 90° - \beta$) are:

$$V^L = \frac{\pi}{3} W^2 h - \frac{\pi}{3} h'^2 (3R_1 - h') \tag{4.1}$$

$$A^{SL} = \pi W \sqrt{W^2 + h^2} \tag{4.2}$$

$$A^{LV} = 2\pi R_1 h' \tag{4.3}$$

where

$$\emptyset = \frac{\pi}{2} - (\theta + \beta) \tag{4.4}$$

$$W = R_1 \sin\emptyset \tag{4.5}$$

$$h = \frac{W}{\tan\emptyset} \tag{4.6}$$

$$h' = R_1 - R_1 \cos\emptyset \tag{4.7}$$

Combining equations (4.4) to (4.7) with equations (4.1) to (4.3) results in:

$$V^L = \frac{\pi}{3} {R_1}^3 \left[\frac{\cos^3(\theta + \beta)}{\tan\beta} - 2 + 3\sin(\theta + \beta) - \sin^3(\theta + \beta) \right] \tag{4.8}$$

$$A^{SL} = \pi {R_1}^2 \left[\frac{\cos^2(\theta + \beta)}{\sin\beta} \right] \tag{4.9}$$

$$A^{LV} = 2\pi {R_1}^2[1 - \sin(\theta + \beta)] \tag{4.10}$$

Moreover the area of the solid−vapor interface can be obtained from:

$$A^{SV} = \text{whole solid interface} - A^{SL} \tag{4.11}$$

The next step is calculating dV^L, dA^{SL}, dA^{SV}, and dA^{LV}. When the solid geometry is specified, the contact angle and the principal radii of the curvature are the only independent variables. Hence each of the above derivatives can be written in terms of $d\theta$ and dR_1, considering $R_1 = R_2$ for the liquid−vapour interface which is part of a sphere in this case.

The derivatives are therefore as follows:

$$dV^L = \pi {R_1}^2 \left[\frac{\cos^3(\theta + \beta)}{\tan\beta} - 2 + 3\sin(\theta + \beta) - \sin^3(\theta + \beta)\right] dR_1 + \frac{\pi}{3} {R_1}^3 \left[\frac{-3\cos^2(\theta + \beta)\sin(\theta + \beta)}{\tan\beta} + 3\cos(\theta + \beta) - 3\sin^2(\theta + \beta)\cos(\theta + \beta)\right] d\theta \tag{4.12}$$

$$dA^{SL} = 2\pi R_1 \left[\frac{\cos^2(\theta + \beta)}{\sin\beta}\right] dR_1 - 2\pi {R_1}^2 \left[\frac{\cos(\theta + \beta)\sin(\theta + \beta)}{\sin\beta}\right] d\theta \tag{4.13}$$

$$dA^{SV} = -dA^{SL} \tag{4.14}$$

$$dA^{LV} = 4\pi R_1[1 - \sin(\theta + \beta)]dR_1 - 2\pi {R_1}^2[\cos(\theta + \beta)]d\theta \tag{4.15}$$

Substituting equations (4.12) to (4.15) into equation (3.20), results in the following equation after some rearrangements:

$$\left\{(P^L - P^V)(\pi R_1{}^2)\left[\frac{\cos^3(\theta+\beta)}{\tan\beta} - 2 + 3\sin(\theta+\beta) - \sin^3(\theta+\beta)\right]\right.$$

$$\left. +(\gamma^{SV} - \gamma^{SL})(2\pi R_1)\left[\frac{\cos^2(\theta+\beta)}{\sin\beta}\right] - \gamma^{LV}4\pi R_1[1 - \sin(\theta+\beta)]\right\} dR_1$$

$$+\left\{(P^L - P^V)\frac{\pi}{3}R_1{}^3\left[\frac{-3\cos^2(\theta+\beta)\sin(\theta+\beta)}{\tan\beta} + 3\cos(\theta+\beta) - 3\sin^2(\theta+\beta)\cos(\theta+\beta)\right]\right. \tag{4.16}$$

$$\left. -(\gamma^{SV} - \gamma^{SL})(2\pi R_1{}^2)\left[\frac{\cos(\theta+\beta)\sin(\theta+\beta)}{\sin\beta}\right] + \gamma^{LV}(2\pi R_1{}^2)[\cos(\theta+\beta)]\right\} d\theta = 0$$

For any virtual displacement around equilibrium, equation (4.16) is zero, only when both of the coefficients of dR_1 and $d\theta$ are zero, i.e:

$$(P^L - P^V)(\pi R_1{}^2)\left[\frac{\cos^3(\theta+\beta)}{\tan\beta} - 2 + 3\sin(\theta+\beta) - \sin^3(\theta+\beta)\right]$$

$$+(\gamma^{SV} - \gamma^{SL})(2\pi R_1)\left[\frac{\cos^2(\theta+\beta)}{\sin\beta}\right] - \gamma^{LV}4\pi R_1[1 - \sin(\theta+\beta)] = 0 \tag{4.17}$$

and,

$$(P^L - P^V)\frac{\pi}{3}R_1{}^3\left[\frac{-3\cos^2(\theta+\beta)\sin(\theta+\beta)}{\tan\beta} + 3\cos(\theta+\beta) - 3\sin^2(\theta+\beta)\cos(\theta+\beta)\right]$$

$$-(\gamma^{SV} - \gamma^{SL})(2\pi R_1{}^2)\left[\frac{\cos(\theta+\beta)\sin(\theta+\beta)}{\sin\beta}\right] + \gamma^{LV}(2\pi R_1{}^2)[\cos(\theta+\beta)] = 0 \tag{4.18}$$

Solving these two equations simultaneously to find $(P^V - P^L)$ and $(\gamma^{SV} - \gamma^{SL})$ results in the Laplace–Young equation (2.15) and the Young equation (2.16):

$$P^a - P^b = \frac{2\gamma^{ab}}{R_m} \tag{2.15}$$

where in this case a is vapour phase, b is liquid phase, and R_m is equal to R_1.

$$\gamma^{SV} - \gamma^{SL} = \gamma^{LV} \cos\theta \tag{2.16}$$

In a similar way, for the case of liquid formation with convex liquid−vapour interface ($\theta > 90° - \beta$), with the appropriate equations for the volume of the new phase and surface area of the interfaces, it can be shown that the Laplace−Young equation (2.15) and the Young equation (2.16) are obtained from the conditions for equilibrium.

Table 4-1 presents the equations for the liquid volume and the surface areas that are formed as a result of liquid phase formation from the bulk vapour phase. Although the formula is the same for both cases of concave and convex meniscus, it should be noted that R_1 must be inserted with a negative sign in the case of convex meniscus. This is in accordance with our convention that by defining ΔP as $P^V - P^L$, R_1 would be negative if the center of the circle is on the liquid side. Also in each case, the contact angle would automatically account for the concavity of the liquid−vapour interface.

Table 4-1 Liquid volume and the surface areas for liquid phase formation from the bulk vapour phase in a conical pit.

$V^L = \frac{\pi}{3} {R_1}^3 \left[\frac{\cos^3(\theta+\beta)}{\tan\beta} - 2 + 3\sin(\theta+\beta) - \sin^3(\theta+\beta)\right]$	(4.8)
$A^{SL} = \pi {R_1}^2 \left[\frac{\cos^2(\theta+\beta)}{\sin\beta}\right]$	(4.9)
$A^{LV} = 2\pi {R_1}^2 [1 - \sin(\theta+\beta)]$	(4.10)

The next step is to analyse the stability of the liquid phase being formed out of a vapour phase. From Table 3-6, the equation of the free energy for the liquid formation from bulk vapour phase is:

$$B = B_0 + \frac{2\gamma^{LV}}{R_C} V^L + \left(-\gamma^{LV}\cos\theta\right) A^{SL} + \gamma^{LV} A^{LV} \tag{3.59}$$

For either case of concave or convex meniscus, the liquid volume and the surface areas from Table 4-1 are to be replaced in equation (3.59). For an arbitrary solid material and the fluid of interest, the equilibrium contact angle is considered to be known from experiments. Therefore the radius of curvature of the liquid−vapour interface is the only independent variable in the free energy function, and stability analysis is determined based on the size of this radius, as described in 2.4. In this case where $R_1 = R_2$, the size of the radius of curvature at the equilibrium condition ($R_{1,e}$) can be obtained from solving the following equation:

$$\left(\frac{\partial B}{\partial R_1}\right)_{\theta=\theta_e} = 0 \tag{4.19}$$

where θ_e is the contact angle at equilibrium condition.

The stability of the liquid−vapour interface (stable, unstable, or metastable), can be analysed according to the sign of the second derivative of the free energy with respect to the radius of the curvature at equilibrium condition, i.e. $\left(\frac{\partial^2 B}{\partial {R_1}^2}\right)_{\substack{R_1=R_{1,e}\\ \theta=\theta_e}}$, where the free energy is known from equation (3.59).

$$\left(\frac{\partial^2 \mathrm{B}}{\partial {\mathrm{R}_1}^2}\right)_{\substack{\mathrm{R}_1=\mathrm{R}_\mathrm{C}\\ \theta=\theta_\mathrm{e}}} = 2\pi\gamma^{\mathrm{LV}}\left(\frac{2\cos^3(\theta_\mathrm{e}+\beta)}{\tan\beta} - 2 + 4\sin(\theta_\mathrm{e}+\beta) - 2\sin^3(\theta_\mathrm{e}+\beta) - \cos(\theta_\mathrm{e})\frac{\cos^2(\theta_\mathrm{e}+\beta)}{\sin\beta}\right) \tag{4.20}$$

4.1.1. Stability of the liquid phase being formed from a bulk vapour phase inside a conical pit: concave meniscus

When the meniscus is concave, the centre of the radius of curvature of the liquid−vapour interface is located in the vapour phase, as shown in Figure 4-1. This requires R_1 (= R_2 = R_C) to be positive, according to our convention stated in 2.1.3, where the pressure difference is defined as $\Delta P = P^V - P^L$. The positive R_1, equivalent to positive Kelvin radius, is only possible at vapour pressures below the saturation pressure ($P^V < P_\infty$) according to section 3.7.1.

For vapour pressures less than the saturation pressure for which it is possible to have a concave meniscus, equation (4.20) is always positive. Hence at the equilibrium state, the free energy is a minimum, and the equilibrium state is stable. This stable equilibrium state and the corresponding minimum are shown in Figure

4-2 on the free energy curve vs. scaled size of the curvature ($\frac{R_1}{R_C}$), using Mathematica 8.0 software. This graph is for a solid cone with a half angle of 10° and the equilibrium contact angle equal to zero. Water is selected as the pure component of the liquid and vapour phases at 20°C. Fluid properties at this condition can be obtained from Table 3-7. The vapour pressure is set to be 0.9P∞ (less than the saturation pressure). At these conditions the Kelvin radius of the system is found from equation (2.20) to be 1.02×10^{-8} m.

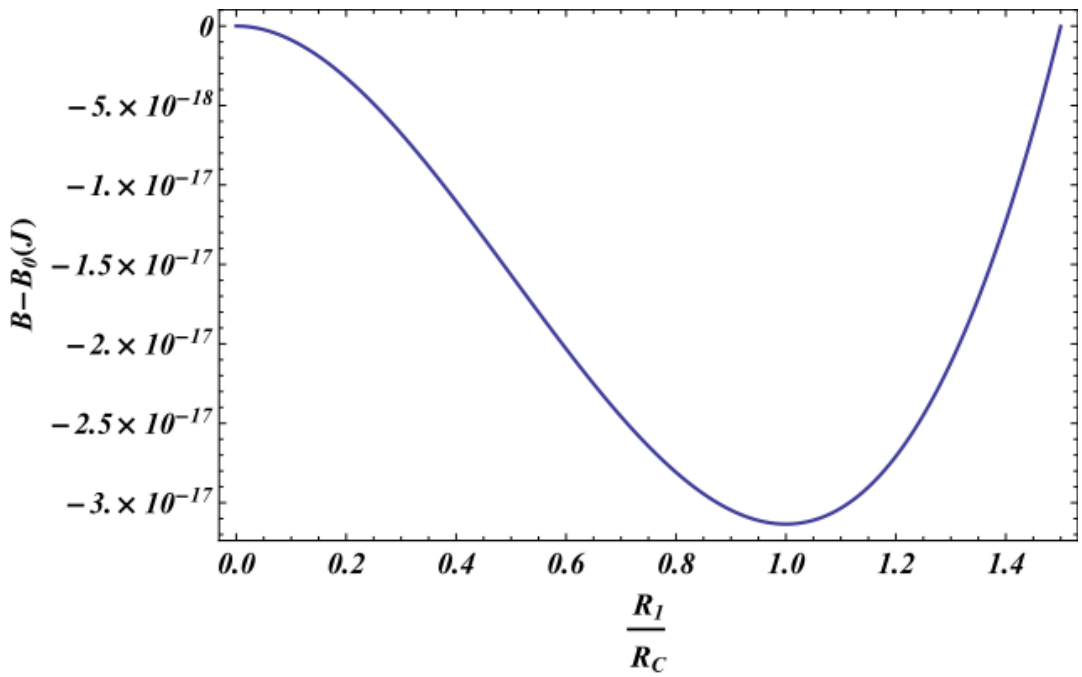

Figure 4-2 Free energy vs. scaled size of the liquid phase formed out of a bulk vapour phase for H_2O at 20°C, $P^V=0.9P_\infty$, contact angle of θ=0° (concave meniscus), and solid half angle of β=10°.

The liquid bridge forms spontaneously since there is no energy barrier (no maximum point) to be overcome, and hence the phase transition is not a nucleation process.

4.1.1.1. Effect of equilibrium contact angle on the stability of the system for liquid phase formation out of a bulk vapour phase inside a conical pit: concave meniscus

This section is dedicated to the impact of the equilibrium contact angle on the energy level and stability of the liquid formation with concave meniscus. The specifications of the system, other than the equilibrium contact angle, are the same as those used for Figure 4-2.

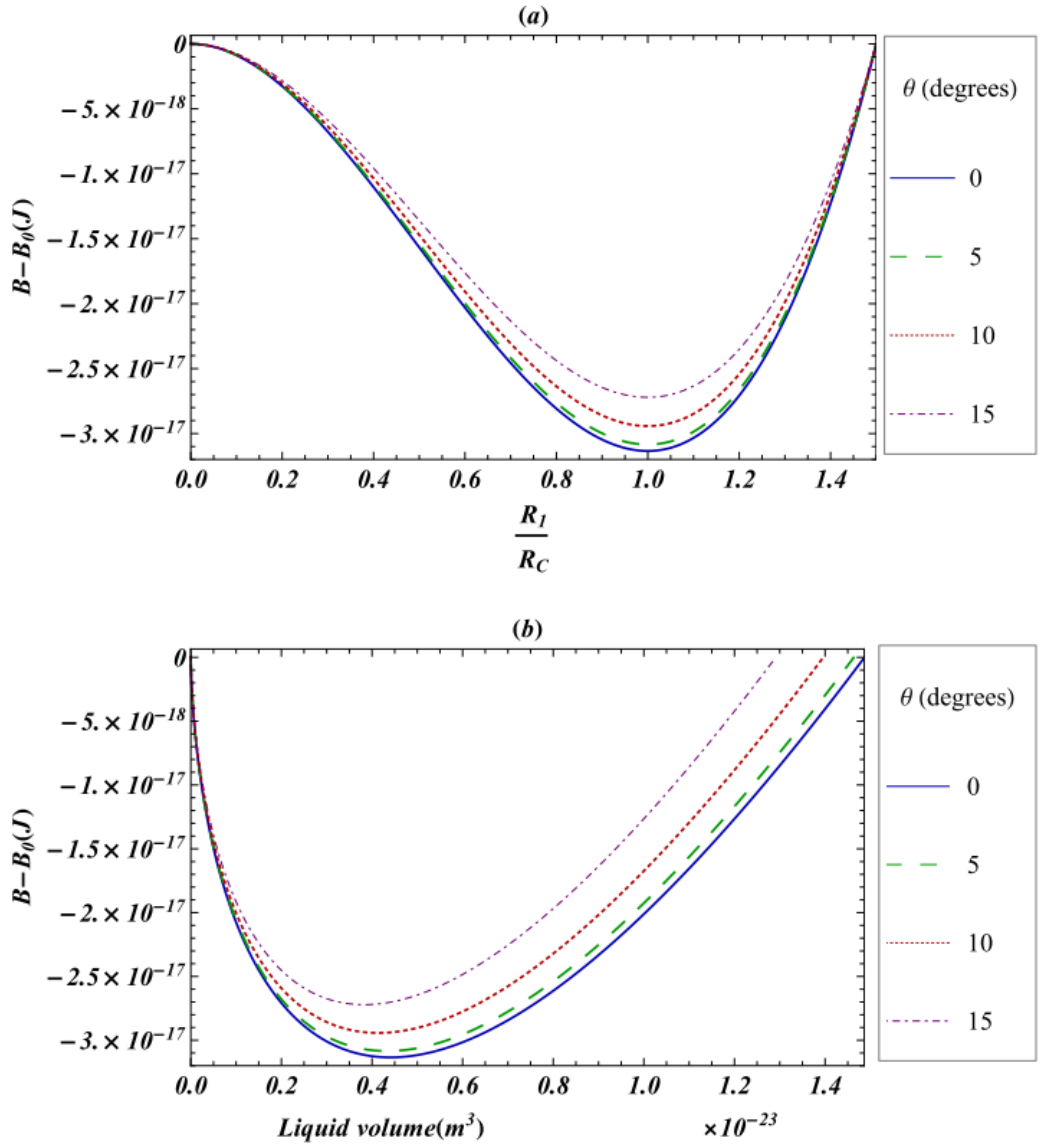

Figure 4-3 Effect of equilibrium contact angle, θ, on the free energy of the liquid phase formed out of a bulk vapour phase for H_2O at 20°C and P^V=0.9P_∞, and solid half angle of β=10°, for various contact angles that result in a concave meniscus: (a) Free energy vs. scaled radius of curvature, (b) Free energy vs. volume of the liquid phase.

It can be seen from Figure 4-3 that as the equilibrium contact angle increases, the free energy minimum becomes shallower (less stable). In Figure 4-3 (b) it is shown that as the equilibrium contact angle increases, a smaller volume of liquid is formed from the bulk vapour phase.

It should be noted that for any equilibrium contact angle, the principal radius of the liquid−vapour interface at the minimum free energy point is R_C, since $R_1=R_2$ due to considering the liquid−vapour interface to be part of a sphere.

Also in Figure 4-3, it can be seen that for the same number of degrees change in contact angle of 5°, the free energy curves of θ=0° and θ=5° have small relative differences, in comparison to the free energy curves of θ=5° and θ=10°. Therefore it is concluded that the effect of a specific number of degrees change in contact angle (5° for example) is more important when the initial equilibrium contact angle is closer to the ***transition contact angle.***

The ***transition contact angle*** for the cone with a half angle of 10° is equal to 80° (90°–10°). For a closer look at this issue, compare the two cases in Figure 4-4.

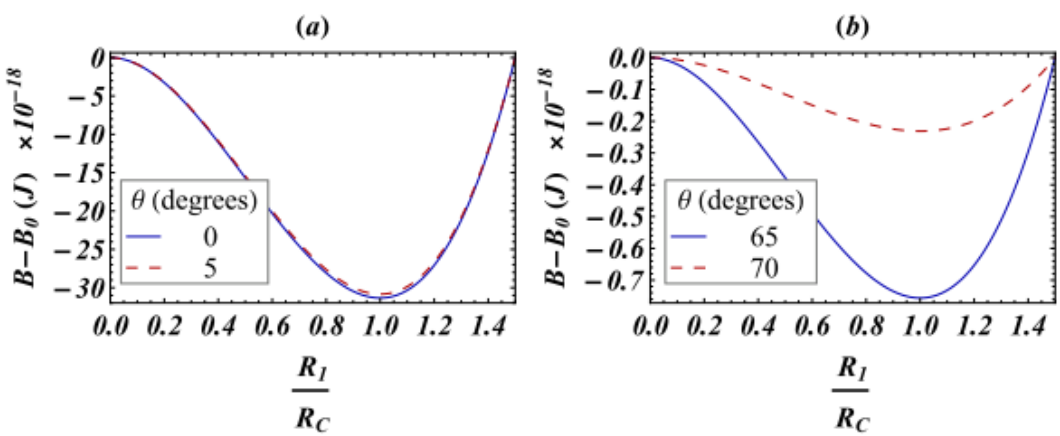

Figure 4-4 Comparing the effect of a certain number of degrees (5°) change in the equilibrium contact angle on the free energy of the system when a liquid phase is formed out of a bulk vapour phase for H_2O at 20°C and $P^V=0.9P_\infty$ and solid half angle of β=10° for various contact angles that result in a concave meniscus. (a) Far from the transition contact angle, (b) Close to the transition contact angle.

The comparison of cases (a) and (b) of Figure 4-4 can be fulfilled through the comparison of the relative difference in the energy level of their extrema. The relative difference is:

$$\left|\frac{\text{Property@ condition 1} - \text{Property @ condition 2}}{\text{Property@ condition 1}}\right| \times 100 \tag{4.21}$$

In part (a) of Figure 4-4, the equilibrium contact angle is changed by 5° from 0° to 10°, both are far from the ***transition contact angle***. As a result the free energy of the minimum point is changed from −31.34 aJ (attojoule) to −30.85 aJ. From equation (4.21) the relative difference in free energy of the minimum point in case (a) is 1.56%.

In part (b) of Figure 4-4, the equilibrium contact angle is changed 5° from 65° to 70°, which are close to the ***transition contact angle.*** In this situation, the free energy of the minimum point is changed from −0.76 aJ to −0.23 aJ. Although the absolute change in free energy is less than case (a), the relative difference for this condition is much higher (69.74%):

This result shows that in the case of $\theta < 90° - \beta$, approximating small contact angles (far from the ***transition contact angle***) with zero is a good approximation in understanding and predicting stability behaviour and also in calculating size of the equilibrium bridge.

4.1.1.2. Effect of the cone apex angle on the stability of the system for liquid formation out of a bulk vapour phase inside a conical pit: concave meniscus

In Figure 4-5, the free energy curve is plotted for three different cone apex angles. Properties other than the cone apex angle are kept the same as the properties in Figure 4-2.

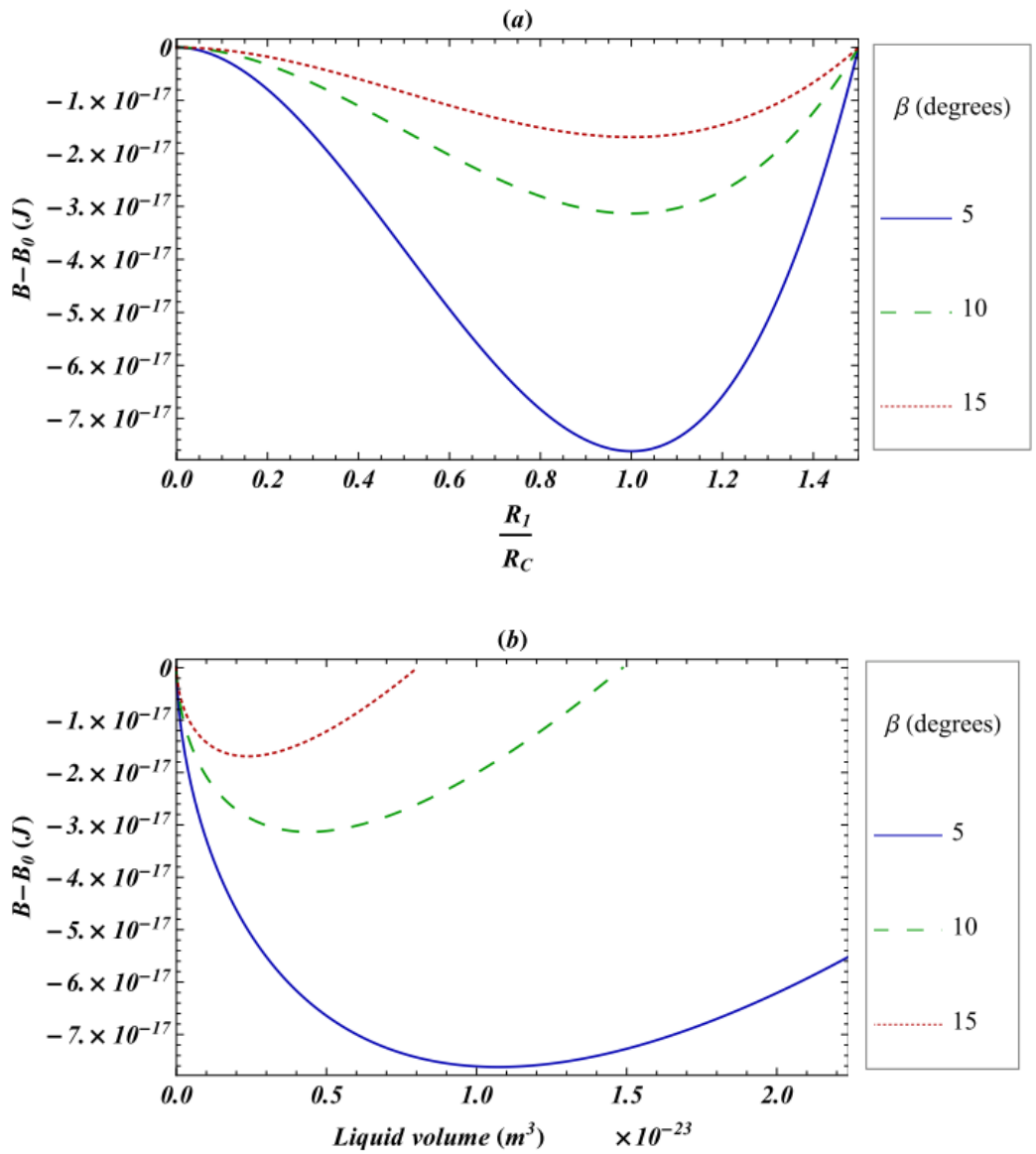

Figure 4-5 Effect of cone apex angle on the free energy of the system when a liquid phase is formed out of a bulk vapour phase for H_2O at 20°C and P^V=0.9P_∞ and θ=0° (concave meniscus). (a) Free energy vs. scaled radius of curvature, (b) Free energy vs. volume.

In Figure 4-5, the free energy minimum is more stable (deeper) for the smaller cone apex angle. Thus liquid formation out of the bulk vapour in a conical pit with a solid material such that $\theta < 90° - \beta$ becomes more stable as the cone apex angle decreases. Due to considering the liquid−vapour interface to be part of a sphere, for any cone apex angle, the equilibrium radius of curvature is always the same and

equal to the Kelvin radius (Figure 4-5(a)). On the other hand as shown in Figure 4-5(b), at smaller cone apex angle, a higher volume of the liquid must be formed to meet the stable equilibrium condition and reach the Kelvin radius (R_C).

4.1.2. Stability of the liquid phase being formed from a bulk vapour phase inside a conical pit: convex meniscus

From geometrical considerations the convex meniscus is only possible if $\theta > 90° - \beta$, and the principal radii of curvature are negative (located on the liquid side) when the pressure difference is defined as $P^V - P^L$, as illustrated in Figure 4-1.The negative R_1, equivalent to negative Kelvin radius, is only possible at vapour pressures above the saturation pressure ($P^V > P_\infty$) according to section 3.7.1.

To analyse the stability of the liquid being formed, the sign of $\left(\frac{\partial^2 B}{\partial {R_1}^2}\right)_{\substack{R_1=R_C \\ \theta=\theta_e}}$ is to be determined. For $\theta > 90° - \beta$, equation (4.20) is always negative. Therefore the free energy would be maximum at the equilibrium condition, denoting an unstable equilibrium. Figure 4-6 represents this unstable equilibrium state. This graph is for a solid cone with the half angle of 10° and the equilibrium contact angle equal to 180°. Water is chosen as the pure component at 20°C. Fluid properties at this condition can be obtained from Table 3-7. The vapour pressure, that should be higher than saturation pressure, is considered to be $1.1P_\infty$. For these conditions, the Kelvin radius is -1.13×10^{-8} m from equation (2.20) where the negative sign indicates that the center of the radius is located on the liquid side.

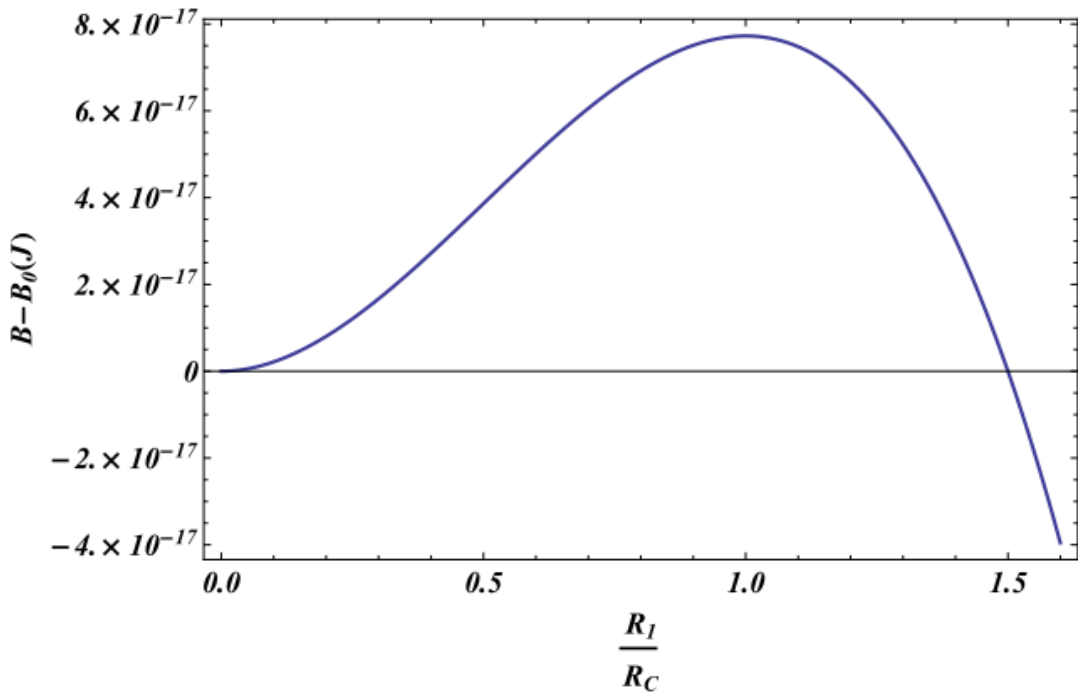

Figure 4-6 Free energy vs. scaled size of liquid phase formed out of a bulk vapour phase for H_2O at 20°C and $P^V=1.1P_\infty$, contact angle of θ=180° (convex meniscus), and solid half angle of β=10°.

This maximum in the free energy represents the energy barrier that must be overcome for the new phase to be formed. Therefore the phase transition is a nucleation phenomenon. Passing the maximum point, the curve is ever decreasing, and no minimum point exists. This means that all the vapour phase would turn into liquid, once the barrier is overcome.

4.1.2.1. Effect of equilibrium contact angle on the stability of the system for liquid phase formation out of a bulk vapour phase inside a conical pit: convex meniscus

The effect of the equilibrium contact angle on the free energy of the liquid formation with convex meniscus is investigated in this section. Other than the equilibrium contact angle, the system has the same specifications as those for Figure 4-6.

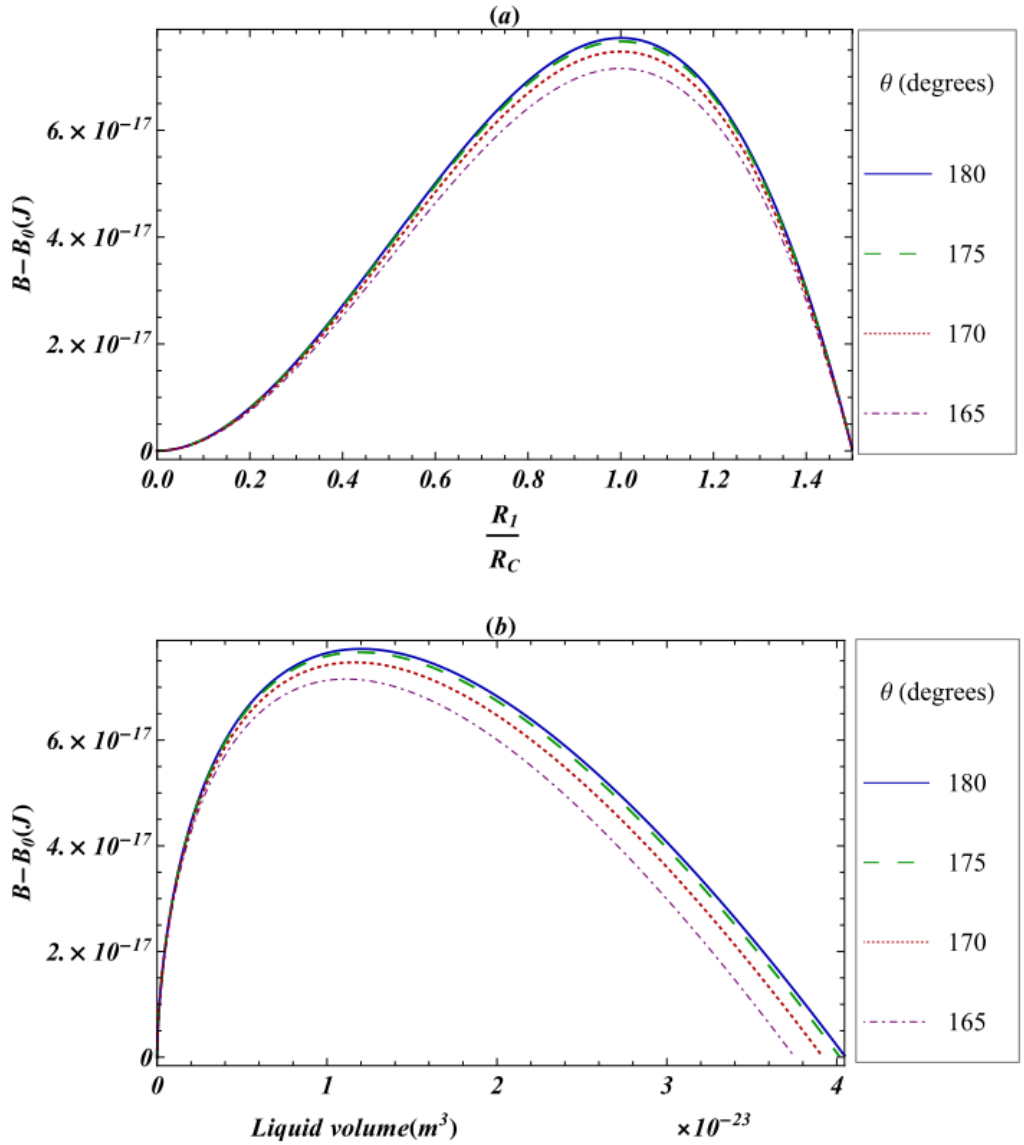

Figure 4-7 Effect of equilibrium contact angle on the free energy vs. volume of the liquid phase formed out of a bulk vapour phase for H_2O at 20°C and $P^V=1.1P_\infty$, and solid half angle of β=10°, for various contact angles that result in a convex meniscus. (a) Free energy vs. scaled radius of curvature, (b) Free energy vs. volume of the liquid phase.

As the equilibrium contact angle decreases, the free energy barrier becomes smaller and the unstable equilibrium is formed with less amount of liquid volume.

Also it can be seen in Figure 4-7 that, similarly to the previous case, the effect of specific changes in contact angle is less important when the initial equilibrium

contact angle is far from the ***transition contact angle.*** As mentioned in section 4.1.1.1 the ***transition contact angle*** for the cone with the half angle of 10° is equal to 80°. For better clarity, a certain number of degrees change in contact angle for two conditions of far from, and close to, the ***transition contact angle*** is examined in Figure 4-8:

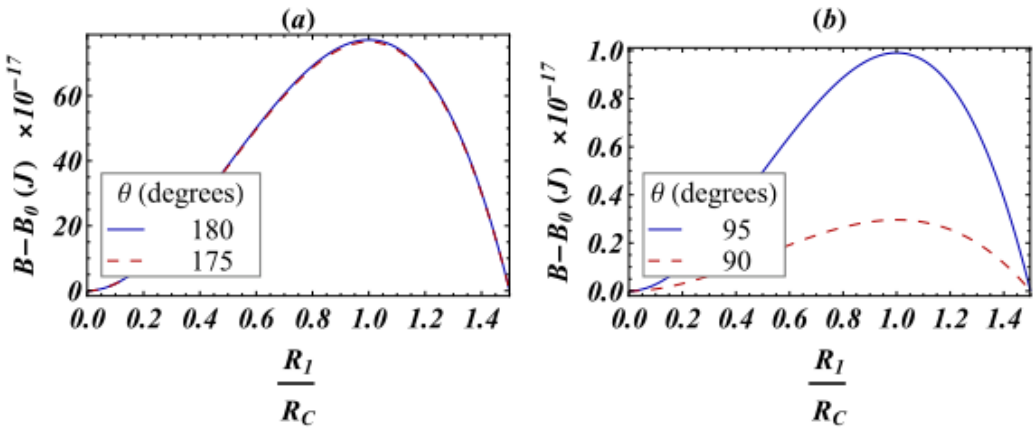

Figure 4-8 Comparing the effect of a certain number of degrees (5°) change in the equilibrium contact angle on the free energy of the system when a liquid phase is formed out of a bulk vapour phase for H_2O at 20°C and $P^V=1.1P_\infty$ and solid half angle of β=10° for various contact angles that result in a convex meniscus. (a) Far from the transition contact angle, (b) Close to the transition contact angle.

In Figure 4-8 (a) the equilibrium contact angle changes from 180° to 175°, with both being far from the transition contact angle. The free energy of the maximum point changes from 77.26 aJ to 76.62 aJ. The relative difference in the free energy of the maximum point is 0.83% from equation (4.21). In Figure 4-8 (b) the equilibrium contact angle changes from 95° to 90°, with both being close to the ***transition contact angle.*** The free energy of the maximum point changes from 0.99 aJ to 0.30 aJ, with a relative difference of 69.70% from equation (4.21).

This shows that a certain amount of error in measuring the contact angle has a greater impact for contact angles close to the ***transition contact angle***. The focus of

this conclusion is the relative difference of the energy barrier; however in this particular case of Figure 4-8 both the absolute and relative changes in the free energy were larger near the ***transition contact angle***.

4.1.2.2. Effect of cone apex angle on the stability of the system for liquid phase formation out of a bulk vapour phase inside a conical pit: convex meniscus

In Figure 4-9 the free energy curve is plotted for three different cone apex angles. Properties other than the cone apex angle are kept the same as for the first case of section 4.1.2 (Figure 4-6) .

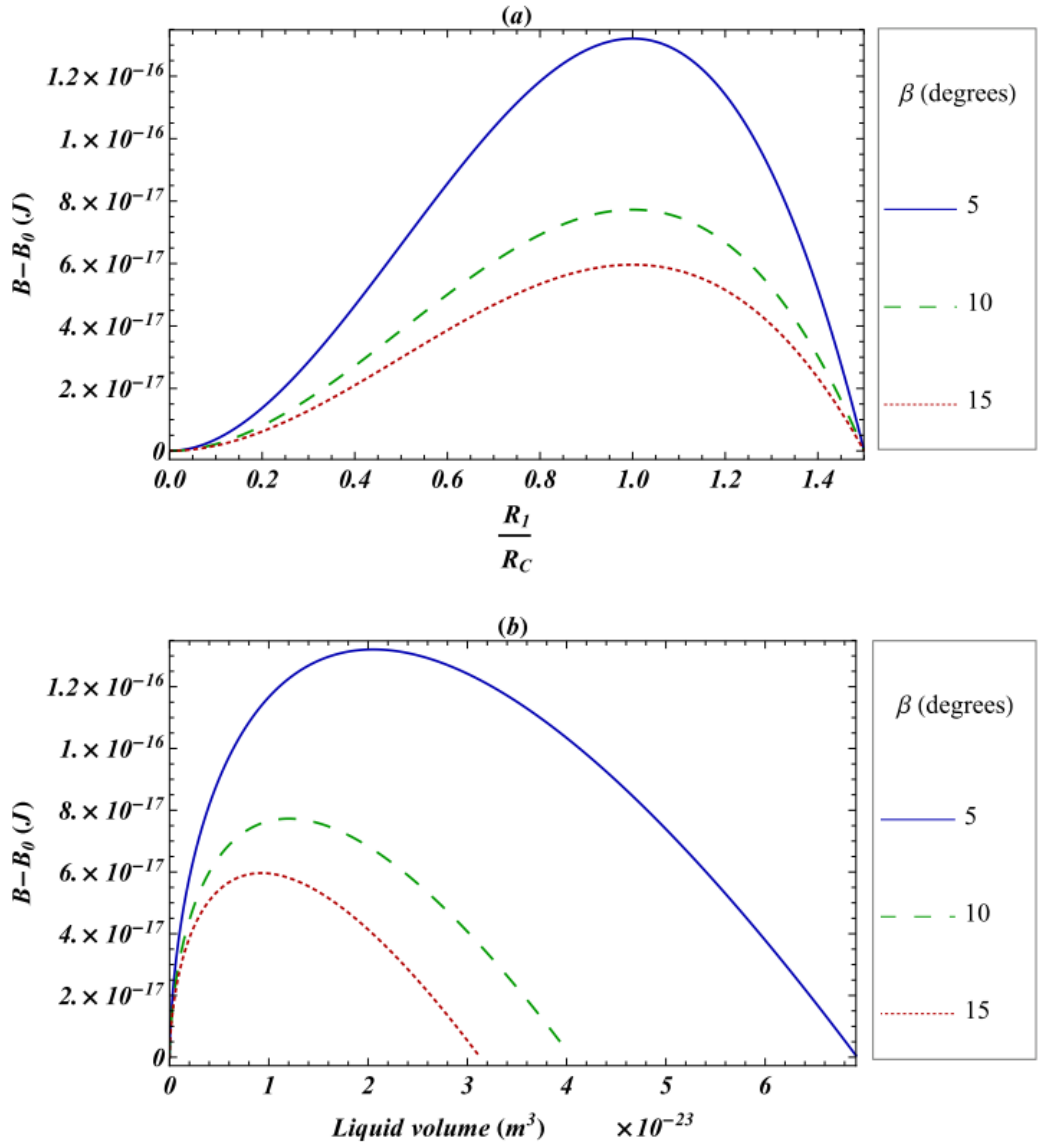

Figure 4-9 Effect of cone apex angle on the free energy of the system when a liquid phase is formed out of a bulk vapour phase for H_2O at 20°C and P^V=1.1P_∞ and θ=180° (convex meniscus). (a) Free energy vs. scaled radius of curvature, (b) Free energy vs. volume.

According to Figure 4-9, a higher energy barrier must be overcome for the smaller cone apex angle. Thus liquid formation out of the bulk vapour phase in the cone of the solid material that enforces $\theta > 90° - \beta$, becomes less favourable as the apex cone apex angle decreases. Considering the liquid−vapour interface as part of a sphere, for any cone apex angle the equilibrium radius of curvature is always the

same and equal to the Kelvin radius, as shown in Figure 4-9 (a). Also as shown in Figure 4-9 (b), as cone apex angle gets smaller, a higher volume of the liquid must be formed and fill the cone before getting to the unstable condition (the Kelvin radius).

4.2. Vapour phase formation from a bulk liquid phase inside a conical pit

The constraints of the system in which vapour is formed out of a bulk liquid phase are as shown in Table 3-3. The conditions for equilibrium are as presented in Table 3-4 (b), for the *curved* solid interfaces (equations (3.22) to (3.26)).

The liquid−vapour interface is considered to be part of a sphere, using the same justifications as in section 4.1. The notations that are assigned to describe the geometry of the problem are presented in Figure 4-10. It should be noted that the contact angle is being measured from the liquid side, as set by convention. By this convention, the ***transition contact angle*** in the case of vapour formation inside a cone with cone apex angle 2β is equal to $90° + \beta$. The meniscus is concave if $\theta > 90° + \beta$ and is convex if $\theta < 90° + \beta$.

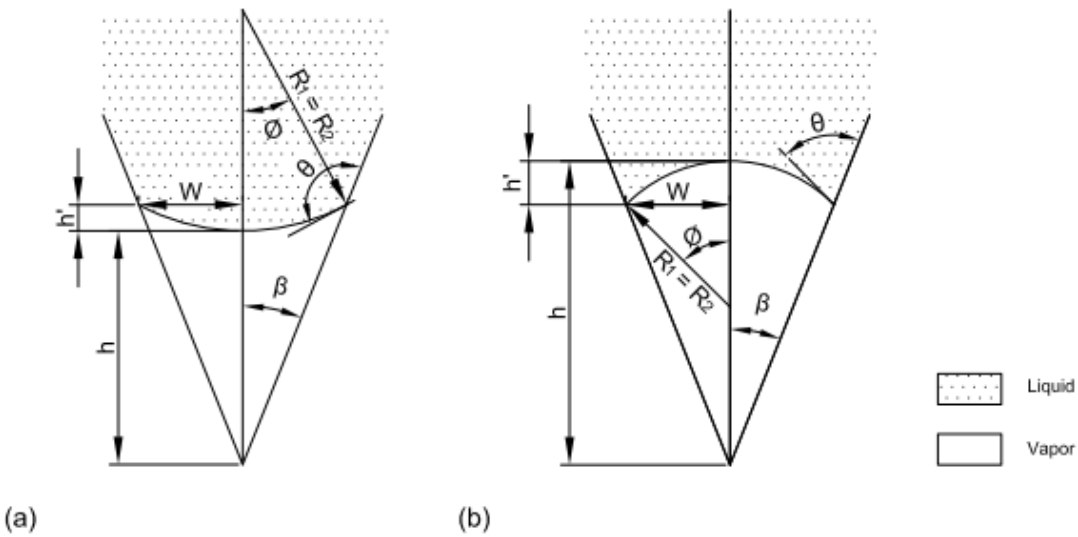

Figure 4-10 Schematic of liquid formation inside a conical pit and the definition of cone apex angle 2β, contact angle θ, principal radii of curvature R_1=R_2, radius of the three−phase contact circle W, height of interface h, distance between the highest and the lowest parts of the liquid−vapour interface h′, and half−filling angle of the new phase ∅, for cases of a) concave ($\theta > 90° + \beta$) and b) convex ($\theta < 90° + \beta$) meniscus.

Relations for the volume of the vapour phase and the surface areas are presented in the following table, having been derived from the formulas of volume and surface area of a cone and a spherical cap [42]. The radius R_1 should be inserted with the appropriate sign in each case, i.e. positive sign for the concave meniscus ($\theta > 90° + \beta$) and negative for the convex meniscus ($\theta < 90° + \beta$) when ΔP is defined as $P^L - P^V$.

Table 4-2 Vapour volume and the surface areas for vapour phase formation from the bulk liquid phase in a conical pit.

$V^V = \frac{\pi}{3} {R_1}^3 \left[\frac{-\cos^3(\theta-\beta)}{\tan\beta} - 2 + 3\sin(\theta-\beta) - \sin^3(\theta-\beta)\right]$	(4.22)
$A^{SL} = \pi {R_1}^2 \left[\frac{\cos^2(\theta-\beta)}{\sin\beta}\right]$	(4.23)
$A^{LV} = 2\pi {R_1}^2 [1 - \sin(\theta-\beta)]$	(4.24)

To analyse the stability of the vapour phase being formed out of the liquid, the vapour volume and surface areas are to be replaced in the equation for free energy in Table 3-6. It should be noted that the pressure difference is defined as $P^L - P^V$ here.

Once the solid material is known, the equilibrium contact angle is assumed to be fixed, and free energy is only a function of the principal radii of curvature. The size of the principal radii of curvature at the equilibrium condition can either be obtained from the extermum of the curve of free energy vs. size of the new phase, or by solving equation (4.19), as was stated in part 4.1. Again for this case where the liquid−vapour interface is considered to be part of a sphere, R_1 is equal to R_2, and both are equal to the Kelvin radius.

The second derivative of free energy with respect to the principal radius of curvature is derived for this case of vapour formation out of the bulk liquid phase. The stability of the vapour phase being formed out of the liquid phase can be determined based on the sign of this expression.

$$\left(\frac{\partial^2 B}{\partial {R_1}^2}\right)_{\substack{R_1=R_C \\ \theta=\theta_e}} = 2\pi\gamma^{LV}\left(\frac{-2\cos^3(\theta_e-\beta)}{\tan\beta} - 2 + 4\sin(\theta_e-\beta) - 2\sin^3(\theta_e-\beta) + \cos(\theta_e)\frac{\cos^2(\theta_e-\beta)}{\sin\beta}\right) \quad (4.25)$$

4.2.1. Stability of the vapour phase being formed from a bulk liquid phase inside a conical pit: concave meniscus

In the case of vapour formation with a concave meniscus $\theta > 90° + \beta$, with the pressure difference being defined as $P^L - P^V$, R_1 (= R_2 = R_C) is to be positive due to its center being located in the liquid phase, as shown in Figure 4-10. Positive R_1, equivalent to positive Kelvin radius, is only possible at liquid pressures above the saturation pressure ($P^L > P_\infty$) according to section 3.7.1.

In this case where $\theta > 90° + \beta$, equation (4.25) is always positive. This positive sign indicates that the extremum in the free energy of the system will be a minimum, as shown in Figure 4-11. Therefore the equilibrium condition of the system is stable. Figure 4-11 is for the case where the half angle of the solid cone is chosen to be 10° and the solid is made up of a material such that the equilibrium contact angle is 180°. The pure fluid in the system is H_2O at 20°C, with the fluid properties given in Table 3-7. The liquid pressure is set to be $1.1P_\infty$. The Kelvin radius of the system is 6.22×10^{-4} m from equation (2.23).

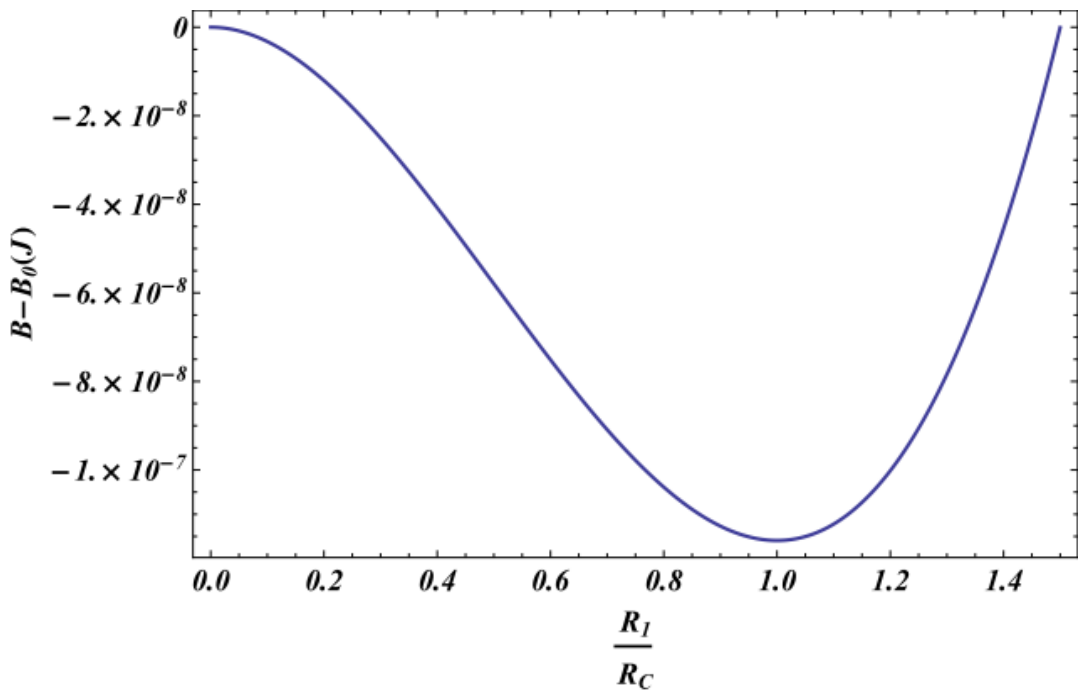

Figure 4-11 Free energy vs. scaled size of vapour phase formed out of a bulk liquid phase for H_2O at 20°C and $P^L=1.1P_\infty$, contact angle of θ=180° (concave meniscus), and solid half angle of β=10°.

No energy barrier is to be overcome to reach the stable equilibrium condition, as shown in Figure 4-11. Therefore the vapour phase formation out of the liquid phase is not a nucleation phenomenon in the case of concave meniscus.

4.2.1.1. Effect of equilibrium contact angle on the stability of the system for vapour phase formation out of a bulk liquid phase inside a conical pit: concave meniscus

The impact of the equilibrium contact angle is investigated for systems with the same properties as those in Figure 4-11, except that the equilibrium contact angle is changing.

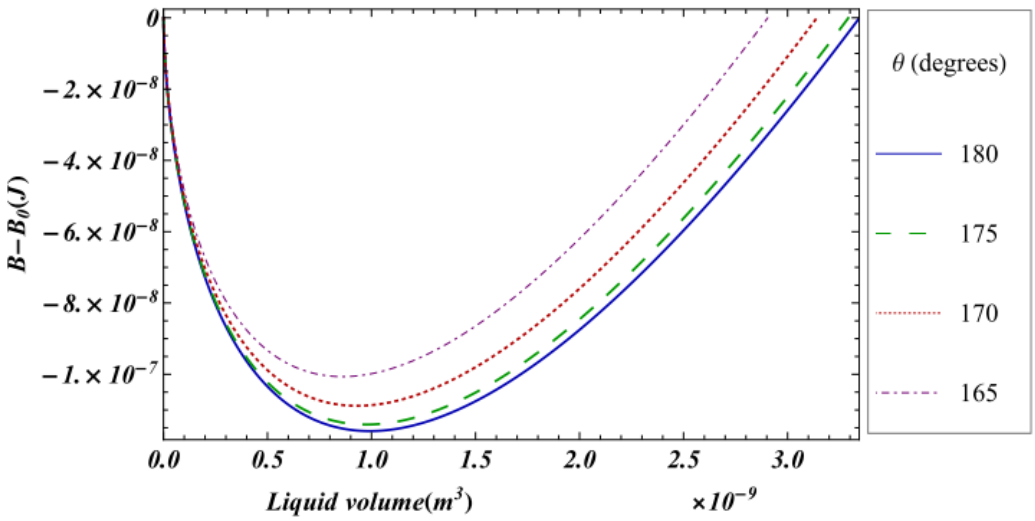

Figure 4-12 Effect of equilibrium contact angle on the free energy vs. volume of the vapour phase formed out of a bulk liquid phase for H_2O at 20°C and P^L=1.1P_∞ and solid half angle of β=10°, for various contact angles that results in a concave meniscus.

As the equilibrium contact angle gets smaller (gets closer to the ***transition contact angle***), while it is kept above $90° + \beta$, the stable equilibrium condition becomes less stable, with less volume of vapour being formed.

Also it can be seen in Figure 4-12 that for the same number of degrees change in the equilibrium contact angle (5° here) , the changes cause greater relative difference when the contact angle is closer to the ***transition contact angle***, which *is* $90° + \beta$.

4.2.1.2.Effect of cone apex angle on the stability of the system for vapour phase formation out of a bulk liquid phase inside a conical pit: concave meniscus

The effect of cone apex angle is being investigated for the same system as Figure 4-11, with different cone apex angles.

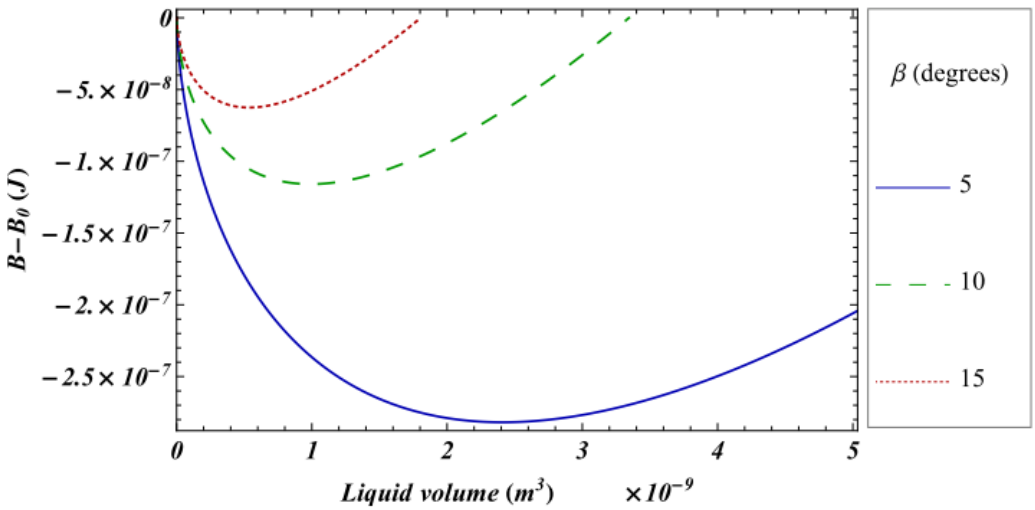

Figure 4-13 Effect of cone apex angle on the free energy vs. volume of the vapour phase formed out of a bulk liquid phase for H_2O at 20°C and P^L=1.1P_∞ and θ=180° (concave meniscus).

The cone with the smaller apex angle results in the more stable equilibrium condition, with a higher volume of the new phase, i.e. the vapour phase, at equilibrium.

4.2.2. Stability of the vapour phase being formed from a bulk liquid phase inside a conical pit: convex meniscus

As shown in Figure 4-10, the principal radius of curvature R_1 (= R_2 = R_C) is negative for the case of vapour formation out of a bulk liquid phase, with the pressure difference is defined as $P^L - P^V$. For the radius R_1, and equivalently the Kelvin radius, the bulk liquid pressure must be less than the saturation pressure ($P^L < P_\infty$) according to section 3.7.1.

For the meniscus to be convex, the equilibrium contact angle must be in the range of $\theta < 90° + \beta$, which results in equation (4.25) being always negative. The

negative sign in the second derivative of the free energy corresponds to a maximum point indicating an unstable equilibrium state, as presented in Figure 4-14. For Figure 4-14, the half angle of the solid cone is chosen to be 10° and the solid is made up of a material such that the equilibrium contact angle is 0°. The pure fluid component is H_2O at 20°C, with its properties as presented in Table 3-7. The liquid pressure is chosen to be $0.9P_{\infty}$, for which the Kelvin radius of the system is -6.22×10^{-4} m from equation (2.23).

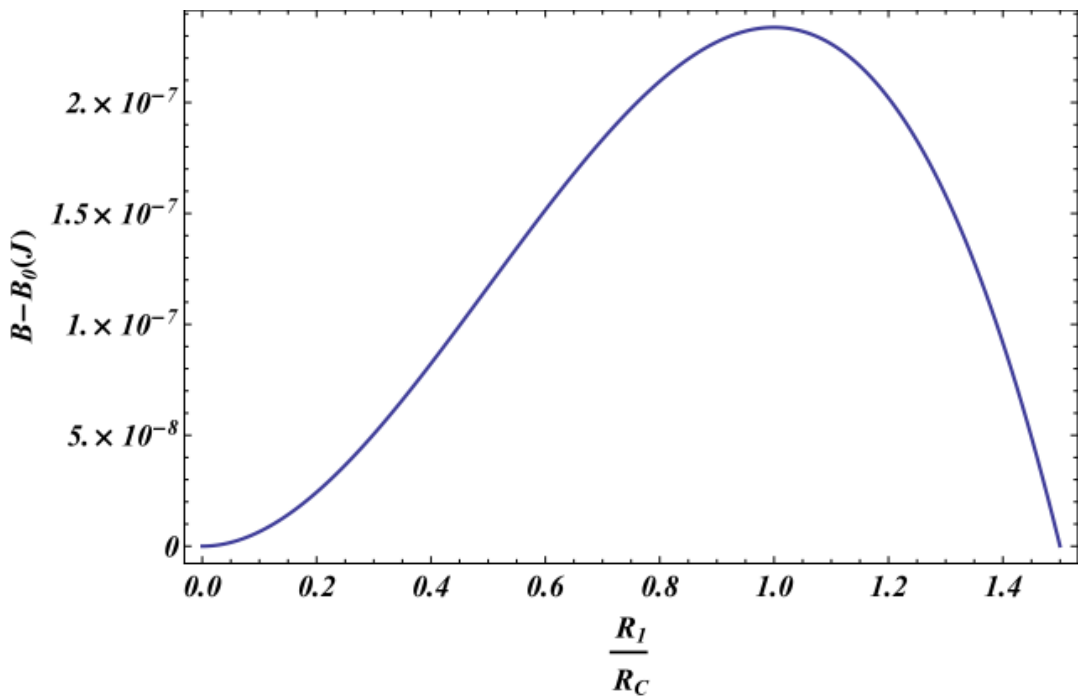

Figure 4-14 Free energy vs. scaled size of the vapour phase formed out of a bulk liquid phase for H_2O at 20°C and $P^L=0.9P_{\infty}$, contact angle of θ=0° (convex meniscus), and solid half angle of β=10°.

The maximum in the free energy represents the barrier to be overcome for the nucleation of a vapour phase out of a bulk liquid phase. Passing the maximum point, the ever descending curve shows the spontaneous change of all liquid into vapour, once the barrier is overcome.

4.2.2.1. Effect of equilibrium contact angle on the stability of the system for vapour phase formation out of a bulk liquid phase inside a conical pit: convex meniscus

The free energy curve is shown for different equilibrium contact angles, in the system with the same characteristics as the one in Figure 4-14.

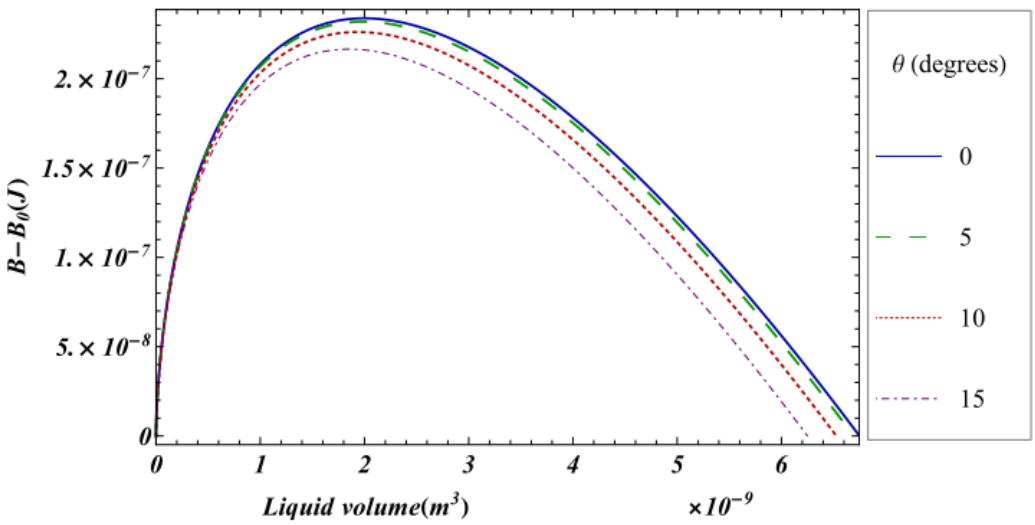

Figure 4-15 Effect of equilibrium contact angle on the free energy vs. volume of the vapour phase formed out of a bulk liquid phase for H_2O at 20°C and P^L=0.9P_∞ and solid half angle of β=10°, for various contact angles that result in a convex meniscus.

It can be seen in the above figure that the smaller the equilibrium contact angle, the higher would be the barrier to be overcome. Also far from the transition contact angle $90° + \beta$, the effect of changes in the contact angle is negligible.

4.2.2.2. Effect of cone apex angle on the stability of the system for vapour phase formation out of a bulk liquid phase inside a conical pit: convex meniscus

The same system as the one in Figure 4-14 is chosen, and the free energy for different cone apex angles is presented in Figure 4-16.

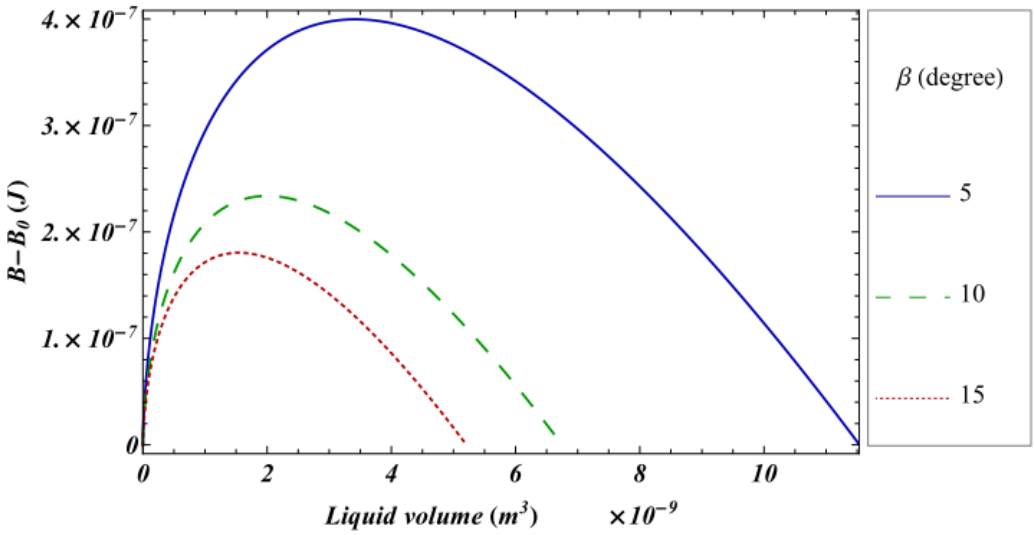

Figure 4-16 Effect of cone apex angle on the free energy vs. volume of the vapour phase formed out of a bulk liquid phase for H_2O at 20°C and $P^L=0.9P_\infty$ and θ=0° (convex meniscus).

According to the above figure, a higher energy barrier is to be overcome for the vapour phase to be formed in the cone with the smaller apex angle. Also as the apex angle gets smaller, a higher volume of the vapour must be formed to meet the unstable equilibrium condition.

4.3. Conclusion

In this chapter the liquid−vapour system inside a conical pit was studied under the condition of constant bulk phase pressure and constant mass. Gravitational effects have been neglected which is reasonable based on the explanations of section 3.2 .

There are two possible systems with a liquid−vapour interface inside a conical pit (or any other geometry): (1) liquid formation from a bulk vapour phase (section 4.1) and (2) vapour formation from a bulk liquid phase (section 4.2). Each of these cases might have a concave outward or a convex outward interface.

Thermodynamic stability analysis was performed on each of these cases. Also the effects of the solid geometry parameters (cone apex angle) and the contact angle on the stability of the system were investigated.

The following table is a summary of what has been discussed in sections 4.1 and 4.2.

Table 4-3 Summary of liquid phase formation out of a bulk vapour phase and vapour phase formation out of a bulk liquid phase inside a conical pit with a half apex angle of β, and effect of the involved parameters. In this table θ denotes the equilibrium contact angle being measured from inside the denser phase (liquid), θ_t is the *transition contact angle*, R_1 (= R_2) is the principal radius of curvature of the liquid-vapour interface, P^L denotes the liquid pressure, and P^V is the vapour pressure.

Case		Definition of ΔP	Sign of R_1 (=R_2=R_C) based on ΔP definition	Bulk pressure	Equilibrium state	Increase in θ	Increase in β
Liquid Formation from vapour ($\theta_t = 90° - \beta$)	Concave ($\theta < 90° - \beta$)	$P^V - P^L$	+	$P^V < P_\infty$	1 stable	~ Closer to θ_t →Less stability	→Less stability
	Convex ($\theta > 90° - \beta$)	$P^V - P^L$	–	$P^V > P_\infty$	1 unstable	~ Farther from θ_t →Larger barrier	→Smaller barrier
Vapour formation from liquid ($\theta_t = 90° + \beta$)	Concave ($\theta > 90° + \beta$)	$P^L - P^V$	+	$P^L > P_\infty$	1stable	~ Farther from θ_t →More stability	→Less stability
	Convex ($\theta < 90° + \beta$)	$P^L - P^V$	–	$P^L < P_\infty$	1 unstable	~ Closer to θ_t →Smaller barrier	→Smaller barrier

From what has been discussed, it can be concluded that for formation of liquid from a bulk vapour phase, or vapour from a bulk liquid phase inside a conical pit:

1) For any new phase, with the liquid−vapour interface being considered as part of a sphere, there exists one and only one equilibrium state (either stable or unstable), and for that equilibrium state $R_{1,e} = R_{2,e} = R_C$.

   This is due to the fact that when the liquid−vapour interface is part of a sphere, then $R_1 = R_2$ and for these radii to satisfy equation (2.21), the principal radii of the curvature are to be equal to the Kelvin radius.

2) If only one unstable condition (maximum point) exists in the free energy curve vs. the size of the new phase, the curve would be ever descending after that unstable point. In this situation all of the bulk phase would change into the new phase once the nucleation barrier is overcome.

3) In the formation of liquid from a bulk vapour phase inside a conical pit, one of the following would happen based on the solid material:

   - For wettable solid materials where the meniscus is concave ($\theta < 90° - \beta$), liquid formation would be a spontaneous non−nucleating phenomena, filling the conical pit up to the stable equilibrium size. Such a concave meniscus can only exists at $P^V < P_\infty$ and this phenomenon is called capillary condensation [1].
   - For non−wettable solid materials where the meniscus is convex ($\theta > 90° - \beta$), liquid formation is a nucleation phenomena, i.e. phase transfer happens once some energy barrier is overcome. After passing the nucleation barrier,

all the vapour phase would condense into the liquid. Such a convex meniscus can only exists at $P^V > P_\infty$.

4) In the formation of vapour from a bulk liquid phase inside a conical pit, one of the following would happen based on the solid material:

- For non−wettable solid materials where the meniscus is concave ($\theta > 90° + \beta$), vapour formation would be a spontaneous non−nucleating phenomena, filling the conical pit up to the stable equilibrium size. Such a concave meniscus can only exists at $P^L > P_\infty$ and this phenomenon is called capillary evaporation [1].
- For wettable solid materials where the meniscus is convex ($\theta < 90° + \beta$), vapour formation is a nucleation phenomena and would happen only once the nucleation barrier is overcome. After passing the energy barrier all the liquid phase would evaporate into the vapour. Such a convex meniscus can only exists at $P^L < P_\infty$.

5) Effect of the contact angle:

- When the meniscus is concave, getting farther from the ***transition contact angle*** results in more stability of the stable equilibrium condition. The meniscus is concave for $\theta < 90° - \beta$ and $P^V < P_\infty$ in the case of liquid formation from a bulk vapour phase, and for $\theta > 90° + \beta$ and $P^L > P_\infty$ in the case of vapour formation from a bulk liquid phase.

  In the case of liquid formation with a concave meniscus from a bulk vapour phase, decrease of the contact angle results in getting farther from the ***transition contact angle***. For vapour formation with a concave meniscus

from a bulk liquid phase, increasing the contact angle is equivalent to getting farther from the ***transition contact angle***.

Translating the changes in the contact angle into getting farther from the ***transition contact angle*** unifies the description of the liquid formation and vapour formation cases which otherwise would be different due to the convention of measuring the contact angle from the liquid side.

- When the meniscus is convex, getting farther from the ***transition contact angle*** increases the amount of the energy barrier. The meniscus is convex for $\theta > 90° - \beta$ and $P^V > P_\infty$ in the case of liquid formation from a bulk vapour phase, and for $\theta < 90° + \beta$ and $P^L < P_\infty$ in the case of vapour formation from a bulk liquid phase. In the case of liquid formation with a convex meniscus from a bulk vapour phase, increase of the contact angle results in getting farther from the ***transition contact angle***. For vapour formation with a convex meniscus from a bulk liquid phase decreasing the contact angle is equivalent to getting farther from the ***transition contact angle***.

6) A certain number of degrees change in the equilibrium contact angle has more effect on the free energy curve and the volume of the new phase, when the contact angle is close to the ***transition contact angle.***

7) Effect of the cone apex angle:

- In the case of a concave meniscus (liquid formation or vapour formation), the conical solid with greater cone apex angle creates a less stable equilibrium state.

- In the case of a convex meniscus (liquid formation or vapour formation), the conical solid with greater cone apex angle results in a smaller energy barrier.

5. Liquid−vapour system between two flat plates

In this chapter fluid confined in the gap between two flat plates is investigated. The focus of this study is a pure fluid system of constant mass and constant pressure (imposed by the reservoir). For this geometry, the solid−liquid and solid−vapour interfaces are *flat*. When the upper and lower plates are both of the same material, the liquid−vapour interface should meet the solid surfaces at identical contact angles at any contacts.

Thermodynamic stability analysis is performed for both cases of liquid formation out of a bulk vapour phase (section 5.1), and vapour formation out of a bulk liquid phase (section 5.2), using the equations and definitions of chapter 3. For any vapour−liquid system the meniscus may either be concave or convex. Sections 5.1.1 and 5.1.2 discuss liquid formation with concave and convex menisci respectively. For vapour formation, concave and convex menisci are explained in sections 5.2.1 and 5.2.2 respectively. The effects of different parameters on the stability of these liquid−vapour systems are studied. Sections 5.1.1.1, 5.1.2.1, 5.2.1.1, and 5.2.2.1 are about the impact of the contact angle. How the distance between the two flat plates affects the stability of the liquid−vapour system is explained in sections 5.1.1.2, 5.1.2.2, 5.2.1.2, and 5.2.2.2. In section 5.3 all of these

investigations are put together and conclusively show the complete picture of different liquid−vapour systems between two flat plates and the effects of equilibrium contact angle and plate separation distance on the stability of the system.

5.1. Liquid phase formation from a bulk vapour phase between two flat plates

The constraints on the system when liquid is being formed between two *flat* plates can be found in Table 3-2. Conditions for equilibrium are to be obtained from Table 3-4 (a) in which the last stated equation (equation (3.26)) leads to the Laplace−Young equation (equation (2.13)) and the Young equation (equation (2.16)).

Due to the small size of the newborn liquid phase compared with the capillary length (from equation (3.2)), the gravitational force is assumed to be negligible compared to the surface forces. Ignoring gravitational effects implies constant pressure in both the liquid and the vapour phases. Then according to the Kelvin equation (equation (2.20)), the liquid−vapour interface is to be a surface of constant curvature, i.e. R_1 and R_2 are to be such that R_m in equation (2.14) is constant at any point. Through the numerical computation of the shape of the liquid−vapour interface at equilibrium, the liquid−vapour interface of a liquid bridge has been shown to be accurately approximated by a toroidal surface when the liquid bridge half width is equal to or greater than 6.5 times the Kelvin radius (R_C) [18]. That simulation was performed for the case of a liquid bridge between a flat plate and a

sphere, for various sphere sizes. The case of a liquid bridge between two planar plates is equivalent to the case of a liquid bridge between a sphere of infinite radius and a flat plate. Hence the approximation of the liquid−vapour interface as a toroidal surface (i.e., considering the vertical section of the interface to be an arc of a circle) is assumed to be valid with the same criteria of the liquid bridge half width being equal to or greater than 6.5 times the Kelvin radius (R_C) for the case in this chapter. The toroidal liquid−vapour interfaces being considered are shown schematically in Figure 5-1.

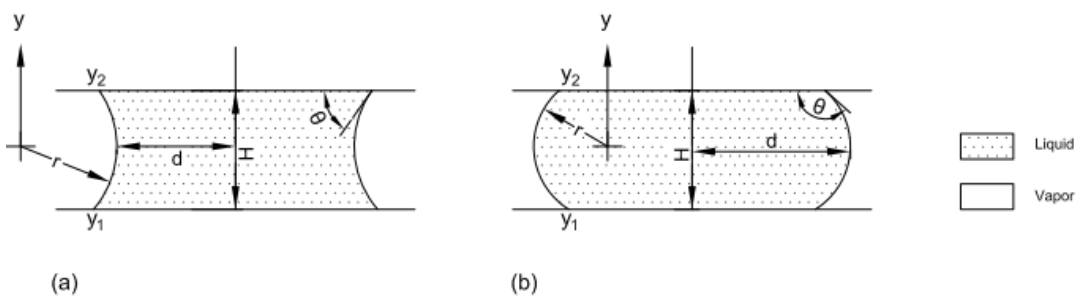

Figure 5-1 Schematic of a liquid bridge – a) concave ($\theta < 90°$) and b) convex ($\theta > 90°$) − between two flat plates, where θ is the equilibrium contact angle, r is the radius of the circle approximating the vertical section of the liquid−vapour interface, d is the liquid bridge half width, H is the distance between the two plates, y_1 is the three phase contact with the lower plate and y_2 is the three phase contact with the upper plate.

Based on the solid material that imposes the equilibrium contact angle, the liquid−vapour interface is either concave ($\theta < 90°$) or convex ($\theta > 90°$). The ***transition contact angle*** at which the meniscus changes from concave to convex is 90° for this geometry. It is worth noting that the equilibrium contact angle is being measured through the denser phase (liquid).

When approximating the liquid−vapour interface by a toroidal surface, the magnitudes of the principal radii of curvature are $|R_1| = r$ and $|R_2| = d$. The signs of the principal radii of curvature are determined based on the definition of ΔP, and

according to the concavity of the meniscus. Here ΔP is defined as $P^V - P^L$. For the case of concave meniscus, R_1 is positive since the centre of the circle is in the vapour phase ($R_1 = r$) and R_2 is negative ($R_2 = -d$) due to its centre being inside the liquid phase. In the same way, for the convex case both of the radii are negative ($R_1 = -r$ and $R_2 = -d$).

V^L and A^{LV} are the volume and surface area of revolution of the liquid−vapour interface curve, *F(y)*, around the y−axis. The volume of revolution can be computed by adding up a sequence of thin flat washers [43]. The appropriate equations giving V^L, A^{SL} and A^{LV} are presented in Table 5-1[44].

Table 5-1 The liquid volume, the solid−liquid and the liquid−vapour surface areas for a liquid bridge between two flat plates [43, 44].

$V^L = \pi \int_{y_1}^{y_2} F(y)^2 dy$	(5.1)		
$A^{SL} = \pi\,[F(y_1)^2 + F(y_2)^2]$	(5.2)		
$A^{LV} = 2\pi \int_{y_1}^{y_2} F(y)\sqrt{1 + F'(y)^2}\,dy$	(5.3)		
Concave meniscus (θ < 90º)		**Convex meniscus (θ > 90º)**	
$F(y) = r + d - \sqrt{r^2 - y^2}$	(5.4)	$F(y) = -r + d + \sqrt{r^2 - y^2}$	(5.5)
$y_1 = -r\cos\theta$	(5.6)	$y_1 = r\cos\theta$	(5.7)
$y_2 = r\cos\theta$	(5.8)	$y_2 = -r\cos\theta$	(5.9)

To analyse the stability of the liquid bridge, the equation for the change in free energy upon the liquid formation is as stated in Table 3-6:

$$B - B_0 = \frac{2\gamma^{LV}}{R_C} V^L + (-\gamma^{LV}\cos\theta) A^{SL} + \gamma^{LV} A^{LV} \qquad (3.59)$$

where V^L, A^{SL} and A^{LV} are to be substituted from Table 5-1.

The equilibrium contact angle is assumed to be known from experiments for the solid material of the plates. The amount of r $(= |R_1|)$ is imposed by the distance between the two plates and the equilibrium contact angle. For the case of concave meniscus,

$$r = \frac{H}{2\cos\theta} \tag{5.10}$$

and for the case of convex meniscus,

$$r = \frac{-H}{2\cos\theta} \tag{5.11}$$

The dependant variable of the free energy function (equation (3.59)) would be d $(= |R_2|)$. The equilibrium size of the liquid bridge is either obtained from the extremum of the curve of the free energy vs. liquid bridge half length, d, or from the roots of the derivative of the free energy with respect to the liquid bridge half length, d, i.e. $\left(\frac{\partial B}{\partial d}\right)_{\theta=\theta_e} = 0$.

The stability of the liquid bridge can then be found according to the sign of the derivative at the equilibrium point. A maximum point denotes an unstable equilibrium, the global minimum of the curve denotes a stable equilibrium, and any local minimum represents a metastable equilibrium.

5.1.1. Stability of the liquid phase being formed from a bulk vapour phase between two flat plates: concave meniscus ($\theta < 90^o$)

For the case of liquid formation with a concave meniscus, with the pressure difference being defined as $\Delta P = P^V - P^L$, R_1 is positive and R_2 is negative since the centre of the radius is in the vapour for R_1 and in the liquid for R_2. Hence the mean radius of curvature from equation (2.14) is:

$$\frac{1}{R_m} = \frac{1}{2}\left(\frac{1}{r} - \frac{1}{d}\right) \tag{5.12}$$

where R_m is identical to Kelvin radius (R_C) at equilibrium conditions, according to equation (2.21).

For various plate separation distances, and equilibrium contact angles of interest, it has been observed that at the equilibrium conditions, r is less than d. This would result in positive R_m according to equation (5.12), and therefore in positive R_C. For R_C to be positive, the vapour pressure must be below the saturation pressure ($P^V < P_\infty$) according to section 3.7.1.

Thermodynamic stability analysis for liquid formation with a concave meniscus is to be performed through the curve of free energy vs. scaled concave liquid bridge size ($\frac{d}{R_C}$). A typical example of such a curve is presented in Figure 5-2 for n−dodecane as the pure confined vapour at 24°C (the same condition as in [18]). Fluid properties at this condition are presented in Table 3-7.The vapour pressure is set to be $0.9P\infty$ (less than the saturation pressure), for which the Kelvin radius of

the system is 4.39×10^{-8} meters from equation (2.20). The contact angle is considered to be 0° and the separation distance of the two flat plates to be equal to $0.97R_C$.

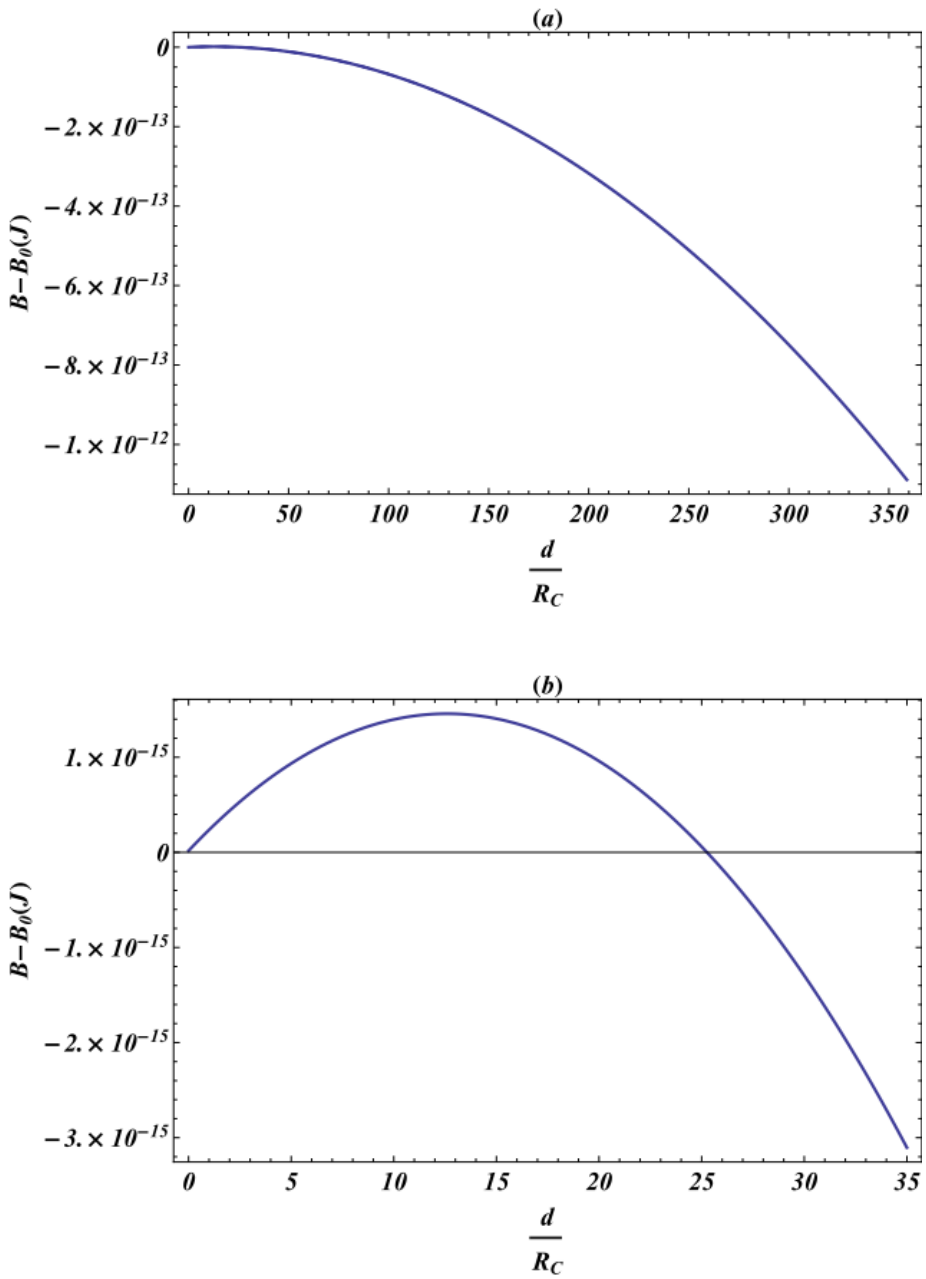

Figure 5-2 (a) Free energy vs. scaled liquid bridge half width ($\frac{d}{R_C}$) between two flat plates, for n−dodecane at 24°C, $P^V=0.9P_\infty$, θ= 0°, and $H=0.97R_C$, (b) Magnification of the region close to d = 0.

After passing the maximum point, the curve continuously descends. This means that once the energy barrier is overcome and the nucleation event has occurred, all the vapour would change into liquid, filling the space between the plates.

5.1.1.1. Effect of equilibrium contact angle on the stability of the system for liquid phase formation out of a bulk vapour phase between two flat plates: concave meniscus

In this section the effect of equilibrium contact angle on the free energy and stability of liquid formation with a concave meniscus is studied. The properties of the system other that the equilibrium contact angle are kept the same as those in Table 5-2.

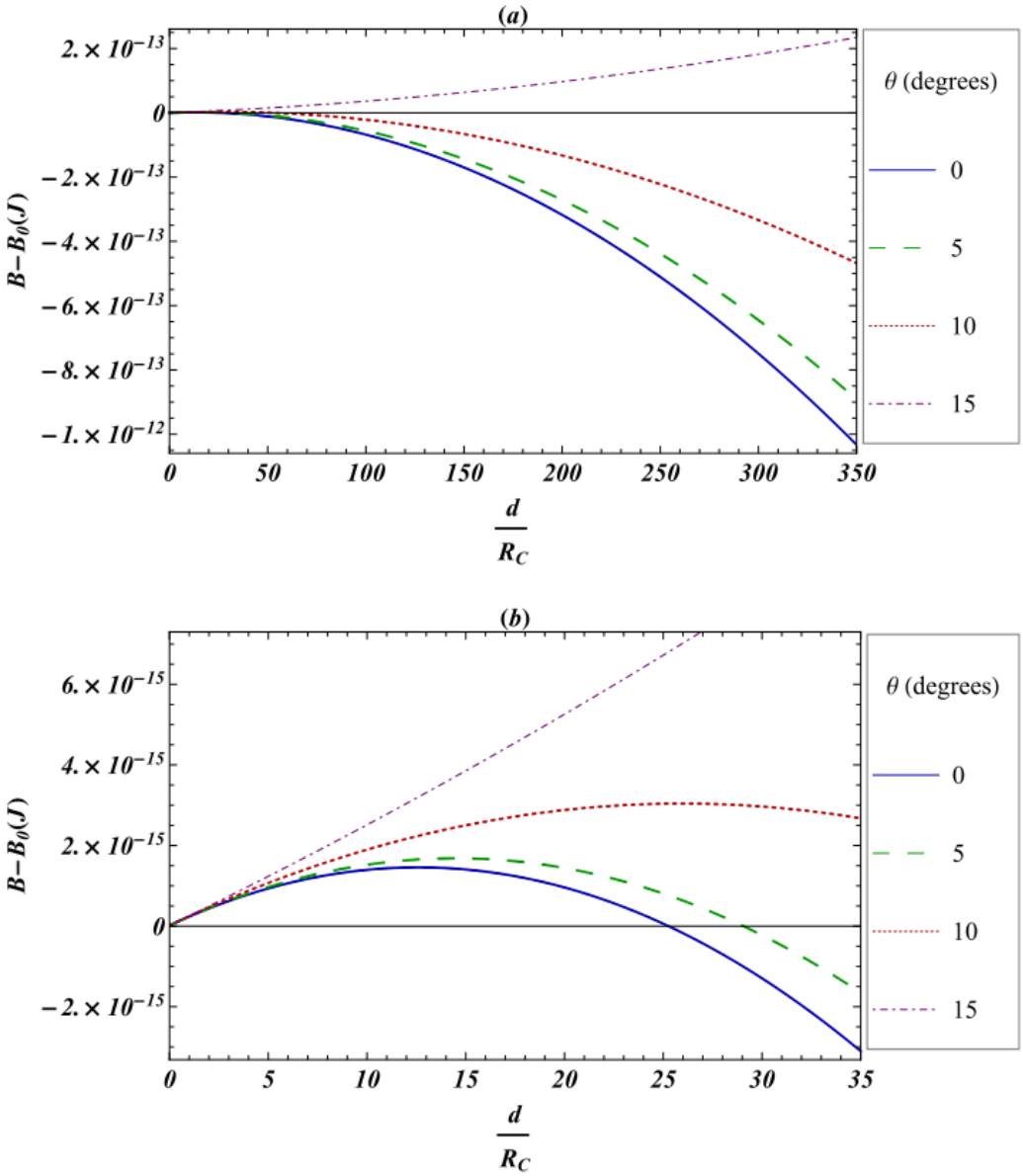

Figure 5-3 (a) Effect of the equilibrium contact angle on the curve of free energy vs. liquid bridge half width between two flat plates, for n−dodecane at 24°C, P^V=0.9P_∞, for various contact angles less than 90° (concave meniscus), and H=0.97R_C, (b) Magnification of the unstable equilibrium point.

It can be seen in Figure 5-3 for liquid formation with a concave meniscus, that as the contact angle increases (gets closer to the ***transition contact angle***) the energy barrier becomes greater; until at some equilibrium contact angle below the ***transition contact angle*** (for example at θ=14.1° for the conditions of Figure 5-3)

the curve becomes continuously increasing where the formation of the liquid turns out to be unfavourable. Also from part (b) of Figure 5-3, with the increase of the equilibrium contact angle, the unstable equilibrium is seen to happen at larger liquid bridge lengths.

A specific number of degrees changes in contact angle results in larger relative changes to the energy barrier for contact angles closer to the ***transition contact angle***. The following figure demonstrates the above statement.

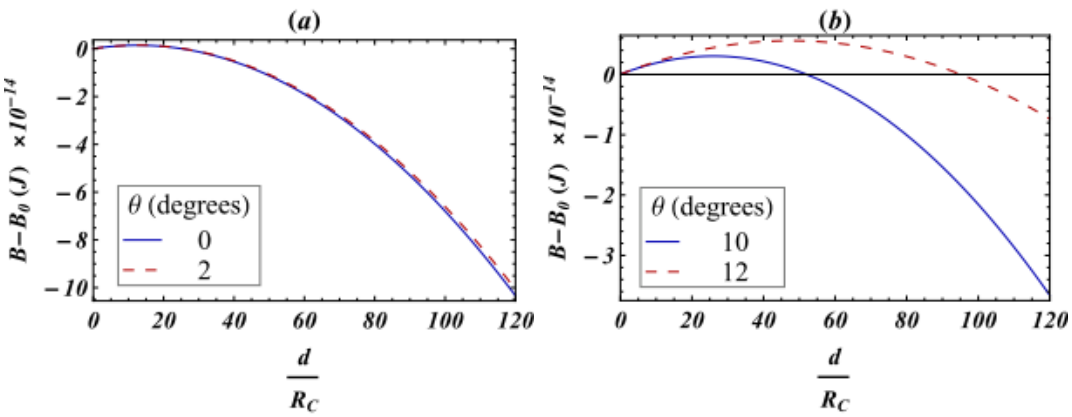

Figure 5-4 Comparison of the effect of a specific number of degrees change (2°) in the equilibrium contact angle on the free energy of liquid formation with a concave meniscus (θ< 90°) between two flat plates, for n−dodecane at 24°C, $P^V=0.9P_\infty$, and $H=0.97R_C$ (a) far from the transition contact angle, (b) Closer to the transition contact angle

The *transition contact angle* for this geometry is 90° as mentioned previously. In part (a) of Figure 5-4 where the contact angle is changing from 0° to 2°, the energy level of the barrier is changing from 1.46×10^{-15} to 1.49×10^{-15} J, for a relative difference of 2.05 %, according to equation (4.21). In part (b) for the contact angle changing from 10° to 12°, which is closer to the ***transition contact angle*** (in comparison to 0° to 2°) , the energy level of the barrier changes from 3.04×10^{-15}J to 5.59×10^{-15}J, with a relative difference of 83.88%.

This explanations justifies the approximation of small contact angles with zero, which has been used in many calculations as a matter of simplification [18].

It should be noted that the above pattern (according to which specific changes in the contact angle result in more relative difference as one gets closer to the ***transition contact angle)*** is based on the comparison of the level of the energy barrier at the maximum point (the equilibrium state), only around which the definition of the energy with respect to the reference point is valid.

Upon further increasing the contact angle (for example above θ=14.1° for the conditions of Figure 5-3 or Figure 5-4), the energy curve becomes monotonically increasing. For monotonically increasing curves, the pattern is different. The relative differences in the energy curves caused by certain changes to the contact angle get smaller as one gets closer to the transition contact angle. Figure 5-5 demonstrates this phenomenon.

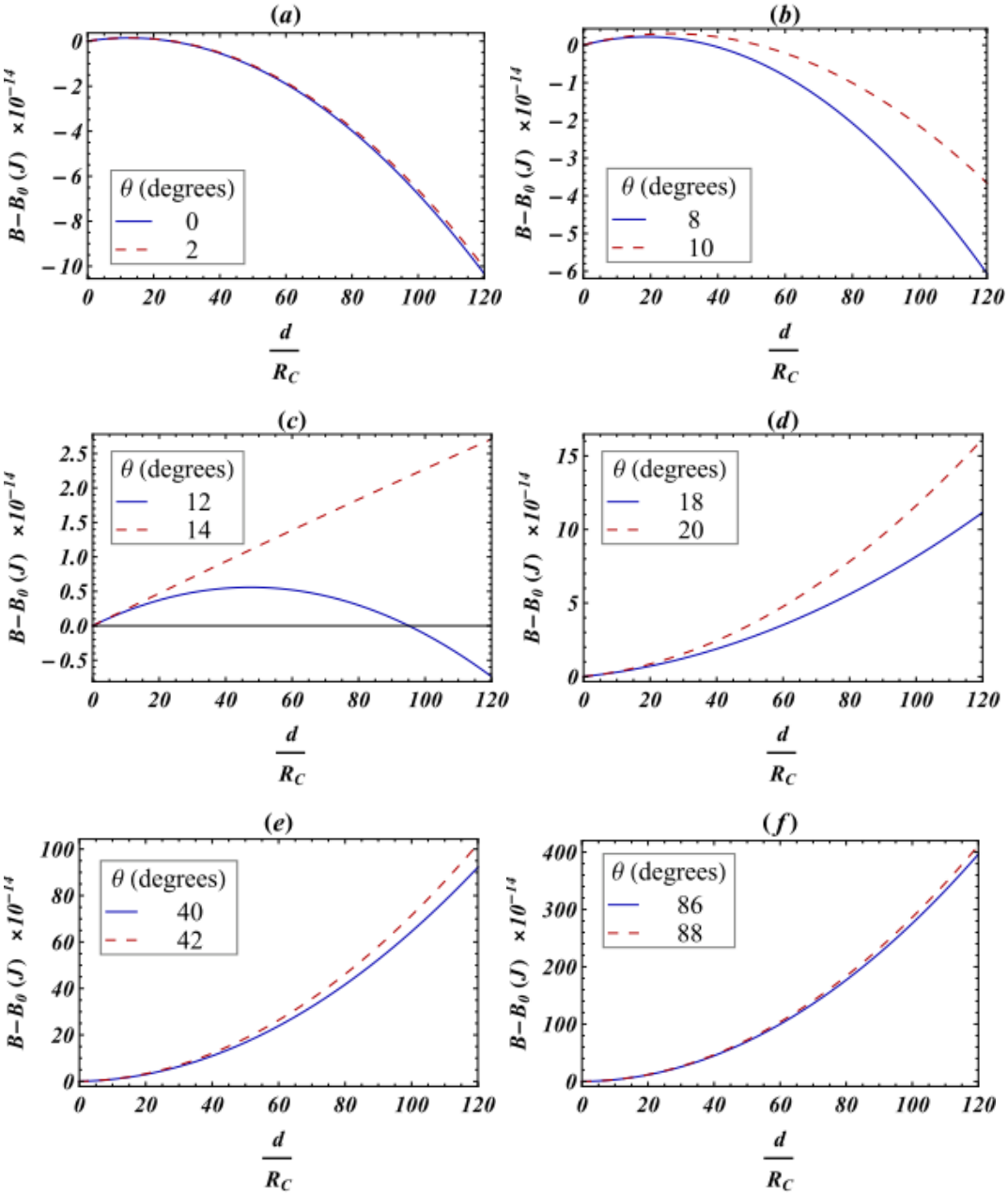

Figure 5-5 Specific changes (2°) in the contact angle affect the free energy of liquid formation with a concave meniscus (θ < 90°) between two flat plates, for n−dodecane at 24°C, P^V=0.9P_∞, and H=0.97R_C. The relative difference in the free energy gets less important far from the transition contact angle in the case of having an energy barrier (a,b), becomes maximum when the energy curve changes to monotonically increasing, and gets less important as one gets closer to the *transition contact angle* in the case of monotonically increasing curves (d,e,f).

5.1.1.2. Effect of the flat plate separation distance on the stability of the system for liquid phase formation out of a bulk vapour phase between two flat plates: concave meniscus

The distance between the two flat plates impacts the stability of the system for liquid formation with a concave meniscus as illustrated in Figure 5-6.

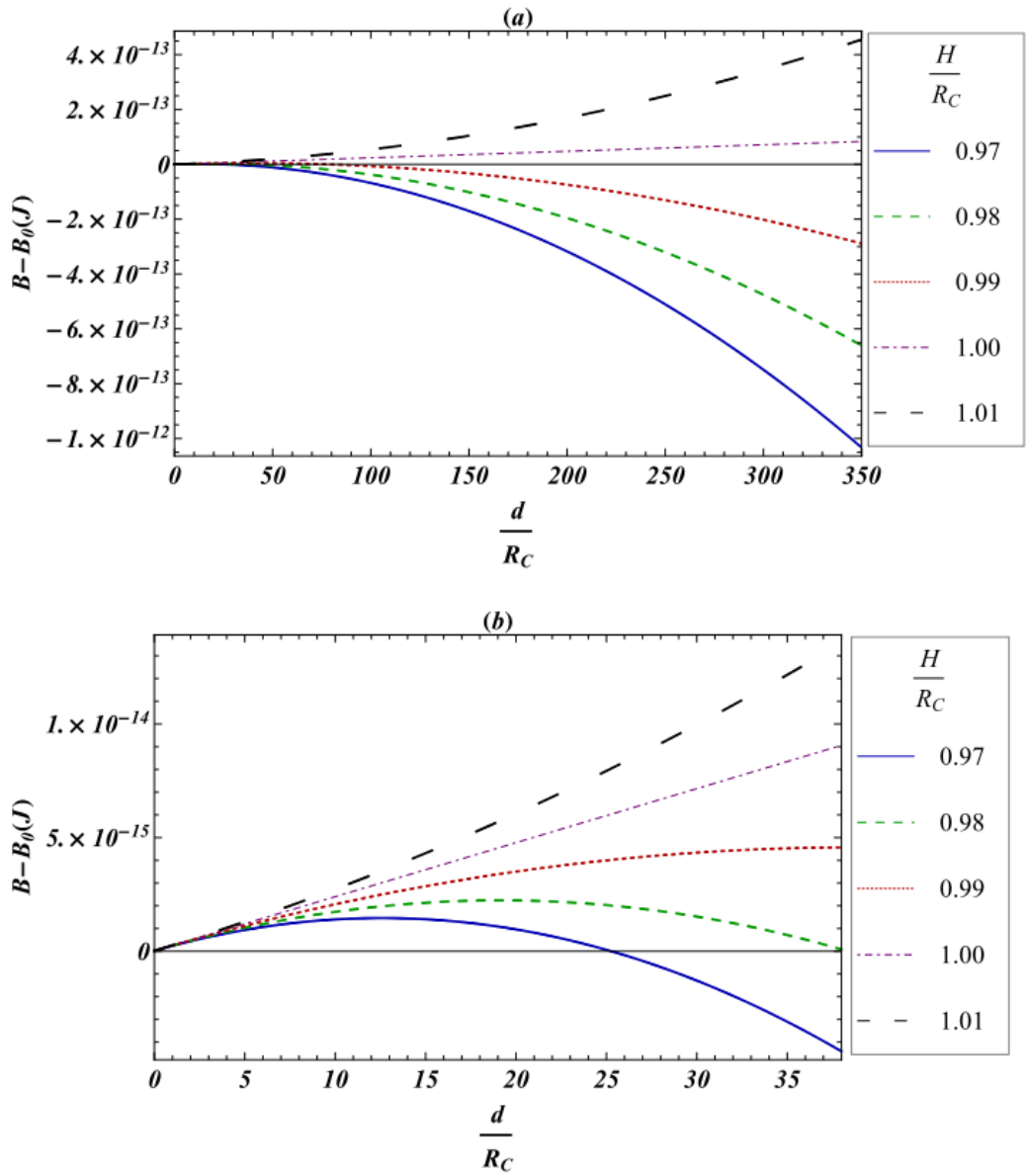

Figure 5-6 (a) Effect of the flat plate separation distance on the curve of free energy vs. liquid bridge half width between two flat plates, for n−dodecane at 24°C, P^V=0.9P_∞, θ=0°, (b) magnification of the unstable equilibrium point.

From part (b) of Figure 5-6 it can be seen that as the distance between the two flat plates increases, the level of the energy barrier increases, and the larger the liquid bridge has to be to pass the unstable point.

According to part (a), the formation of the liquid phase becomes unfavourable (monotonically increasing curve) at and above $H=R_C$ for this case of zero contact angle. Considering the effect of contact angle that was described in section 5.1.1, for greater contact angles the liquid formation becomes unfavourable even at some distance less than R_C. Hence it would be generally true for any contact angle that liquid formation with concave meniscus is unfavourable for $H \geq R_C$. Below R_C further investigation is required for any specific contact angle to judge whether liquid formation with concave meniscus is favourable. The separation distance above which liquid formation with concave meniscus between two flat plates becomes unfavourable is well predicted by $R_C \cos\theta$, which is proposed in previous works [12, 24] for confinement geometry of a flat plate and a sphere. (More explanation about this is given in chapter 6, at section 6.1.1.2)

5.1.2. Stability of the liquid phase being formed from a bulk vapour phase between two flat plates: convex meniscus ($\theta > 90^o$)

To have contact angle greater than 90° (equivalent to convex meniscus), with the pressure difference defined by $P^V - P^L$, both R_1 and R_2 are negative with their centers being located inside the liquid phase.

The mean radius of the curvature from equation (2.14) is then:

$$\frac{1}{R_m} = \frac{1}{2}\left(-\frac{1}{r} - \frac{1}{d}\right) \tag{5.13}$$

At the equilibrium condition R_m is equivalent to the Kelvin radius, R_C, according to equation (2.21).

According to equation (5.13), R_m, which is identical to R_C, is negative. Negative R_C is only possible when vapour pressure is greater than the saturation pressure ($P^V > P_\infty$), as discussed in section 3.7.1.

Figure 5-7 is a typical free energy curve in this case where the liquid bridge has a convex meniscus. This demonstration is for n−dodecane at 24°C, with fluid properties as reported in Table 3-7.The vapour pressure is fixed at $1.1P_\infty$ (above the saturation pressure), which results in a Kelvin radius of -4.85×10^{-8} meters from equation (2.20). Consider a contact angle of 160° and a separation distance of the two flat plates equal to $0.97\left|R_C\right|$.

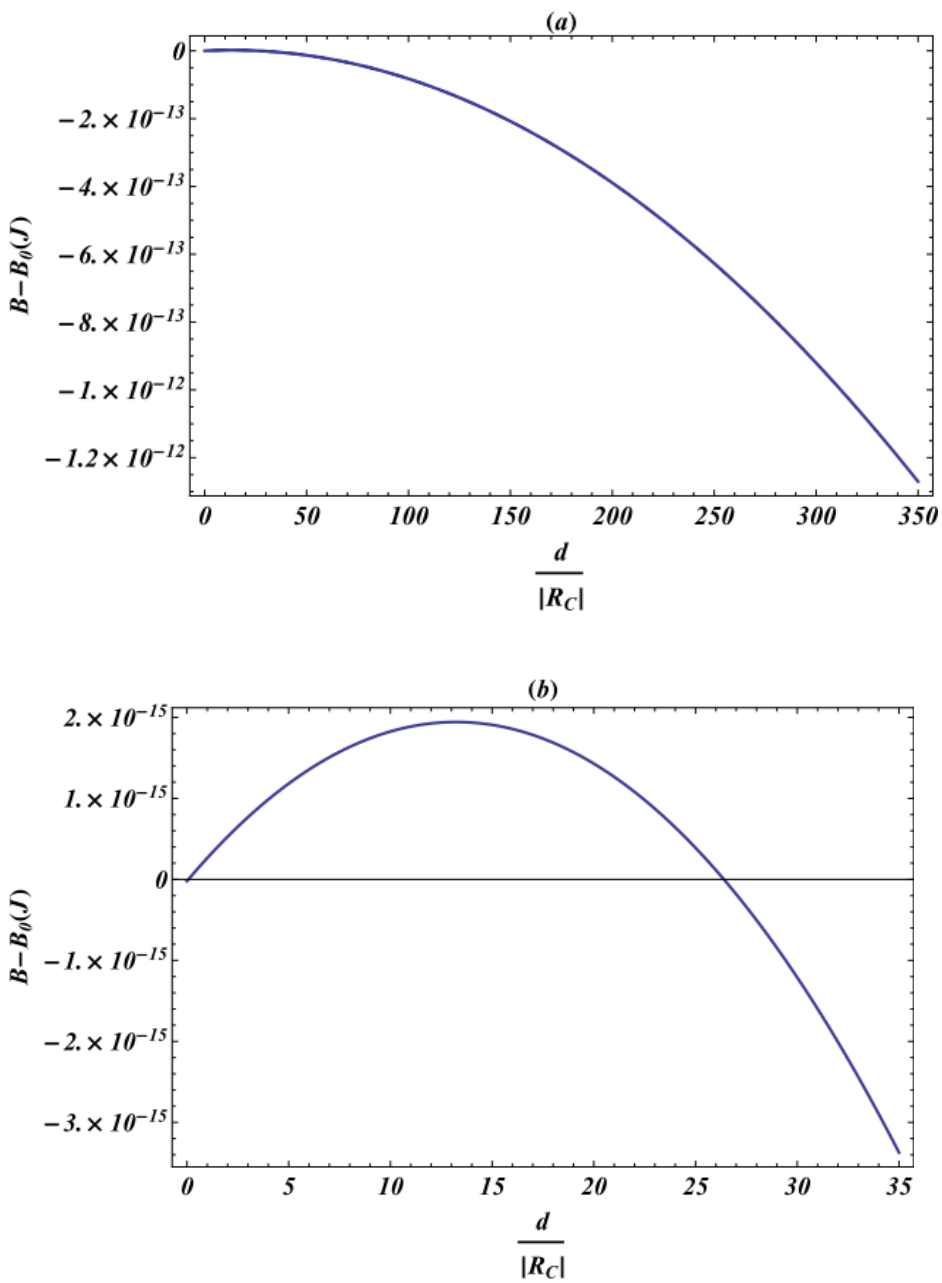

Figure 5-7 (a) Free energy vs. scaled liquid bridge half width ($\frac{d}{R_C}$) between two flat plates, for n−dodecane at 24°C, P^V=1.1P_∞, θ = 160°, and H=0.97$|R_C|$, (b) Magnification of the region close to d = 0.

The curve is monotonically increasing after passing a maximum which means that all the vapour would change to liquid after passing the energy barrier.

5.1.2.1. Effect of equilibrium contact angle on the stability of the system for liquid phase formation out of a bulk vapour phase between two flat plates: convex meniscus

The effect of the equilibrium contact angle on the free energy level of the system for liquid formation between two flat plates is investigated in this section, while the geometry and other properties are kept the same as introduced in section 5.1.2 and Figure 5-7 .

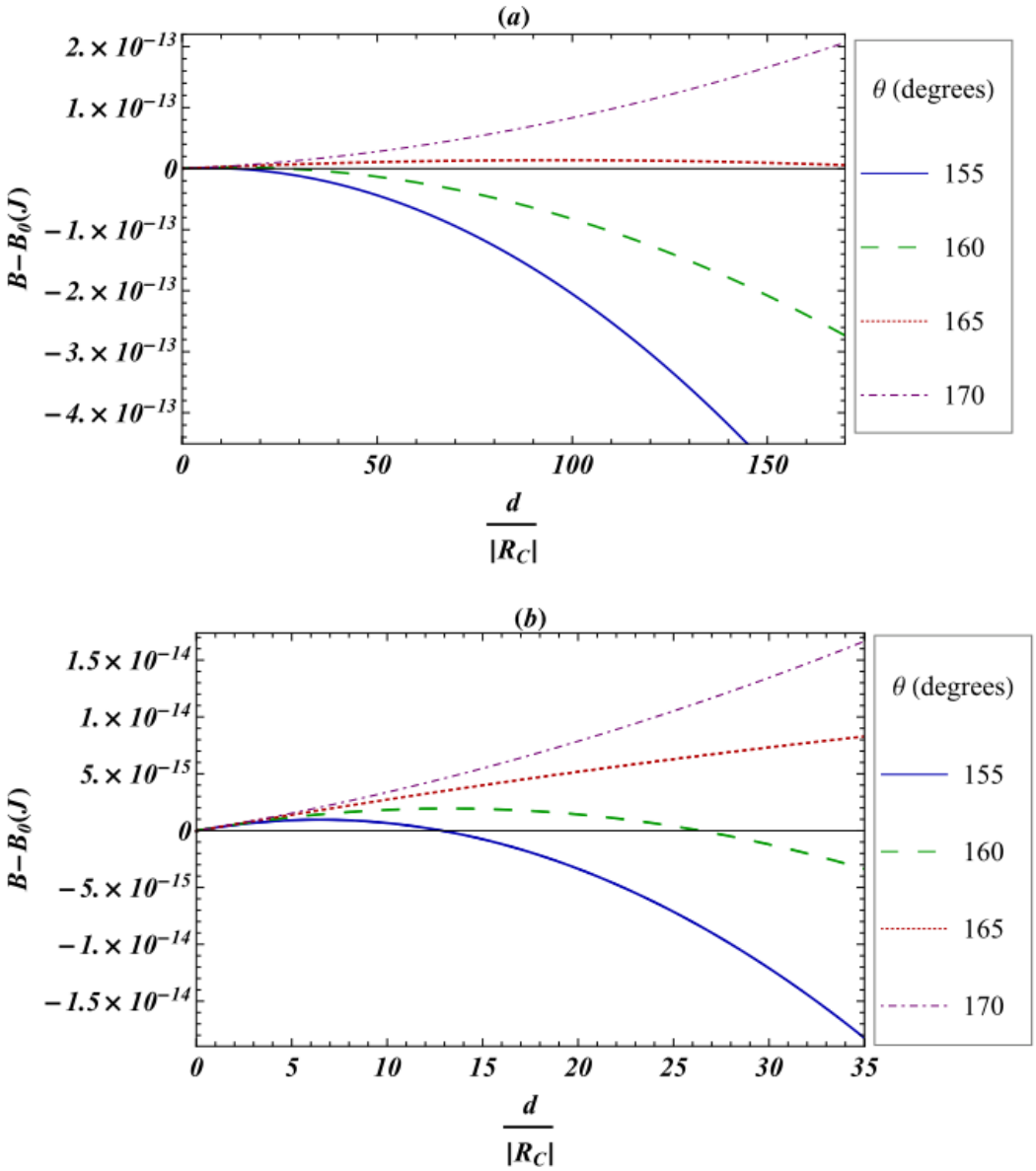

Figure 5-8 (a) Effect of the equilibrium contact angle on the curve of free energy vs. liquid bridge half width between two flat plates, for n−dodecane at 24°C, P^V=1.1P_∞, for various contact angles higher than 90° (convex meniscus), and H=0.97 $|R_C|$, (b) Magnification of the unstable equilibrium point.

In this case of convex liquid−vapour meniscus formation, an increase in the equilibrium contact angle is equivalent to getting farther from the ***transition contact angle***. Any increase in the contact angle makes the energy barrier larger, until at some equilibrium contact angle the curve becomes monotonically

increasing indicating that formation of the liquid phase is unfavourable. Also part (b) of Figure 5-8 shows that with an increase of the equilibrium contact angle, the unstable equilibrium would happen at larger liquid bridge widths.

5.1.2.2. Effect of the flat plate separation distance on the stability of the system for liquid phase formation out of a bulk vapour phase between two flat plates: convex meniscus

Figure 5-9 illustrates the free energy curves for different flat plate separation distances in the case of liquid formation with a convex meniscus.

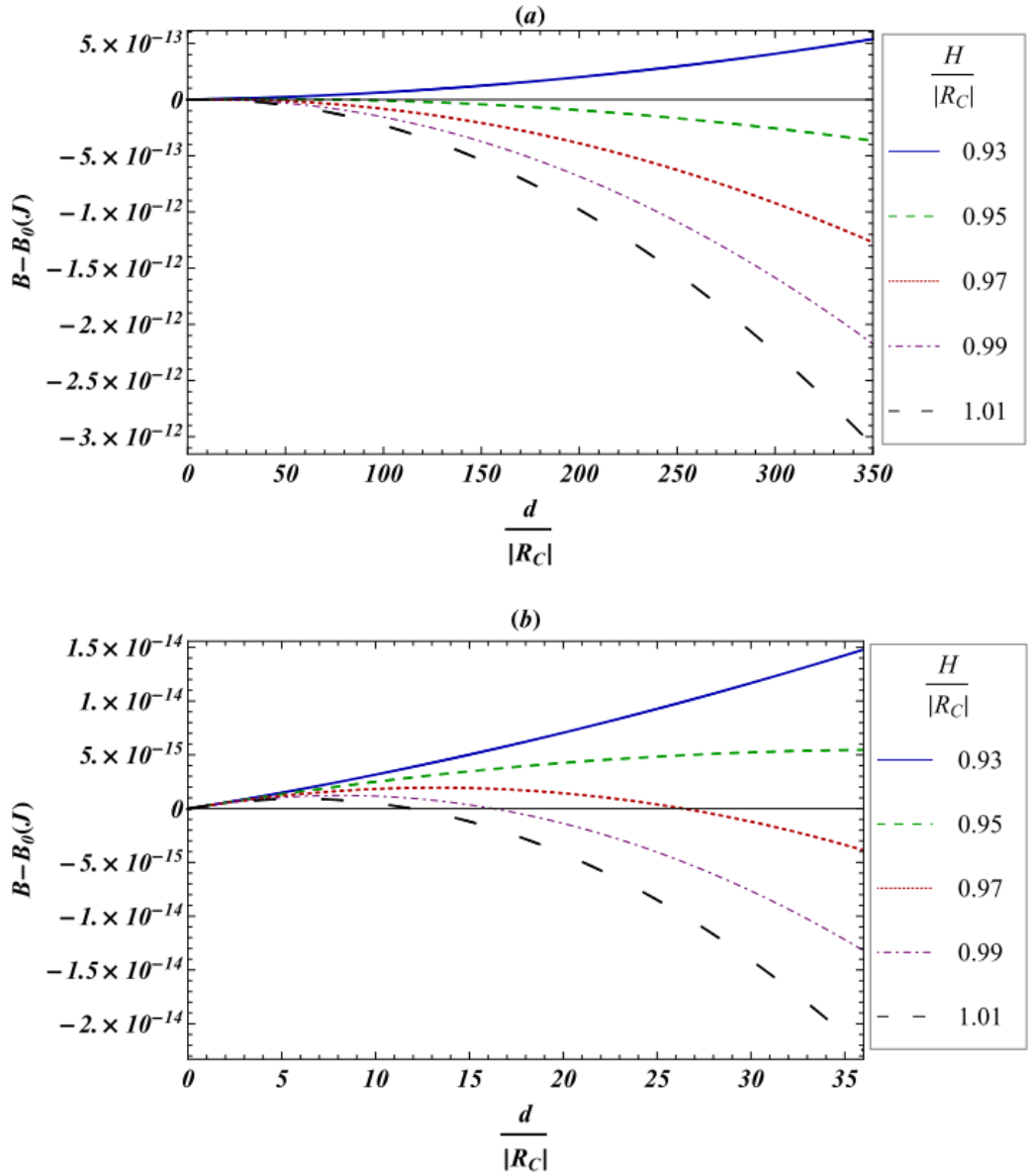

Figure 5-9 (a) Effect of the flat plate separation distance on the curve of free energy vs. liquid bridge half width between two flat plates, for n−dodecane at 24°C, P^V=1.1P_∞, θ=160°, (b) Magnification of the unstable equilibrium point.

As illustrated in Figure 5-9, the formation of a liquid phase with a convex meniscus is unfavourable for plates at close distance. As the plate separation gets larger, liquid formation with a convex liquid−vapour interface becomes favourable at some large enough plate separation distance. Further increase in the plate

separation distance makes the energy barrier less, and a smaller liquid bridge needs to be formed to overcome the unstable equilibrium point.

For contact angle equal to 180°, while other properties are kept the same as for Figure 5-9, phase transition from vapour confined by non-wettable walls to liquid is favourable for plate separation distance above R_C. Considering the effect of contact angle as discussed in section 5.1.2.1 (maximum point happens at smaller bridge length with less energy as contact angle get closer to the ***transition contact angle***), liquid phase formation is favourable when plates are separated by a distance above the Kelvin radius, regardless of the amount of contact angle. Free energy curves for different contact angles and different separation distances show that $|R_C cos\theta|$ is the distance below which phase transition from confined vapour with non-wettable walls into liquid is unfavourable. The primary idea of this amount came from literature [12, 24], while their concern was to find the separation distance above which concave liquid formation between a sphere and a flat plate is unfavourable.

5.2. Vapour phase formation from a bulk liquid phase between two flat plates

The constraints on the system in which vapour is formed from a liquid phase between two flat plates are given in Table 3-3. Equilibrium conditions are obtained through Table 3-4 (b) for the case of flat solid surface.

When gravitational effects are neglected, through the same justifications as in section 5.1, the liquid−vapour interface is approximated by a toroidal surface as

long as the liquid bridge half width is equal to or greater than 6.5 times the Kelvin radius (R_C) [18]. The following figure illustrates such liquid−vapour interfaces. The contact angle (θ) is measured through the liquid phase as per convention.

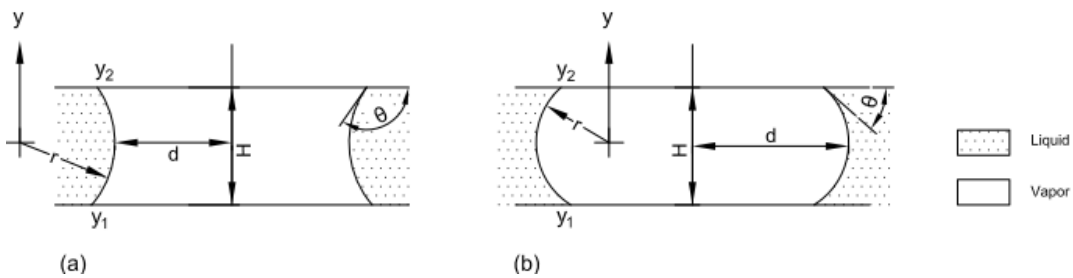

Figure 5-10 Schematic of a vapour bridge – a) concave ($\theta > 90°$) and b) convex ($\theta < 90°$) − between two flat plates, where θ is the equilibrium contact angle, r is the radius of the circle approximating the vertical section of the liquid−vapour interface, d is the vapour bridge half width, H is the distance between the two plates, y_1 is the three phase contact with lower plate and y_2 is the three phase contact with the upper plate.

The liquid−vapour interface is either concave ($\theta > 90°$) or convex outward ($\theta < 90°$) for this case of vapour formation. For this geometry, the ***transition contact angle*** at which the meniscus changes from concave to convex is 90°.

The sizes of the principal radii of curvature are $|R_1| = r$ and $|R_2| = d$. The sign of the principal radii of curvature is determined based on the definition of ΔP, and according to the concavity of the meniscus. Here ΔP is defined as $P^L - P^V$. For the case of concave meniscus R_1 ,with its center located at liquid phase, is positive ($R_1 = r$) and R_2 is negative ($R_2 = -d$) due to its centre being inside the vapour phase. In the same way, for the convex outward case both of the radii are negative ($R_1 = -r$ and $R_2 = -d$).

Vapour volume, V^V, and surface area, A^{LV}, of the revolution of the liquid−vapour interface curve around the y−axis, and A^{SV} can be obtained from Table 5-2 [43, 44].

Table 5-2 The vapour volume, the solid–liquid and the solid–vapour surface areas for a vapour bridge between two flat plates [43, 44].

$V^V = \pi \int_{y_1}^{y_2} F(y)^2 dy$			(5.14)
$A^{SV} = \pi\,[F(y_1)^2 + F(y_2)^2]$			(5.15)
$A^{LV} = 2\pi \int_{y_1}^{y_2} F(y)\sqrt{1 + F'(y)^2}\,dy$			(5.16)
Concave meniscus (θ > 90º)		**Convex meniscus (θ < 90º)**	
$F(y) = r + d - \sqrt{r^2 - y^2}$	(5.17)	$F(y) = -r + d + \sqrt{r^2 - y^2}$	(5.18)
$y_1 = r\cos\theta$	(5.19)	$y_1 = -r\cos\theta$	(5.20)
$y_2 = -r\cos\theta$	(5.21)	$y_2 = r\cos\theta$	(5.22)

The equation of the free energy for vapour formation is as stated in Table 3-6:

$$B - B_0 = \frac{2\gamma^{LV}}{R_C} V^v + (\gamma^{LV}\cos\theta) A^{SV} + \gamma^{LV} A^{LV} \tag{3.62}$$

where V^V, A^{SV} and A^{LV} are to be substituted from Table 5-2.

For a specific solid material, the equilibrium contact angle is assumed to be known from experiments. The amount of $r\ (= |R_1|)$ is imposed by the distance between the two flat plates and the equilibrium contact angle. For the case of a concave meniscus,

$$r = \frac{-H}{2\cos\theta} \tag{5.23}$$

and for the case of a convex meniscus,

$$r = \frac{H}{2\cos\theta} \tag{5.24}$$

Then the free energy function, equation (3.62), is only a function of d $(= |R_2|)$. The equilibrium size of the vapour bridge is either obtained from the extremum of the curve of the free energy vs. vapour bridge half length (d) or from the roots of the derivative of the free energy with respect to the vapour bridge half length, i.e. $\left(\frac{\partial B}{\partial d}\right)_{\theta=\theta_e} = 0$. The stability of the vapour bridge can then be found according to the sign of the derivative at the equilibrium point.

5.2.1. Stability of the vapour phase being formed from a bulk liquid phase between two flat plates: concave meniscus (θ > 90º)

For such a concave meniscus, R_1 is positive and R_2 is negative when the pressure difference is defined as $\Delta P = P^L - P^V$. Hence the mean radius of curvature from equation (2.14) is:

$$\frac{1}{R_m} = \frac{1}{2}\left(\frac{1}{r} - \frac{1}{d}\right) \tag{5.25}$$

where R_m is identical to the Kelvin radius (R_C) at equilibrium conditions, according to equation (2.21).

For various plate separation distances, and equilibrium contact angles of interest, at the equilibrium conditions r is less than d. As a result R_m is positive according to equation (5.25), which is equivalent to positive R_C. According to section 3.7.1, positive R_C is only possible if the bulk liquid pressure is above the saturation pressure ($P^L > P_\infty$).

A typical curve of the free energy vs. scaled convex vapour bridge size ($\frac{d}{R_C}$) is presented in Figure 5-11 for water at 20°C. Fluid properties at this condition are presented in Table 3-7.The liquid pressure is set to be $1.1P_\infty$. The Kelvin radius of the system at such conditions is 6.22×10^{-4} meters from equation (2.23). The equilibrium contact angle is 180°, and the separation distance of the two flat plates is equal to $0.97R_C$.

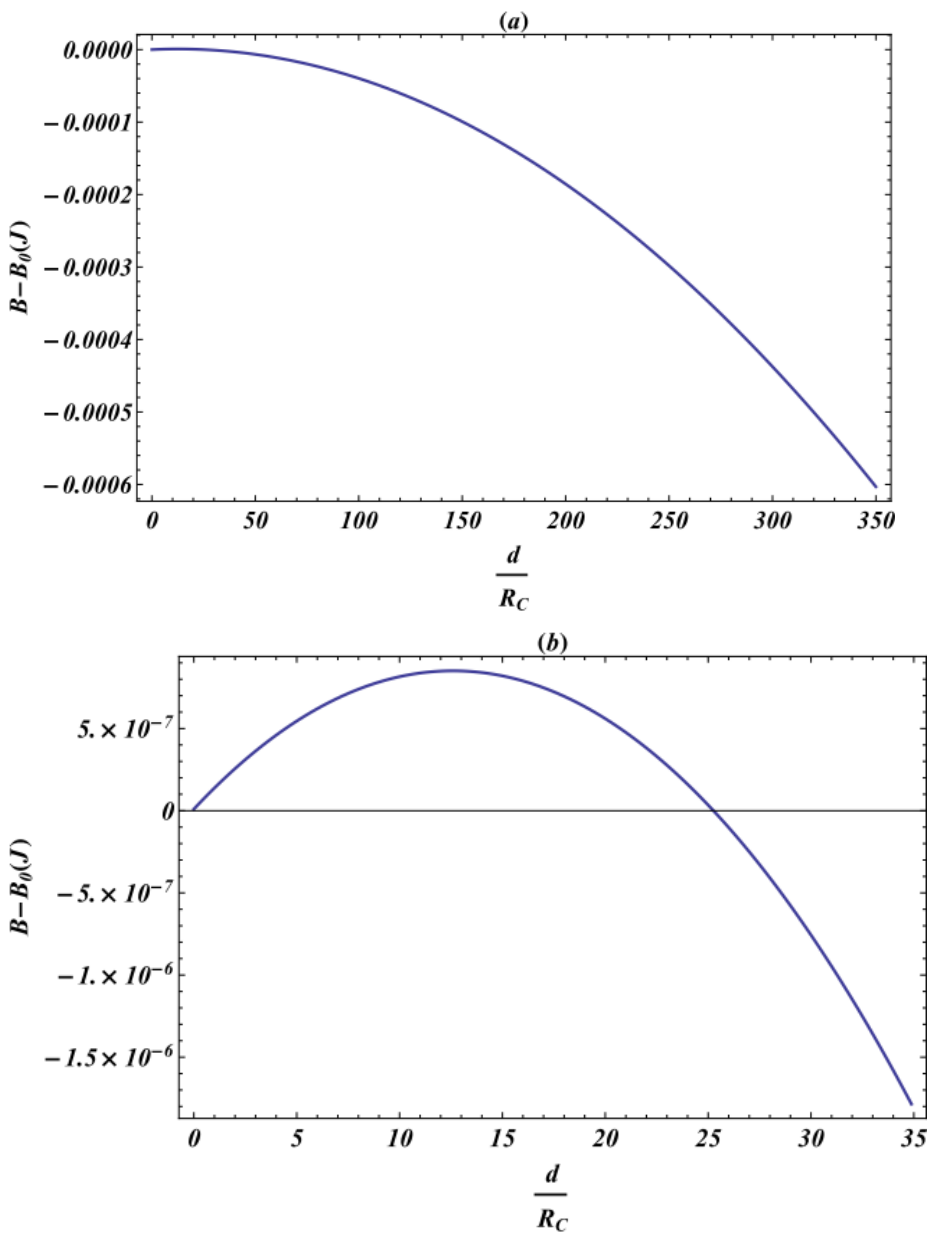

Figure 5-11 (a) Free energy vs. scaled vapour bridge half width ($\frac{d}{R_C}$) between two flat plates, for water at 20°C, P^L=1.1P_∞, θ=180°, and H=0.97R_C, (b) Magnification of the region close to d=0

As Figure 5-11 indicates, after passing the energy barrier, all the liquid would change into vapour and there is no stable size for the vapour.

5.2.1.1. Effect of equilibrium contact angle on the stability of the system for vapour phase formation out of a bulk liquid phase between two flat plates: concave meniscus

The effect of the equilibrium contact angle on the free energy of a vapour phase with a concave meniscus is investigated in this section. The properties of the system other than the equilibrium contact angle are kept the same as those in Figure 5-11.

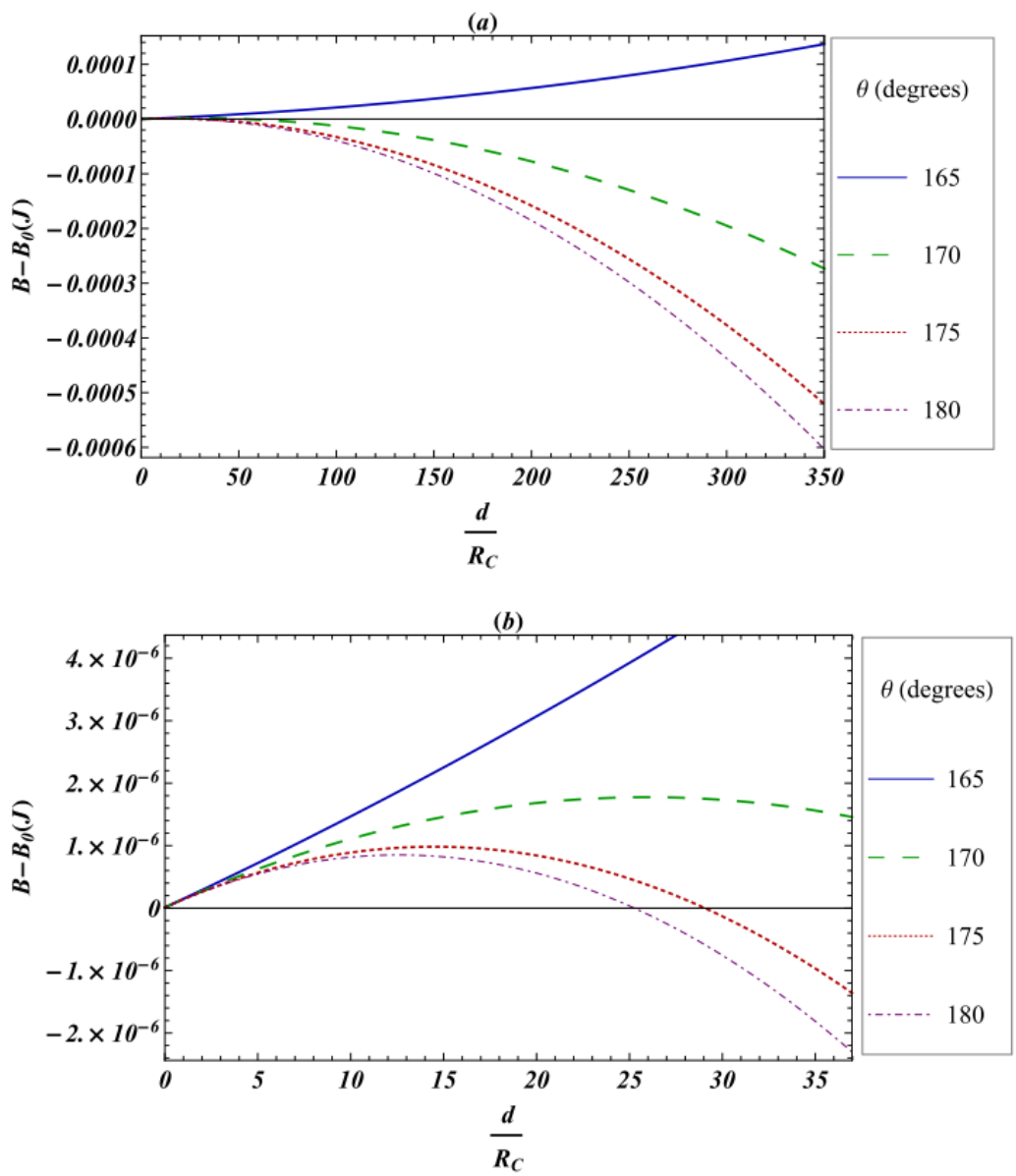

Figure 5-12 (a) Effect of the equilibrium contact angle on the curve of free energy vs. vapour bridge half width between two flat plates, for water at 20°C, P^L=1.1P_∞, for various contact angles higher than 90° (concave meniscus), and H=0.97R_C, (b) Magnification of the unstable equilibrium point.

As contact angle decreases and gets closer to the ***transition contact angle***, the energy barrier increases and the unstable equilibrium vapour bridge gets larger; until at some contact angle the curve becomes monotonically increasing where the formation of the liquid turns out to be unfavourable.

For the same number of degrees change in the contact angle, higher relative changes in the free energy curve occur close to the *transition contact angle*. This is similar to the case of concave meniscus liquid formation from the bulk vapour phase. This fact is valid for contact angles resulting in curves having a maximum point, as illustrated in Figure 5-13.

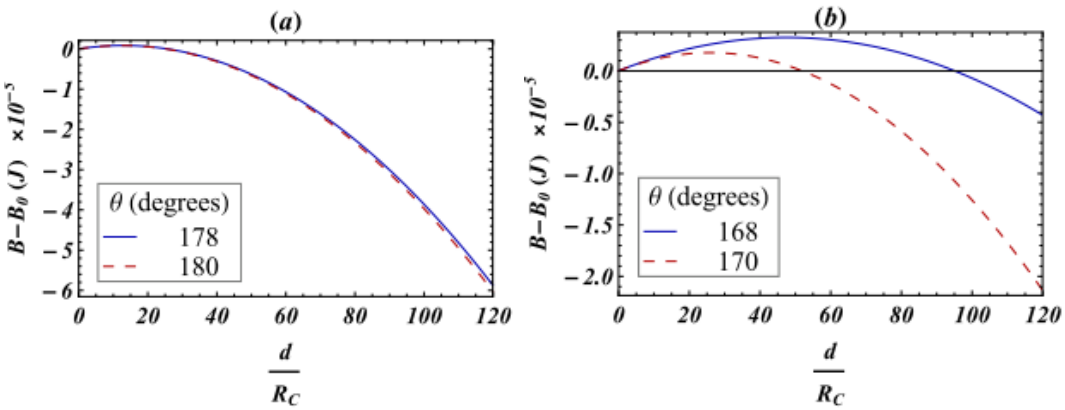

Figure 5-13 Comparison of the effect of a specific number of degrees (2º) change in the equilibrium contact angle on the free energy of vapour formation with a concave meniscus (θ > 90º) between two flat plates, for water at 20°C, P^V=1.1P_∞, and H=0.97R_C (a) far from the transition contact angle, (b) closer to the transition contact angle.

The *transition contact angle* for this geometry is 90º. In part (a) of Figure 5-13 where the contact angle is changing from 178º to 180º, the height of the barrier changes from 8.70×10^{-7} J to 8.51×10^{-7} J, for a relative difference of 2.21 %, from equation (4.21). In part (b) for the contact angle changing from 168º to 170º, which is closer to the ***transition contact angle***, the height of the barrier changes from 3.26×10^{-6} J to 1.77×10^{-6} J, with a relative difference of 83.81%, from equation (4.21).

5.2.1.2. Effect of the flat plate separation distance on the stability of the system for vapour phase formation out of a bulk liquid phase between two flat plates: concave meniscus

Figure 5-14 shows the free energy of the concave vapour phase for various plates' separation distances.

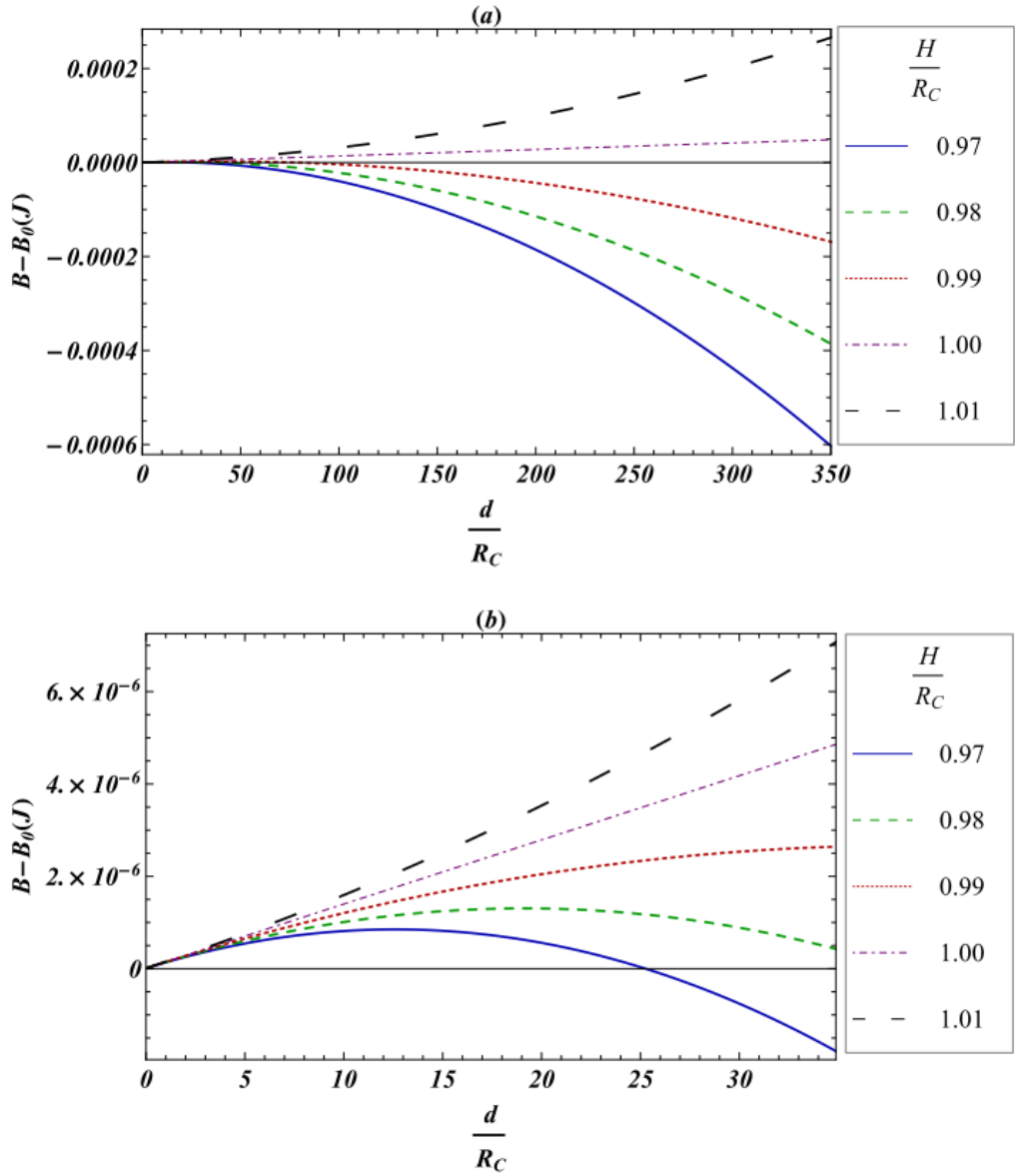

Figure 5-14 (a) Effect of the flat plate separation distance on the free energy vs. vapour bridge half width between two flat plates, for water at 20°C, θ =180°, and P^L=1.1P_∞, (b) Magnification of the unstable equilibrium point.

As illustrated in Figure 5-14, the energy barrier becomes higher as the plate separation distance increases, until at some distance the formation of the vapour phase is no longer favourable. For smaller contact angles (with the effect of contact angle as described in section 5.2.1.1), vapour formation with concave meniscus becomes unfavourable even at some distance less than R_C. Therefore it can be

concluded that for any contact angle, vapour formation with concave meniscus is unfavourable for $H \geq R_C$. Below R_C further investigation is required for any specific contact angle. Modifying what has been proposed in literature [12, 24] for the case of liquid formation with concave meniscus between a sphere and a flat plate, vapour formation with concave meniscus between two flat plates becomes unfavourable for plate separation distance above $-R_C \cos\theta$.

5.2.2. Stability of the vapour phase being formed from a bulk liquid phase between two flat plates: convex meniscus (θ < 90º)

For the pressure difference being defined as $P^L - P^V$ and for the convex meniscus (θ < 90º), both R_1 and R_2 are negative with their centers being located inside the vapour phase.

With $r = |R_1|$ and $d = |R_2|$, the mean radius of the curvature from equation (2.14) is:

$$\frac{1}{R_m} = \frac{1}{2}\left(-\frac{1}{r} - \frac{1}{d}\right) \tag{5.26}$$

where R_m is equal to Kelvin radius (R_C) at equilibrium condition, according to equation (2.21).

R_m , which is identical to R_C, is negative according to equation (5.26). For R_C to be negative, bulk liquid pressure must be less than the saturation pressure ($P^L < P_\infty$) as discussed in section 3.7.1.

A typical free energy curve vs. scaled convex vapour bridge size ($\frac{d}{R_C}$) is shown in Figure 5-15. The case is water at 20°C, with properties given in Table 3-7. The liquid pressure is set to be $0.9P_\infty$. The Kelvin radius of the system at these conditions is -6.22×10^{-4} meters from equation (2.23). First let us set the equilibrium contact angle to 20°, and the separation distance of the two flat plates to $0.97\left|R_C\right|$.

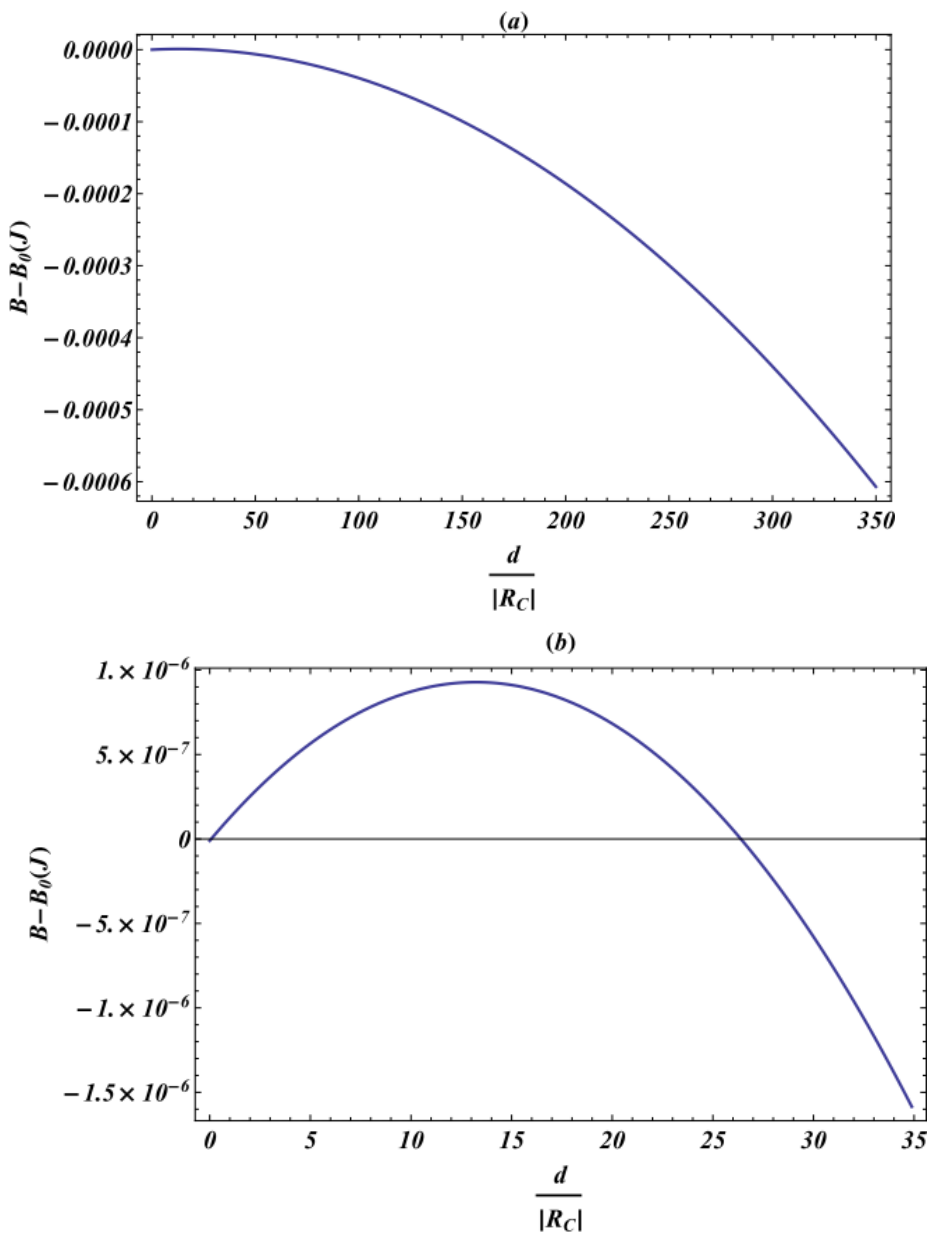

Figure 5-15 (a) Free energy vs. scaled vapour bridge half width ($\frac{d}{R_C}$) between two flat plates, for water at 20°C, P^L=0.9P_∞, θ=20°, and H=0.97 $|R_C|$, (b) Magnification of the region close to d=0.

After passing a maximum point, the curve is monotonically decreasing which means all the liquid would turn into vapour after passing the energy barrier.

5.2.2.1. Effect of equilibrium contact angle on the stability of a vapour phase being formed from the liquid phase between two flat plates: convex meniscus

The geometry and other properties are kept the same as presented in Figure 5-15, and the effect of the equilibrium contact angle is investigated.

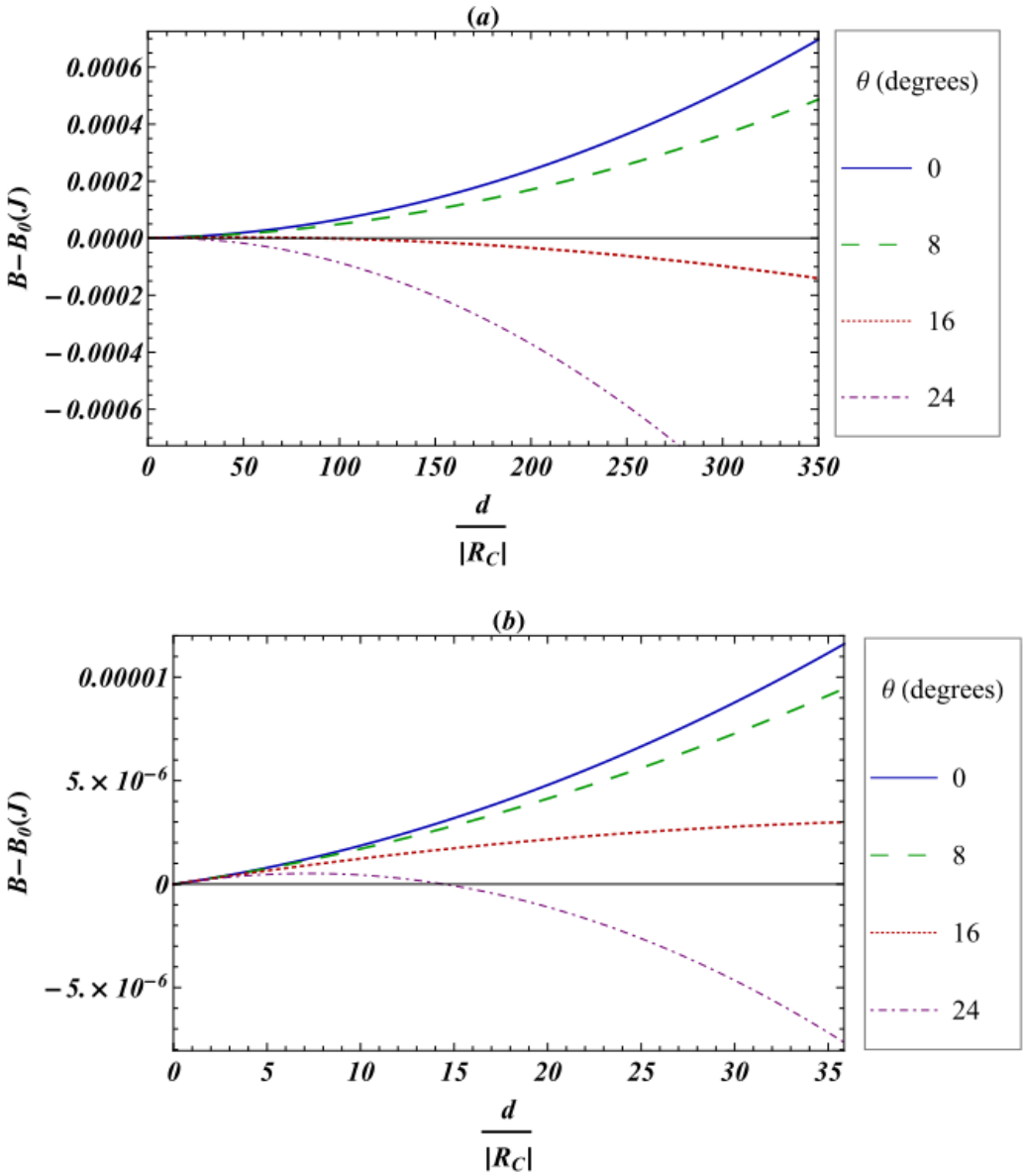

Figure 5-16 (a) Effect of the equilibrium contact angle on the free energy vs. vapour bridge half width between two flat plates, for water at 20°C, $P^L=0.9P_\infty$, for various contact angles less than 90° (convex meniscus), and $H=0.97\,|R_C|$, (b) Magnification of the unstable equilibrium point.

In the formation of the convex vapour phase, any decrease in the equilibrium contact angle (i.e. getting farther from the ***transition contact angle***), increases the height of the energy barrier and the unstable condition happens at higher volume of the vapour phase. At some equilibrium contact angle far enough from the

transition contact angle, the curve becomes monotonically increasing indicating that it is not favourable to nucleate a new phase.

5.2.2.2. Effect of the flat plate separation distance on the stability of a vapour phase being formed from the liquid phase between two flat plates: convex meniscus

The flat plate separation distance, *H*, is an important factor that determines whether the vapour formation with a convex meniscus is favourable in the first place, and also determines the size of the energy barrier when vapour bridge formation is possible. Figure 5-17 displays the effect of flat plate separation distance.

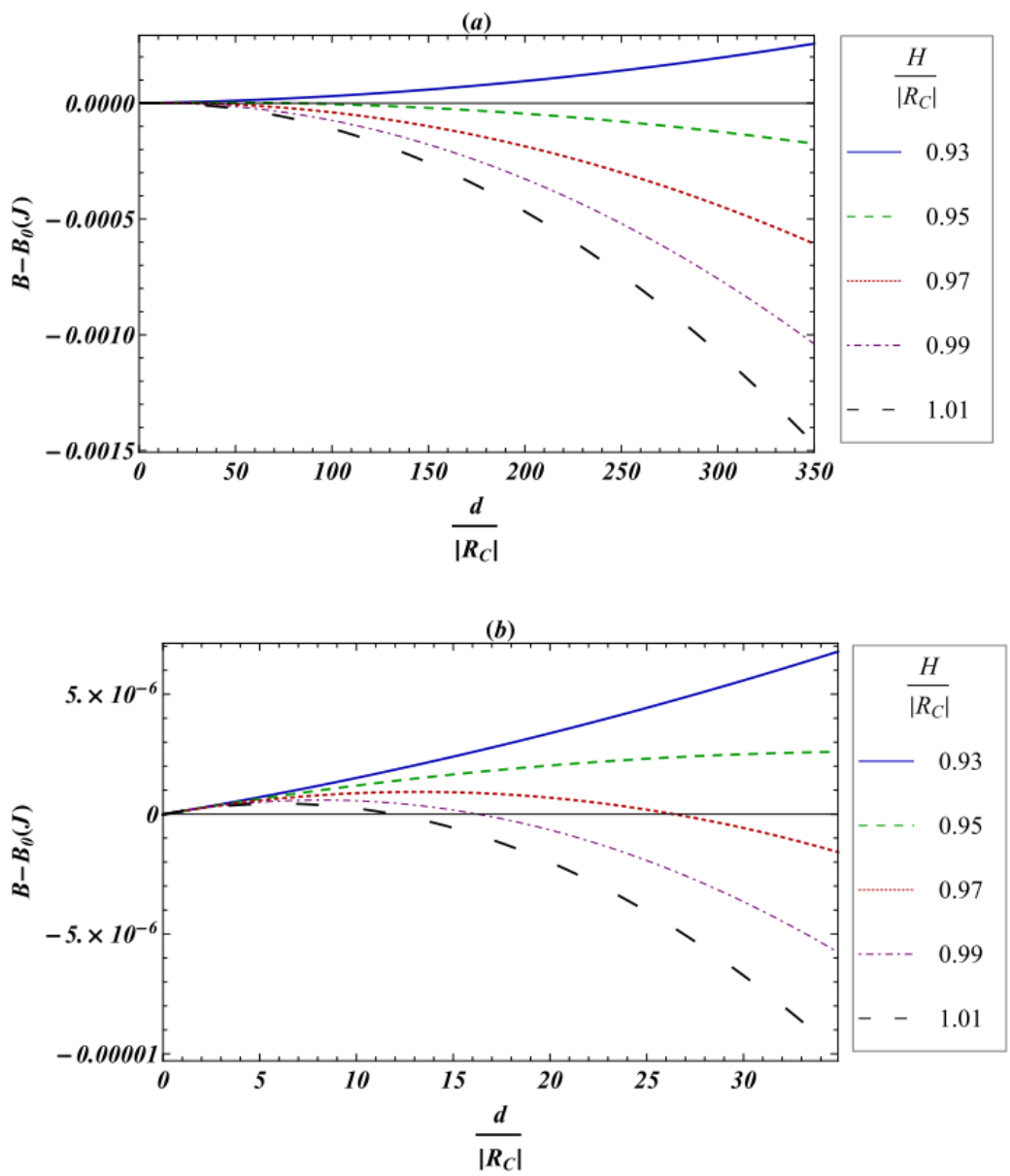

Figure 5-17 (a) Effect of the flat plate separation distance on the free energy vs. vapour bridge half width between two flat plates, for water at 20°C, θ =20°, and P^L=0.9P_∞, (b) Magnification of the unstable equilibrium point.

As shown in Figure 5-17, the formation of the vapour phase with a convex meniscus is unfavourable at small flat plate separation distances. Vapour formation with a convex liquid−vapour interface becomes favourable at some large enough separation distance. Further increase in the distance makes the energy barrier

smaller, and a smaller vapour bridge needs to be formed to overcome the unstable equilibrium point.

Closer examinations were performed to find the amount of plate separation distance below which vapour formation is impossible due to wettable plates that tightly confine the liquid phase. For contact angle equal to 0°, while other properties are kept the same as Figure 5-17, phase transition from liquid being confined by wettable walls to vapour is favourable for plate separation distance above R_C. Considering the effect of contact angle as discussed in section 5.1.2.1 liquid phase formation is favourable, regardless of the amount of contact angle, for plate separation distances above the Kelvin radius. Through further examination of the free energy curve for different contact angles, $|R_C cos\theta|$ is found to be the distance below which phase transition from confined liquid with wettable walls into vapour is unfavourable. This amount is inspired by the amount proposed in literature [12, 24] for the separation distance above which concave liquid formation between a sphere and a flat plate is unfavourable.

5.3. Conclusion

The focus of this chapter has been the liquid−vapour system between two flat plates under the condition of constant bulk phase pressure and constant mass. Two possible systems with the liquid−vapour interface were investigated: (1) liquid formation from a bulk vapour phase and (2) vapour formation from a bulk liquid phase. Each of these might have a concave outward or a convex outward interface.

Thermodynamic stability analysis was performed on each of these cases. The effects of the contact angle and of the flat plate separation distance on the stability of the system were investigated in separate sections.

The following table, Table 5-3, summarizes the results in sections 5.1 and 5.2.

Table 5-3 Summary of liquid phase formation out of a bulk vapour phase and vapour phase formation out of a bulk liquid phase between two flat plates, and the effect of the equilibrium contact angle, θ, and the plate separation distance, H, on the stability of the system. θ_t is the transition contact angle, R_1 & R_2 are the principal radii of the liquid-vapour interface, P^L is the liquid phase pressure, and P^V is the vapour phase pressure.

Case		Arbitrary Definition of ΔP	Sign of R_1 & R_2 according to ΔP definition	Bulk pressure	Equilibrium state	Increase in θ	Increase in H
Liquid Formation from vapour ($\theta_t = 90^o$)	Concave ($\theta < 90^o$)	$P^V - P^L$	R_1 (+) R_2 (−)	$P^V < P_\infty$	1 unstable	~ Closer to θ_t →Larger barrier (ultimately unfavourable new phase formation)	→Larger barrier
	Convex ($\theta > 90^o$)	$P^V - P^L$	R_1 (−) R_2 (−)	$P^V > P_\infty$	1 unstable	~Farther from θ_t →Larger barrier (ultimately unfavourable new phase formation)	→Smaller barrier
Vapour formation from liquid ($\theta_t = 90^o$)	Concave ($\theta > 90^o$)	$P^L - P^V$	R_1 (+) R_2 (−)	$P^L > P_\infty$	1 unstable	~Farther from θ_t →Smaller barrier	→Larger barrier
	Convex ($\theta < 90^o$)	$P^L - P^V$	R_1 (−) R_2 (−)	$P^L < P_\infty$	1 unstable	~Closer to θ_t →Smaller barrier	→Smaller barrier

From what has been discussed, it can be concluded that for formation of a liquid from a bulk vapour phase, or a vapour from a bulk liquid phase, between two flat plates:

1) In the formation of a liquid from a bulk vapour phase between two flat plates, one of the following would happen:
   - Liquid formation with concave meniscus is possible if and only if bulk vapour pressure is below the saturation pressure ($P^V < P_\infty$) as discussed in section 5.1.1. Also a concave meniscus is only possible for vapour phase inside a confinement with wettable solid walls, that allows for $\theta < 90^o$. With all these conditions being satisfied ($P^V < P_\infty$ and solid material such that $\theta < 90^o$) liquid formation with concave meniscus is still unfavourable for high plate separation distance, and/or for contact angles close to the ***transition contact angle***. For the cases where liquid formation with concave meniscus is favourable, after passing the nucleation barrier, all the vapour phase would condense into liquid. Hence no liquid phase with concave meniscus can exist in a stable condition. This phenomenon of phase transition from vapour to liquid at pressure below the satiation pressure ($P^V < P_\infty$) is well known as capillary condensation.
   - Liquid phase formation with convex meniscus is possible if and only if bulk vapour pressure is above the saturation pressure ($P^V > P_\infty$) as discussed in section 5.1.2. Such a convex meniscus is only achievable through non-wettable confinement that results in $\theta > 90^o$. Even when all

these conditions are met ($P^V > P_\infty$ and solid material such that $\theta > 90^o$), for some small values of separation distance (H), and/or some contact angle far from the ***transition contact angle***, the free energy curve turns into a constantly increasing curve and liquid formation with convex meniscus is unfavourable. This is interesting that even at bulk vapour pressure above the saturation pressure confinement with non-wettable walls prevent phase transition from vapour to liquid, which would occur at saturation pressure for a non-confined liquid. If the parameters (H and θ) are such that liquid formation with convex meniscus is favourable, some nucleation barrier is to be overcome. Once this nucleation barrier is overcome, all the vapour phase turns into the liquid phase (the free energy curve is ever ascending after the maximum point). It should be highlighted that between two flat plates, a liquid bridge with convex meniscus can never exist in a stable condition.

2) In the formation of vapour from a bulk liquid phase between two flat plates, one of the following would occur:

- Vapour formation with concave meniscus is possible if and only if bulk liquid pressure is above the saturation pressure ($P^L > P_\infty$) as discussed in section 5.2.1. Such a concave meniscus is only achievable through non-wettable confinement walls for which $\theta > 90^o$. Under these conditions ($P^L > P_\infty$) and solid such that $\theta > 90^o$), vapour formation with concave meniscus is still impossible (the free energy curve is monotonically increasing) for some contact angle close to the ***transition contact angle*** and/or for plates

with large separation distance. When vapour phase formation with concave meniscus becomes favourable, it would happen only once the nucleation barrier is overcome, and after that all the liquid phase would evaporate into vapour. It should be noted that a vapour phase with concave meniscus cannot exist in a stable condition. This phenomenon of phase transition inside a confinement from liquid phase at pressure above the saturation pressure to vapour phase is called capillary evaporation.

- Vapour formation with convex meniscus is possible if and only if bulk liquid pressure is below the saturation pressure ($P^L < P_\infty$) as discussed in section 5.2.2. Such a convex meniscus only happens in a confinement with wettable walls for which $\theta < 90^o$. Even at these condition ($P^L < P_\infty$ and wettable solid that makes $\theta < 90^o$), phase transition from liquid to vapour can be unfavourable (i.e. monotonically increasing energy curve) for contact angles far from the ***transition contact angle***, and/or for small plate separation distances. It is interesting that phase transition from liquid at pressure below the saturation pressure ($P^L < P_\infty$) to vapour is prevented by tight confinement of the liquid phase with wettable walls, while for an unconfined liquid this phase transition happens at the saturation pressure. If the parameters (H and θ) are such that phase transition is possible, vapour formation would happen once the nucleation barrier is overcome, after which all the liquid phase would evaporate into vapour. It should be highlighted that no stable vapour phase with convex meniscus can exist.

3) For cases where only an unstable condition (maximum point) exists in the free energy curve vs. the size of the new phase, the curve would decrease monotonically after that unstable point. In this situation all of the bulk phase would change into the new phase once the nucleation barrier is overcome.

4) Effect of the contact angle:

- When the meniscus is concave, getting farther from the ***transition contact angle*** results in a smaller energy barrier and advances the nucleation process. In the case of liquid formation from a bulk vapour phase, the meniscus is concave for $P^V < P_\infty$ and for a wettable confinement ($\theta < 90^o$). In the case of vapour formation from a bulk liquid phase, a concave meniscus is possible for $P^L > P_\infty$ and for non-wettable confinement ($\theta > 90^o$). For concave liquid formation from a bulk vapour phase, decrease of the contact angle results in getting farther from the ***transition contact angle***. For concave vapour formation from a bulk liquid phase, increasing the contact angle is equivalent to getting farther from the ***transition contact angle***.
- When the meniscus is convex, getting farther from the ***transition contact angle*** increases the amount of the energy barrier; until at some far enough contact angle the curve becomes ever increasing and the new phase formation becomes unfavourable. In the case of liquid formation from a bulk vapour phase, the meniscus is convex for $P^V > P_\infty$ and for a non-wettable confinement ($\theta > 90^o$). In the case of vapour formation from a bulk liquid phase, a convex meniscus is possible for $P^L < P_\infty$ and for wettable confinement ($\theta < 90^o$). For convex liquid formation from a bulk vapour

phase, increase of the contact angle results in getting farther from the ***transition contact angle***. For convex vapour formation from a bulk liquid phase decreasing the contact angle is equivalent to getting farther from the ***transition contact angle***.

5) In new phase formation with a concave meniscus, changing the contact angle by a specific number of degrees results in larger relative changes of the energy barrier for contact angles close to the ***transition contact angle*** (90º). The focus of this statement is contact angles for which new phase formation is favourable (the free energy vs. new phase size curve is not constantly increasing).

6) Effect of the flat plate separation distance:

- In the case of concave meniscus (liquid formation or vapour formation) larger separation distances increase the height of the energy barrier; until at some large enough separation distance the new phase formation becomes unfavourable. New phase formation with concave meniscus is certainly unfavourable for plate separation distance above R_C, regardless of the amount of the contact angle. The separation distance above which new phase formation is unfavourable can be more accurately predicted by $|R_C cos\theta|$, which is a modification of what is proposed in literature [12, 24] for liquid formation with concave meniscus between a sphere and a flat plate.
- When having a convex meniscus (liquid formation or vapour formation) a larger separation distance promotes the new phase formation by decreasing the energy barrier. New phase formation with convex meniscus out of a fluid confined between two flat plats is prevented if the plate separation distance

is below $|R_C cos\theta|$. It shows that while phase transition happens at the saturation pressure for a fluid without any confinement, confinement may prevent the phase transition: Vapour being confined by non-wettable plates separated by a distance less than $|R_C cos\theta|$ does not turn into liquid, even though $P^V > P_\infty$. Liquid being confined by wettable plates of distance below $|R_C cos\theta|$ does not turn into vapour, even though $P^L < P_\infty$.

6. Liquid−vapour system between a sphere and a flat plate

The solid geometry of concern is the gap between a solid sphere and a solid plate. The sphere−plate geometry is the shape of the confinement in many practical cases. For the study of this chapter, the liquid−vapour system is considered to be pure with constant mass and constant bulk phase pressure (imposed by a reservoir). The solid interfaces (solid−liquid and solid−vapour) are *flat* for the solid plate, and are *curved* for the solid sphere. According to Table 3-4, a solid sphere, being a *curved* surface, results in an extra equilibrium condition, which is the equality of the chemical potential of the solid component in the solid phase with the chemical potential of the solid component adsorbed at the solid−liquid and the solid−vapour interfaces. This will affect the surface tensions of the solid–liquid and the solid solid−vapour interfaces (γ^{SL}, γ^{SV}) which in turn affects the equilibrium contact angle according to the Young equation (equation (2.16)). Therefore this equilibrium condition may cause the equilibrium contact angle to be different for the solid sphere and the solid plate, even though both the sphere and the plate are made of the same solid material.

Given that for the cases of interest, the distance between the sphere and the plate is very small compared to the radius of the sphere (for example a sphere of radius of several millimetres in comparison with a separation distance of less than 100 nm), we assume that the shape of the upper sphere has a negligible effect on contact angle. Therefore the contact angle with the upper spherical solid is assumed to be equal to the contact angle with the lower flat plate, provided both the sphere and the plate are made from the same solid material.

The assumption of equal upper and lower contact angles has been applied to the fluid confined between a sphere and a flat plate in many experimental studies [11, 12, 24]. It should be noted that spherical shape of the upper particle is accounted for in geometry relations, i.e. in calculating the volume of a new phase and the solid sphere surface area.

Both liquid formation from a bulk vapour phase, and vapour formation from a bulk liquid phase are investigated from the thermodynamic stability point of view (following the equations of chapter 3) in sections 6.1 and 6.2 respectively. Each of these sections is divided into two parts based on the concavity of the meniscus. Sections 6.1.1 and 6.1.2 consider liquid formation with concave and convex menisci correspondingly, and sections 6.2.1 and 6.2.2 discus vapour formation with concave and convex menisci. Different parameters have an effect on the stability of each of these cases. The effect of contact angle is explained in sections 6.1.1.1, 6.1.2.1, 6.2.1.1, and 6.2.2.1. The effect of the distance between the sphere and the flat plate is discussed in sections 6.1.1.2, 6.1.2.2, 6.2.1.2, and 6.2.2.2. The effect of

the solid sphere size on the thermodynamic stability of the system is also explained in sections 6.1.1.3, 6.1.2.3, 6.2.1.3, and 6.2.2.3. All these pieces are put together in section 0, and a conclusive picture of a confined fluid between a sphere and a flat plate is given.

6.1. Liquid phase formation from a bulk vapour phase between a sphere and a flat plate

The constraints of the system in which liquid forms out of a bulk vapour phase between a sphere and a flat plate, are presented in Table 3-2. The conditions for equilibrium of such a system are as presented in Table 3-4 (a).

As illustrated in section 2.4, the gravitational force can be neglected compared to the surface forces if the characteristic length of the new born phase is much smaller than the capillary length of the new born phase. This criterion is examined for n−dodecane at 24°C (same condition as [18], with the properties given in Table 3-7) and at bulk vapour phase pressure of $0.9P_\infty$ as an example. The Kelvin radius of the system at such conditions is 4.39×10^{-8} meters from equation (2.20). Also from Table 3-1, the capillary length of n−dodecane at 24°C is 1.85×10^{-3} meters. The capillary length is much larger than the Kelvin radius (supposed to be the characteristic length). Therefore gravitational effects can be ignored, and the pressure is assumed to be constant throughout the liquid phase as well as the vapour phase. Constant pressures imply the liquid−vapour interface must be a surface of constant curvature according to the Kelvin equation (2.20).

As mentioned in the previous chapter, a toroidal interface can accurately approximate the liquid−vapour interface for liquid bridge half widths greater than or equal to 6.5×R_C [18]. Pakarinen et al. [10] also calculated the exact shape of a liquid meniscus through the Kelvin radius. They showed, by comparing the capillary force calculated once for the exact profile and then for the circular approximation, that the circular profile approximation for the meniscus is justified in the validity range of continuum modeling (macroscopic physics) [10]. Such a liquid−vapour interface is shown in Figure 6-1.

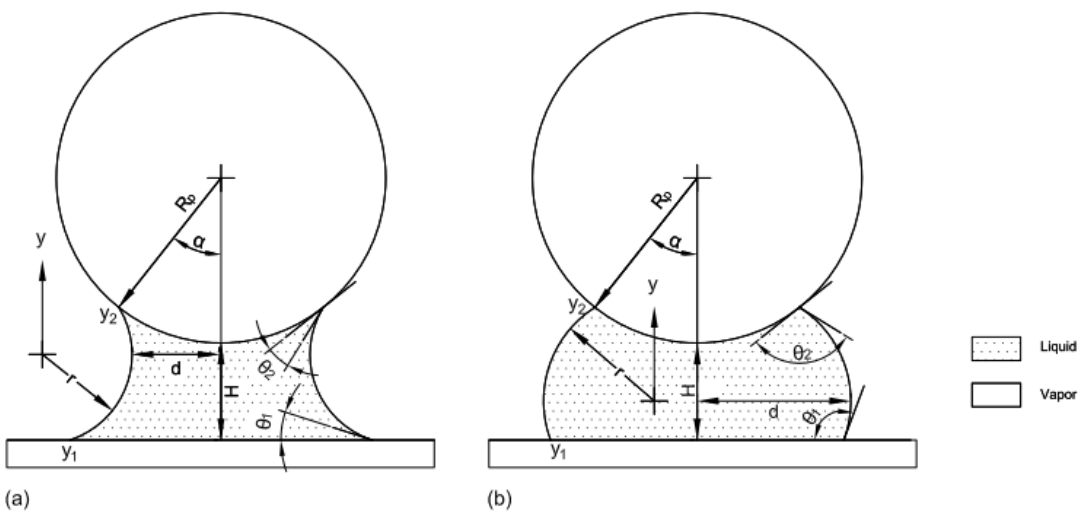

Figure 6-1 Schematic of a liquid bridge –a) concave and b) convex– between a flat plate and a sphere, where θ_1 and θ_2 are the equilibrium contact angles for the lower and upper surfaces, r is the radius of the circle approximating the vertical section of the liquid−vapour interface, d is the liquid bridge half width, H is the distance between the sphere and the flat plate, α is the half filling angle of the liquid in the bridge, y_1 is the three phase contact with the lower particle, y_2 is the three phase contact with the upper particle, and R_P is the radius of the spherical particle.

As presented in Figure 6-1, the interface is either concave or convex depending on the solid material. For identical contact angles at the upper and lower solid surfaces ($\theta_1 = \theta_2 = \theta$), the ***transition contact angle*** is $\frac{180°-\alpha}{2}$. The meniscus is hence concave for $\theta < \frac{180°-\alpha}{2}$ and is convex for $\theta > \frac{180°-\alpha}{2}$.

For the liquid−vapour interface of constant curvature being approximated by a toroidal surface, the principal radii of curvature, R_1 and R_2, have the size of $|R_1| = r$ and $|R_2| = d$, as shown in Figure 6-1. The signs of the principal radii of curvature are determined based on the definition of ΔP, and according to the concavity of the meniscus. Here ΔP is defined as $P^V - P^L$ for the case of liquid formation. For a concave meniscus, R_1 is positive since the centre of the circle is in the vapour phase ($R_1 = r$) and R_2 is negative ($R_2 = -d$) due to its centre being inside the liquid phase. In the same way for the convex case, both of the radii are negative ($R_1 = -r$ and $R_2 = -d$).

The volume of revolution of a curve, $F(y)$, around the y−axis is equivalent to the summation of a sequence of thin flat washers [43]. To find the liquid volume (V^L), the volume of the part of the solid sphere immersed in the liquid (V_S) should then be deducted from the calculated volume of revolution. A^{LV} can be computed from the surface of revolution around the y−axis [44]. The appropriate equations giving V^L, A^{SL} and A^{LV} are presented in Table 6-1.

Table 6-1 Liquid volume, solid–liquid and liquid–vapour surface area for liquid bridge formation between a flat plate and a sphere.

$V^L = \pi \int_{y_1}^{y_2} F(y)^2 dy - V_S$	(6.1)		
$V_S = \frac{\pi}{3} R_P{}^3 (1 - \cos\alpha)^2 (2 + \cos\alpha)$	(6.2)		
$A^{SL} = \pi \left[F(y_1)^2 + 2R_P{}^2 (1 - \cos\alpha) \right]$	(6.3)		
$A^{LV} = 2\pi \int_{y_1}^{y_2} F(y) \sqrt{1 + F'(y)^2} dy$	(6.4)		
Concave meniscus ($\theta < \frac{180° - \alpha}{2}$)		**Convex meniscus ($\theta > \frac{180° - \alpha}{2}$)**	
$F(y) = r + d - \sqrt{r^2 - y^2}$	(6.5)	$F(y) = -r + d + \sqrt{r^2 - y^2}$	(6.6)
$y_1 = -r\cos\theta$	(6.7)	$y_1 = r\cos\theta$	(6.8)
$y_2 = r\cos\theta$	(6.9)	$y_2 = -r\cos\theta$	(6.10)

To perform the stability analysis of the liquid bridge, the equation of the free energy for the liquid formation (from Table 3-6) is to be calculated:

$$B - B_0 = \frac{2\gamma^{LV}}{R_C} V^L + (-\gamma^{LV} \cos\theta) A^{SL} + \gamma^{LV} A^{LV} \tag{3.59}$$

where V^L, A^{SL} and A^{LV} are to be substituted from Table 6-1. For a defined problem in which γ^{LV}, R_C, and θ are known, equation (3.59) after substitution of all geometric relations would be in terms of r and d, both of which can be written as a function of the half filling angle, α. For the case of the concave meniscus,

$$r = \frac{R_P(1 - \cos\alpha) + H}{\cos(\theta + \alpha) + \cos\theta} \tag{6.11}$$

$$d = R_P \sin\alpha - r[1 - \sin(\theta + \alpha)] \tag{6.12}$$

and for the case of the convex meniscus,

$$r = \frac{R_P(1 - \cos\alpha) + H}{-\cos(\theta + \alpha) - \cos\theta} \tag{6.13}$$

$$d = R_P \sin\alpha + r[1 - \sin(\theta + \alpha)] \tag{6.14}$$

The equilibrium state of the liquid bridge and its size can be obtained from the extremum of the curve of the free energy (B–B_0) of the system vs. the liquid bridge half length (d), or from the roots of $\left(\frac{\partial B}{\partial d}\right)_{\theta=\theta_e} = 0$ alternatively.

The stability of the liquid bridge is then obtained according to the type of the extremum point: a maximum point represents an unstable equilibrium, the global minimum corresponds to the stable equilibrium state, and any local minimum would be a metastable condition.

6.1.1. Stability of the liquid phase being formed from a bulk vapour phase between a sphere and a flat plate: concave meniscus

When the pressure difference is defined to be $\Delta P = P^V - P^L$, R_1 is positive and R_2 is negative since the centre of the radius is in the vapour for R_1 and in the liquid for R_2. Hence the mean radius of curvature from equation (2.14) is:

$$\frac{1}{R_m} = \frac{1}{2}\left(\frac{1}{r} - \frac{1}{d}\right) \tag{6.15}$$

and R_m is identical to Kelvin radius (R_C) at the equilibrium condition, according to equation (2.21).

As explained in the previous chapter, for various sphere–plate separation distances and equilibrium contact angles, it has been observed that at the equilibrium

conditions r is less than d. This would result in positive R_m according to equation (6.15), and therefore in positive R_C. For R_C to be positive, the vapour pressure must be below the saturation pressure ($P^V < P_\infty$) according to section 3.7.1.

The curve of the free energy vs. scaled liquid bridge half width ($\frac{d}{R_C}$) is shown in Figure 6-2 for n–dodecane at 24°C (the properties of which are reported in Table 3-7) as an example. The vapour pressure is set to be 0.9 P_∞ for which the Kelvin radius is 4.39×10^{-8} meters from equation (2.20). The equilibrium contact angle is set to 0°, the separation distance of the sphere and the flat plate is set equal to $0.97R_C$, and the solid sphere is taken to be of a radius of 2.5 cm. This is a reproduction of the calculations by Elliott and Voitcu [18] and the results are in good agreement.

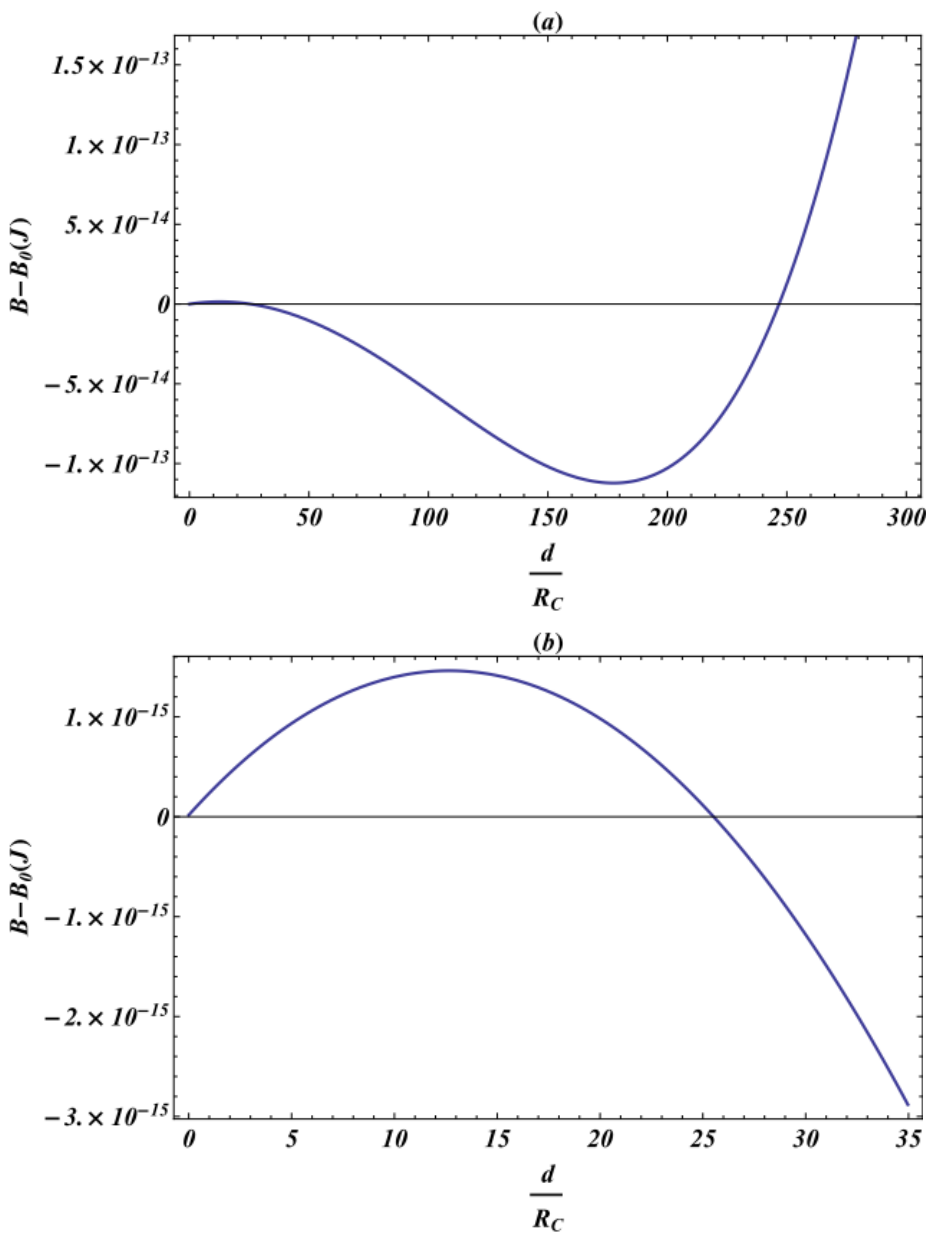

Figure 6-2 (a) Free energy vs. scaled liquid bridge half width ($\frac{d}{R_C}$) between a flat plate and a sphere, for n−dodecane at 24°C, P^V=0.9P_∞, θ=0°, H=0.97R_C, R_p=2.5 cm, (b) Magnification of the region close to d=0

There is a maximum point in the free energy curve, demonstrating an energy barrier to be overcome for the phase transition. The phase transition therefore is a nucleation phenomenon. Once this barrier is overcome the energy barrier gets to a minimum point and the liquid bridge stays at its stable equilibrium size.

6.1.1.1. Effect of equilibrium contact angle on the stability of the system for liquid phase formation out of a bulk vapour phase between a flat plate and a sphere: concave meniscus

Thermodynamic stability analysis has been performed by others, while considering only zero contact angle [18]. In this section, the role of the equilibrium contact angle on the free energy curve will be investigated. The properties of the system other that the equilibrium contact angle are kept the same as those in Figure 6-2.

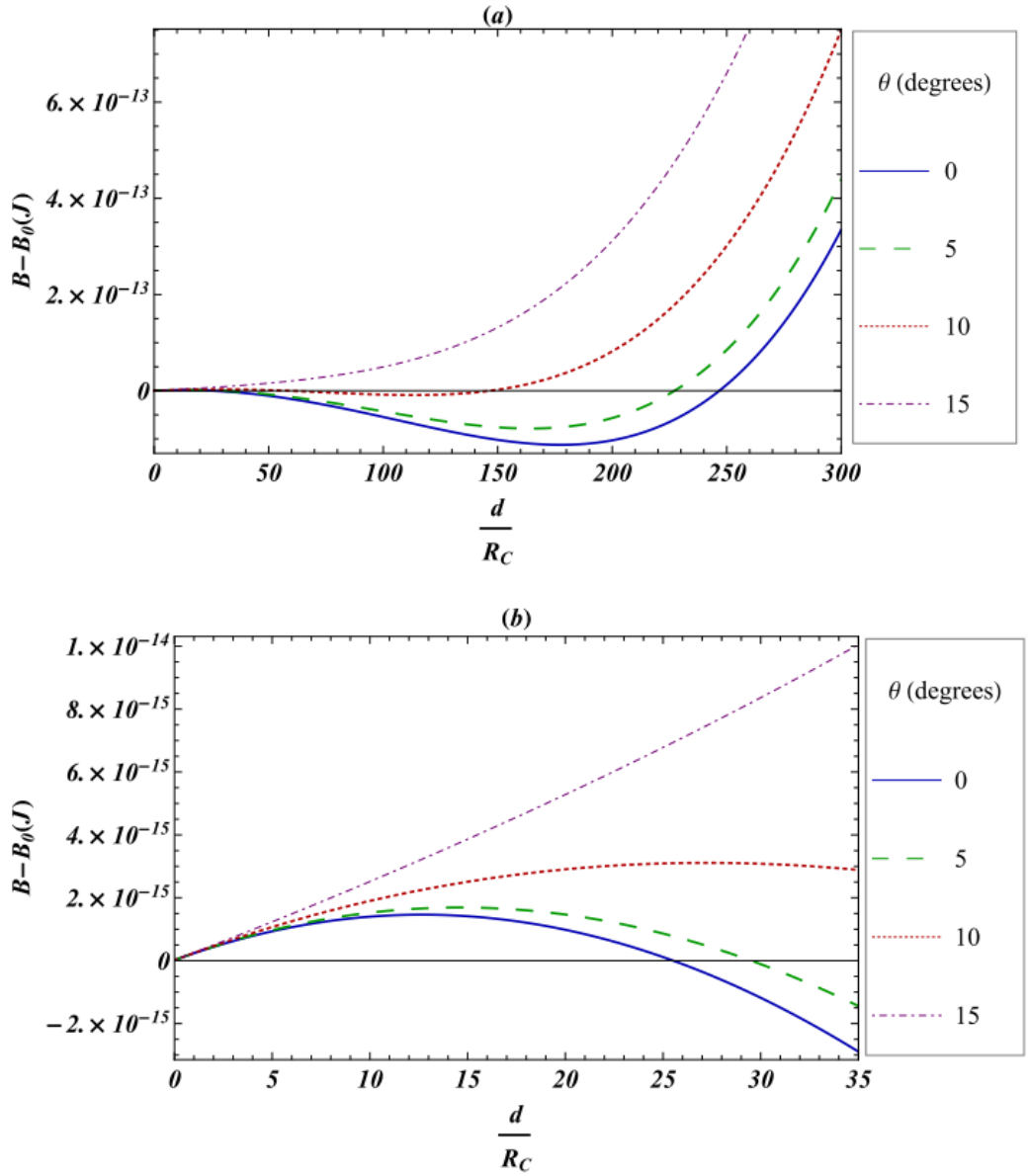

Figure 6-3 (a) Effect of the equilibrium contact angle on the free energy vs. scaled liquid bridge half width between a flat plate and a sphere, for n−dodecane at 24ºC, P^V=0.9P_∞, H=0.97R_C, R_p=2.5 cm, for various contact angles that result in concave meniscus (b) Magnification of the unstable equilibrium point.

For this case of liquid formation with concave meniscus, as contact angle increases (get closer to the ***transition contact angle***) an increase occurs in the height of the energy barrier, and the unstable liquid bridge is formed at larger bridge width. The increase of the contact angle (closer to the ***transition contact angle***) also results in

a shallower stable equilibrium state with a smaller size of the bridge, i.e. a smaller amount of liquid would form with less stability.

As the increase of the contact angle continues, at a certain contact angle the curve becomes monotonically increasing where the formation of the liquid turns out to be unfavourable.

From further investigations it has been found that a specific number of degrees change in the contact angle results in larger relative changes in the energy barrier and the energy level of the minimum point for contact angles closer to the ***transition contact angle***. This statement only applies to the cases where liquid formation is possible (and the curve has a maximum point, followed by a minimum point), and not the cases where liquid formation is unfavourable (the energy curve is constantly increasing). Figure 6-4 illustrates the above statement.

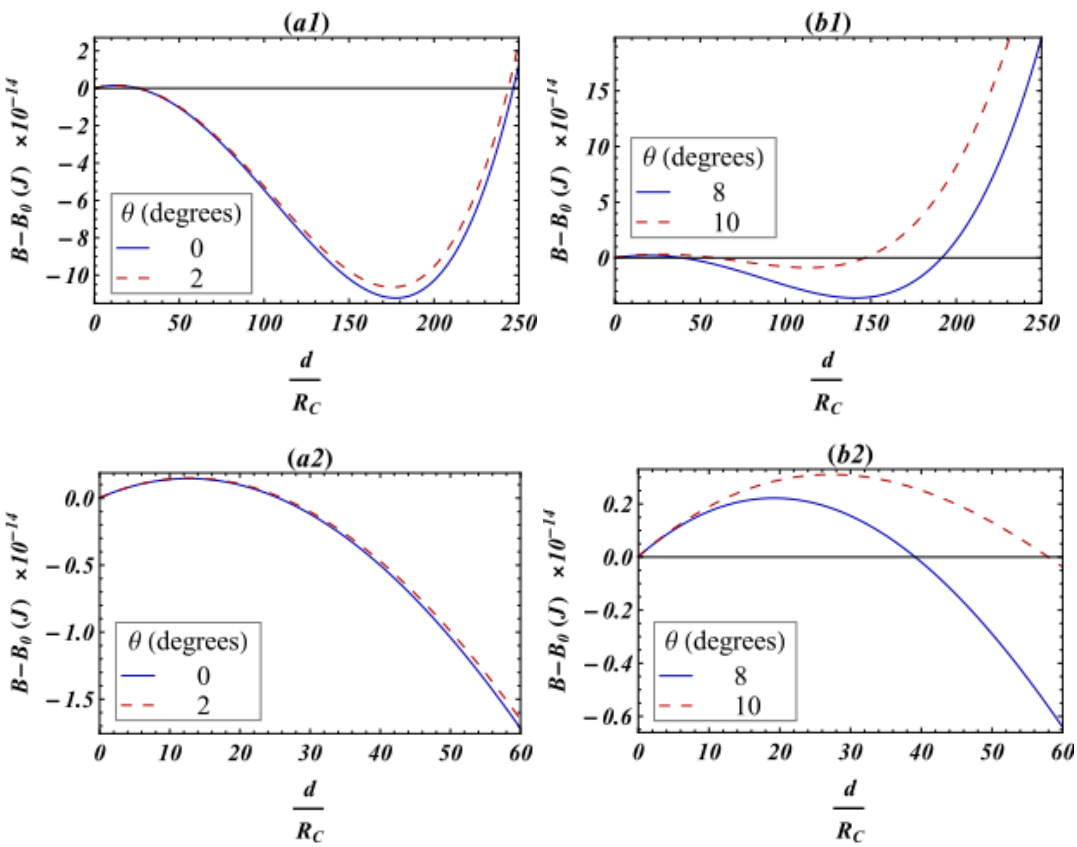

Figure 6-4 Comparison of the effect of a specific number of degrees change (2°) in the equilibrium contact angle on the free energy of liquid formation with a concave meniscus between a flat plate and a sphere, for n−dodecane at 24°C, P^V=0.9P_∞, H=0.97R_C, R_p=2.5 cm, (a1) far from the transition contact angle, (b1) closer to the transition contact angle. (a2) and (b2) are magnifications of (a1) and (b1) respectively.

In (a1) and (a2) of Figure 6-4 where the contact angle is changing from 0° to 2° far from the ***transition contact angle***, the energy level of the barrier is changed from 1.46×10^{-15} J to 1.49×10^{-15} J, and the energy level of the stable point is changed from -1.12×10^{-13} J to -1.06×10^{-13} J. In (b1) and (b2) when the contact angle changes from 10° to 12°, which is closer to the ***transition contact angle***, the energy level of the barrier is changed from 2.22×10^{-15} J to 3.11×10^{-15} J, and the energy level of the stable point is changed from -3.61×10^{-14} J to -8.88×10^{-15} J. The relative difference, being calculated from equation (4.21), is presented in Table 6-2 for each case.

Table 6-2 Relative differences in the free energy level of the maximum and minimum points as a result of a certain number of degrees (2°) change in the contact angle for the case of liquid formation with concave meniscus out of a bulk vapour phase.

$\theta_1 \rightarrow \theta_2$	Relative difference in energy level of the maximum point	Relative difference in energy level of the minimum point
0°→2° (far from θ_t)	2.22%	5.15%
8°→10° (close to θ_t)	40.24%	75.41%

6.1.1.2. Effect of the solid surface separation distance on the stability of the system for liquid phase formation out of a bulk vapour between a sphere and a flat plate: concave meniscus

Figure 6-5 shows the effect of the solid surface separation distance on the free energy curve of liquid formation with a concave meniscus.

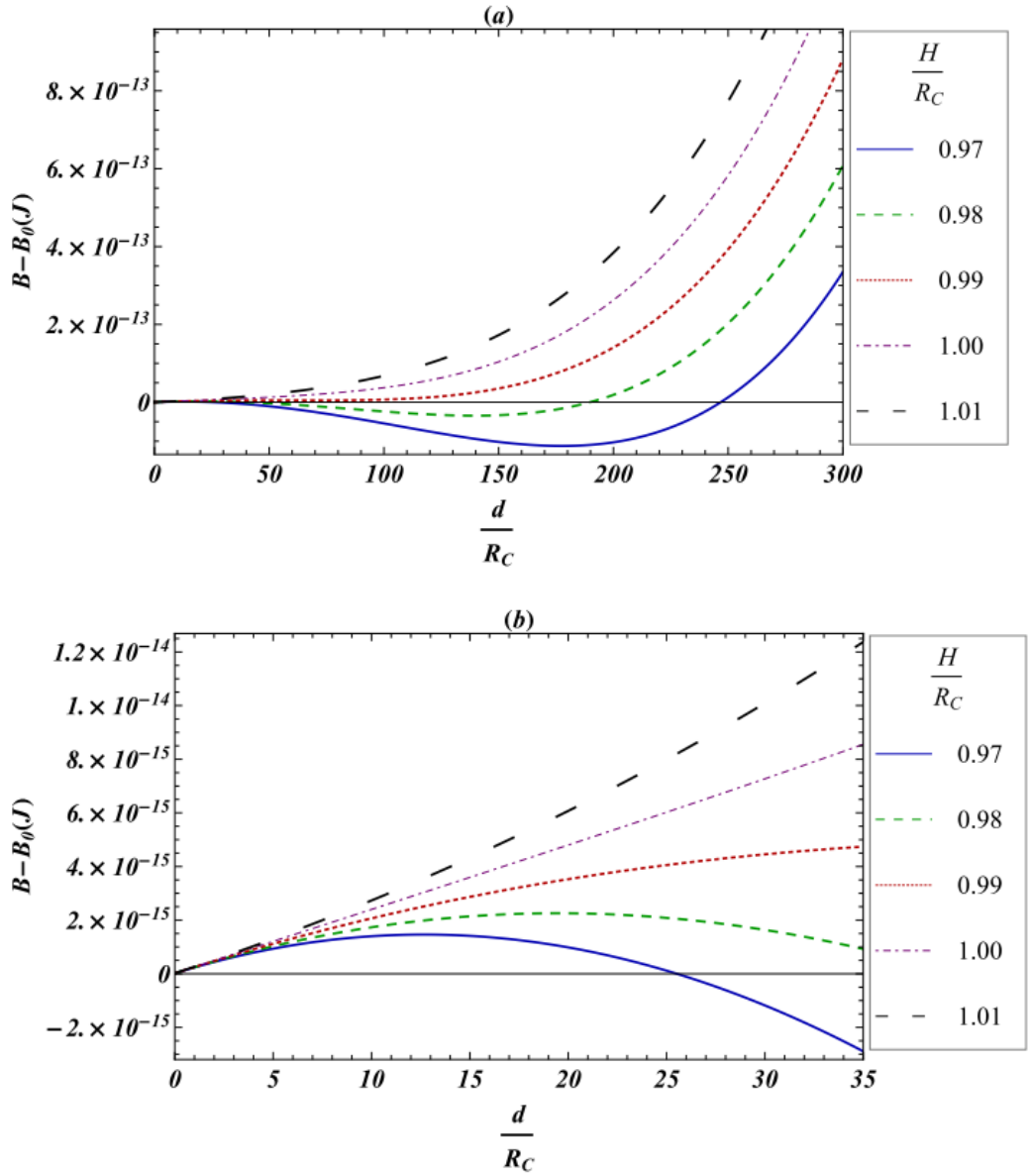

Figure 6-5 (a) Effect of the solid surface separation distance on the free energy vs. scaled liquid bridge half width between a flat plate and a sphere, for n−dodecane at 24ºC, P^V=0.9P_∞, θ=0º, R_p=2.5 cm, (b) Magnification of the unstable equilibrium point.

Figure 6-5 is a reproduction of, and is in good agreement with, the study which has previously been performed [18]. A higher energy barrier with a larger liquid bridge width is to be overcome as the separation distance between a sphere and a flat plate increases. Larger sphere–plate separation distance also causes less stability

(shallower minimum) and shorter liquid bridge width for the stable equilibrium state.

Further increase in the sphere–plate separation distance makes the free energy curve constantly ascending and the formation of the liquid phase to be unfavourable. The solid surface separation distance above which the liquid formation becomes unfavourable (the liquid bridge breaks from its stable condition) is called the ***breakage distance*** (H_{Break}) [18].

For liquid formation in this geometry, the breakage distance is approximated by the ***critical distance*** (H_{Break}) in terms of the Kelvin radius and the contact angle, for the cases where $R_P >> |d| >> H$, and for small contact angles [24]. Fisher and Israelachvili used some different notations and definitions in their work, for example the mean radius of curvature is defined as $\frac{1}{R_m} = (\frac{1}{R_1} + \frac{1}{R_2})$, rather than $\frac{1}{R_m} = \frac{1}{2}(\frac{1}{R_1} + \frac{1}{R_2})$ as in our work and many others [18]. Translating their notations and definitions into ours, the critical distance is given by:

$$H_{Break} = R_C \cos\theta \left\{ 1 - \frac{3}{\left(\frac{32 R_P \cos\theta}{R_C}\right)^{1/3}} \right\} \tag{6.16}$$

as stated in [24].

Equation (6.16) for the critical distance is obtained through geometrical relations between d, r, and H, and equation (2.21), which makes it possible to write H in terms of d, R_P, θ, and R_C. Then with constant R_P and θ for a defined problem, and

constant R_C at fixed vapour pressure, H and d are the only variables. Therefore the maximum of H, equivalent to H_{Break}, can be obtained in terms of the constants R_P, θ, and R_C, through the derivative of H with respect to d. The value of H_{Break} is very insensitive of R_P, and is approximated by $R_C \cos\theta$ [24]. This is a good approximation for large enough $\frac{R_P}{R_C}$ values. For example for n–dodecane at 24ºC, $P^V=0.9P_\infty$, and $\theta=0^o$, the breakage distance is approximated to be equal to R_C. However from equation (6.16), the breakage distance is $0.990\times R_C$ for a sphere of 2.5cm ($\frac{R_P}{R_C}$ = 5.7×10^5) and is $0.978\times R_C$ for a sphere of 2.5 mm ($\frac{R_P}{R_C}$ = 5.7×10^4).

The breakage distance is less than R_C for any contact angle according to equation (6.16) . Thus liquid formation between a sphere and a flat plate is certainly unfavourable, regardless of the contact angle, for any sphere–plate separation distance of above R_C ($H>R_C$). For $H< R_C$, further investigation is to be done for each contact angle of interest to figure out the favourability of liquid formation at H close to R_C.

A closer look is given to liquid formation with concave meniscus, and $\theta=0^o$, between a sphere and a flat plate, at separation distance near the breakage distance.

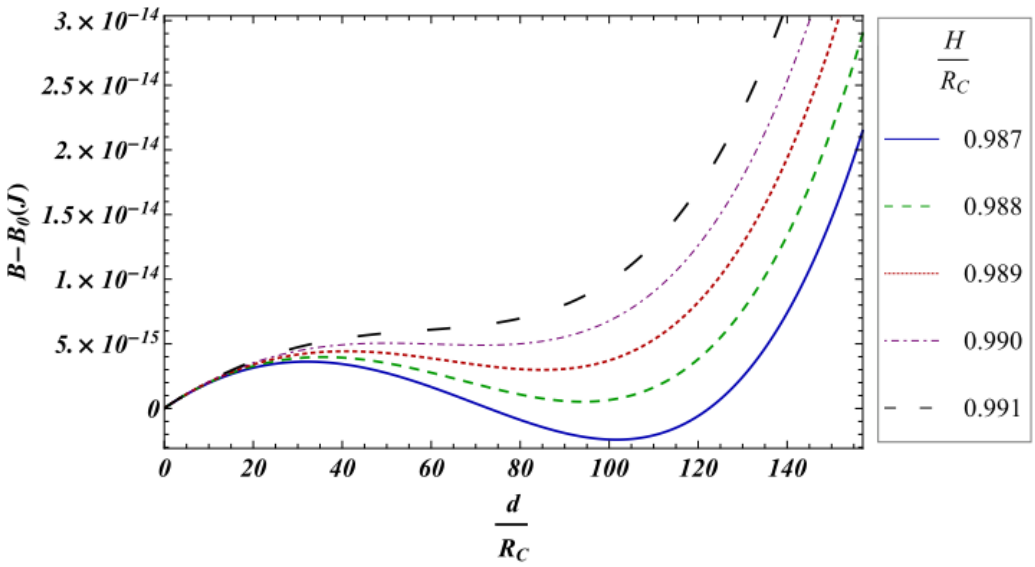

Figure 6-6 Energy level of the maximum and minimum points at sphere–plate separation distance close to the breakage distance for a liquid bridge between a flat plate and a sphere, for n−dodecane at 24°C, P^V=0.9P_∞, θ=0°, R_p=2.5 cm.

Figure 6-6 is also a reproduction of previous studies, indicating a breakage distance of 0.990×R_C [18], which is in good agreement with the breakage distance calculated from equation (6.16), and slightly smaller than a breakage distance obtained from $R_C \cos\theta$ (equal to R_C in this case where θ is 0°).

As the sphere–plate separation distance increases to the breakage distance, the free energy of the stable equilibrium becomes approximately identical to the free energy of the unstable equilibrium as illustrated in Figure 6-6. Hence natural fluctuations large enough to overcome the nucleation barrier are also large enough to allow the bridge to disappear. This leads to fluctuations of the liquid bridge size between the unstable and the stable liquid bridge sizes. Elliott and Voitcu explain this as a thermodynamic understanding of the "diffuse liquid−vapour interface" [18].

In experiments by Maeda et al. on n-hexadecane, two different behaviours have been observed at sphere–plate separation distance equal to H_{Break} (for the case where contact angle is zero, and $H_{Break}=R_C$) based on how this separation distance is approached [12]:

1) If the separation distance is initially above H_{Break}, and it decreases to H_{Break}, the bridge that forms at H_{Break} has density between the densities of liquid and vapour, and behaves like a fluid above its critical point [12].
2) If the separation distance is initially below H_{Break}, and it increases to H_{Break}, the reflective index of the bridge remains that of a bulk liquid at H_{Break} [12].

This process-based behaviour at H_{Break} can be described as follow:

1) In the first case where the sphere–plate separation distance is initially above and then decreases to H_{Break} , the free energy curve changes from steadily increasing (no liquid existence) for $H> H_{Break}$, to a curve with an unstable followed by a stable state at $H= H_{Break}$. Thus in this approach, at $H= H_{Break}$ liquid is to be formed after passing a nucleation barrier, while the possibility of liquid nucleation did not exist at previous steps where $H> H_{Break}$. Longer time is required, due to the necessity of passing a nucleation barrier, before the system can reach its stable equilibrium. Before reaching the stable equilibrium condition, the energy fluctuates between the maximum and minimum points and this can potentially described a non-uniform density profile and a diffuse liquid-vapour interface as previously described [18].
2) In the second process, a sphere and a flat plate were initially separated by a distance below H_{Break} , which then increases to H_{Break} . At $H<H_{Break}$, with the

free energy curve having an unstable and a fairly more stable state, the liquid bridge has already been formed. As the separation distance increases, the liquid bridge which already exists, should only adjust itself to a new (smaller) stable size. Here since the liquid bridge already exists and no nucleation is necessary, no fluctuations happen. Hence at $H=H_{Break}$, simply the size of the bridge shrinks and gets stable to its new stable size.

It should be mentioned that as the focus is the thermodynamic equilibrium state, non- equilibrium transitions as a result of mechanical instabilities (coalescence as a result of van der Waals force when the separation distance is decreasing, and snapping as a result of Rayleigh instability when the separation distance is increasing rapidly [12]) are not in the perspective of this research.

At the other side when the distance between a sphere and a flat plate decreases to zero (the sphere and plate are touching), the energy barrier is eliminated and the phase transition would be a non−nucleating spontaneous process as shown in Figure 6-7. In fact the contact point of the two solids acts as an agent for the new phase formation with concave meniscus. Decreasing the separation distance to zero, also results in the most stable equilibrium with the greatest liquid bridge width.

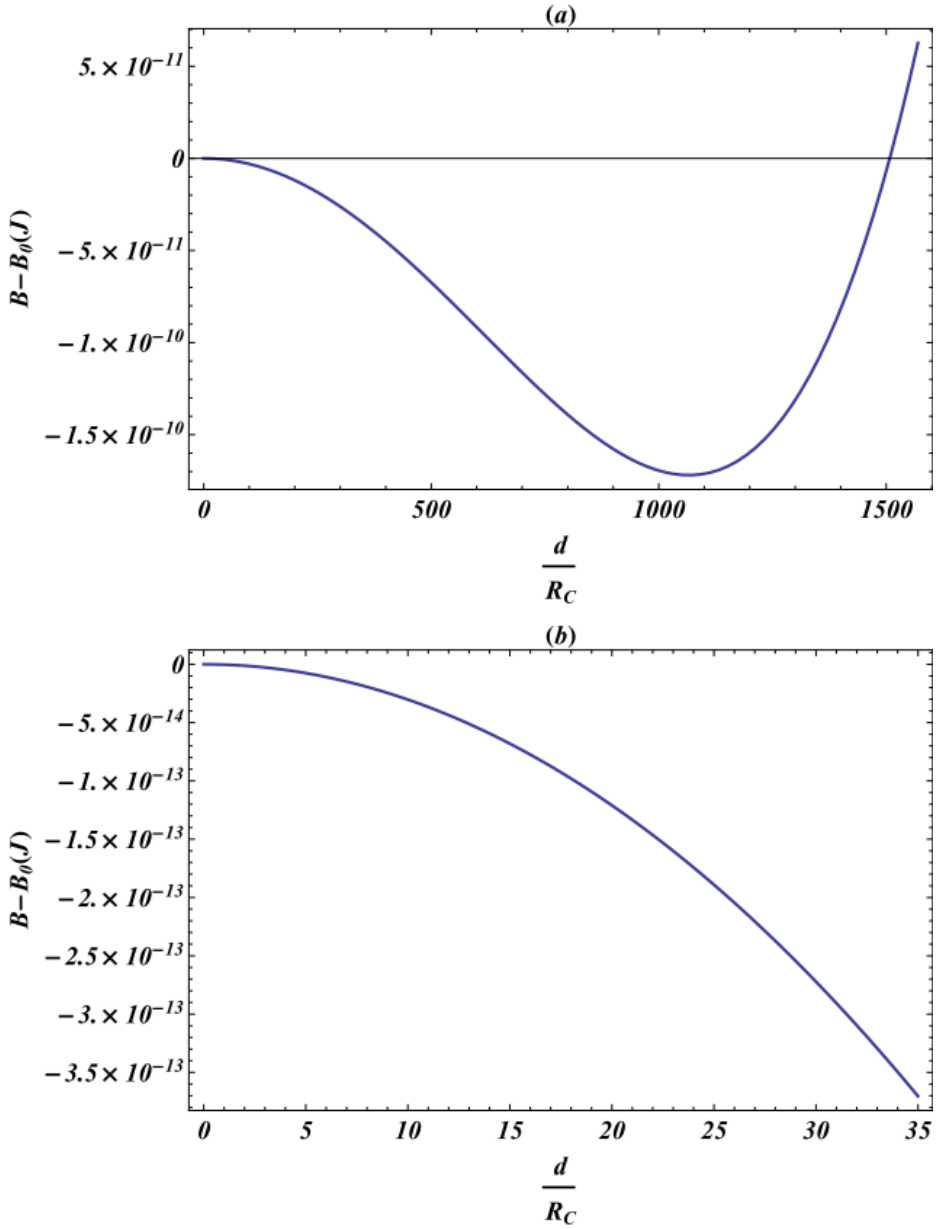

Figure 6-7 (a) Free energy vs. scaled liquid bridge half width between a flat plate and a sphere, for n−dodecane at 24°C, P^V=0.9P_∞, θ=0°, H=0, R_p=2.5 cm. (b) Magnification of the calculation at small bridge width.

Another interesting point is that when a flat plate and a sphere are in contact (H=0), there is always a stable liquid bridge for any contact angle or any sphere size. For example for a sphere and a plate at H=0.97R_C (and the conditions of Figure 6-2) the liquid formation becomes unfavourable for contact angles above 11.5°, whereas

with H=0 liquid formation is favourable for all the contact angles below the ***transition contact angle***, for which the meniscus is concave (for example a stable liquid bridge with a scaled bridge width of $\frac{d}{R_C}$ = 93 is formed when the contact angle is 89.5°).

6.1.1.3. Effect of solid sphere size on the stability of the system for a liquid phase being formed out of a bulk vapour phase between a flat plate and a sphere: concave meniscus

The effect of size of the sphere on the stability behaviour of a liquid bridge with a concave meniscus between a sphere and a flat plate is studied in this section. The properties of the system other than the radius of the solid sphere are kept the same as those in Figure 6-2.

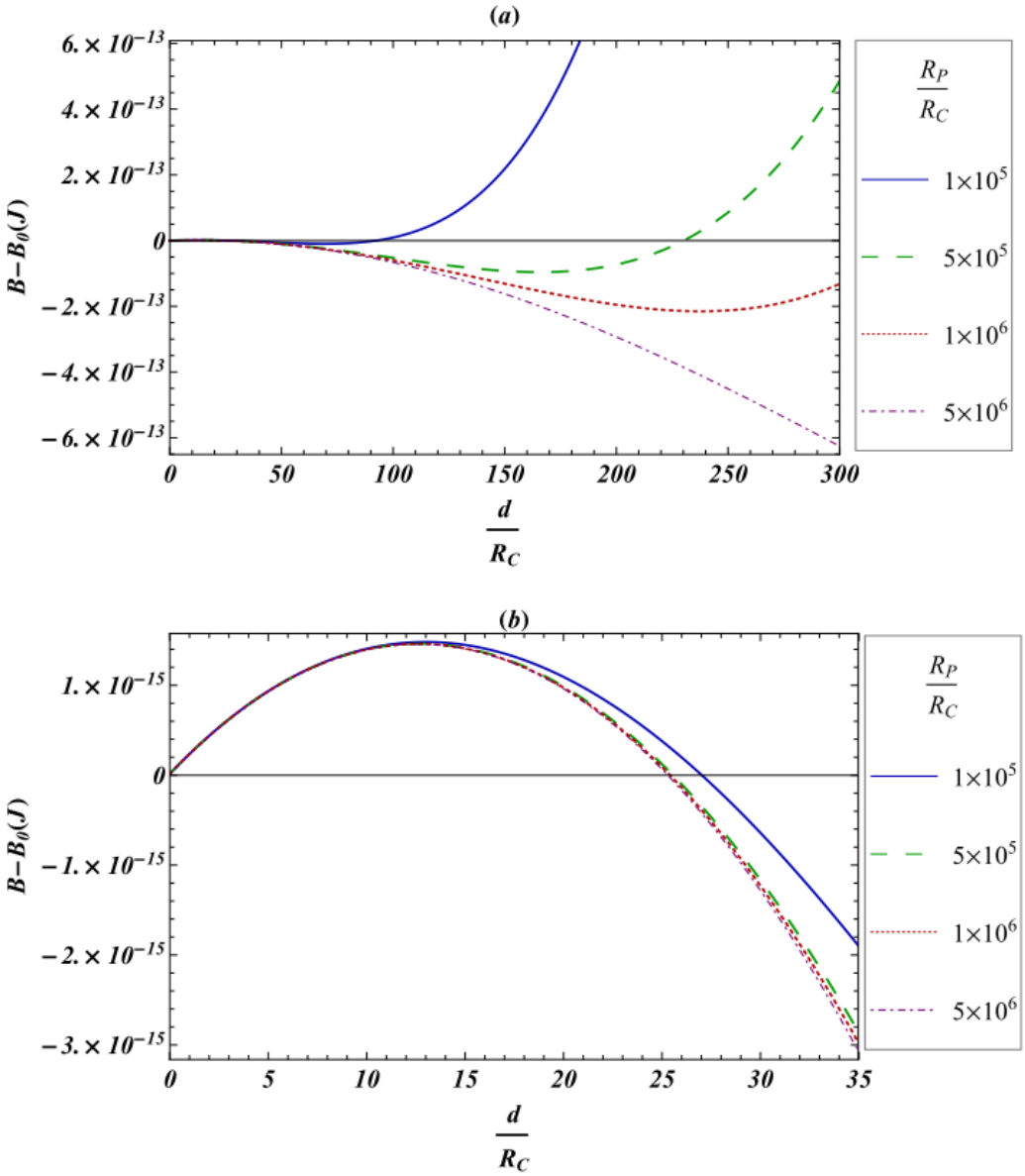

Figure 6-8 (a) Effect of the solid sphere size on the free energy vs. scaled liquid bridge half width between a flat plate and a sphere, for n−dodecane at 24°C, P^V=0.9P_∞, θ=0°, H=0.97R_C and P^V=0.9P_∞, (b) Magnification of the unstable equilibrium point.

In Figure 6-8, the radius of the solid sphere is changing from millimetres ($10^5 \times R_C$) to decimetres ($5\times10^6 \times R_C$). Increase in the radius of the solid sphere results in more stability (deeper minimum) and larger width of the liquid bridge. The extreme as the sphere gets larger is when the radius of the upper sphere becomes infinity, and simply the case would change to the liquid bridge between two flat plates. As

shown in the previous chapter, there would be no minimum point for the liquid bridge between two flat plates, and all the liquid would change into the vapour once the barrier is overcome.

For the solid sphere of radius smaller than $2\times10^6\times R_C$, the separation distance in Figure 6-8 is above the breakage distance of the system, therefore liquid formation becomes unfavourable.

As can be seen from part (b) of Figure 6-8, as the upper solid sphere gets bigger, there occurs only a very small decrease in the level of the energy barrier and the width of the unstable concave liquid bridge.

The effect of the solid sphere size on the unstable free energy and the unstable liquid bridge widh is minor. For example in Figure 6-8, while the sphere radius increases from $10^5\times R_C$ (4.39 mm) to $10^6\times R_C$ (4.39 cm) by an order of magnitude, the energy level of the maximum point decreases from 1.48×10^{-15} J to 1.46×10^{-15} J and the scaled unstable liquid bridge half width changes from 13.00 to 12.63. Even for the geometry of the confined space between two flat plates, which is equivalent to the upper sphere radius being infinite, the energy level of the barrier is 1.46×10^{-15}J and the scaled unstable liquid bridge half width is 12.59. The reason behind this is the large size of the sphere in comparison to the separation distance of the sphere and plate. Even for the smallest sphere where R_P is $10^5\times R_C$ (4.39 mm), the sphere radius is almost 10^5 times the separation distance. Therefore a sphere of radius $10^5\times R_C$ (4.39 mm) or $10^6\times R_C$ (4.39 cm) being located at distance equal to $0.97\times R_C$ from a flat plate, is similar to a sphere of radius 100 or 1000 meters at a distance of

1 millimetre from a plate. At small liquid bridge width (small *d's*), the new phase cannot sense how different the amount of the curvature of these two spheres is.

6.1.2. Stability of the liquid phase being formed from a bulk vapour phase between a sphere and a flat plate: convex meniscus

For liquid formation having convex meniscus with pressure difference being defined as $P^V - P^L$, both R_1 and R_2 are negative due to their center being located in the liquid phase.

Accordingly the mean radius of the curvature from equation (2.14) is as follows:

$$\frac{1}{R_m} = \frac{1}{2}\left(-\frac{1}{r} - \frac{1}{d}\right) \tag{6.17}$$

and R_m is identical to the Kelvin radius (R_C) at the equilibrium condition based on equation (2.21).

From Equation (6.17), R_m is negative since both r and d are positive numbers as they are the magnitudes of the principal radii of curvature. Equivalently R_C is to be negative, which is only satisfied at vapour phase pressures above the saturation pressure ($P^V > P_\infty$), according to section 3.7.1.

A typical curve of free energy vs. scaled liquid bridge half width ($\frac{d}{R_C}$) is presented in Figure 6-9 for n−dodecane at 24°C (the properties of which are reported in Table 3-7) as an example. The vapour phase pressure is set at 1.1 P_∞ for which the Kelvin radius is -4.85×10^{-8} meters from equation (2.20). The equilibrium contact angle is

set to 160°, the separation distance of the sphere and the flat plate is set to $0.97R_C$, and the solid sphere is assumed to have a radius of 2.5 cm.

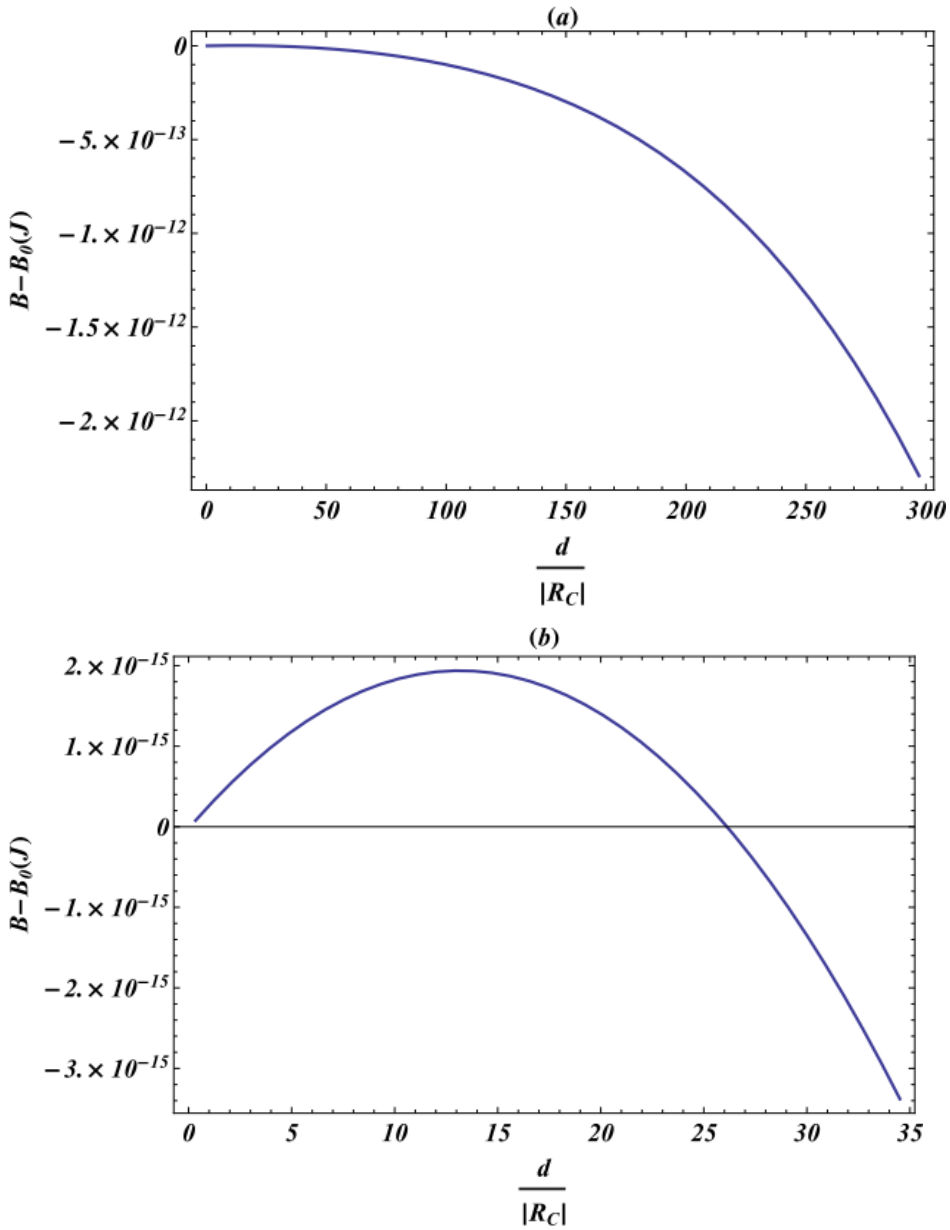

Figure 6-9 (a) Free energy vs. scaled liquid bridge half width ($\frac{d}{|R_C|}$) between a flat plate and a sphere, for n−dodecane at 24°C, P^V=1.1P_∞, θ=160°, H=0.97$|R_C|$, R_p=2.5 cm, (b) Magnification of the region close to d=0.

The formation of a convex liquid bridge between a spherical particle and a flat plate is a nucleation phenomenon for which an energy barrier is to be overcome.

After passing that maximum point, the curve would be ever descending and all the vapour would change into liquid.

6.1.2.1. Effect of equilibrium contact angle on the stability of the system for liquid phase formation out of a bulk vapour phase between a flat plate and a sphere: convex meniscus

In this section, the free energy curves for various contact angles are presented, while the properties of the system other than the equilibrium contact angle are kept the same as those in Figure 6-9.

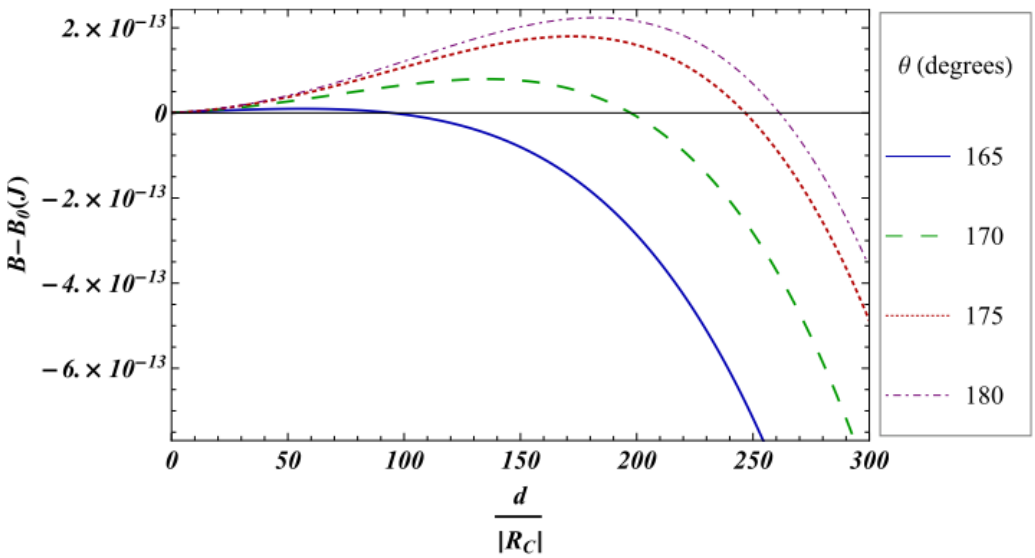

Figure 6-10 Effect of the equilibrium contact angle on the free energy vs. scaled liquid bridge half width between a flat plate and a sphere, for n−dodecane at 24°C, P^V=1.1P_∞, H=0.97$|R_C|$, R_P=2.5cm and, for various contact angles that results in a convex meniscus.

For liquid formation with a convex meniscus between a sphere and a flat plate, any increase in contact angle (getting farther from the ***transition contact angle***) causes the barrier to get larger, and the unstable liquid bridge is formed at larger width. In contradiction to the case of convex liquid bridge formation between <u>two flat plates</u>, even for the greatest possible contact angle (180°), the curve does not become

monotonically increasing. However for the specification of Figure 6-10 with the contact angle equal to 180°, the width of the unstable bridge would be so large ($\frac{d}{|RC|}$ =182.53) with the energy of 2.24×10^{-13} J, in comparison to the case of contact angle of 155° (with other condition kept the same) for which $\frac{d}{|RC|}$ =6.46 and the energy barrier is 6.15×10^{-16} J.

6.1.2.2. Effect of the solid surface separation distance on the stability of the system for liquid phase formation out of a bulk vapour between a sphere and a flat plate: convex meniscus

Sphere–plate separation distance plays an important role in the stability of the liquid phase. This effect is illustrated in Figure 6-11.

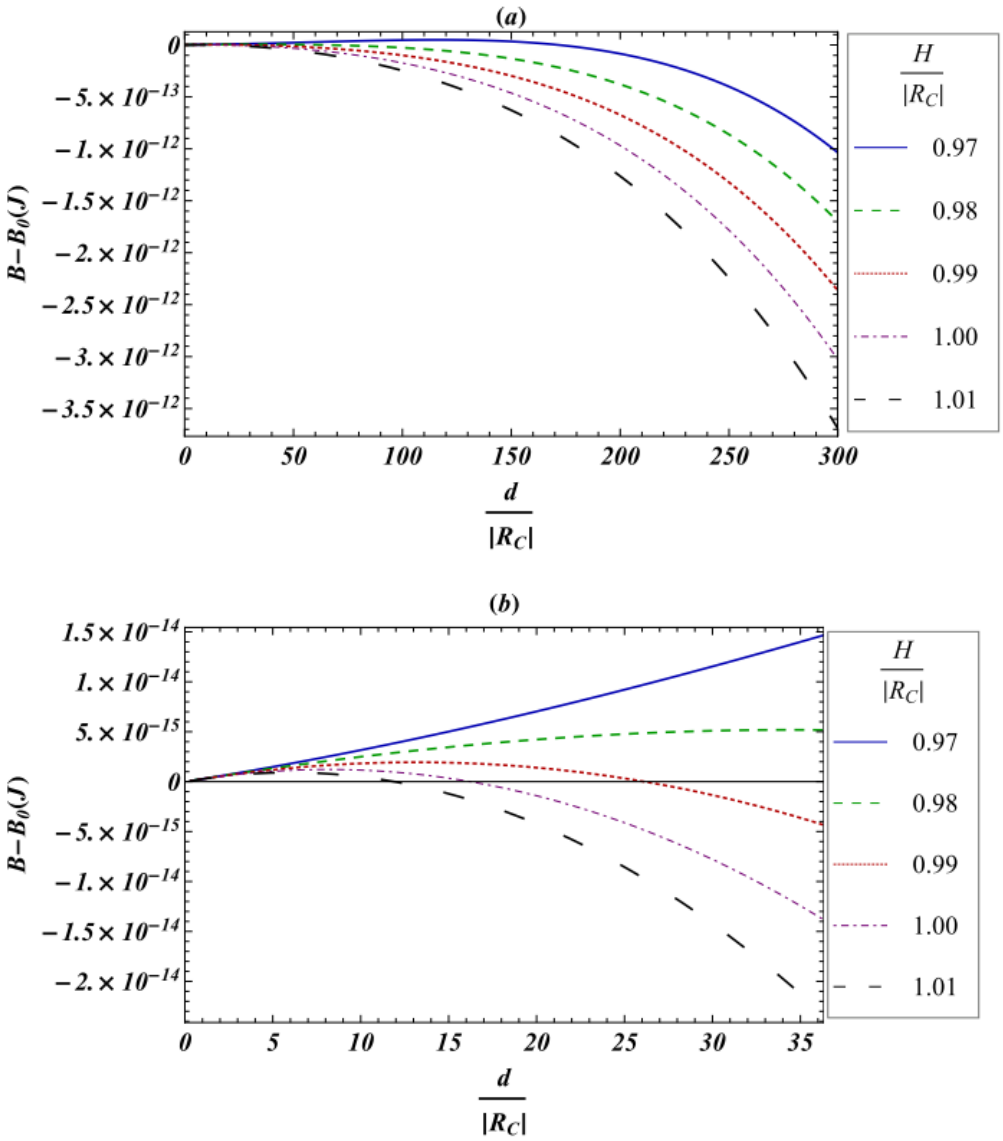

Figure 6-11 (a) Effect of the solid surface separation distance on the free energy vs. scaled liquid bridge half width between a flat plate and a sphere, for n−dodecane at 24ºC, P^V=1.1P_∞, θ=160º, and R_p=2.5 cm, (b) Magnification of the unstable equilibrium point.

As the sphere–plate separation distance decreases, a higher energy barrier with a larger liquid bridge width is to be overcome. In contradiction to the case of convex liquid bridge between two flat plates, in this case even for a sphere and flat plate at contact (*H*=0) formation of a liquid bridge would be still possible and the curve does not become constantly increasing. However for a sphere and a flat plate in

contact, the width of the unstable liquid bridge and the amount of the barrier to be overcome are both large, as shown in Figure 6-12.

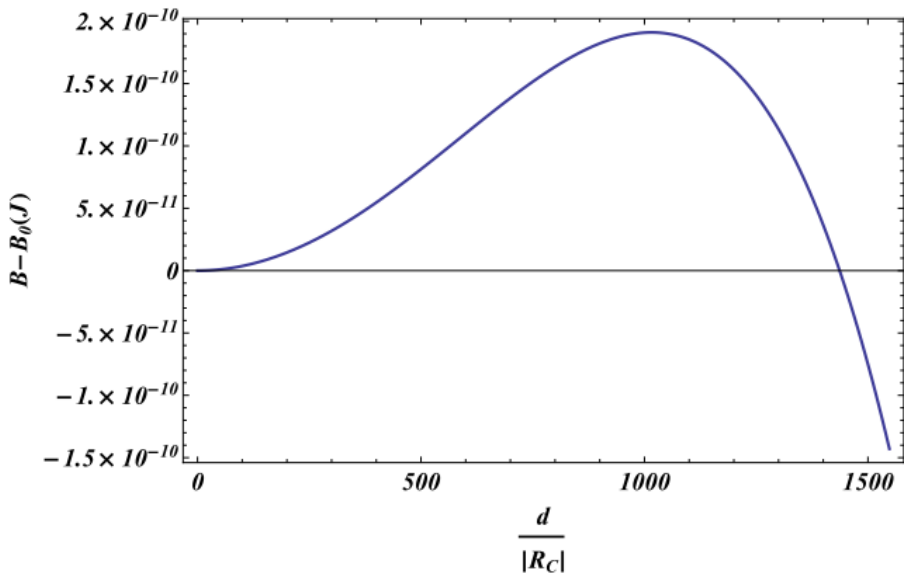

Figure 6-12 Curve of free energy vs. scaled liquid bridge half width between a flat plate and a sphere for n−dodecane at 24°C, P^V=1.1P_∞, θ =180°, H=0, and R_p=2.5 cm.

For the convex liquid bridge between two flat plates the vertical distance between the plates remains constant at different distances from the center line (different *d*). In the case of the convex liquid bridge between a flat plate and a sphere, the vertical distance between the sphere and the plate gets larger as we get farther from the center line (as *d* increases). Therefore in sphere–plate geometry, even when two solid surfaces are touching, somewhere far enough from the centerline the distance becomes large enough to allow the formation of the unstable convex liquid bridge.

6.1.2.3. Effect of solid sphere size on the stability of the system for liquid phase formation out of a bulk vapour phase between a flat plate and a sphere: convex meniscus

In Figure 6-13, for different solid sphere sizes, the free energy curve of the convex liquid bridge is presented. The properties of the system other than the radius of the solid sphere are kept the same as those in Figure 6-9.

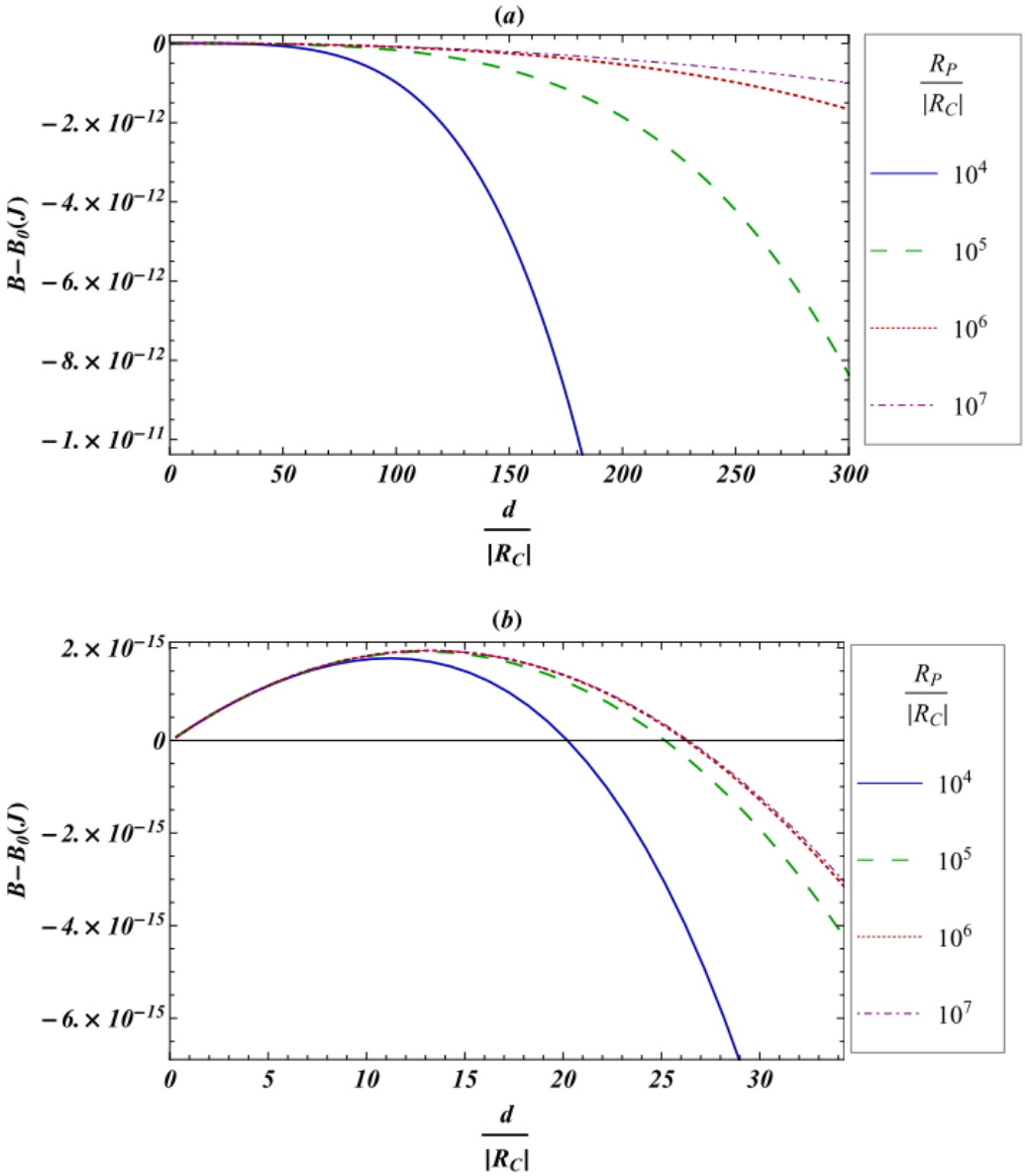

Figure 6-13 (a) Effect of the solid sphere size on the free energy vs. liquid bridge half width between a flat plate and a sphere, for n−dodecane at 24°C, P^V=1.1P_∞, θ=160°, and H=0.97$|R_C|$, (b) Magnification of the unstable equilibrium point

In contrast to the case of concave liquid formation here as the upper solid sphere radius increases, the level of the energy barrier and the width of the unstable concave liquid bridge would also increase. The highest energy barrier is for the case of the solid sphere of infinite radius, identical to the convex liquid bridge formation between two flat plates.

For any sphere size other than infinity (the case of the two flat plates), the curve of the free energy never becomes monotonically increasing even at the smallest separation distance or for the farthest contact angle from the transition contact angle, i.e. contact angle of 180°. However if the sphere is large enough, the nucleation happens at a very large liquid width with a relatively high barrier. For example for a sphere of radius $10^9 \times |R_C| = 48$ meters touching the flat plate (H=0), the unstable bridge has a width of $\frac{d}{|RC|} = 4.3\times10^4$ (d~ 2 mm) with an energy barrier of 3.26×10^{-7} J.

For the case of two flat plates (equivalent to an upper sphere of radius of infinity) the curve might be monotonically increasing if the flat plates' separation distance is smaller than a certain amount. In Figure 6-13 where the separation distance is $H=0.97|R_C|$, convex vapour formation is always possible. Even when the case changes to the case of two flat plates, the convex vapour formation happens after passing an energy barrier of 1.94×10^{-15} J at vapour bridge half width of $13.23|R_C|$.

6.2. Vapour phase formation from a bulk liquid phase between a sphere and a flat plate

In this section, vapour formation out of a bulk liquid phase with constant pressure will be investigated. In the absence of a gravitational field, the vapour phase pressure is constant throughout and the liquid phase pressure is constant throughout, though they are not equal. Constant pressures imply constant Kelvin radius according to equation (2.20). As a result the liquid−vapour interface is to be

a surface of constant curvature due to the equality of the mean radius of curvature with the Kelvin radius.

This liquid−vapour interface with constant mean curvature can accurately be approximated by a toroidal interface for bridge half width greater than or equal to $6.5 \times R_C$ [18]. The illustration of such liquid−vapour interfaces is presented in Figure 6-14:

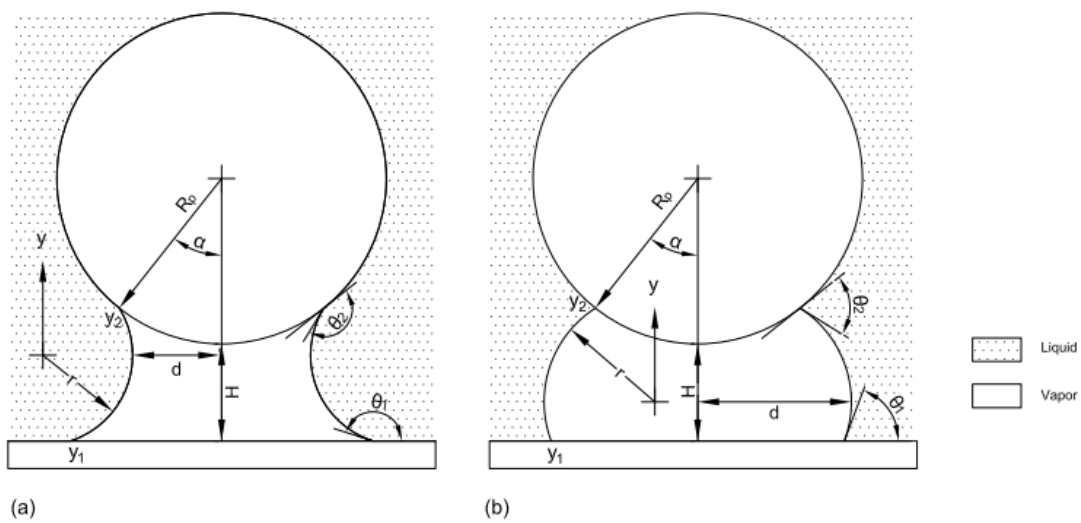

Figure 6-14 Schematic of a vapour bridge – a) concave and b) convex – between a flat plate and a sphere, where θ_1 and θ_2 are the equilibrium contact angles, r is the radius of the circle approximating the vertical section of the liquid−vapour interface, d is the vapour bridge half width, H is the distance between the two plates, α is the half filling angle of the vapour in the bridge, y_1 is the three phase contact with the lower solid surface, y_2 is the three phase contact with the upper solid surface, and R_P is the radius of the spherical particle .

The solid interface is *flat* for the plate and is *curved* for the spherical particle. The constraints of the system in which vapour is being formed between a flat plate and a sphere are shown in Table 3-2, in *flat* and *curved* sections respectively. The conditions for equilibrium are presented in Table 3-4 (b). As reported in Table 3-4 (b), there is one extra equilibrium condition for *curved* interfaces, which is the equality of the chemical potential of the solid material in the solid phase with the

chemical potential of the same component at the solid−liquid and the solid−vapour interfaces. This affects the interfacial tension, which in turn influences the amount of the equilibrium contact angle. Therefore it is possible that the equilibrium contact angle can have a slightly different value at the sphere than at the flat plate.

When the distance between the sphere and the flat plate is much smaller than the radius of the spherical particle, we assume that the *curved* surface of the sphere acts negligibly on the contact angle, leading to identical equilibrium contact angles for the upper and lower (sphere and flat plate) solids if both of them are made from the same solid material. There are two cases of concave or convex liquid−vapour interface according to Figure 6-14. For identical contact angles for the upper and the lower solids, the ***transition contact angle*** is $\frac{180°+\alpha}{2}$. The meniscus is concave for $\theta > \frac{180°+\alpha}{2}$ and is convex for $\theta < \frac{180°+\alpha}{2}$.

R_1 and R_2 are the principal radii of curvature of the toroidal surface representing the liquid−vapour interface of constant curvature. The magnitudes of these principal radii are described with r and d, where $|R_1| = r$ and $|R_2| = d$. With ΔP being defined as $P^L - P^V$, the sign of the principal radius of curvature is positive when its center is located in the liquid phase, and is negative if its center is in the vapour phase. For the concave outward meniscus, R_1 is positive ($R_1 = r$) and R_2 is negative ($R_2 = -d$). For the convex outward case, both of the radii are negative ($R_1 = -r$ and $R_2 = -d$).

The vapour volume, V^V, can be computed from the volume of revolution of the liquid−vapour interface curve [43] and then subtracting the immersed part of the spherical particle, V_S. A^{LV} is the surface of revolution around the y−axis [44]. The appropriate formulas for V^V, A^{SV} and A^{LV} are presented in Table 6-3:

Table 6-3 Vapour volume, solid−vapour and liquid−vapour surface areas for vapour bridge formation between a flat plate and a sphere.

$V^V = \pi \int_{y_1}^{y_2} F(y)^2 dy - V_S$	(6.18)		
$V_S = \frac{\pi}{3} R_P{}^3 (1 - \cos\alpha)^2 (2 + \cos\alpha)$	(6.19)		
$A^{SV} = \pi \left[F(y_1)^2 + 2R_P{}^2 (1 - \cos\alpha) \right]$	(6.20)		
$A^{LV} = 2\pi \int_{y_1}^{y_2} F(y) \sqrt{1 + F'(y)^2} dy$	(6.21)		
Concave meniscus ($\theta > \frac{180° + \alpha}{2}$)		**Convex meniscus ($\theta < \frac{180° + \alpha}{2}$)**	
$F(y) = r + d - \sqrt{r^2 - y^2}$	(6.22)	$F(y) = -r + d + \sqrt{r^2 - y^2}$	(6.23)
$y_1 = r\cos\theta$	(6.24)	$y_1 = -r\cos\theta$	(6.25)
$y_2 = -r\cos(\theta - \alpha)$	(6.26)	$y_2 = r\cos(\theta - \alpha)$	(6.27)

Stability analysis of the vapour bridge is achievable through the equation of the free energy of the system for vapour formation as stated in Table 3-6:

$$B - B_0 = \frac{2\gamma^{LV}}{R_C} V^v + (\gamma^{LV} \cos\theta) A^{SV} + \gamma^{LV} A^{LV} \tag{3.62}$$

where V^V, A^{SV} and A^{LV} are to be substituted from Table 6-3. After these substitutions for a defined problem in which γ^{LV}, R_C, and θ are known, equation (3.62) would be a function of r and d, both of which can be written as a function of the half filling angle, α. For the case of the concave meniscus,

$$r = \frac{R_P(1 - \cos\alpha) + H}{-\cos(\theta - \alpha) - \cos\theta} \tag{6.28}$$

$$d = R_P \sin\alpha - r[1 - \sin(\theta - \alpha)] \tag{6.29}$$

and for the case of the convex meniscus,

$$r = \frac{R_P(1 - \cos\alpha) + H}{\cos(\theta - \alpha) + \cos\theta} \tag{6.30}$$

$$d = R_P \sin\alpha + r[1 - \sin(\theta - \alpha)] \tag{6.31}$$

The equilibrium state of the vapour bridge and its size can be obtained from the extremum of the curve of the free energy of the system vs. the vapour bridge half length (d), or alternatively from the roots of $\left(\frac{\partial B}{\partial d}\right)_{\theta=\theta_e} = 0$.

The stability of the vapour bridge is then obtained according to the type of the extremum point: a maximum point represents an unstable equilibrium, the global minimum corresponds to the stable equilibrium state, and any local minimum would indicate a metastable condition.

6.2.1. Stability of the vapour phase being formed from a bulk liquid phase between a sphere and a flat plate: concave meniscus

With the pressure difference defined as $\Delta P = P^L - P^V$, R_1 is positive and R_2 is negative since the centre of the radius is in liquid for R_1 and in vapour for R_2. The mean radius of curvature from equation (2.14) is as follows:

$$\frac{1}{R_m} = \frac{1}{2}\left(\frac{1}{r} - \frac{1}{d}\right) \tag{6.32}$$

and R_m is identical to the Kelvin radius (R_C) at the equilibrium condition, according to equation (2.21).

As explained in the previous chapter (section 5.2), for various sphere–plate separation distances, and equilibrium contact angles, it has been observed that at the equilibrium conditions r is less than d. Then according to equation (6.32), R_m is positive and R_C would be positive. For R_C to be positive the liquid pressure must be above the saturation pressure ($P^L > P_\infty$) as explained in section 3.7.1.

A typical curve of the free energy vs. the scaled vapour bridge half width ($\frac{d}{R_C}$) at such a condition is shown in Figure 6-15 for water at 20°C, with its properties as reported in Table 3-7. The liquid pressure is set at $1.1P_\infty$. The Kelvin radius from equation (2.20) is 6.22×10^{-4} meters. The equilibrium contact angle is set to be 180°, the separation distance of the two flat plates is set at $0.5R_C$ (300μm), and the solid sphere is taken to have radius of $10^3\times R_C$ (62 cm).

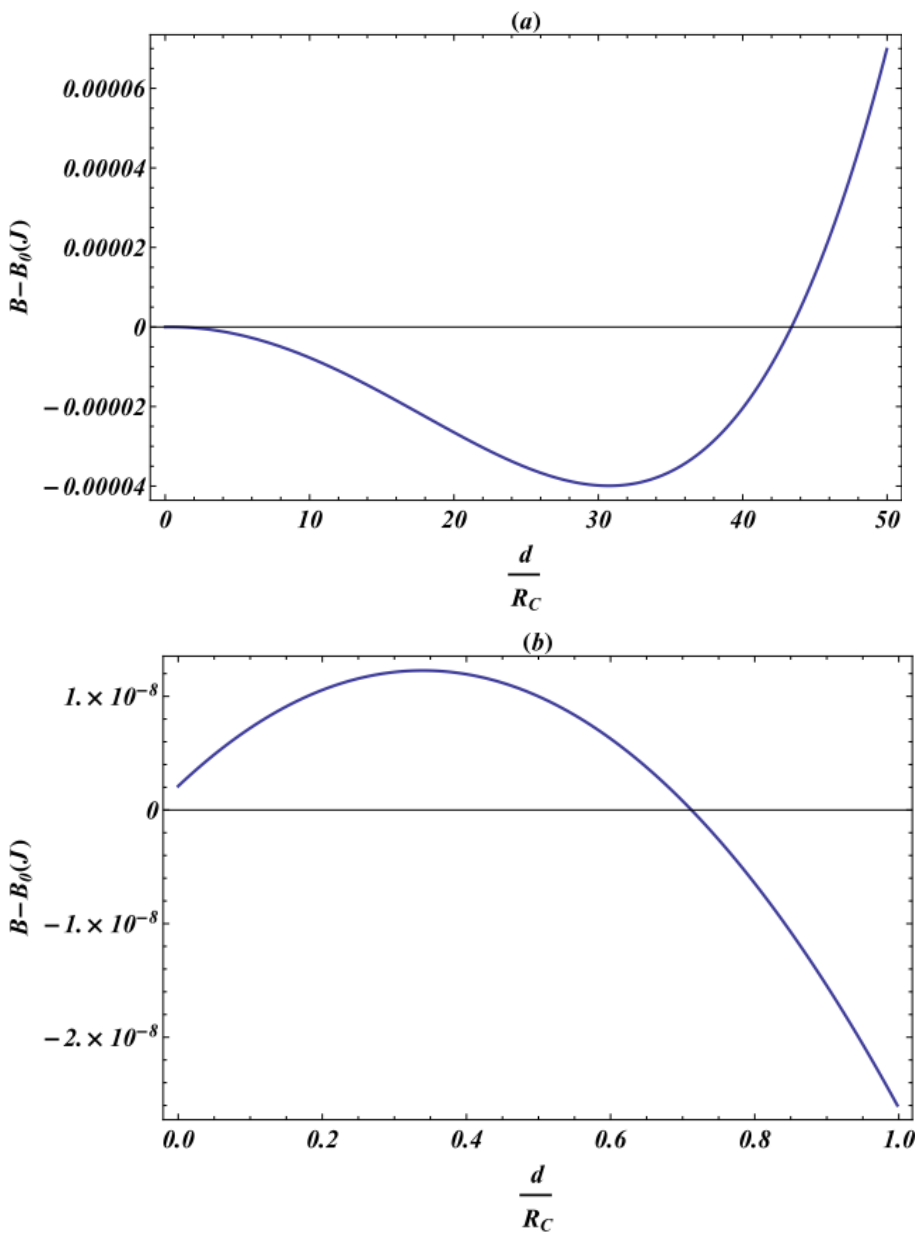

Figure 6-15 (a) Free energy vs. vapour bridge half width between a flat plate and a sphere, for water at 20°C, P^L=1.1P_∞, H=0.5R_C (300μm), θ=180°, R_p=10^3×R_C (62 cm), (b) Magnification of the region close to d=0.

There is a maximum point at a very small vapour bridge width (*d* much smaller than 6.5×R_C). Although the value of the energy barrier cannot be trusted because of the very small vapour bridge width (where the toroidal surface assumption is no longer valid), the graph gives a good prediction of the behaviour of the system. The

vapour formation can only happen after passing an energy barrier, i.e. the phase transition is a nucleation phenomena. After passing the barrier, the vapour phase grows until it reaches its stable condition, corresponding to the minimum point in the graph.

6.2.1.1. Effect of the equilibrium contact angle on the stability of the system for vapour phase formation out of a bulk liquid phase between a flat plate and a sphere: concave meniscus

The effect of the equilibrium contact angle on the free energy of the concave vapour formation is studied in this section. The properties of the system other than the contact angle are the same as those presented in Figure 6-15.

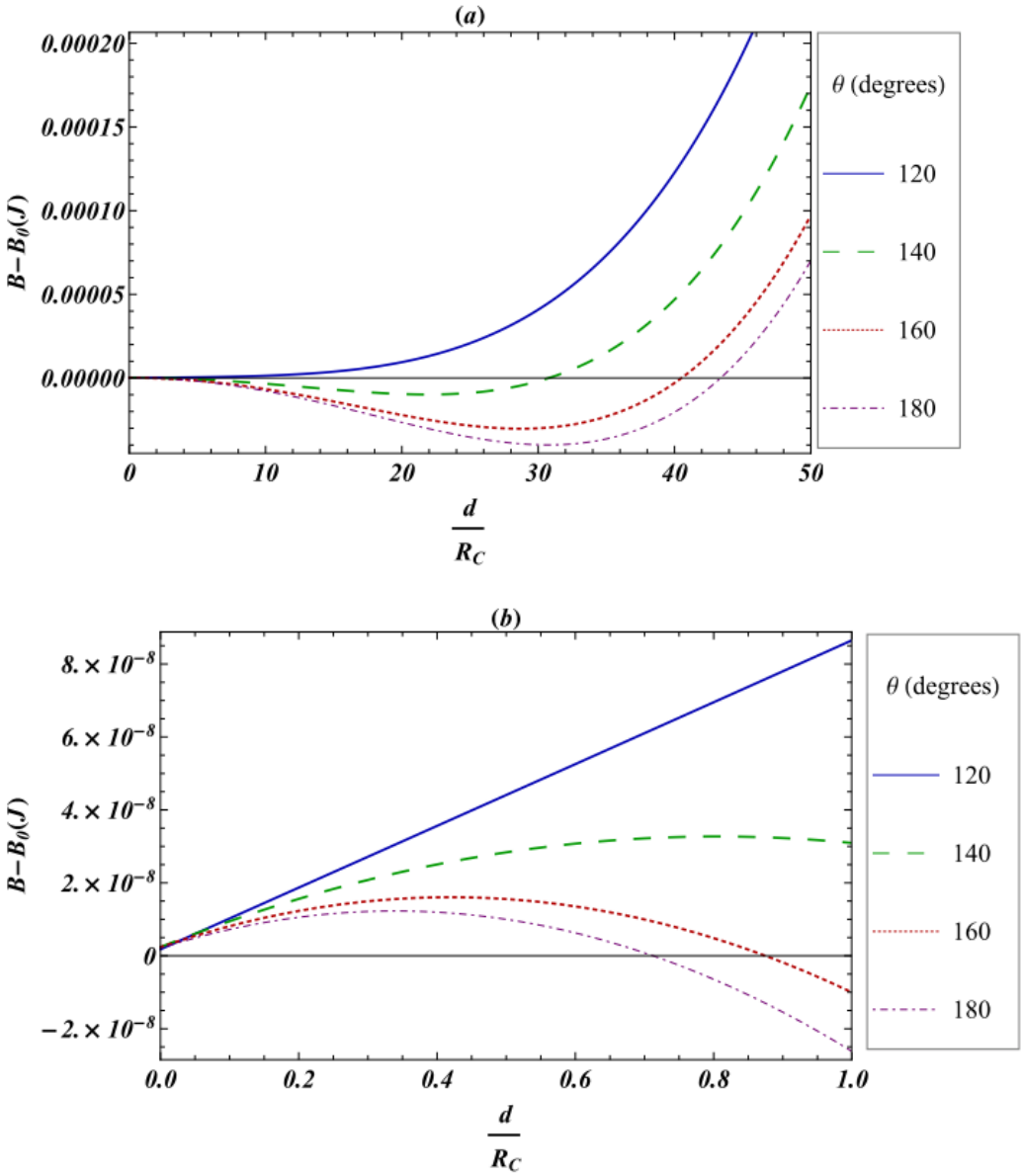

Figure 6-16 (a) Effect of the equilibrium contact angle on the free energy vs. scaled vapour bridge half width between a flat plate and a sphere, for water at 20°C, P^L=1.1P_∞, H=0.5R_C (300μm), R_p=10^3×R_C (62 cm), for various contact angles that result in concave meniscus, (b) Magnification of the unstable equilibrium point.

Getting closer to the ***transition contact angle*** (equivalently a decrease in the contact angle) results in an increase in the energy barrier and a larger unstable vapour bridge length. It also causes less stability with shorter vapour bridge width in the stable equilibrium state. Getting closer to the ***transition contact angle***, at

some point the curve becomes monotonically increasing, i.e. the formation of the concave vapour phase would become unfavourable.

In studying the case more closely, it has been found that a specific number of degrees change in the contact angle results in a large relative change of the energy barrier and the energy level of the stable state for contact angles closer to the ***transition contact angle***, as shown in Figure 6-17.

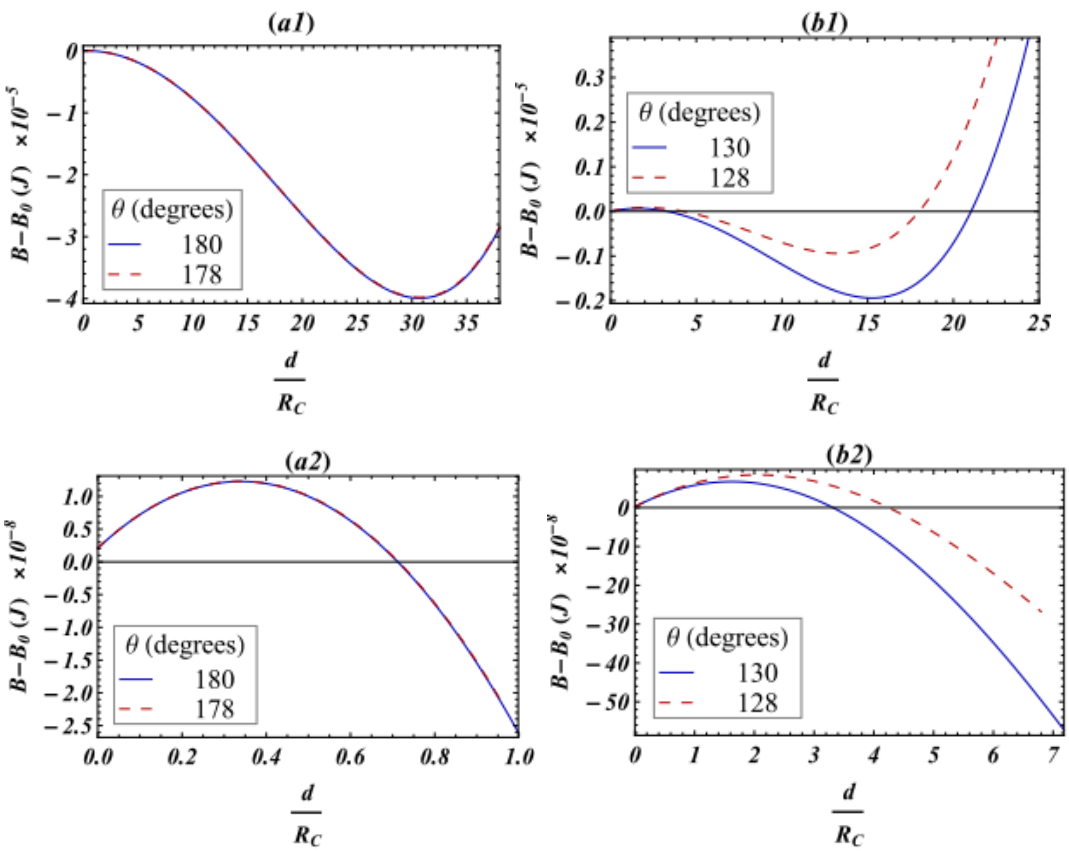

Figure 6-17 Comparison of the effect of a specific number of degrees change (2°) in the equilibrium contact angle on the free energy of vapour formation with a concave meniscus between a flat plate and a sphere, for water at 20°C, $P^L=1.1P_\infty$, $H=0.5R_C$ (300μm), $R_p=10^3\times R_C$ (62 cm), (a1) far from the transition contact angle, (b1) closer to the transition contact angle. (a2) and (b2) are magnifications of (a1) and (b1) respectively.

In parts (a1) and (a2) of Figure 6-17 far from the ***transition contact angle*** the contact angle is changing from 180° to 178°. In (b1) and (b2) the changes in the

contact angle happen closer to the ***transition contact angle*** and the contact angle is changing from 130º to 128º. The relative differences in the free energy levels of the maximum and minimum points calculated from equation (3.5) are presented in the following table for each case.

Table 6-4 Concave vapour formation between a flat plate and a sphere, relative differences in the free energy levels of the maximum and minimum points as a result of a certain number of degrees (2º) change in the contact angle, for water at 20ºC, $P^L=1.1P_\infty$, $H=0.5R_C$ (300μm), $R_p=10^3\times R_C$

Relative difference in	180º→178º (far from θ_t)	130º→128º (close to θ_t)
energy level of the maximum point	0.37 %	26.28 %
scaled bridge length of the maximum point	0.26 %	26.65 %
energy level of the minimum point	0.29 %	51.42%
scaled bridge length of the minimum point	0.07 %	12.88 %

6.2.1.2. Effect of the solid surface separation distance on the stability of the system for liquid phase formation out of a bulk vapour between a sphere and a flat plate: concave meniscus

The effect of the sphere–plate separation distance on the free energy curve of the concave vapour formation is investigated in this section.

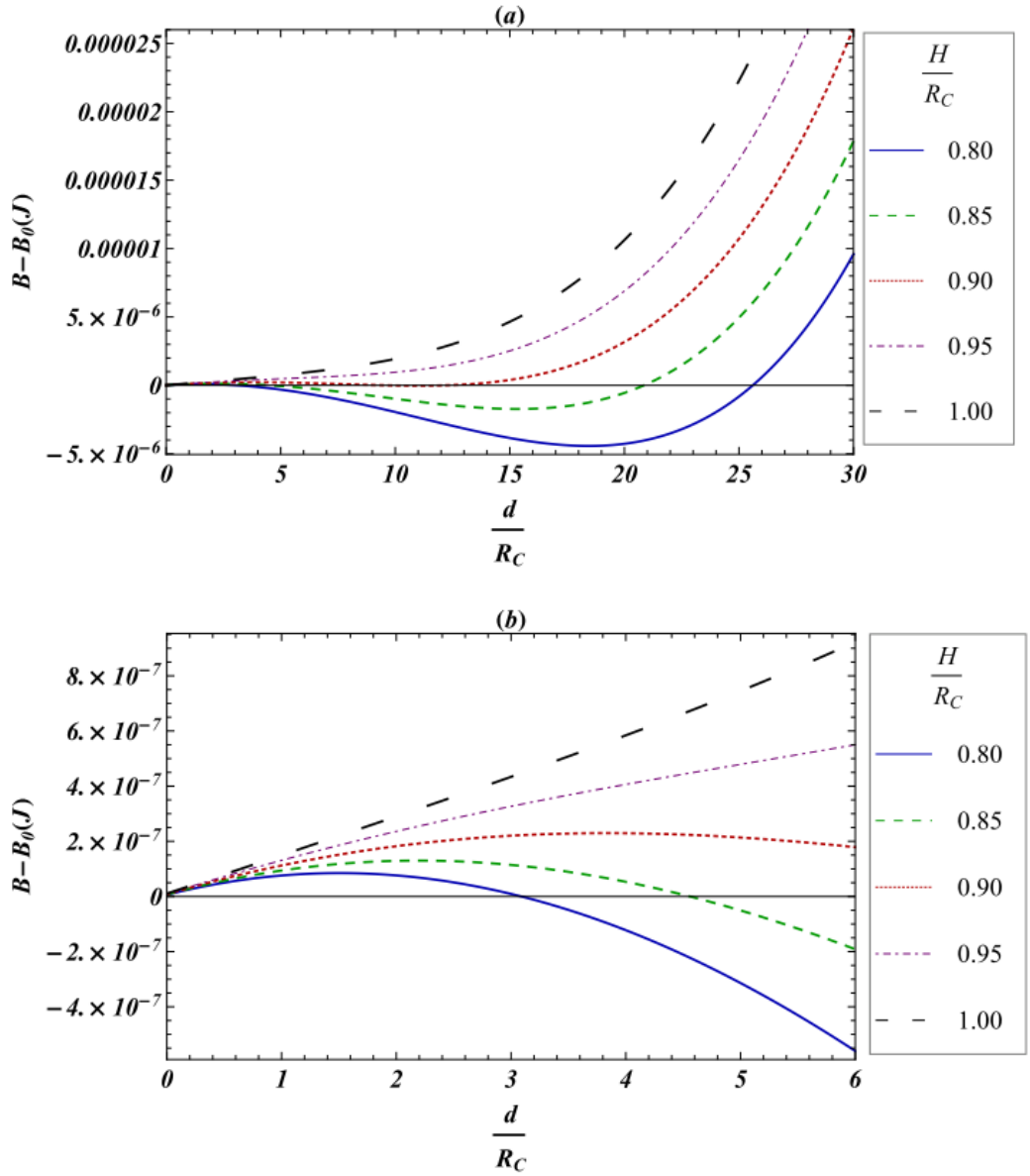

Figure 6-18 Effect of the solid surface separation distance on the free energy vs. scaled liquid bridge half width between a flat plate and a sphere, for water at 20°C, P^L=1.1P_∞, θ=180°, R_p=10^3×R_C (62 cm), (b) Magnification of the unstable equilibrium point.

As the separation distance of a sphere and a flat plate increases, the stable equilibrium state is formed with less stability and at shorter vapour bridge width. A larger separation distance also causes higher energy barrier with larger vapour bridge width to be overcome.

For separation distances higher than a certain amount, the free energy curve becomes monotonically increasing and the formation of the vapour phase would be unfavourable. In the case where the contact angle is 180° (farthest from the ***transition contact angle***) and the sphere radius is $10^3 \times R_C$, vapour formation becomes unfavourable at a sphere–plate separation distance of about $0.92 \times R_C$.

Considering the effect of contact angle, for contact angles less than 180° (closer to the ***transition contact angle***), the vapour formation would be unfavourable even at separation distances less than $0.92 \times R_C$ when the spherical sphere radius is $10^3 \times R_C$. Also the effect of particle size, as will be discussed in the next section, is such that as the spherical particle gets bigger, the sphere–plate separation distance can be larger before the concave vapour phase formation becomes unfavourable. Even in the case where the radius of the spherical particle becomes infinity (the case simply changes to the case of two flat plates), concave vapour phase formation becomes unfavourable at $H=R_C$. Hence it can be concluded that for an arbitrary contact angle and sphere size, the vapour formation is unfavourable for $H \geq R_C$. Below R_C further investigation is required for any specific contact angle and/or particle size to judge whether the concave vapour formation is favourable.

If any concave vapour phase has already been formed, increasing the separation distance would make it smaller until it would completely break apart at the critical distance which is mentioned above. This critical distance is called the ***breakage distance*** as mentioned in section 6.1, which depends on the Kelvin radius, the

equilibrium contact angle and the particle size. The breakage distance is always less than R_C according to the discussion of the previous paragraph.

Modifying equation (6.16) based on the negative sign of the term $cos\theta$ (because $\theta > \frac{180°+\alpha}{2}$), the potential equation for the breakage distance for the case of concave vapour formation out of a bulk liquid phase is:

$$H_{Break} = -R_C \cos\theta \left\{ 1 + \frac{3}{\left(\frac{32 R_P \cos\theta}{R_C}\right)^{1/3}} \right\} \tag{6.33}$$

However as stated in section 6.1, this equation works if $R_P >> |d| >> H$. For water at 20ºC, $P^L = 1.1P_\infty$, $\theta = 180°$, $R_p = 10^3 \times R_C$ (62 cm), the breakage distance from the graph is $0.92 \times R_C$, while from equation (6.33) it is $0.997 \times R_C$. That much of difference is because $R_P >> |d| >> H$ is not satisfied in this case where $R_p = 10^3 \times R_C$.

As discussed in the concave liquid formation section 6.1, the energy level of the unstable and stable equilibrium points becomes almost equal as the particles' distance increases to the breakage distance. Due to this almost equal energy level of the unstable and the stable points, there occurs some fluctuation in the vapour bridge width, before the system reaches to its stable condition. Therefore some part of the gap between two particles would have the density between that of the liquid and vapour.

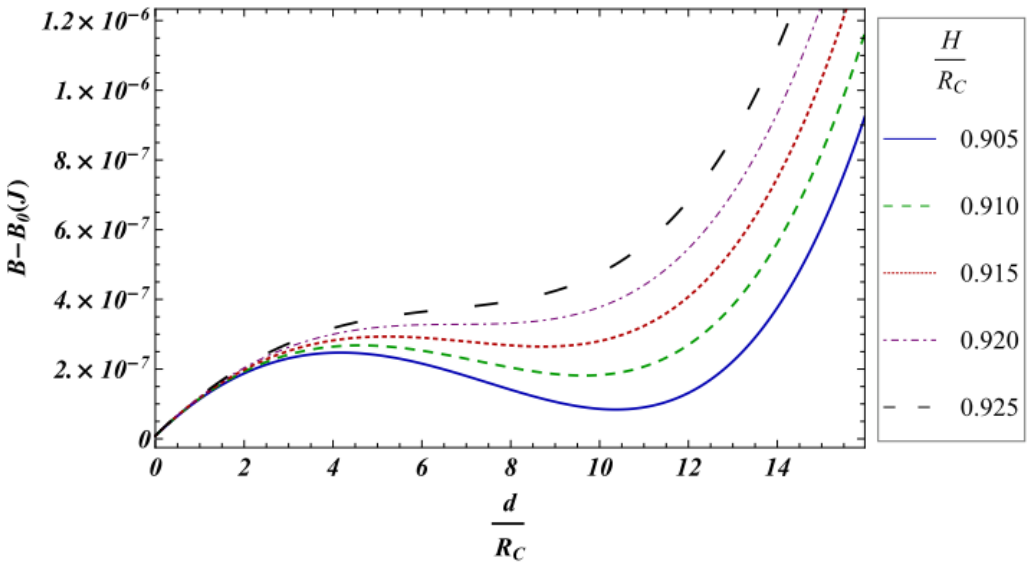

Figure 6-19 Energy levels of the maximum and minimum points at separation distances close to the breakage distance for a vapour bridge between a flat plate and a sphere, for water at 20°C, $P^L=1.1P_\infty$, θ=180°, $R_p=10^3\times R_C$ (62 cm)

The other side of the story occurs when the distance between the sphere and the flat plate reduces to zero. For concave vapour formation between a sphere and a flat plate that are touching, the new phase formation happens through a non−nucleating phenomenon with no energy barrier to be overcome. Decreasing the separation distance to zero also results in the most stable equilibrium with the greatest liquid bridge width.

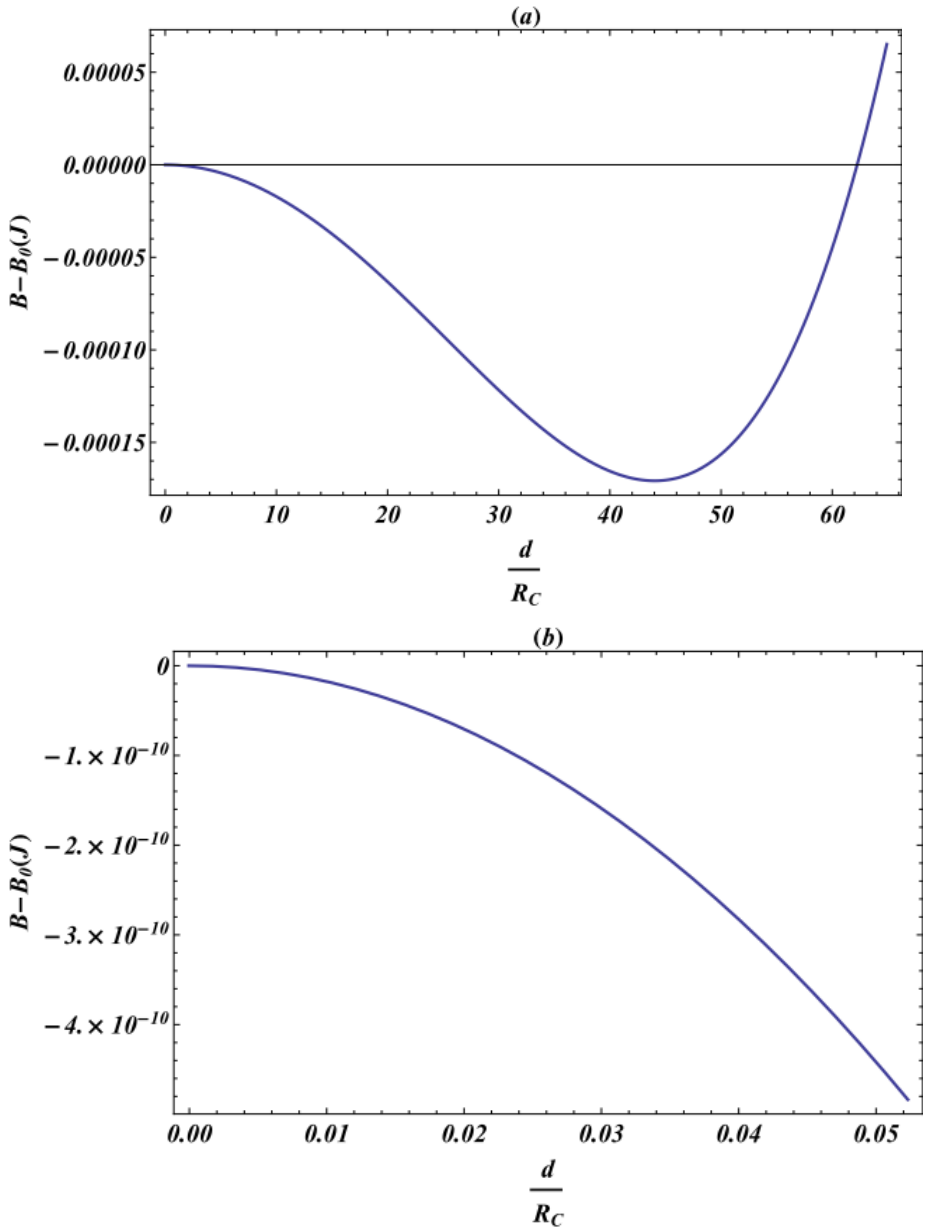

Figure 6-20 Free energy vs. vapour bridge half width between a sphere and a flat plate, for water at 20°C, P^L=1.1P_∞, θ=180°, H=0, R_p=10^3×R_C (62 cm), (b) Magnification of the curve at small value of bridge width.

6.2.1.3. Effect of solid sphere size on the stability of the system for a vapour phase being formed out of a bulk liquid phase between a flat plate and a sphere: concave meniscus

The impact of the size of the spherical solid particle on the energy level of the concave vapour bridge is examined in this section. The properties of the system other than the radius of the solid sphere are kept the same as those in Figure 6-15.

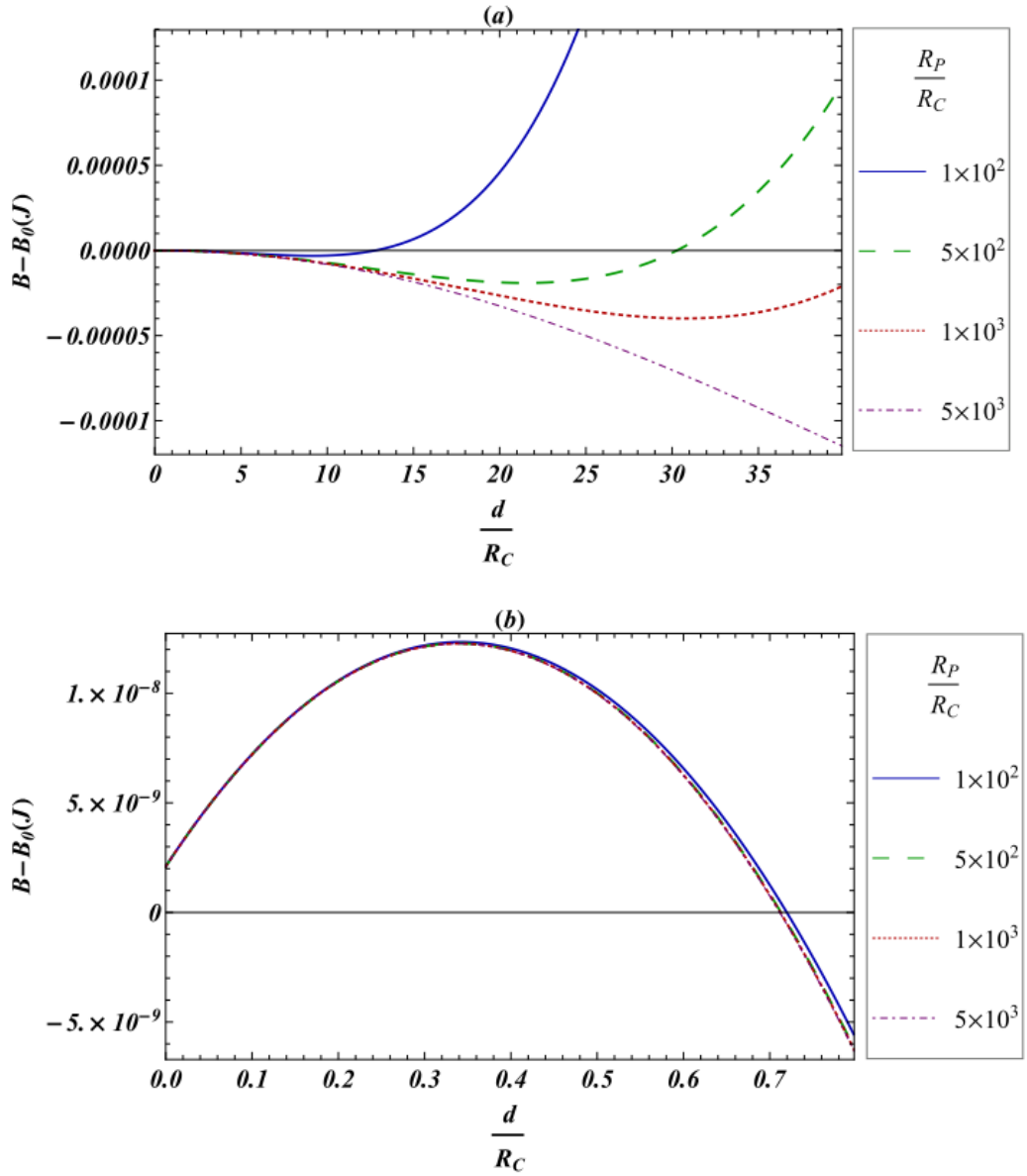

Figure 6-21 Effect of the solid sphere size on the free energy vs. vapour bridge half width between a flat plate and a sphere, for water at 20°C, P^L=1.1P_∞, θ=180°, H=0.5×R_C (300μm), (b) Magnification of the unstable equilibrium point.

The radius of the spherical particle is changed from several centimetres ($10^2 \times R_C$) to several meters ($5\times10^3 \times R_C$). As the spherical particle gets larger, at some point the concave vapour formation becomes possible after passing an energy barrier and the concave vapour phase becomes stable at some vapour bridge width. For larger spherical particles, the energy barrier gets smaller and the concave vapour phase

gets stable at lorger bridge width with deeper energy levels. In the case of an upper sphere of infinite radius (equivalent to the case of two flat plates), the energy barrier is at its lowest level, and all of the liquid phase would change into vapour once the energy barrier is overcome.

As illustrated in part (b) of Figure 6-21, the effect of the solid sphere size on the unstable free energy and the unstable liquid bridge width is minor. The reason behind this can be explained as follows: The separation distance is much smaller than the spherical particle's radius, and the unstable state happens at such a small bridge width that a concave vapour bridge does not sense the size and changes in the curvature of the spherical solid, especially when the contact angle is far from the ***transition contact angle***. As the concave vapour width gets larger and we get farther from the center line, the curvature of the solid sphere would significantly affect the energy level of the system, as it does for the stable equilibrium state.

For a solid sphere of radius smaller than $3.2\times R_C$ (2 mm), the separation distance ($H=0.5\times R_C$) in Figure 6-21 is higher than the breakage distance of the system, therefore liquid formation becomes unfavourable.

6.2.2. Stability of the vapour phase being formed from a bulk liquid phase between a sphere and a flat plate: convex meniscus

Both R_1 and R_2 are negative in a case of the convex vapour meniscus, with pressure difference being defined as $P^L - P^V$, following the convention and according to Figure 6-14.

Accordingly the mean radius of curvature from equation (2.14) is:

$$\frac{1}{R_m} = \frac{1}{2}\left(-\frac{1}{r} - \frac{1}{d}\right) \tag{6.34}$$

From equation (6.34) R_m is negative, since both r and d are magnitudes of the principal radii of curvature and are positive. Also based on equation (2.21), R_m is identical to the Kelvin radius, R_C, at equilibrium condition. Therefore R_C is negative, where according to section 3.7.1, this is only satisfied at liquid pressures below the saturation pressure ($P^L < P_\infty$).

Figure 6-22 demonstrates a typical free energy vs. scaled vapour bridge half width ($\frac{d}{R_C}$) for water at 20°C with its properties reported in Table 3-7. The liquid phase pressure is set to be $0.9P_\infty$. The Kelvin radius from equation (2.20) is -6.22×10^{-4} meters at this liquid pressure. The equilibrium contact angle is 0°, the separation distance between the sphere and the flat plate is $0.5\left|R_C\right|$ (300μm), and the solid sphere has a radius of $10^3\times\left|R_C\right|$ (62 cm).

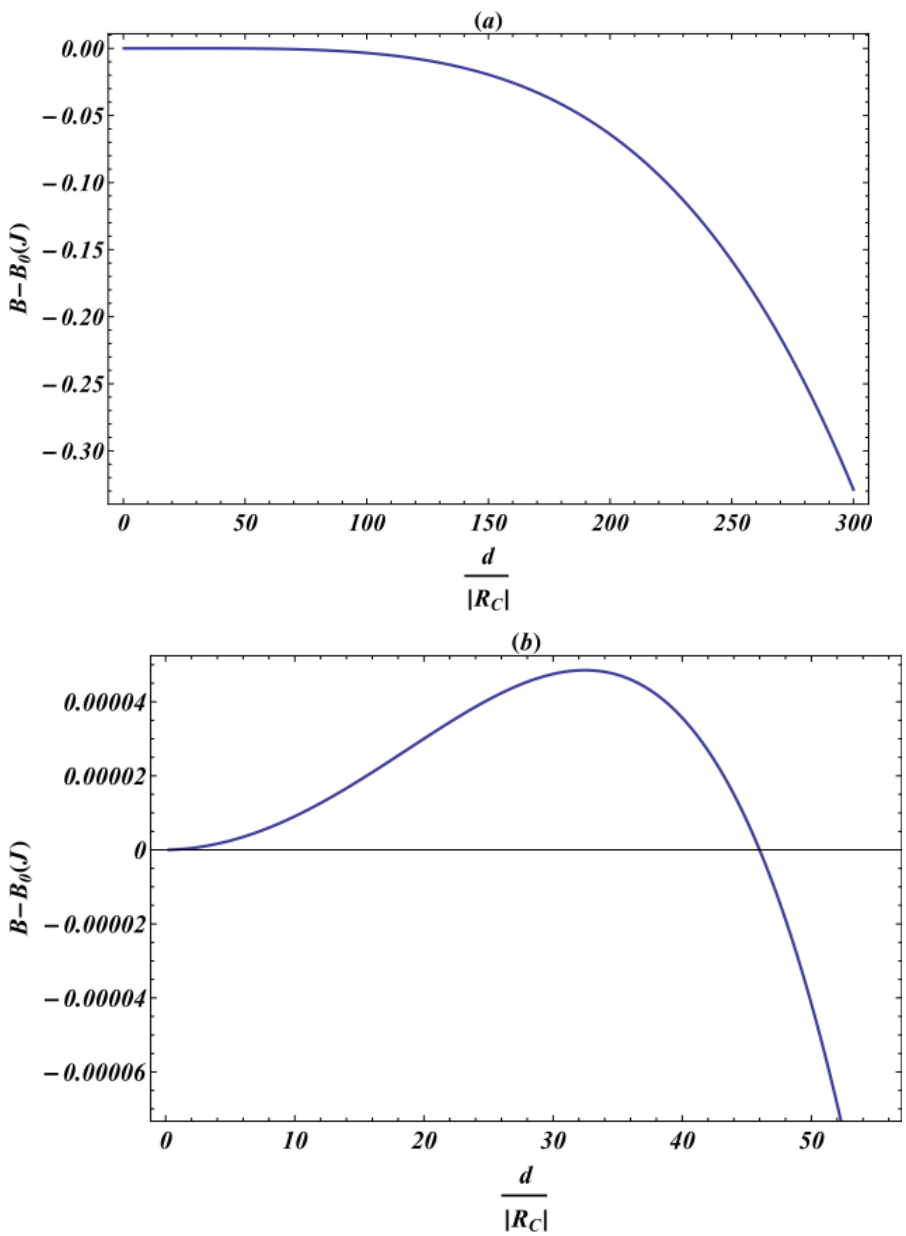

Figure 6-22 (a) Free energy vs. scaled vapour bridge half width between a flat plate and a sphere, for water at 20°C, $P^L=0.9P_\infty$, θ=0°, H=0.5 | R_C | (300μm), $R_p=10^3\times$ | R_C | (62 cm), (b) Magnification of the region close to d=0.

There exists an energy barrier to be overcome for convex vapour formation out of a bulk liquid phase between a spherical particle and a flat plate, i.e. the phase transition is the nucleation phenomena. The curve is ever decreasing after that and all the liquid would change into vapour.

6.2.2.1. Effect of equilibrium contact angle on the stability of the system for vapour phase formation out of a bulk liquid phase between a flat plate and a sphere: convex meniscus

Properties of the system other than the equilibrium contact angle are kept the same as for Figure 6-22, and the effect of the contact angle on the free energy is investigated.

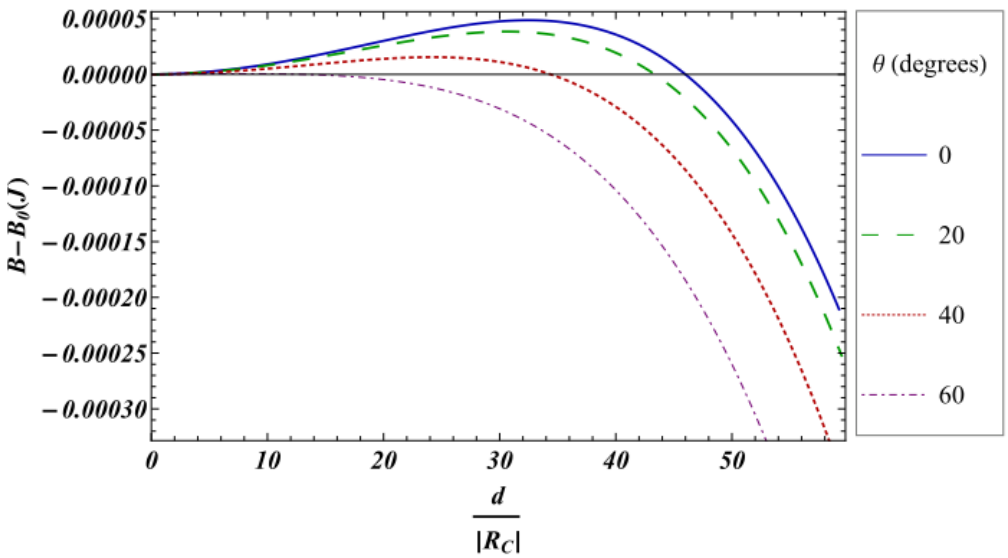

Figure 6-23 Effect of the equilibrium contact angle on the free energy vs. scaled vapour bridge half width between a flat plate and a sphere, for water at 20°C, $P^L=0.9P_\infty$, $H=0.5|R_C|$ (300μm), $R_p=10^3\times|R_C|$ (62 cm).

As we get farther from the ***transition contact angle*** (equivalent to smaller contact angle), the energy barrier for the formation of the convex vapour phase becomes greater.

Although the curve is never monotonically increasing, for very large upper sphere radii with contact angles far from the ***transition contact angle*** (small contact angle in convex vapour formation), an extremely large vapour bridge with a huge energy barrier must be formed for nucleation to be possible. For example for R_P =

$10^8 \times |R_C|$ (62 km) and θ=0°, the vapour bridge width of the maximum point is $10^4 \times |R_C|$, with an energy barrier of 4.4 J. At the extreme where the upper sphere turns into a flat plate (radius of infinity), vapour formation with convex meniscus is unfavourable (the free energy curve is monotonically increasing) for contact angles far from the ***transition contact angle*** (small contact angle in convex vapour formation).

6.2.2.2. Effect of the solid surface separation distance on the stability of the system for vapour phase formation out of a bulk liquid between a sphere and a flat plate: convex meniscus

The effect of the distance between a sphere and a flat plate on the free energy of the convex vapour formation is illustrated in Figure 6-24:

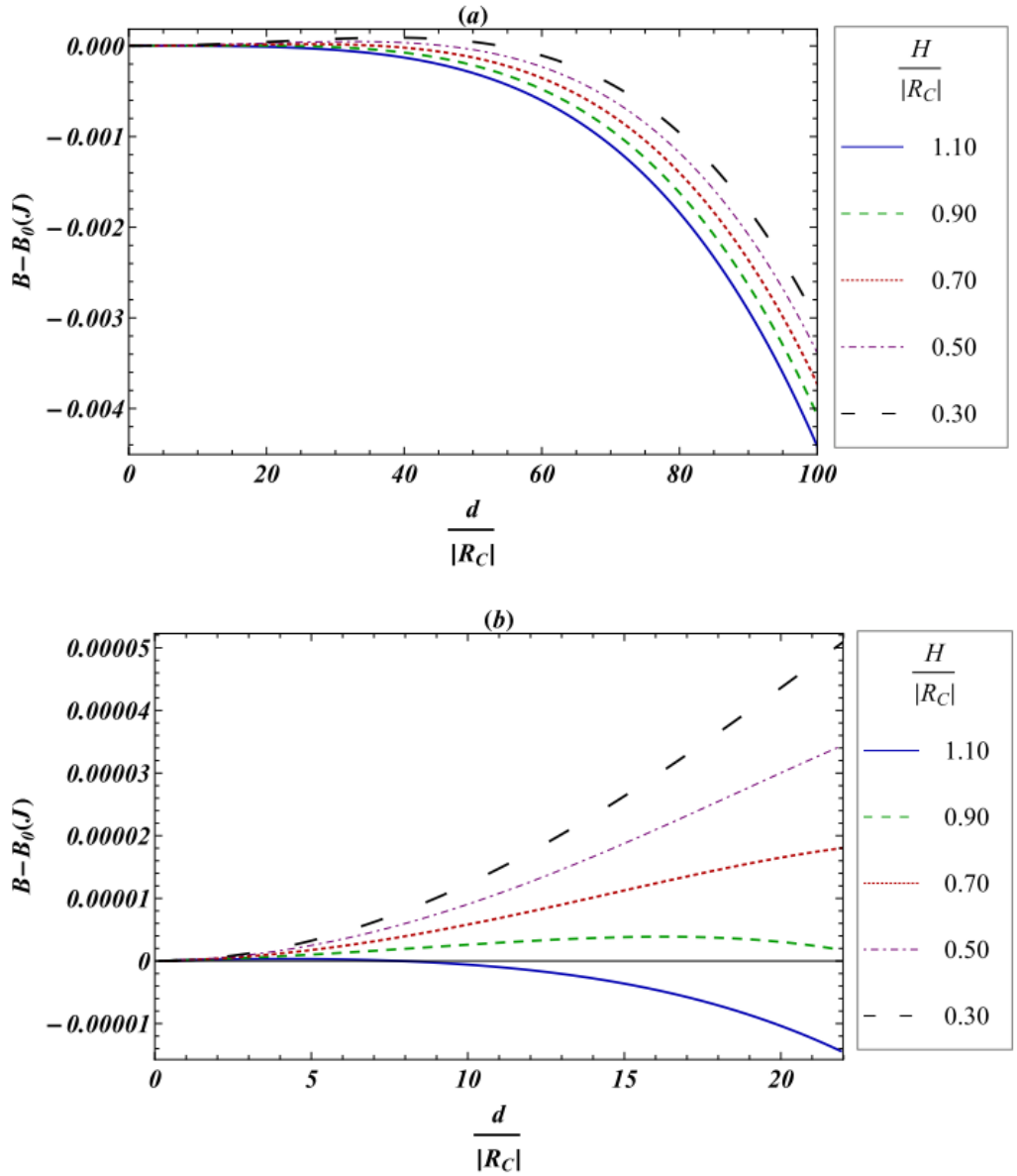

Figure 6-24 Effect of the solid surface separation distance on the free energy vs. scaled vapour bridge half width between a flat plate and a sphere, for water at 20°C, $P^L=0.9P_\infty$, θ=0° $R_p=10^3\times|R_C|$ (6.2 km), concave meniscus, (b) Magnification of the unstable equilibrium point.

For smaller separation distances, the convex vapour formation is possible after passing a higher energy barrier. In convex vapour formation between two flat plates, new phase formation becomes unfavourable below a certain separation distance, as demonstrated in section 5.2.2.2. In contradiction to the case of a

convex vapour bridge between two flat plates, in this case of a spherical particle and a flat plate even for two touching solids, convex vapour formation is still possible after passing a relatively high energy. This contradiction can be explained as follows: For convex vapour formation between two flat plates, the vertical distance of the plates remains constant at different distances from the center line (different *d*). In the case of convex vapour formation between a flat plate and a sphere, the vertical distance between the sphere and flat plate gets larger as we get farther from the center line (as *d* increases). Therefore even when the two solids are touching, somewhere far enough from the centerline the separation distance becomes large enough to allow the formation of the unstable convex vapour bridge (Figure 6-25).

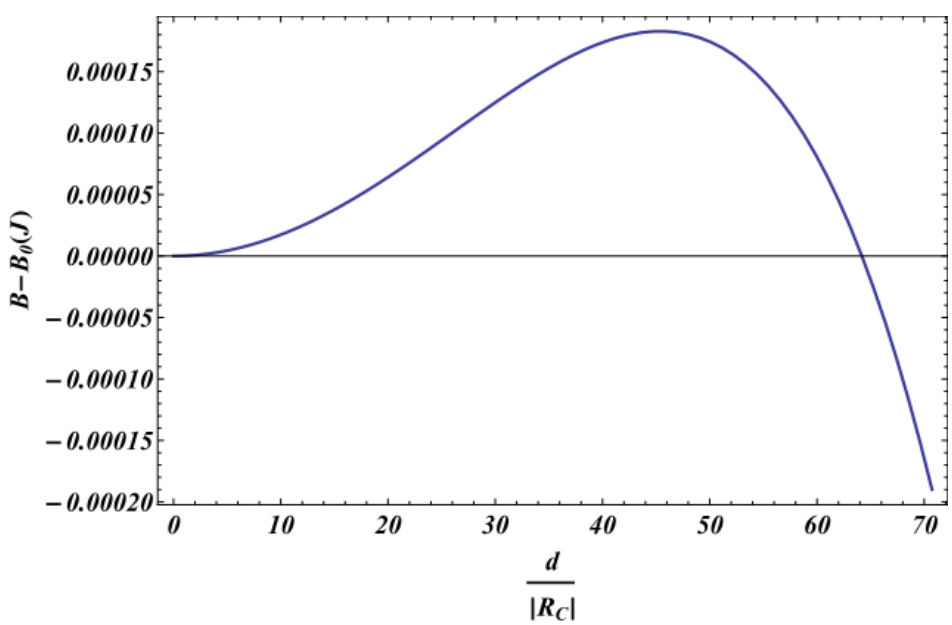

Figure 6-25 Curve of free energy vs. scaled liquid bridge half width between a flat plate and a sphere for water at 20°C, P^L=0.9P_∞, θ=0°, H=0, and R_p=10^3×│R_C│(6.2 km).

6.2.2.3. Effect of solid sphere size on the stability of the system for vapour phase formation out of a bulk liquid phase between a flat plate and a sphere: convex meniscus

The impact of the spherical particle's size is studied in this section. The properties of the system other than the radius of the solid sphere are kept the same as those in Figure 6-22.

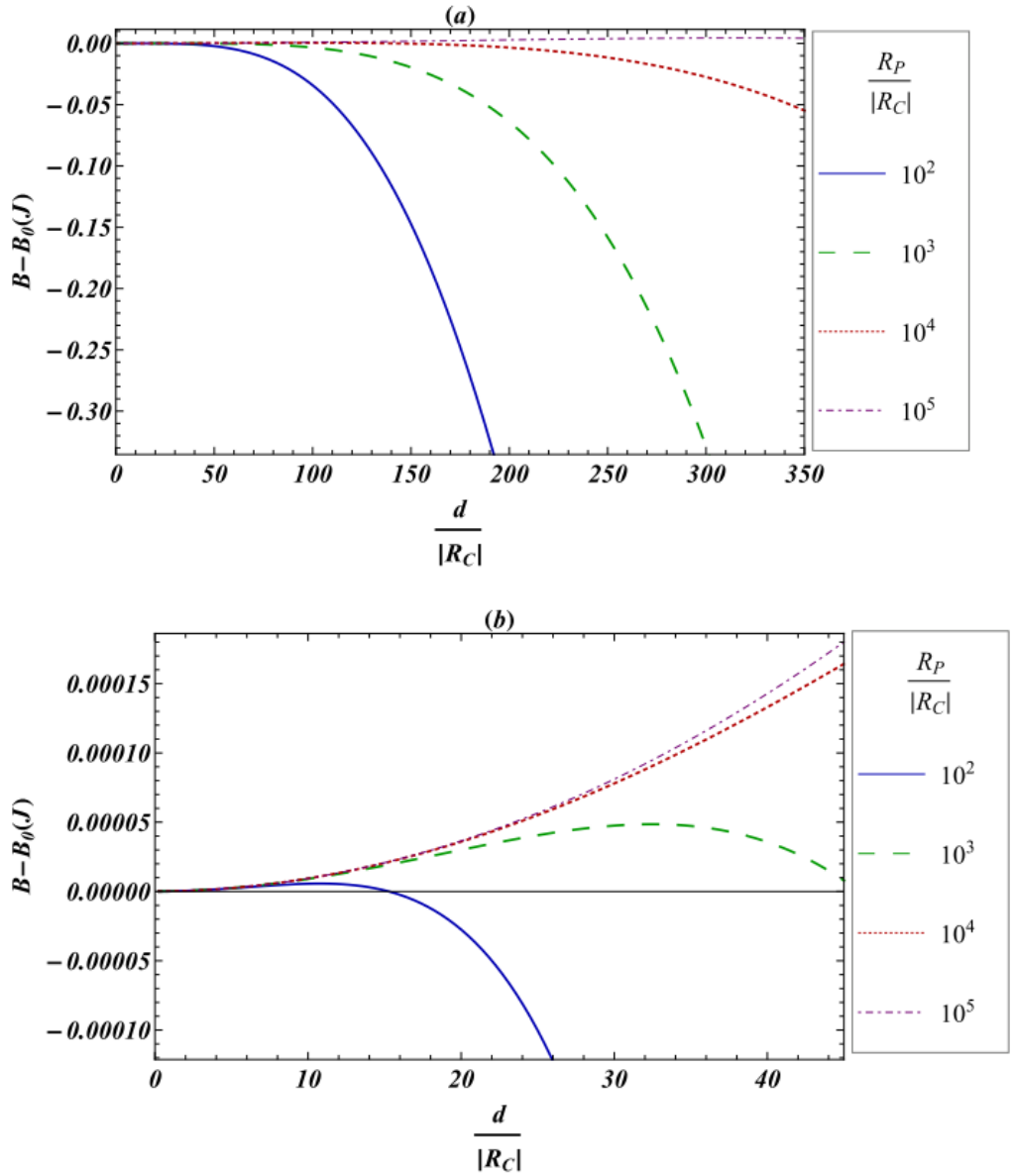

Figure 6-26 Effect of the solid sphere size on the free energy vs. vapour bridge half width between a flat plate and a sphere, for water at 20°C, P^L=0.9P_∞, θ=0°, and H=0.5│R_C│(300μm), (b) Magnification of the unstable equilibrium point.

An increase in the upper sphere size results in a higher energy barrier and a larger unstable convex vapour bridge. In the extreme case, for an upper sphere with radius of infinity (equivalent to a flat plate), either the highest energy barrier (in comparison to various cases of sphere with finite size) must be overcome for vapour formation, or vapour formation would not be possible at all (monotonically

increasing energy curve), depending on the amount of separation distance and the contact angle. For any sphere size other than infinity (the case of the two flat plates), the curve of the free energy never turns into monotonically increasing even at the smallest separation distance or for the farthest contact angle from the transition contact angle (0°). However if the sphere is very large, the nucleation happens at a very large vapour width with a relatively high energy barrier. For example for a sphere of radius $10^9 \times \left| R_C \right|$ (~ 620 kilometres) touching a flat plate (H=0), the unstable bridge has a width of $\frac{d}{|RC|} = 4.4\times10^4$ (d~ 28 m) with an energy level of 173 J. In this case the energy level of the nucleation barrier is so large that it might take forever for the nucleation to happen.

6.3. Conclusion

In this chapter bulk fluid confined between a sphere and a flat plate has been studied, while the temperature, bulk phase pressure, and mass of the system are constant. There are two cases based on the state of the fluid: (1) liquid formation from a bulk vapour phase, (2) vapour formation from a bulk liquid phase. In each of these cases, according to the bulk phase pressure (above or below the saturation pressure) the meniscus is either concave or convex. Thermodynamic stability analysis was performed on each case, and the effects of different parameters including equilibrium contact angle, separation distance between the sphere and the flat plate, and the size of the sphere was investigated. The results of sections 5.1 and 5.2 are summarized in Table 6-5 as follows:

Table 6-5 Summary of liquid phase formation out of a bulk vapour phase and vapour phase formation out of a bulk liquid phase between a flat plate and a sphere, and the effects of the equilibrium contact angle, θ, the separation distance, H, and the sphere size, R_P, on the stability of the system. θ_t is the transition contact angle, R_1 & R_2 are the principal radii of the liquid-vapour interface, P^L is the liquid phase pressure, and P^V is the vapour phase pressure.

(a) liquid phase formation out of a bulk vapour phase

Case		Arbitrary Definition of ΔP	Sign of R_1 & R_2 according to ΔP definition	Bulk pressure	Equilibrium state	Increase in θ	Increase in H	Increase in R_P
Liquid Formation from vapour	Concave ($\theta < \frac{180°-\alpha}{2}$)	$P^V - P^L$	R_1 (+) R_2 (−)	$P^V < P_\infty$	1 unstable 1 stable	~ Closer to θ_t →(1) Larger barrier →(2) Less stability of the stable point (ultimately unfavourable new phase formation)	→(1) Larger barrier →(2) Less stability of the stable point (unfavourable new phase formation for $H > H_{Break}$)	→(1) Smaller barrier →(2) More stability of the stable point
	Convex ($\theta > \frac{180°-\alpha}{2}$)	$P^V - P^L$	R_1 (−) R_2 (−)	$P^V > P_\infty$	1 unstable	~ Farther from θ_t →Larger barrier	→Smaller barrier	→Larger barrier

Table 6-5 Summary of liquid phase formation out of a bulk vapour phase and vapour phase formation out of a bulk liquid phase between a flat plate and a sphere, and the effects of the equilibrium contact angle, θ, the separation distance, H, and the sphere size, R_P, on the stability of the system. θ_t is the transition contact angle, R_1 & R_2 are the principal radii of the liquid-vapour interface, P^L is the liquid phase pressure, and P^V is the vapour phase pressure.

(b) Vapour phase formation out of a bulk liquid phase

Case		Arbitrary Definition of ΔP	Sign of R_1 & R_2 according to ΔP definition	Bulk pressure	Equilibrium state	Increase in θ	Increase in H	Increase in R_P
Vapour Formation from liquid	Concave ($\theta > \frac{180°+\alpha}{2}$)	$P^L - P^V$	R_1 (+) R_2 (−)	$P^L > P_\infty$	1 unstable 1 stable	~ Farther from θ_t →(1) Smaller barrier →(2) More stability of the stable point	→(1) Larger barrier →(2) Less stability of the stable point (unfavourable new phase formation for $H > H_{Break}$)	→(1) Smaller barrier →(2) More stability of the stable point
	Convex ($\theta < \frac{180°+\alpha}{2}$)	$P^L - P^V$	R_1 (−) R_2 (−)	$P^L < P_\infty$	1 unstable	~ Closer to θ_t →Smaller barrier	→Smaller barrier	→Larger barrier

Several conclusions about new phase formation out of a bulk fluid phase in between a sphere and a flat plate are presented here:

1) When vapour is the bulk fluid between a sphere and a flat plate, two possible cases exist:
   - Formation of a liquid phase with concave meniscus can take place if and only if the bulk vapour pressure is below the saturation pressure ($P^V < P_\infty$) as discussed in the beginning of section 6.1.1. For the meniscus to be concave the confinement walls should be wettable such that $\theta < \frac{180° - \alpha}{2}$. Even when the vapour pressure is below the saturation pressure, and the contact angle is such that the meniscus is concave, liquid phase formation might or might not be possible depending on the value of different parameters including the contact angle (θ), separation distance (H), and sphere size (R_P). If liquid formation is favourable, after passing an energy barrier, the new liquid phase reaches to and remains at its stable size. This phenomenon is well known as capillary condensation.
   - Liquid phase formation with convex meniscus is possible if and only if bulk vapour pressure is above the saturation pressure ($P^V > P_\infty$). Such a convex meniscus is only achievable through non-wettable confinement that results in $> \frac{180° - \alpha}{2}$. The free energy curve for this case goes through a maximum point, and is constantly decreasing after passing that maximum. This indicates that the phase transition is a nucleation phenomenon, and

once the barrier is passed all the bulk vapour phase turn into liquid phase. It should be highlighted that between a sphere and a flat plate a liquid bridge with a convex meniscus can never exist in stable condition. Depending on the parameters (contact angle (θ), separation distance (H), and sphere size (R_P), the nucleation energy barrier might be so high that the nucleation never happens in practice; but the free energy curve never turns into monotonically increasing.

2) When the bulk fluid between a sphere and a flat plate is liquid, there are two possible cases of vapour formation out of bulk liquid phase:

- Vapour phase formation with concave meniscus may happen if and only if the bulk liquid pressure is above the saturation pressure ($P^L > P_\infty$). The confinement walls should be non–wettable such that $\theta > \frac{180° + \alpha}{2}$ for the concave meniscus. Even when the liquid phase pressure is above the saturation pressure, and the contact angle is such that the meniscus is concave, vapour phase formation might or might not be possible depending on the value of different parameters including the of contact angle (θ), separation distance (H), and sphere size (R_P). If vapour formation is favourable, after passing an energy barrier, the new vapour phase reaches to and remains at its stable size. This phenomenon is called capillary evaporation.
- Vapour phase formation with convex meniscus is possible if and only if bulk liquid pressure is below the saturation pressure ($P^L < P_\infty$). Such a convex meniscus is only possible if the confinement walls are wettable and

result in $< \frac{180^\circ + \alpha}{2}$. The free energy curve for this case goes through a maximum point, and is constantly decreasing after passing that maximum. The phase transition is a nucleation phenomenon and all the bulk liquid phase turn into vapour phase once the barrier is passed. It should be highlighted that between a sphere and a flat plate a vapour bridge with a convex meniscus can never exist in a stable condition. Depending on the parameters (contact angle (θ), separation distance (H), and sphere size (R_P), the nucleation energy barrier might be so high that it takes so long before it can be overcome that the nucleation will never happen in practice; but the free energy curve never turns into monotonically increasing.

3) Effect of the contact angle (θ):

- For any new phase formation with a <u>concave</u> meniscus, getting farther from the ***transition contact angle*** makes the energy barrier smaller, and the stable point more stable. For liquid formation out of a bulk vapour phase, a concave meniscus is possible for $P^V < P_\infty$, and $< \frac{180^\circ - \alpha}{2}$, and getting farther from the ***transition contact angle*** happens as the contact angle decreases. For vapour formation out of a bulk liquid phase, a concave meniscus is possible for $P^L > P_\infty$, and $> \frac{180^\circ + \alpha}{2}$, and getting farther from the ***transition contact angle*** is equivalent to increasing the contact angle. New phase formation between a sphere and a flat plate at separation distance H ($H \neq 0$) with concave meniscus becomes ultimately impossible for some contact angles close to the ***transition contact angle***.

- For any new phase formation with a <u>convex</u> meniscus, getting farther from the ***transition contact angle*** increases the height of the energy barrier. Liquid formation out of a bulk vapour phase with convex meniscus is only possible for $P^V > P_\infty$, and $> \frac{180° - \alpha}{2}$, and getting farther from the ***transition contact angle*** happens as the contact angle increases. Vapour formation out of a bulk liquid phase with convex meniscus only happens if $P^L > P_\infty$, and $> \frac{180° + \alpha}{2}$, and getting farther from the ***transition contact angle*** is equivalent to decreasing the contact angle. The free energy curve for the new phase formation with convex meniscus between a sphere and a flat plate never gets monotonically increasing, even for the farthest amount of contact angle from the ***transition contact angle*** (in contrast to the case of new phase formation with convex meniscus between two flat plates, for which the free energy curve gets monotonically increasing at some contact angle far enough from the ***transition contact angle***). However the energy level of the nucleation barrier might get so large (also depending on separation distance (H), and sphere size (R_P)), that it takes so long for the barrier to be overcome, and nucleation never happens in practice.

4) Effect of the separation distance between a sphere and a flat plate (H):

- For any new phase formation (liquid formation or vapour formation) with a <u>concave</u> meniscus, an increase in the separation distance results in a higher energy barrier and less stability of the stable state of the system. New phase

formation with concave meniscus becomes unfavourable above a certain distance, called the ***breakage distance*** (H_{Break}) [18].

For liquid formation with concave meniscus, equation (6.16) is found in the literature [24], describing the ***breakage distance*** for the condition where $R_P >> |d| >> H$. The ***breakage distance*** sensitively depends on the Kelvin radius, and is also a less sensitive function of the sphere radius and contact angle according to equation (6.16). Equation (6.33) is the analogous equation for the case of vapour formation with concave meniscus.

From further investigation it is found that new phase formation with concave meniscus is certainly not possible for separation distance above the Kelvin radius ($H > R_C$) for any sphere size and with any contact angle. Therefore H_{Break} is always less than R_C, regardless of the amount of contact angle and size of the sphere.

At the ***breakage distance***, the free energy of the stable equilibrium is approximately equal to the free energy of the unstable equilibrium. Natural fluctuations between the unstable and stable points can be considered as a reason for a "diffuse liquid−vapour interface" [18]. Such a diffuse liquid-vapour interface is experimentally observed at separation distance equal to the breakage distance, in the process of reducing H from $H > H_{Break}$ to the breakage distance [12].

As a sphere and a flat plate come into contact (separation distance of zero), the most stable bridge with concave meniscus is formed through a spontaneous non-nucleating phenomenon (zero energy barrier).

Investigations showed that for a sphere and a flat plate in contact ($H=0$), new phase formation with concave meniscus is always possible (never becomes unfavourable) for any contact angle (even for the closest contact angle to the ***transition contact angle***) and any sphere size.

For any new phase formation (liquid formation or vapour formation) with <u>convex</u> meniscus, an increase in the separation distance makes the energy barrier smaller. Reduction of the separation distance, even to $H=0$, will not cause new phase formation with convex meniscus to be unfavourable (in contrast to new phase formation with convex meniscus in between two flat plates, for which new phase formation is unfavourable below some separation distance). However, at small separation distances the energy barrier might have such a huge value that it takes so long before it can be overcome, that the nucleation doesn't happen in practice.

5) Effect of the sphere size (R_P):

- For any new phase formation (liquid formation or vapour formation) with <u>concave</u> meniscus, increase in the radius of the solid sphere results in shorter energy barrier and more stability (deeper minimum) and larger bridge width at the stable condition. The extreme as the sphere gets larger occurs when the radius of the upper sphere becomes infinity, where the geometry would simply change to that of two flat plates. For two flat plates, all of the bulk phase would change into the new phase once the energy barrier is overcome.

It is remarkable that the effect of the solid sphere size on the unstable free energy barrier and the unstable liquid bridge width is minor in comparison to

its effect on the stable point. This can be described as follows: at small liquid bridge width (small *d's*), the new phase cannot sense the difference of the amount of the curvature of spheres of various sizes. However, as the bridge width gets larger the location of the stable size is strongly affected by curvature.

- For any new phase formation (liquid formation or vapour formation) with <u>convex</u> meniscus, increase in the radius of the solid sphere causes a higher energy barrier. The new phase formation is still thermodynamically favourable for any sphere of finite radius, although the barrier might be so large that such a long time is required before it can be overcome, that the nucleation doesn't happen in practice.

6) It should be noted that for any new phase formation (liquid formation or vapour formation) with <u>convex</u> meniscus between a sphere and a flat plate, the free energy curve of the system never (for any value of θ, H, and R_P) changes to monotonically increasing. This is in contradiction with the new phase formation with convex meniscus between two flat plates, where for some contact angle far from the ***transition contact angle***, or at some small separation distance the phase transition will become unfavourable. This contradiction happens as a result of the geometry of the confinement: As we get farther from the center line (as bridge width, *d*, gets larger), while the vertical distance of the solids between two flat plates remains constant, the vertical distance between a sphere and a flat plate gets larger and larger. Therefore between a sphere and a flat plate, even when the two solids are touching or the contact angle is near the

transition contact angle, at some large enough bridge width (somewhere far enough from the centerline) the gap becomes large enough to allow the formation of the unstable new phase with convex bridge.

7. Conclusion

Confined fluid behaves in a different way from a bulk fluid, as has been observed in various natural and industrial cases. In this thesis, the behaviour of a confined fluid has been discussed from a surface thermodynamics point of view (the basics of which were presented mainly in chapter 3), for three different geometries: i) inside a cone, ii) between two flat plates, and iii) between a sphere and a flat plate. The fluid was considered to be pure (single component), and the temperature and bulk phase pressure of the confined fluid assumed to be constant. The system was closed to any mass exchange.

Thermodynamic stability analysis was performed by examining the curve of free energy of the system vs. size of the new phase being formed out of the confined fluid. From that curve it was predicted whether new phase formation is favourable, and if the new phase can exist in a stable condition. For each of the geometries, the effect of the equilibrium contact angle, and also geometrical factors (the effect of cone angle for the cone geometry, the effect of plate separation distance for the geometry of two flat plates, and effects of solid separation distance and spherical particle size for the sphere and flat plate geometry) have been studied.

7.1. New phase formation – two types based on the curvature shape: concave or convex

7.1.1. New phase formation with concave meniscus

- Liquid formation with a concave meniscus out of a confined vapour phase is possible only at vapour phase pressures below the saturation pressure ($P^V < P_\infty$). In addition, at vapour phase pressure below the saturation pressure, only a liquid phase with concave meniscus has the possibility to form. This has been discussed in section 3.7.1, and the beginning of sections 4.1.1, 5.1.1, and 6.1.1 for each of the geometries. Also the solid walls must be wettable to have a concave meniscus. Wettable walls can equivalently be described as a situation for which γ^{SL} is lower than γ^{SV} [45]. The free energy of the system in this case can be obtained from equation (3.59).
- Vapour phase formation with a concave meniscus out of a confined liquid phase is possible if and only if the liquid phase pressure is above the saturation pressure ($P^L > P_\infty$), as explained in section 3.7.2, and the beginning of sections 4.2.1, 5.2.1, and 6.2.1. The free energy of the system in this case can be obtained from equation (3.62). For the vapour phase to form with a concave meniscus, the confinement walls must be non–wettable. There are fewer of such non–wettable solids (in comparison with the wettable case) in practice. For example according to Ward and Levart [16], only a few of the plastics, such as polytetra–fluoroethylene, make a contact angle greater than 90° with water. Many other materials such as a clean metal or glass in contact with water show the contact angle of zero.

Typical curves of free energy vs. new phase size are shown for new phase formation with concave meniscus in the different geometries in Table 7-1.

Table 7-1 Curves of free energy vs. new phase size for new phase formation with concave meniscus

Geometry	Cone	Plate–Plate	Sphere–Plate
Liquid formation with concave meniscus out of a confined vapour phase (at $P^V < P_\infty$), inside confinement of wettable walls. 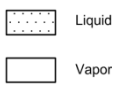	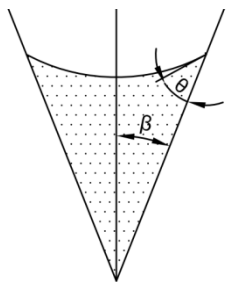 $0 \le \theta < 90^o - \beta$	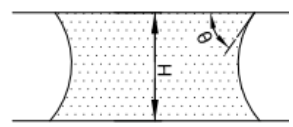 $0 \le \theta < 90^o$	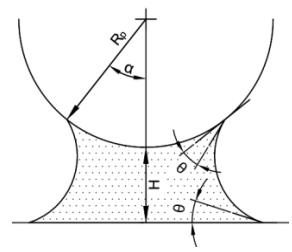 $0 \le \theta < 90^o - \frac{\alpha}{2}$
Vapour formation with concave meniscus out of a confined liquid phase (at $P^L > P_\infty$), confinement of non–wettable walls. 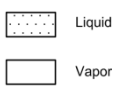	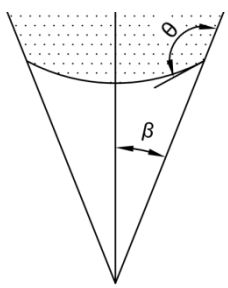 $90^o + \beta < \theta \le 180^o$	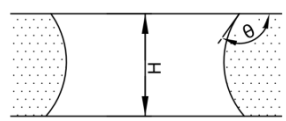 $90^o < \theta \le 180^o$	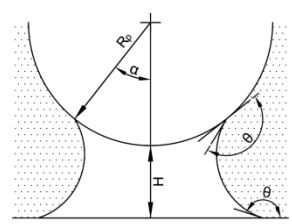 $90^o + \frac{\alpha}{2} < \theta \le 180^o$
Typical curve of free energy vs. size of a new phase with concave meniscus	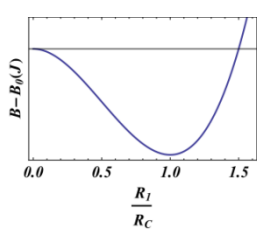	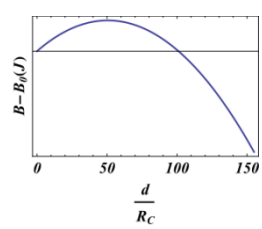 (~ for $H < \lvert R_C \cos\theta \rvert$)	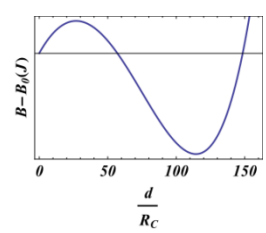 (for $H < H_{Break}$)

A stable new phase with a concave meniscus can be formed out of a fluid phase being confined inside a cone or between a sphere and a flat plate. The stable new phase with concave meniscus forms spontaneously (without any energy barrier) for

the cone geometry and the sphere–plate geometry when H=0, and after overcoming an energy barrier for the sphere–plate geometry when $H \neq 0$. For fluid being confined between two flat plates, the whole confined fluid changes into the new phase once the barrier is overcome, i.e. there is no coexistence of the two phases (the confined fluid and the new phase) in a stable condition.

It should be noted that while inside a cone, a new phase with concave meniscus can always form in a stable condition, whereas for the gap between two flat plates or between a sphere and a flat plate, new phase formation becomes unfavourable (monotonically increasing free energy curve) above a certain separation distance and/or for some contact angles close to the ***transition contact angle*** (contact angle at which the meniscus changes from concave to convex). This will be explained in more detail in sections 7.2 and 7.3 (effects of solid separation distance and equilibrium contact angle).

Contact angle is measured from inside a denser phase (liquid) according to convention. That is why the ranges are different for liquid formation or vapour formation, although both have a concave meniscus. The range of contact angle for which the meniscus is concave, also depends on the geometry of the confinement. For example for liquid formation inside a sphere–plate geometry, the meniscus is concave if $0 \leq \theta < 90^{o} - \frac{\alpha}{2}$, where α is the half–filling angle. For an upper sphere of comparatively large size, and tiny separation distance, α is small even for large bridge length (d). That describes why using $\theta < 90^{o}$ as a criterion for having a

liquid bridge with a concave meniscus is a good assumption, as in literature where sphere radius is 2.5 cm and separation distance is on the order of nanometres [12].

7.1.2. New phase formation with convex meniscus

- Liquid formation with convex meniscus out of a bulk vapour phase is possible if and only if the vapour phase pressure is above the saturation pressure ($P^V > P_\infty$).This has been explained in section 3.7.1, and the beginning of sections 4.1.2, 5.1.2, and 6.1.2 for each of the geometries. Confinement walls must be non-wettable for the liquid phase to have a convex meniscus. It should be noted that for wettable walls, the liquid would have already formed from the vapour phase below (as discussed in 7.1.1) or at the saturation pressure. The free energy of the system in this case can be obtained from equation (3.59).
- Vapour phase formation with convex meniscus out of a confined liquid phase is possible if and only if liquid pressure is below the saturation pressure ($P^L < P_\infty$), as explained in section 3.7.2, and the beginning of sections 4.2.2, 5.2.2, and 6.2.2. For the vapour phase to have a convex meniscus, the confinement walls must be wettable. It should be noted that for non–wettable walls, the vapour would have already formed from the liquid phase above (as discussed in 7.1.1) or at the saturation pressure. The free energy of such system can be calculated from equation (3.62).

Typical curves of free energy of a system vs. size of the new phase with convex meniscus are shown for different geometries in Table 7-2.

Table 7-2 Curves of free energy vs. new phase size for new phase formation with convex meniscus

Geometry	Cone	Plate–Plate	Sphere–Plate
Liquid formation with convex meniscus out of a confined vapour phase (at $P^V > P_\infty$), confinement of non–wettable walls. 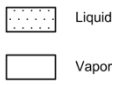	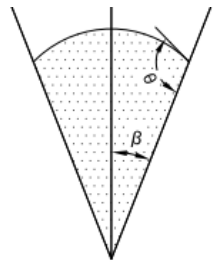 $90^o - \beta < \theta \leq 180^o$	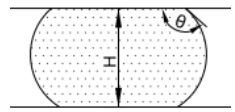 $90^o < \theta \leq 180^o$	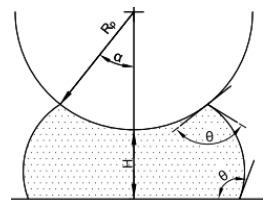 $90^o - \frac{\alpha}{2} < \theta \leq 180^o$
Vapour formation with convex meniscus out of a confined liquid phase (at $P^L < P_\infty$), confinement of wettable walls. 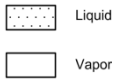	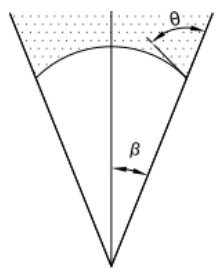 $0 \leq \theta < 90^o + \beta$	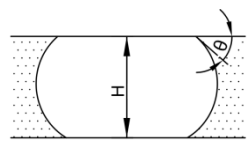 $0 \leq \theta < 90^o$	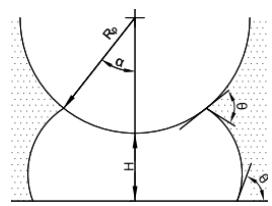 $0 \leq \theta < 90^o + \frac{\alpha}{2}$
Typical curve of free energy vs. size of a new phase with convex meniscus	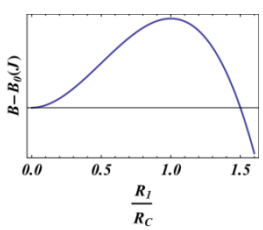	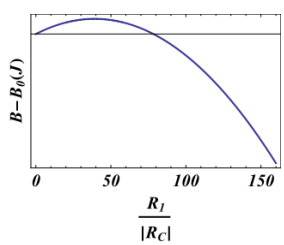 (~ for H > $\lvert R_C \cos\theta \rvert$)	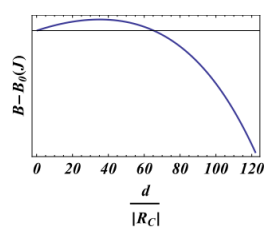

Free energy curves for new phase formation with convex meniscus go through a maximum point, and are constantly decreasing after that. The phase transition is a nucleation phenomena, i.e. a nucleation barrier must be overcome. Once the nucleation barrier is overcome, all of the confined phase turns into the new phase. Therefore with a new phase having a convex meniscus, two phases cannot coexist in a stable condition, i.e. no convex meniscus is stable for the case of a pure fluid.

Inside a cone, the new phase free energy curves never become ever–ascending and new phase formation is always possible. For the gap between a sphere and a flat plate, the free energy curve never becomes monotonically increasing; however for small separation distances and/or equilibrium contact angles far from the ***transition contact angle*** (θ_t) the energy barrier might be so high that nucleation never occurs in practice. Inside the gap between two flat plates, the free energy curve becomes constantly increasing for small separation distances and/or equilibrium contact angles far from the ***transition contact angle*** (θ_t). The effects of solid separation distance and equilibrium contact angle are fully discussed in sections 7.2 and 7.3.

7.2. Effect of equilibrium contact angle on the stability of the system when a new phase is formed from a confined fluid

7.2.1. Effect of equilibrium contact angle, for new phase formation with concave meniscus

For new phase formation with concave meniscus, getting farther from the ***transition contact angle*** (θ_t) makes the unstable point (maximum point) occur at a smaller volume with a lower energy level (lower energy barrier) and the stable point occur with a larger volume and more stability (deeper minimum point, and lower energy level). The effect of contact angle on the curve of free energy vs. new phase size is shown for different geometries in Table 7-3.

Table 7-3 Effect of contact angle on curves of free energy vs. new phase size for new phase formation with concave meniscus. The solid line shows the free energy as contact angle gets farther from the transition contact angle.

Geometry	Cone	Plate–Plate	Sphere–Plate
Schematic of new phase formation with concave meniscus out of a confined phase for different continent geometries New Phase Confined Fluid	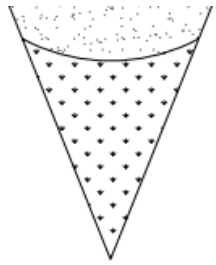	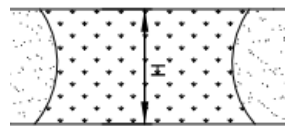	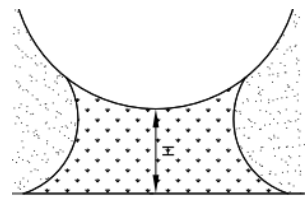
Effect of contact angle on the curve of free energy vs. size of a new phase with concave meniscus	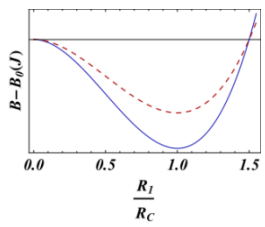	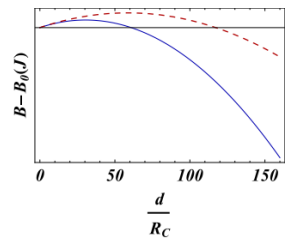 (~ for H < | $R_C\cos\theta$ |)	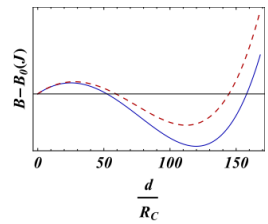 (for H < H_{Break})

For the geometry of interest, in either case of liquid formation or vapour formation, the shape of the meniscus alters in the same way when contact angle gets farther from the ***transition contact angle***. However in terms of increase/decrease in contact angle, getting farther from the ***transition contact angle*** corresponds to opposite terms for liquid formation and vapour formation. This is due to the convention of contact angle being measured from inside a denser phase (liquid). For liquid formation with a concave meniscus out of a confined vapour phase, decrease in contact angle results in getting farther from the ***transition contact angle***. For vapour formation with a concave meniscus out of a confined liquid phase, increase in contact angle is equivalent to getting farther from the ***transition contact angle***. This shows how defining the ***transition contact angle*** facilitates a

unique explanation of meniscus changes, regardless of the case being vapour formation or liquid formation.

Inside the gap between two flat plates, or between a sphere and a flat plate (with separation distance other than zero, $H \neq 0$), as equilibrium contact angle gets close to the ***transition contact angle***, the nucleation barrier increases. Finally at some contact angle close to the ***transition contact angle***, the free energy curve becomes monotonically increasing and new phase formation with concave meniscus becomes unfavourable. For the cone geometry, a stable new phase with a concave meniscus can always form out of a confined phase.

Changing the contact angle by a specific number of degrees, results in larger relative changes of the energy level when the contact angle is closer to the ***transition contact angle***. The validity range of this statement is for contact angles which do not result in monotonically increasing curves.

7.2.2. Effect of equilibrium contact angle for new phase formation with convex meniscus

When the meniscus is convex, getting farther from the ***transition contact angle*** increases the level of the energy barrier, and the volume of the unstable bridge.

Table 7-4 Effect of contact angle on curves of free energy vs. new phase size for new phase formation with convex meniscus. The solid line shows the free energy as contact angle gets farther from the transition contact angle.

Geometry	Cone	Plate–Plate	Sphere–Plate
Schematic of new phase formation with convex meniscus out of a confined phase for different continent geometries New Phase Confined Fluid	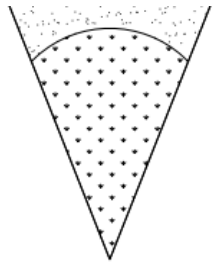	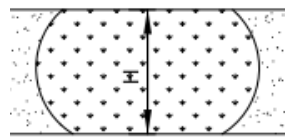	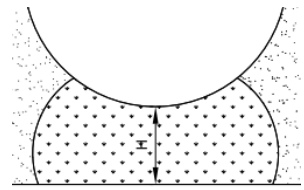
Effect of contact angle on the curve of free energy vs. size of a new phase with convex meniscus	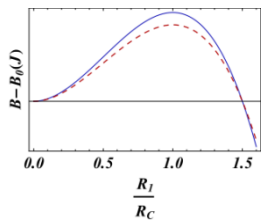	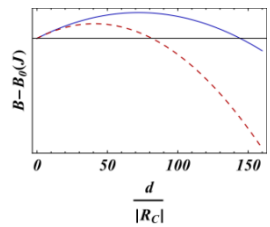 (~ for H > | $R_C\cos\theta$ |)	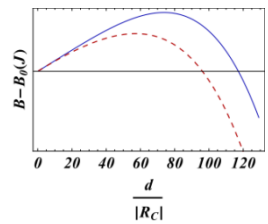

In liquid formation with convex meniscus, the contact angle gets farther from the ***transition contact angle*** as it increases. In vapour formation with convex meniscus, the contact angle should decrease to get farther from the ***transition contact angle***.

7.3. Effect of solid separation distance

In general, a tighter confinement facilitates new phase formation with concave meniscus by reducing the energy barrier and/or results in more stability of the stable condition by lowering the energy level of the minimum point. In contrast for new phase formation with convex meniscus, the tighter the confinement is, the higher the energy barrier that has to be overcome.

For the cone geometry, the apex angle (β) determines how tight the gap is. For the two plates and the sphere–plate geometries, separation distance (H) is indicative of how tight the confinement is.

For confinements where walls meet at some point (for example inside a cone or between a sphere and a flat plate having a contact, i.e. H=0) the free energy curve never becomes monotonically increasing and new phase formation never becomes unfavourable. Also in this case the derivative of free energy with respect to size of new phase is zero at the start point of the curve, i.e. when size is zero. A comparison of free energy curves for two cases of zero and nonzero separation distance for the sphere–plate geometry is illustrated in Table 7-1 for new phase formation with either concave or convex meniscus.

Table 7-5 Comparison of free energy vs. size of the new phase at the start point (new phase size =0) for zero separation distance (H=0), and nonzero separation distance (H≠0).

Case	H=0	H≠0
New phase formation with concave meniscus (sphere–plate geometry)	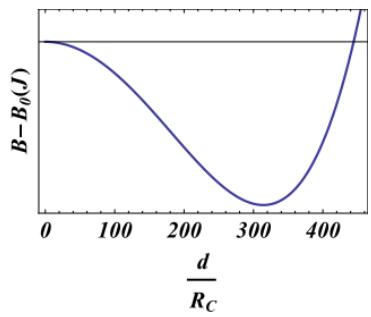	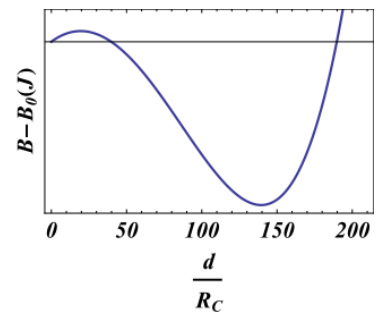
New phase formation with convex meniscus (sphere–plate geometry)	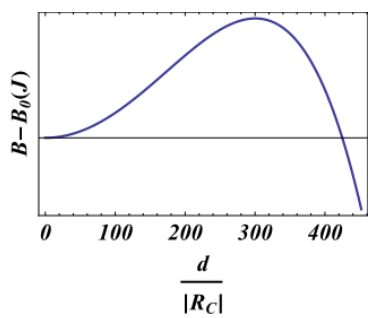	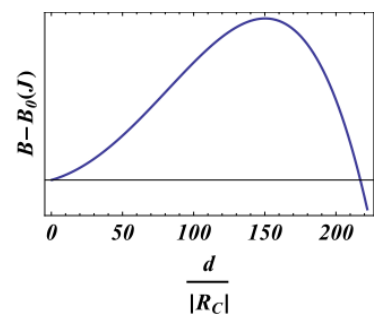

The effect of confinement wall separation distance is fully described for new phase formation with concave meniscus and new phase formation with convex meniscus in the two following sections.

7.3.1. Effect of solid separation distance for new phase formation with concave meniscus

As the confinement walls' separation decreases (decreasing β or H), a new phase with concave meniscus gets more stable, and has higher volume at the stable point. For two flat plates and completely separated sphere–plate ($H\neq0$) geometries, decreasing the separation distance also makes the nucleation energy barrier smaller.

Effect of separation distance on new phase formation with concave meniscus is schematically shown in Table 7-6.

Table 7-6 Effect of solid separation on curves of free energy vs. new phase size for new phase formation with concave meniscus. The dashed curve is the initial condition. The solid line shows the free energy as the walls' separation increases (cone apex (β) or surface distance (H) increases from that of the dashed line). The dot-dashed curve represents unfavourability of new phase formation with concave meniscus inside a gap between two flat plates or a sphere–plate, as H increases over a certain distance (approximately by $|R_C \cos\theta|$).

Geometry	Cone	Plate–Plate	Sphere–Plate
Schematic of new phase formation with concave meniscus out of a confined phase for different continent geometries New Phase Confined Fluid	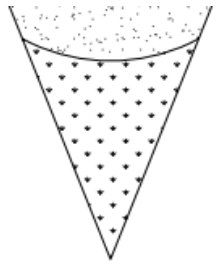	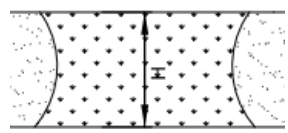	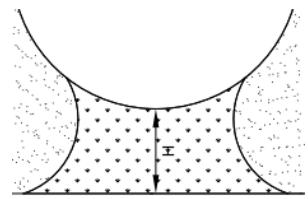
Effect of solid separation (β or H) on the curve of free energy vs. size of a new phase with concave meniscus	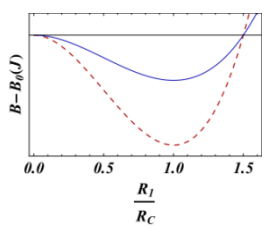	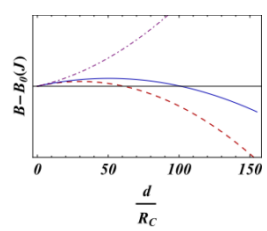	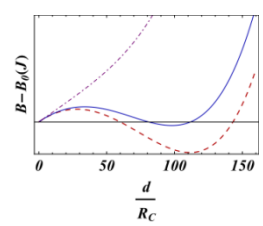

When confinement walls have some common point (inside a cone for any β or inside a gap between a sphere and a plate when H=0), new phase formation with concave meniscus is not a nucleation phenomena (no energy barrier has to be overcome) and it spontaneously reaches to its stable equilibrium. Also for confinement with walls having a common point, the free energy curve never becomes constantly increasing. Therefore for a cone geometry new phase formation with concave meniscus is always favourable regardless of the cone apex angle.

For two flat plates and for the sphere–plate geometry, new phase formation with concave meniscus becomes unfavourable as separation distance increases over a certain amount. For the two flat plates geometry, it has been shown in sections 5.1.1.2 and 5.2.1.2 that $|R_C cos\theta|$ (a modification of what is proposed in literature for the maximum distance of sphere–flat plate that allows for capillary condensation to happen [12, 24]) gives a fair value for the distance above which new phase formation with concave meniscus is unfavourable. For the sphere–plate geometry, the separation distance above which new phase formation with concave meniscus is unfavourable is called the ***breakage distance*** [18]. A new phase with a concave meniscus forms a stable bridge below this distance and breaks at separation distance above this distance. If the sphere radius is much greater that the bridge width, which is in turn much larger than the separation distance ($R_P >> |d| >> H$), the breakage distance can be approximated by $|R_C cos\theta|$ (more precisely from equation (6.16) for liquid formation with concave meniscus [36] or from equation (6.33) for vapour formation with concave meniscus). All in all, for two flat plates and sphere–plate geometries, new phase formation with concave meniscus is confidently unfavourable for separation distances above the Kelvin radius ($H > R_C$). At separation distances below the Kelvin radius, further investigation has to be made based on contact angle and radius size for the sphere–plate case.

7.3.2. Effect of solid separation distance, for new phase formation with convex meniscus

An increase in the solid walls' separation (by increasing cone apex (β) in the cone geometry, or separation distance (H) in the two flat plates or the sphere–plate geometries), reduces the level of the energy barrier.

Table 7-7 presents the effect of the walls' separation on the free energy of the system where new phase formation with convex meniscus happens out of a confined fluid.

Table 7-7 Effect of solid separation on curves of free energy vs. new phase size for new phase formation with convex meniscus. The dashed curve is the initial condition. The solid line shows the free energy as the walls' separation increases (cone apex angle (β) or surface distance (H) increases from that of the dashed line). The dot-dashed curve represents unfavourability of new phase formation with convex meniscus between two flat plates as H decreases over a certain distance (approximately by $|R_C \cos\theta|$).

Geometry	Cone	Plate–Plate	Sphere–Plate
Schematic of new phase formation with convex meniscus out of a confined phase for different continent geometries New Phase Confined Fluid	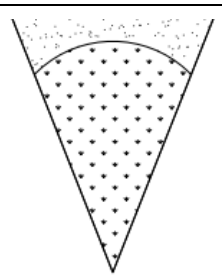	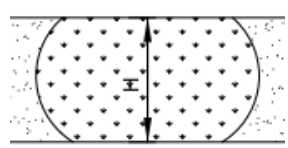	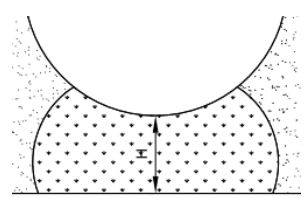
Effect of solid separation (β or H) on the curve of free energy vs. size of a new phase with convex meniscus	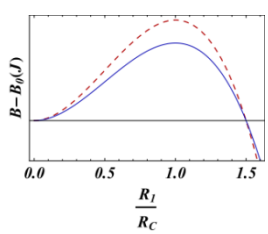	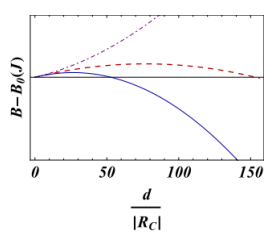	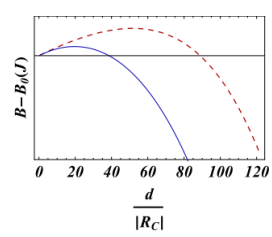

For new phase formation with convex meniscus, as confinement gets tighter (by decreasing the cone apex angle or the separation distance), a higher nucleation

barrier has to be overcome. Inside a cone or a gap between a sphere and a flat plate, new phase formation with convex meniscus never turns out to be unfavourable (monotonically increasing). However for the sphere–plate geometry at very small distance (*H*), the barrier gets so large that the phase transition might be practically impossible (as shown for example for liquid phase formation with convex meniscus in section 6.1.2.2). Between two flat plates, for separation distance below $|R_C cos\theta|$, new phase formation with convex meniscus becomes unfavourable due to constantly increasing free energy curve. $|R_C cos\theta|$ is a modification of what has been proposed [12, 24] for maximum separation distance above which capillary condensation, liquid formation with concave meniscus, becomes impossible.

7.4. Effect of sphere size for the geometry of a sphere and a flat plate

In the sphere–plate geometry, the size of the sphere affects the free energy curve and volume of the unstable and/or stable conditions.

For new phase formation with concave meniscus, increasing the sphere size results in a smaller energy barrier (with less volume of the new phase), and in a more stable minimum point (with higher volume of the new phase). At the extreme case where the sphere radius becomes infinity, equivalent to the case of two flat plates, the whole confined fluid transfers into the new phase once the energy barrier is overcome, i.e. no stable bridge with concave meniscus can be formed.

For new phase formation with convex meniscus, the energy barrier increases as the sphere gets bigger. The highest energy barrier has to be overcome for the case of two flat plates, equivalent to the case of sphere–plate with sphere radius of infinity.

7.5. Results implication

A summary of the comparative investigation of confined fluid for different geometries is presented in Table 7-8.

Table 7-8 Complete picture of thermodynamic stability analysis for confined fluid inside confinements of different geometries.

New phase formation with	Number of equilibrium states for different confinement geometries			Effect of contact angle, getting farther from the ***transition contact angle*** (θ_t)	Effect of separation distance, decrease in H or β	Effect of sphere size for sphere–plate geometry only, increase in R_P
	Cone	Two flat plates	Sphere–plate			
Concave meniscus(1)	1 stable	1 unstable	1 unstable 1 stable	→ Smaller barrier →More stability of stable point	→ Smaller barrier →More stability of stable point	→ Smaller barrier →More stability of stable point
Convex meniscus(2)	1 unstable	1 unstable	1 unstable	→ Larger barrier	→ Larger barrier	→ Larger barrier

(1) Liquid formation at $P^V < P_\infty$ and confinement of wettable walls (capillary condensation) or vapour formation at $P^L > P_\infty$ and confinement of non–wettable walls (capillary evaporation).

(2) Liquid formation at $P^V > P_\infty$ and confinement of non–wettable walls or vapour formation at $P^L < P_\infty$ and confinement of wettable walls.

Such a big picture of the stability of confined fluids can improve modeling techniques, and can describe the reasons behind many intuitive understandings. For example, it describes (in answer to some surprise in literature [46]) why in most experimental observations (and therefore theoretical modeling) a concave profile is considered. As mentioned in section 7.1, stable coexistence of pure liquid and vapour phases at pressures other than the saturation pressure is only possible for a new phase with concave meniscus.

As another example, it has been shown that a smaller liquid bridge (capillary condensation) with less stability forms as the sphere size decreases, or the equilibrium contact angle increases (gets closer to the ***transition contact angle***). This smaller bridge width can explain decrease in the capillary force as a result of the decrease in sphere radius decrease or increase in the equilibrium contact angle, that has been observed in previous modeling with the focus of capillary force calculation [10].

In practice confined fluid behaviour can be manipulated, employing different parameters, as shown in Table 7-8. For example, effective surface treatment is required to prevent capillary condensation in confined humid air (which contains H_2O vapour) at pressures below the saturation pressure that results in a stable concave liquid bridge. Modifying the surface to become non–wettable (equivalent to hydrophobic, when the fluid is H_2O) is one technique to prevent capillary condensation [47].

References

(1) R Roth and, K. M. K. Capillary evaporation in pores. *Journal of Physics: Condensed Matter* **2006**, *18*, 6517.

(2) Andrienko, D.; Patrício, P.; Vinogradova, O. I. Capillary bridging and long-range attractive forces in a mean-field approach. *J. Chem. Phys.* **2004**, *121*, 4414-4423.

(3) Elliott, J. A. W. 2011 NSERC DISCOVERY grant proposal.

(4) Megias-Alguacil, D.; Gauckler, L. J. Analysis of the capillary forces between two small solid spheres binded by a convex liquid bridge. *Powder Technol* **2010**, *198*, 211-218.

(5) Sperry, D. P.; Falconer, J. L.; Noble, R. D. Methanol—hydrogen separation by capillary condensation in inorganic membranes. *J. Membr. Sci.* **1987**, *60*, 185-193.

(6) Neimark, A. V.; Ravikovitch, P. I. Capillary condensation in MMS and pore structure characterization. *Microporous and Mesoporous Materials* **2001**, *44-45*, 697-707.

(7) Chau, A. Theoretical and experimental study of capillary condensation and of its possible application in micro-assembly, Universit´e Libre de Bruxelles, Belgium, 2008.

(8) H.K., C. Phase behaviour in slits—when tight cracks stay wet. *Colloids Surf. Physicochem. Eng. Aspects* **1997**, *123-124*, 355-367.

(9) Tselishchev, Y. G.; Val'tsifer, V. A. Influence of the type of contact between particles joined by a liquid bridge on the capillary cohesive forces. *Colloid Journal of the Russian Academy of Sciences: Kolloidnyi Zhurnal* **2003**, *65*, 385-389.

(10) Pakarinen, O. H.; Foster, A. S.; Paajanen, M.; Kalinainen, T.; Katainen, J.; Makkonen, I.; Lahtinen, J.; Nieminen, R. M. Towards an accurate description of the capillary force in nanoparticle-surface interactions. *Modell Simul Mater Sci Eng* **2005**, *13*, 1175-1186.

(11) Maeda, N.; Israelachvili, J. N. Nanoscale mechanisms of evaporation, condensation and nucleation in confined geometries. *J Phys Chem B* **2002**, *106*, 3534-3537.

(12) Maeda, N.; Israelachvili, J.; Kohonen, M. Evaporation and instabilities of microscopic capillary bridges RID C-4234-2011. *Proc. Natl. Acad. Sci. U. S. A.* **2003**, *100*, 803-808.

(13) Farshchi-Tabrizi, M.; Kappl, M.; Cheng, Y.; Gutmann, J.; Butt, H. -. On the adhesion between fine particles and nanocontacts: An atomic force microscope study. *Langmuir* **2006**, *22*, 2171-2184.

(14) Butt, H.; Kappl, M. Normal capillary forces. *Adv. Colloid Interface Sci.* **2009**, *146*, 48-60.

(15) Willett, C. D.; Adams, M. J.; Johnson, S. A.; Seville, J. Capillary bridges between two spherical bodies. *Langmuir* **2000**, *16*, 9396-9405.

(16) Ward, C.; Levart, E. Conditions for stability of bubble nuclei in solid-surfaces contacting a liquid-gas solution. *J. Appl. Phys.* **1984**, *56*, 491-500.

(17) Ward, C. A.; Johnson, W. R.; Venter, R. D.; Ho, S.; Forest, T. W.; Fraser, W. D. Heterogeneous bubble nucleation and conditions for growth in a liquid-gas system of constant mass and volume. *J. Appl. Phys.* **1983**, *54*, 1833-1843.

(18) Elliott, J. A. W.; Voitcu, O. On the thermodynamic stability of liquid capillary bridges. *Can. J. Chem. Eng.* **2007**, *85*, 692-700.

(19) Eslami, F.; Elliott, J. A. W. Thermodynamic investigation of the barrier for heterogeneous nucleation on a fluid surface in comparison with a rigid surface. *J Phys Chem B* **2011**, *115*, 10646-10653.

(20) Ward, C. A.; Johnson, W. R.; Venter, R. D.; Ho, S.; Forest, T. W.; Fraser, W. D. Heterogeneous bubble nucleation and conditions for growth in a liquid-gas system of constant mass and volume. *J. Appl. Phys.* **1983**, *54*, 1833-1843.

(21) Attard, P. The explicit density functional and its connection with entropy maximization. *JOURNAL OF STATISTICAL PHYSICS* **2000**, *100*, 445-473.

(22) Attard, P. Thermodynamic analysis of bridging bubbles and a quantitative comparison with the measured hydrophobic attraction. *Langmuir* **2000**, *16*, 4455-4466.

(23) Ward, C. A.; Neumann, A. W. On the surface thermodynamics of a two—component liquid-vapor-ideal solid system. *J. Colloid Interface Sci.* **1974**, *49*, 286-290.

(24) Fisher, L. R.; Israelachvili, J. N. Experimental studies on the applicability of the Kelvin equation to highly curved concave menisci. *J. Colloid Interface Sci.* **1981**, *80*, 528-541.

(25) Ghasemi, H.; Ward, C. A. Sessile-water-droplet contact angle dependence on adsorption at the solid-liquid interface. *Journal of Physical Chemistry C* **2010**, *114*, 5088-5100.

(26) Elliott, J. A. W. Class notes for CHE 625, "Advanced macroscopic and statistical thermodynamics", University of Alberta. **2005**.

(27) Callen, H. B. In *Thermodynamics and an introduction to thermostatistics / Herbert B.Callen;* New York : Wiley, c1985; 2nd ed: 1985; .

(28) Ward, C. A. , Class notes through personal communication with Elliott, Janet A.W.

(29) Gibbs, J. W. In *The scientific papers of J. Willard Gibbs / J. Willard Gibbs;* New York, N.Y. : Dover Publications, 1961: 1961; .

(30) Middleman, S. *An Introduction to Fluid Dynamics: Principles of Analysis and Design*. / Wiley,1998.

(31) Hunter, R. J. In *Introduction to modern colloid science / Robert J. Hunter;* Oxford, England ; New York : Oxford University Press, 2002, c1993; 1st ed: 2002; .

(32) Adamson, A. W.; Gast, A. P. In *Physical chemistry of surfaces / Arthur W. Adamson and Alice P.Gast;* New York : Wiley, c1997; 6th ed: 1997; .

(33) Petrov, O.; Furó, I. Curvature-dependent metastability of the solid phase and the freezing-melting hysteresis in pores. *Physical Review E - Statistical, Nonlinear, and Soft Matter Physics* **2006**, *73*.

(34) Elliott, J. A. W. On the Complete Kelvin Equation. *Chemical Engineering Education* **2001**, *35*, 274-279.

(35) J, G. Powles. On the validity of the Kelvin equation. *Journal of Physics A: Mathematical and General* **1985**, *18*, 1551.

(36) Fisher, L. R.; Israelachvili, J. N. Direct measurement of the effect of meniscus forces on adhesion: A study of the applicability of macroscopic thermodynamics to microscopic liquid interfaces. *Colloids and Surfaces* **1981**, *3*, 303-319.

(37) Clift, R.; Grace, J. R.; Weber, M. E. In *Bubbles, drops, and particles / R. Clift, J. R. Grace and M. E.Weber;* New York : Academic Press, 1978: 1978; .

(38) de Gennes, P. G.; Brochard-Wyart, F.; Quéré, D. Capillarity and Wetting Phenomena-Drops, Bubbles, Pearls, Waves. **2004**.

(39) Perry, R. H.; Green, D. W. In *Perry's chemical engineers' handbook [electronic resource];* New York : McGraw-Hill, c2008; 8th ed. / prepared by a staff of specialists under the editorial direction of editor-in-chief, Don W. Green, late editor, Robert H. Perry: 2008; .

(40) Ward, C.; Forest, T. On the relation between platelet adhesion and the roughness of a synthetic biomaterial. *Ann. Biomed. Eng.* **1976**, *4*, 184-207.

(41) Yaws, C. L. In *Yaws' handbook of thermodynamic and physical properties of chemicalcompounds [electronic resource] : physical, thermodynamic and transportproperties for 5,000 organic chemical compounds / Carl L. Yaws;* Norwich, N.Y. : Knovel, c2003: 2003; .

(42) Harris, J.; Stöcker, H. In *Handbook of mathematics and computational science / John W. Harris,Horst Stöcker;* New York : Springer, 1998: 1998; .

(43) Weisstein, E. W. Solid of Revolution. *http://mathworld.wolfram.com/SolidofRevolution.html* (accessed 05/20, 2011).

(44) Thomas, G. B.; Weir, M. D.; Hass, J. In *Thomas' calculus / as revised by Maurice D. Weir, Joel Haas, FrankR. Giordano;* Boston : Pearson Addison Wesley, c2008; Media upgrade, 11th ed: 2008; .

(45) Charlaix, E.; Ciccotti, M. Capillary Condensation in Confined Media. To appear in 2010 in the Handbook of Nanophysics - Vol 1 - Edited by Klaus Sattler - CRC Press, **2009**.

(46) Megias-Alguacil, D.; Gauckler, L. J. Analysis of the capillary forces between two small solid spheres binded by a convex liquid bridge. *Powder Technol* **2010**, *198*, 211-218.

(47) Maboudian, R.; Howe, R. T. Critical review: Adhesion in surface micromechanical structures. *Journal of Vacuum Science and Technology B: Microelectronics and Nanometer Structures* **1997**, *15*, 1-20.

Index

Bond number, *Bo* 37

Capillary length, ℓ_C 38

Free energy (thermodynamic potential) 29

Gibbs free energy 31

Helmholtz free energy 31

Kelvin radius, R_C 27
- for liquid formation
- for vapour formation 28

Laplace–Young equation 22, 23

Mean radius of curvature , R_m 23

Principal radii of curvature 22

Relative difference 81

Thermodynamic potential (free energy) 29

Transition contact angle, θ_t 65

Young equation 25